ERDC Letter Report

Environmental Laboratory

US Army Corps of Engineers®
Engineer Research and Development Center

PCB Transport and Fate Modeling at New Bedford Harbor, MA

Earl Hayter, Lawrence Burkhard, Karl Gustavson, Jarrell Smith, Joseph Gailani, Elaine Stanley, Dave Lederer, and Ellen Iorio

June 2017

SEMS Doc ID 599091

ERDC Letter Report

PCB Transport and Fate Modeling at New Bedford Harbor, MA

Earl Hayter

Environmental Laboratory
U.S. Army Engineer Research and Development Center
3909 Halls Ferry Road
Vicksburg, MS 39180-6199

Lawrence Burkhard

USEPA Environmental Effects Research Laboratory
Mid-Continent Ecology Division/ORD
6201 Congdon Boulevard
Duluth, MN 55804

Karl Gustavson

USEPA Office of Superfund Remediation and Technology Innovation
1200 Pennsylvania Avenue, N. W.
Washington, DC 20460

Jarrell Smith and Joseph Gailani

U.S. Army Engineer Research and Development Center
3909 Halls Ferry Road
Vicksburg, MS 39180-6199

Dave Lederer and Elaine Stanley

U.S. Environmental Protection Agency, Region 1
5 Post Office Square, Suite 100
Boston, MA 02109-3912

Ellen Iorio

U.S. Army Corps of Engineers – New England District
696 Virginia Road
Concord, MA 01742-2751

Prepared for U.S. Environmental Protection Agency, Region 1
Boston, MA 02109-3912

Contents

Figures and Tables

Figures

Tables

Preface

The modeling investigation presented in this report was authorized by the U.S. Army Corps of Engineers New England District (NAE) and by the U.S. Environmental Protection Agency (USEPA) Region 1 to simulate the transport and fate of PCBs under three remedial measures for the New Bedford Harbor Superfund site in New Bedford, MA. David Dickerson, Elaine Stanley and Dave Lederer were the USEPA Remedial Project Managers (RPM) for this Superfund Site over the duration of this project. The technical work was performed by Earl Hayter (EL-EP-W), Karl Gustavson (EL-EP-R), Jarrell Smith (CHL-HF-FO), and Joseph Gailani (CHL-HF-CT). This work was performed at the Environmental Laboratory (EL) of the U. S. Army Engineer Research and Development Center (ERDC) during the period of January 2009 to December 2013 under the direction of Dottie Tillman, Chief of the Water Quality and Contaminant Modeling Branch, Warren Lorentz, Chief of Environmental Processes and Engineering Division, Jack Davis, Deputy Director of EL, and Beth Fleming, Director of EL.

Dr. Jeffrey P. Holland was Director of ERDC. COL Gary Johnston was Commander and Executive Director.

Executive Summary

The U.S. Army Engineer New England District (NAE) and the U.S. Environmental Protection Agency (USEPA) Region 1 requested that the U.S. Army Engineer Research and Development Center (ERDC), Environmental Laboratory (EL) perform a numerical modeling study for the purpose of developing a PCB transport and fate model that will allow multi-decade evaluation of the selected post-remediation scenario in New Bedford Harbor (NBH). A detailed description of the modeling study (including a description of the numerical models used in this study) that was performed to accomplish these two tasks is given in this report.

The post-remediation scenario selected by USEPA was constructed in the LTFATE modeling system that was used to perform this modeling study as follows: a) The bathymetry in the NBH portion of the model domain was updated using the latest bathymetric survey provided by EPA; b) In the Upper harbor, the concentration of total PCBs in the bottom sediment in the subtidal and mudflat areas was set equal to 10 ppm; c) In the Outer harbor, the concentration of total PCBs in the bottom sediment was set equal to 1 ppm; d) The sediment PCB initial concentrations in the non-remediated areas of NBH was re-interpreted using the 2014 LTM PCB data provided by EPA; e) In the Lower Harbor, the PCB bed concentrations was set to 15 ppm in the areas where dredging has been performed and 8 ppm everywhere else; f) The concentration of total PCBs in the lower harbor CAD cell (LHCC) capping material was set equal to 1 ppm.

The following conclusions have been formulated from this modeling study.

- The 30-year post-remediation scenario that was run for New Bedford Harbor using LTFATE revealed very slowly changing PCB concentrations in the harbor. Considering the relatively low energy environment inside the harbor as well as the very small load of clean sediment that is transported into the harbor by the Acushnet River, this is not too surprising.

- Resuspension of sediment in the shallower areas of NBH only occurs during simulated nor'easters. This results in the transfer of more PCBs

from the sediment bed to the water column due to the release of dissolved PCBs in the porewater of the sediment bed as well as particulate PCBs that are adsorbed onto the sediment that is resuspended.

- The diffusive flux of PCBs from the sediment bed to the overlying water column occurs at a very slow rate. This, in combination to a small loss of PCB mass due to volatilization, contribute to the very slow decrease in PCB concentrations, as reflected by the decreasing flux of PCBs out of the harbor, as seen in the model simulation.

- The average annual flux of PCBs to Buzzards Bay at the Hurricane Barrier 30 years after remediation is complete is approximately two orders of magnitude less than that before remediation.

Unit Conversion Factors

Multiply	By	To Obtain
Acres	4,046.873	square meters
acre-feet	1,233.5	cubic meters
cubic feet	0.02831685	cubic meters
cubic inches	1.6387064 E-05	cubic meters
cubic yards	0.7645549	cubic meters
degrees (angle)	0.01745329	Radians
degrees Fahrenheit	(F-32)/1.8	degrees Celsius
Fathoms	1.8288	Meters
Feet	0.3048	Meters
foot-pounds force	1.355818	Joules
Inches	0.0254	Meters
inch-pounds (force)	0.1129848	Newton meters
Knots	0.5144444	meters per second
Microns	1.0 E-06	Meters
miles (nautical)	1,852	Meters
miles (U.S. statute)	1,609.347	Meters
Slugs	14.59390	Kilograms
square feet	0.09290304	square meters
square yards	0.8361274	square meters
Yards	0.9144	Meters

1 Introduction

Background

The U.S. Army Engineer New England District (NAE) and the U.S. Environmental Protection Agency (USEPA) Region 1 requested that the U.S. Army Engineer Research and Development Center (ERDC) perform the following two tasks: 1) update the physical and chemical modeling that was performed at the New Bedford Harbor Superfund Site by Battelle (1990), and 2) perform multi-decade modeling of post-remediation conditions in New Bedford Harbor for the chosen remediation scenario using the updated modeling system. A description of the study plan used to accomplish these two tasks is given following a description of New Bedford Harbor.

Site Description

New Bedford Harbor (NBH) is a small estuary spanning approximately 4 miles between the Acushnet River and Buzzards Bay on the southeastern Massachusetts coast (Figures 1-1, 1-2, 1-3, 1-4). NBH has a mix of land uses, including residential, open space, and commercial uses (*e.g.*, commercial fishing, fish processing, and maritime support). As seen in Figures 1-2 and 1-4, there is a hurricane barrier (constructed in the 1960s) that separates the Lower Harbor from the Outer Harbor. The hurricane barrier is 5.63 km (3.5 miles) in length and has a 46 m (150 ft) wide entrance. The two gates seen in Figure 1-4 can be closed in 12 minutes to prevent a tropical storm induced storm surge from flowing into the harbor. The Upper Harbor is 757 km^2 (187 acres) in size, and the Lower Harbor is 3,035 km^2 (750 acres) in size. Figure 1-3 shows the navigation channel that exists in the Lower and Outer Harbor.

The Acushnet River has a 43 km^2 (16.5 mi^2) drainage basin and discharges into the northern end of NBH. Its estimated average annual discharge is 0.85 m^3/s (30 ft^3/s), which is only approximately 1% of the average tidal prism (the volume of water which flows into and out of NBH over a tidal cycle). As a result, except during high rainfall events this estuary is vertically well mixed. Vertical profiles of temperature and salinity (given in Appendix B) that were measured throughout the harbor during ERDC's field study in November 2008 verified that the water column in NBH is indeed well mixed under normal conditions. There are several

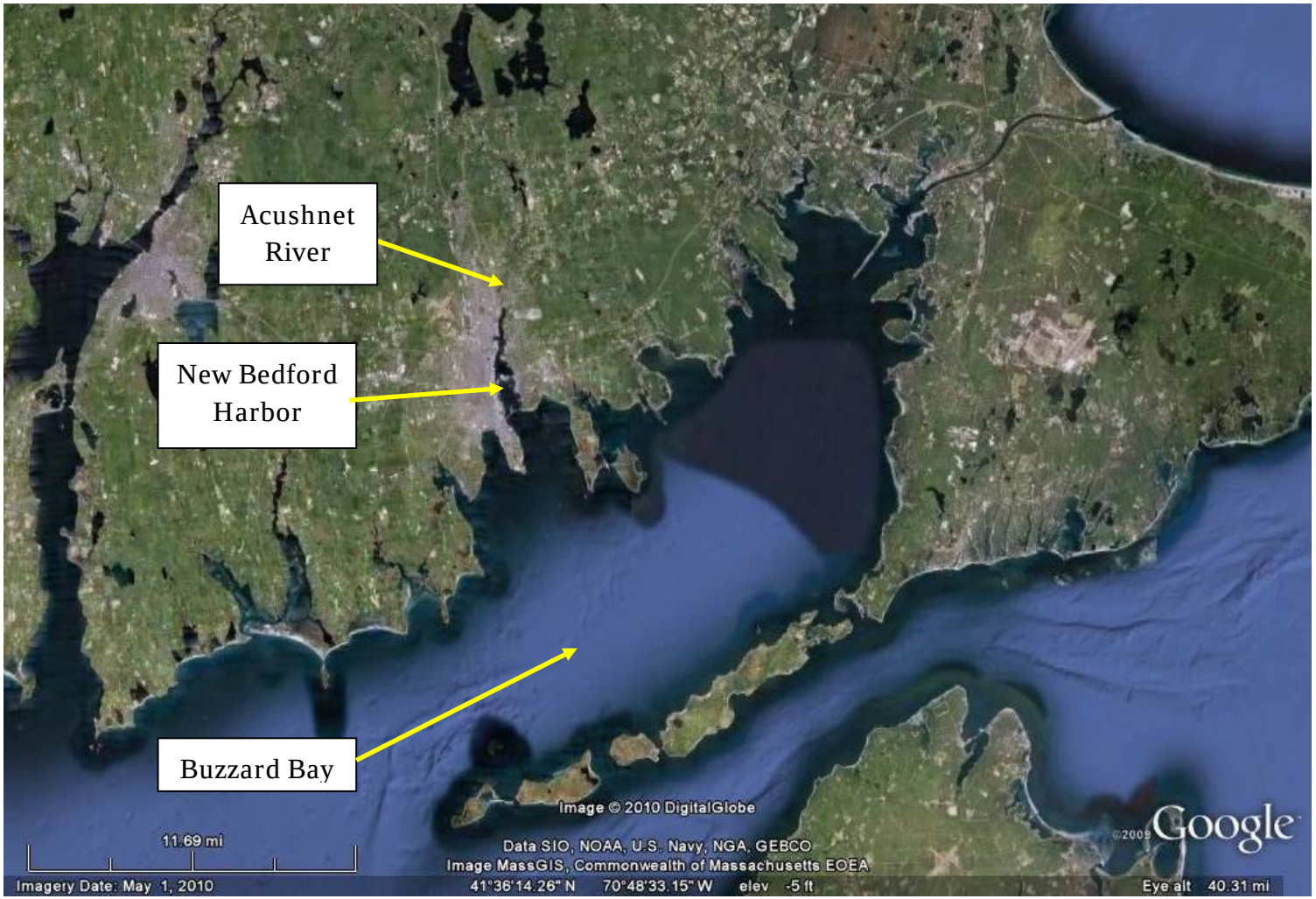

Figure 1-1. Site Map

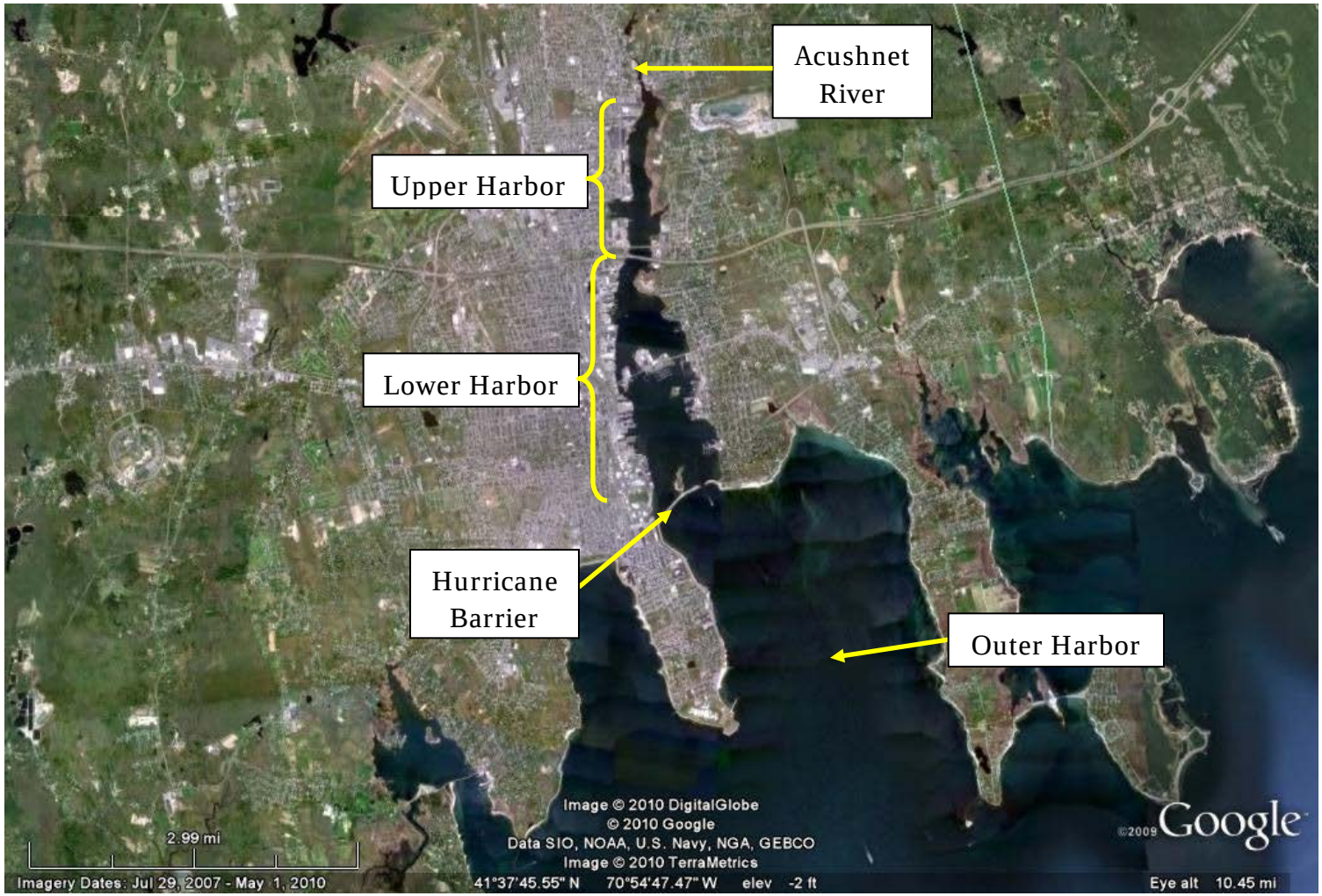

Figure 1-2. New Bedford Harbor, MA

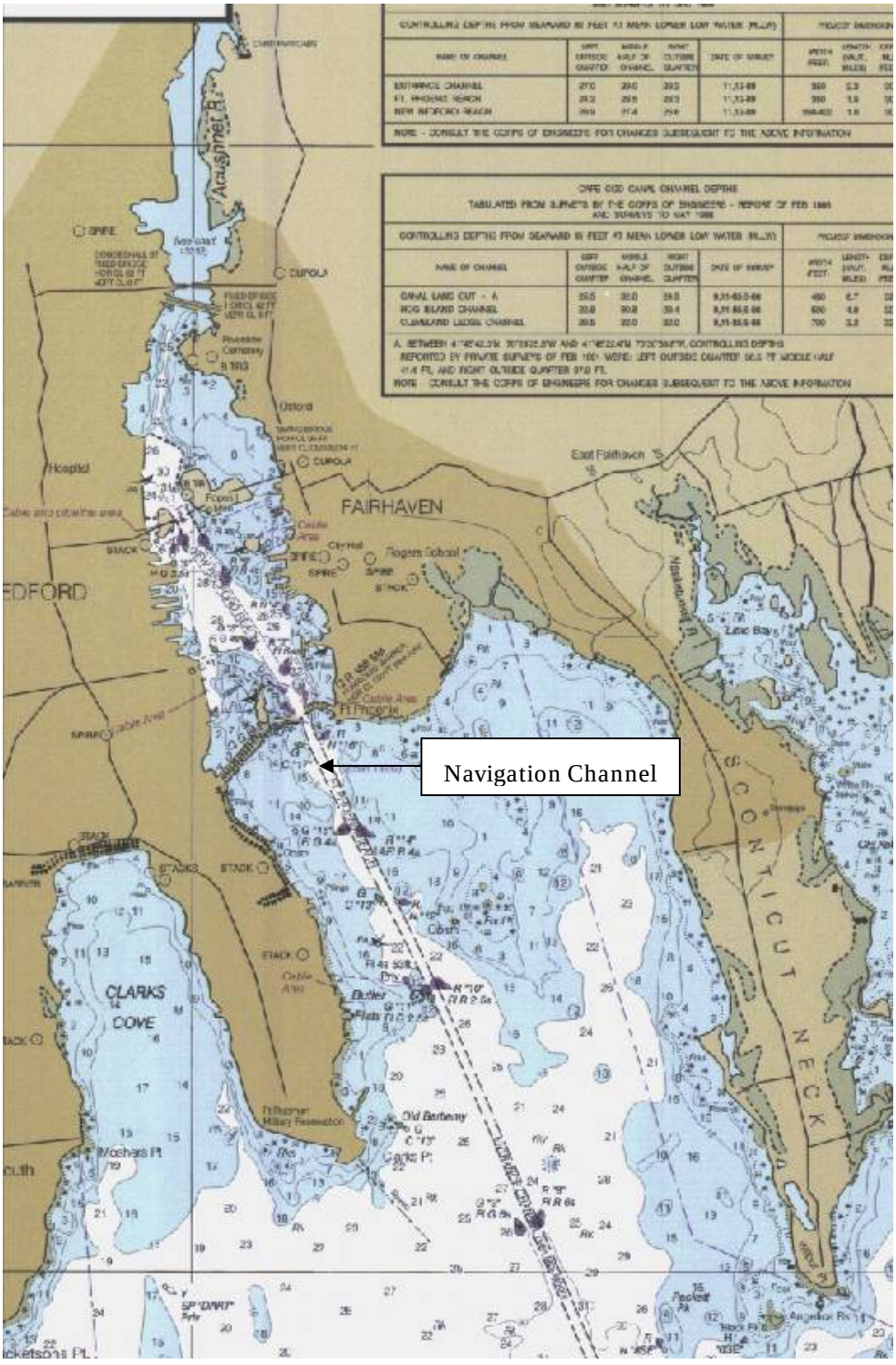

Figure 1-3. Navigation chart (NOAA chart 13230, 6/1999) of New Bedford

Figure 1-4. Hurricane Barrier and Entrance Channel to New Bedford Harbor.

storm drains, combined sewer overflows (CSOs) and industrial discharges as well as small creeks that discharge directly into the harbor.

The currents generated by the semi-diurnal tides in NBH are generally weak. Velocities are generally higher during flood tides than during ebb tides (Summerhayes *et al*., 1977). Currents in the Upper Harbor are relatively low: 0.15 m/s (0.3 knots) on average, and generally less than 0.3 m/s (0.6 knots). In the Lower Harbor, current velocities are generally less than 0.2 m/s (0.4 knots), and the maximum tidal currents in the Outer Harbor are generally comparable to those of the Lower Harbor, at approximately 0.2 m/s (0.4 knots), flowing generally north and south, into and out of NBH through the hurricane barrier opening (Eldridge Tide and Pilot Book, 1994).

The hydrodynamics of NBH have been significantly altered by anthropogenic modifications. The Coggeshall Street Bridge and causeway and the Hurricane Barrier have constricted tidal flow in the Upper Harbor and Lower Harbor, respectively. Currents during flood tides enter the Lower Harbor through the Hurricane Barrier entrance as a jet-type flow with a maximum velocity of approximately 1.2 m/s (2.4 knots). This jet flow and the secondary eddies that form on both sides of it dominates circulation in the Lower Harbor during flood tides. The Coggeshall Street Bridge also causes similar flow patterns in the Upper Harbor (Battelle Ocean Services, 1991; Summerhayes *et al*., 1977). Tidal currents at Coggeshall Street as high as 1.8 m/s (3.5 knots) have been measured during ebb tides (Battelle, 1990).

The Hurricane Barrier appears to have changed the tidal range within NBH as the average tidal range in the Lower Harbor is 1.1 m (3.7 ft) with a spring tidal range of 1.4 m (4.6 ft), while outside the barrier the average tidal range is 1.42 m (4.65 ft) with a spring range of 5.05 ft (1.54 m) (VHB, 1996). With tidal ranges less than 2 m, NBH is classified as a micro-tidal estuary.

Winds also affect the circulation in the Outer Harbor. Moderate southwest winds during summer and strong northwest winds during the winter cause distinctly different seasonal circulation effects. Because of the sheltered nature of NBH, winds would only cause a measurable circulation inside the harbor during storms.

With a fetch of more than 8.7 miles (14 km) is present to the Southwest, and waves in the Outer Harbor at times can reach 2 m (6.5 ft) (Battelle, 1990). While

the Upper and Lower Harbors are generally protected from waves by the Hurricane Barrier, waves as high as 0.9 m (3 ft) have been observed north of Coggeshall Street during storms (Battelle, 1990). Wind-generated waves, in particular during storms, may be the most important factor in generating currents at the bottom and possibly eroding sediment in shallow waters such as those in the Upper Harbor and the undredged portions of the Lower Harbor.

Site Contamination

New Bedford Harbor is contaminated with polychlorinated biphenyls (PCBs). PCBs are a group of 209 congeners with varying substitution of chlorine atoms on a biphenyl backbone. In the United States, PCBs were produced, sold, and subsequently introduced to the environment as mixtures containing subsets of those congeners (known as Aroclors, a trademark of Monsanto). These mixtures, specified by 4-digit numbers (*e.g.*, Aroclor 1016, 1242, or 1260), possessed different amount of chlorine by weight. PCB analysis in environmental samples has been evolving for decades. Over time, techniques have changed from quantifying Aroclor mixtures (by comparing sample chromatographic patterns to pure Aroclor mixtures) (Risebrough *et al.*, 1969) to separation and quantification of individual congeners (Larsen, 1995). While quantifying each of the 209 congeners is not necessary because many congeners have never been detected in environmental samples (McFarland and Clarke, 1989), analyzing PCBs as Aroclor mixtures is not as robust since congener patterns change over time and uptake by biota is not equal across all congeners in an Aroclor mixture (NRC, 2001).

From the 1940s to the 1970s, two electrical capacitor manufacturing plants disposed of industrial wastes containing PCBs directly into New Bedford Harbor and indirectly through the storm sewer system. The combined tidal and riverine flows in the harbor transported the PCBs for about 9.7 km (6 miles) from the Acushnet River into Buzzards Bay. The harbor was placed on USEPA's National Priorities List in 1982. Aroclors 1016, 1242, and 1254 were most commonly used by these electrical capacitor manufacturers (EBASCO, 1990). Studies of the contamination have been ongoing since the 1970s, so a wide variety of historical PCB data (total PCBs defined as Aroclors, homologues, or various congeners) are available. Over time, analytical methods and PCB congeners selected for evaluation in New Bedford Harbor sediment, water, and biota samples have changed. For example, early analytical efforts could only quantify Aroclors (*e.g.*, Hall *et al.*, 1983). Biota collected by the State of Massachusetts in 2005 (State of Massachusetts 2008) were analyzed for 136 congeners and 5 Aroclors; in 2002

(EPA and State of Massachusetts, 2004), five PCB Aroclors and 28 congeners[1] were analyzed. More recently, the Massachusetts Department of Environmental Protection and the Massachusetts Division of Marine Fisheries (2016) issued a monitoring report for seafood harvested in 2015 from the NBH Superfund Site. This report documents the PCB levels in edible seafood species caught in NBH and Buzzards Bay in 2015. As with previous studies, there is a decreasing trend of PCB concentrations in locally caught seafood from the Upper Bay, to Middle Bay, to Lower Bay, and to the Outer Bay. This study found that levels of PCBs in the seafood in NBH are still above the 1998 ROD's target level of 0.02 ppm.

EPA's long-term sediment and biota sampling program that began in 1993 analyzes 18 PCB congeners utilized by the National Oceanic and Atmospheric Administration's (NOAA) Status and Trends Program (Bergen *et al.* 1998; Nelson *et al.* 1996; Nelson and Bergen, 2012). These specific congeners are the most pervasive and make up about half of the total mass of PCBs in marine biota. In Figure 1-5, collection areas are shown for the on-going seafood monitoring program for the New Bedford Harbor Superfund site performed by the State of Massachusetts, Department of Environmental Protection and Division of Marine Fisheries.

In 1998 EPA selected a remediation plan for the widespread PCB contamination in NBH (EPA, 1998). This remedy involves dredging and containment of approximately 688,000 m^3 (900,000 cubic yards) of PCB-contaminated sediment spread over about 1,000 acres. In the Upper Harbor sediments with PCB concentrations above 10 parts per million (ppm) will be removed, while in the Lower Harbor and in salt marshes, sediments with PCB concentrations above 50 ppm will be removed. Intertidal sediments in specific areas will be removed if PCB levels are above specified levels. The main goals of the planned remediation are to reduce health risks due to consumption of PCB-contaminated seafood, and reduce health risks due to contact with PCB-contaminated shoreline sediments.

[1] Eighteen NOAA (National Oceanic and Atmospheric Administration) list congeners and the twelve World Health Organization (WHO) dioxin-like congeners.

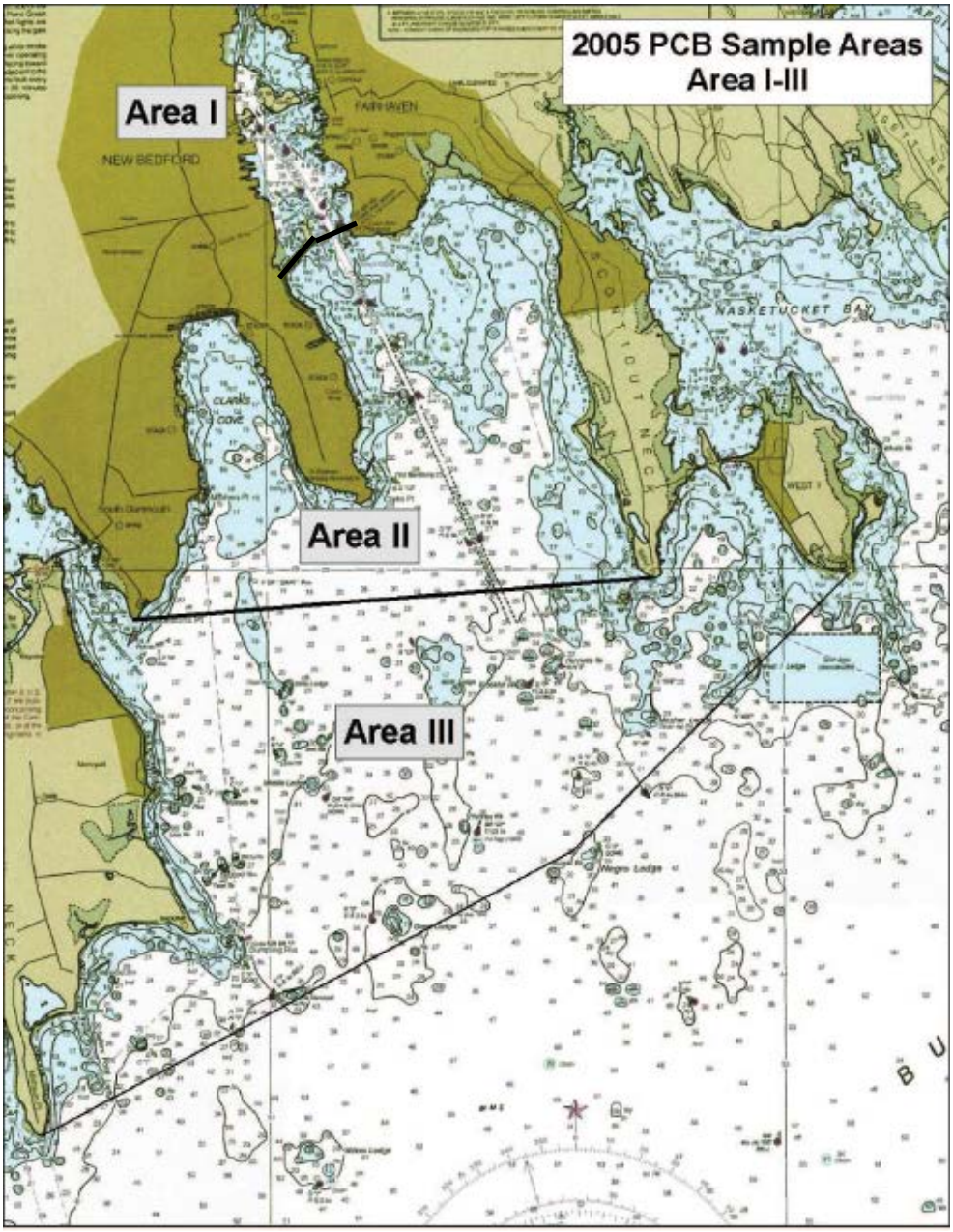

Figure 1-5 Fish closure areas in New Bedford Harbor (after MDEP-MDMF, 2008)

Hydraulic dredging took place in the upper harbor between 2004 and 2015. Prior to the start of the dredging in 2004, EPA and the US Army Corps of Engineers performed several “hot spot” cleanup actions in the harbor and along the shoreline. Through 2015, approximately 311,000 m^3 (407,000 cubic yards) of PCB-contaminated sediment has been remediated. Approximately 99,392 m^3 (130,000 cubic yards) of less contaminated sediment from the Lower and Upper

Harbor has been mechanically dredged and disposed of in the Lower Harbor Confined Aquatic Disposal (CAD) Cell during 2016-17. Additionally, the State Enhanced Remedy (SER) has accounted for about 352,000 m^3 (460,000 cubic yards) of dredging in the Lower Harbor, followed by placement in one of four State SER CAD Cells constructed in the Lower Harbor.

Study Objectives

There are two primary tasks: 1) update the physical, chemical, and biological modeling that was performed at the New Bedford Harbor Superfund Site by Battelle (1990), and 2) perform multi-decade modeling of post-remediation conditions in New Bedford Harbor for the EPA selected remediation alternative using the updated modeling system. Geophysical models can be very useful tools for predicting the future behavior of a physical system, and for providing relative comparisons among proposed remedies.

The original model developed for the site (Battelle 1990) (henceforth called the Battelle model) and its application, while being a state-of-the-art model for that time, contained numerous assumptions and limitations that greatly increased the uncertainties of the results. Most of these limitations and assumptions were not used in the current PCB transport and fare modeling study for NBH. Some of these assumptions and limitations associated with the original model construct are listed below:

- Temporally and spatially constant eddy viscosities and eddy diffusivities were used in the Battelle model.

- Wind waves were assumed not to propagate into the harbor from outside the modeling domain.

- The modeling domain is too small to accurately represent the propagation of the incident and reflected tidal waves within the harbor.

- Sediment bed is limited to one 4-cm layer.

- Parameters used to calibrate the sediment transport module were the mean grain size for noncohesive size fractions, critical shear stresses for each type and size fraction, and erodibility coefficients for cohesive sediments.

- Primary calibration parameter for the contaminant transport model was the bed partitioning coefficients.

- Surface sediment data from the literature are used to represent the properties of the sediment bed.

- Diffusion of dissolved PCBs in the bed is not represented.

- The percentage of organic matter on sediment particles and its effect on adsorbed and dissolved PCB transport is not represented.

- Limited sensitivity and uncertainty analyses and model calibration were performed.

- No model validation was performed.

- Model results from 95-day model simulation using synthetic hydrodynamics linearly extrapolated in two-year increments to estimate fate of the PCBs over 10 years.

- The synthetic 95-day hydrodynamics were generated by piecing together the hydrodynamics computed for the following two 24-hour simulations: fair weather case with northerly winds ranging from 2 to 10 m/s, and a storm event case with southerly winds of 1 to 15 m/s. Both cases were forced by a M2 tide applied at the open water boundary. The synthetic hydrodynamics used to force the sediment and contaminant transport model consisted of the following sequence of the two cases: 31 days of the fair weather case, 1 day of the storm event, 31 days of the fair weather case, 1 day of the storm event, and 31 days of the fair weather case.

The components to the modeling system that were updated in this study were the hydrodynamic, sediment and contaminant transport models. In this context, updating refers to using state-of-the-art sediment and contaminant transport models which represent more transport processes and represent those processes more accurately than models available in the late 1980's and early 1990's. The tremendous increase in computing power since that time permits 1) better representation of the harbor geometry and bathymetry through the use of a finer numerical grid in both the horizontal and vertical dimensions, and 2) expanding

the modeling domain Bay (for the hydrodynamic modeling) to include Buzzards Bay.

The need to model sediment transport in addition to the transport and fate of PCBs is because PCBs preferentially adsorb to organic matter in surface waters, on POC suspended in the water column and deposited on the bed, and on DOC in the water column and in the porewater of the bed. As such, simulation of PCB transport at NBH also requires the simulation of the fine-grain sediment that is the dominant type of sediment throughout the harbor. Accurate simulation of fine-grain (*i.e.*, cohesive) sediment transport requires the measurement of site-specific properties that govern the transport of cohesive sediment in surface waters.

Along with using improved models, new methods for measuring site-specific erosion rates and critical shear stresses of resuspension of fine-grain dominated sediments (as are present in NBH) have been developed since the late 1980's. Most notable is the SEDFLUME, which was used to measure gross erosion rates and critical resuspension shear stresses with depth in sediment cores collected in NBH. A second critical need in modeling contaminated sediment transport is measurement of the site-specific settling velocities of fine-grain sediment flocs. The settling velocities of flocs are functions of, among other factors, concentrations of suspended clay, silt and organic particles; turbulence intensity; salinity; and clay mineralogy. Field studies to perform a SEDFLUME study and to measure floc settling velocities were conducted as a component of this project.

Data Limitations

It is important to state up front that very limited data were available to conduct a thorough calibration and validation of the various models used in this modeling study. A few examples of this are listed below.

- Based on a few isolated measurements, during normal weather conditions only very low suspended sediment loads get transported by the Acushnet River into the Upper Harbor, while during extreme rainfall induced runoff events the suspended sediment loads usually increase by one or more orders of magnitude. Due to the lack of sediment load measurements during such an event, a regional discharge-SSC relationship was used to calculate the SSC time series of the finest cohesive sediment size class as a function of the Acushnet discharge time series.

- No measurements of suspended sediment concentrations at any location in NBH had been made during any significant event, so no data were available to calibrate the suspended sediment transport model. The limited calibration and validation of the sediment transport model that were performed are described in Section 5.

- There were no wave measurements available to calibrate the wave model that was applied to the model domain to simulate the time and space varying locally generated wind waves.

- There were only a limited number of measurements of the dissolved PCB concentrations at a few sampling points in NBH. This limited data did not allow for a thorough calibration and validation of the contaminant transport model.

The impact of the limited data on the modeling study will be discussed throughout this report. As presented in Section 5, despite the data limitation, the modeling system was able come within 20 percent of the measured PCB flux at the entrance to NBH. Since the PCB flux is based on predictions by the hydrodynamic model, the sediment transport model, and the contaminant transport model, this indicates that the performance of the combined modeling system was at least representative of the actual conditions at NBH.

Modeling Approach

The modeling approach used by the ERDC and EPA modeling team is summarized next:

1. A hydrodynamic model that used a coarse curvilinear-orthogonal grid to represent Buzzards Bay was setup and calibrated. This model was used to construct the hydrodynamic boundary conditions to drive a fine grid model of NBH. Tidal constituents contained in the ADCIRC Western North Atlantic Ocean data base (Mukai *et al.*, 2003) were used to construct the tidal boundary conditions at the open water boundaries.

2. A hydrodynamic model that used a nested, non-uniform Cartesian grid for NBH that extended out into Buzzards Bay was setup and calibrated. The tidal

boundary conditions for this model were extracted from the coarse grid hydrodynamic model.

3. A sediment transport model that is capable of simulating the transport of both cohesive and noncohesive sediment was setup using the results of the SEDFLUME tests and settling velocity measurements.

4. A wave transformation model that simulates, among other processes wind-induced generation, shoaling, refraction, diffraction, and breaking was setup and used to generate the temporally varying wave field in the modeling domain. Along with the flows simulated by the hydrodynamic mode, the wave field was used to calculate the current- and wave-induced bed shear stresses that were used in the sediment transport model to determine when erosion and deposition occurred.

5. A contaminant transport model that is capable of simulating 3-phase equilibrium partitioning of PCBs between particulate (sorbed), freely dissolved, and DOC-bound phase, volatilization of PCBs, diffusion of freely dissolved PCBs from the water column to the top sediment bed layer (and vice-versa), and diffusion of freely dissolved PCBs within the layered sediment bed was setup, calibrated and validated.

6. The PCB fate model was used to simulate 30-years of post-remediation conditions in New Bedford Harbor starting with initial conditions that represent the combined efforts of the EPA Superfund cleanup and the State Enhanced Remedy (SER).

Report Organization

Descriptions of the different models used in this modeling study are presented in Chapter 2. The field data collection program performed is described in Chapter 3. The setup of the models is discussed in Chapter 4, and Chapter 5 provides descriptions of the calibration and validation of these models. The simulated modeling scenario and the results of this simulation are described in Chapter 6. Conclusions are provided in Chapter 7.

2 Description of Models

The numerical modeling simulations for the hydrodynamic, sediment transport and contaminant transport modeling components of this study were performed with the LTFATE model, which is the three-dimensional (3D) surface water modeling system supported by ERDC. The hydrodynamic, sediment transport and contaminant transport components of LTFATE are described next.

Hydrodynamic Model

The hydrodynamic model in LTFATE is the Environmental Fluid Dynamics Code (EFDC) model (Hamrick, 2007a, 2007b, and 2007c). EFDC is a 3D finite difference model that contains dynamically linked hydrodynamic, sediment transport and contaminant transport modules. EFDC can simulate barotropic and baroclinic flow in a water body due to astronomical tides, wind, density gradients, and river inflow. It solves the 3D, vertically hydrostatic, free surface, turbulence averaged equations of motion. EFDC is extremely versatile, and can be used for 1D, 2D-laterally averaged (2DV), 2D-vertically averaged (2DH), or 3D simulations of rivers, lakes, reservoirs, estuaries, coastal seas, and wetlands. For realistic representation of horizontal boundaries, the governing equations in EFDC are formulated such that the horizontal coordinates, x and y, are curvilinear. To provide uniform resolution in the vertical direction, the sigma (stretching) transformation is used.

The governing equations that are solved by EFDC are given in Appendix A. They are the 3D Reynolds-averaged equations of continuity (Equation A-1), linear momentum (Equations A-2 and A-3), hydrostatic pressure (Equation A-4), equation of state (Equation A-5), and transport equations for salinity and temperature (Equations A-6 and A-7). These equations of motion and transport solved in EFDC are turbulence-averaged, because prior to averaging, although they represent a closed set of instantaneous velocities and concentrations, they cannot be solved for turbulent flows. A statistical approach is applied, where the instantaneous values are decomposed into mean and fluctuating values to enable the solution. Additional terms that represent turbulence are introduced to the equations for the mean flow. Turbulent equations of motion are formulated to utilize the Boussinesq approximation for variable density. The Boussinesq approximation accounts for variations in density only in the gravity term. This

assumption simplifies the governing equations significantly, but may introduce large errors when density gradients are large. The resulting governing equations, presented in the next chapter, include parameterized, Reynolds-averaged stress and flux terms that account for the turbulent diffusion of momentum, heat and salt. The turbulence parameterization in EFDC is based on the Mellor and Yamada (1982) level 2.5 turbulence closure scheme as modified by Galperin *et al.* (1988) that relates turbulent correlation terms to the mean state variables.

The EFDC model also solves several transport and transformation equations for different dissolved and suspended constituents, including suspended sediments, contaminants, and water quality state variables. An overview of the governing equations is given below; detailed descriptions of the model formulation and numerical solution technique used in EFDC are provided by Hamrick (2007b). Additional capabilities of EFDC include: 1) simulation of wetting and drying of flood plains, mud flats, and tidal marshes; 2) integrated, near-field mixing zone model; 3) simulation of hydraulic control structures such as dams and culverts; and 4) simulation of wave boundary layers and wave-induced mean currents.

Numerically, EFDC is second-order accurate both in space and time. A staggered grid or C grid provides the framework for the second-order accurate spatial finite differencing used to solve the equations of motion. Integration over time involves an internal-external mode splitting procedure separating the internal shear, or baroclinic mode, from the external free surface gravity wave, or barotropic mode. In the external mode, the model uses a semi-implicit scheme that allows the use of relatively large time steps. The internal equations are solved at the same time step as the external equations, and are implicit with respect to vertical diffusion. Details of the finite difference numerical schemes used in the EFDC model are given in Hamrick (2007b), and will not be presented in this report.

Wave Model

The open source SWAN wave model that represents wave generation, propagation, and transformation was used in this study for simulating wind generated surface waves in the model domain in Buzzards Bay and New Bedford Harbor. SWAN (acronym for Simulating WAves Nearshore) is a third-generation wave transformation model for obtaining estimates of wind-generated surface gravity wave parameters (*e.g.*, wave heights and periods) in coastal seas, estuaries and lakes from given wind, bathymetry and current conditions (Booij *et al.*,

1999). The model is based on the wave action balance equation (or energy balance in the absence of currents) with sources and sinks.

The following wave propagation processes are simulated in SWAN:

- rectilinear propagation through geographic space,
- refraction due to spatial variations in bottom and current,
- shoaling due to spatial variations in bottom and current,
- blocking and reflections by opposing currents, and
- transmission through, blockage by, or reflection from sub-grid scale obstacles.

The following wave generation and dissipation processes are represented in SWAN:

- generation by wind,
- dissipation by white-capping,
- dissipation by depth-induced wave breaking,
- dissipation by bottom friction,
- wave-wave interactions (quadruplets and triads), and
- interaction with fixed obstacles.

In addition, the wave-induced set-up of the mean sea surface is computed by SWAN.

Information about the wave field in a water body is contained in the wave variance spectrum or energy density $E(\sigma, \theta)$ that distributes wave energy over frequencies σ (as observed in a reference frame moving with the current) and propagation directions θ which is the direction normal to the wave crest of each spectral component. Usually wave transmission models determine the change of the action density $N(\vec{x}, t, \sigma, \theta)$ in vector space $\vec{x}$ and time t. The action density is defined as $N = E/\sigma$. It is conserved during propagation in the presence of a current field, whereas E is not (Whitman, 1974). It is assumed that the current field is uniform with respect to the vertical coordinate and is denoted as $\vec{U}$.

The change of N with time is governed by the action balance equation, which is given as (Mei, 1983):

$$\frac{\partial N}{\partial t}+\nabla_{\vec{x}}[(\vec{c}_g+\vec{U})N]+\frac{\partial c_\sigma N}{\partial \sigma}+\frac{\partial c_\theta}{\partial \theta}=\frac{S_{tot}}{\sigma} \quad (2\text{-}1)$$

The second term on the left-hand side of this equation represents the propagation of wave energy in two-dimensional space, with the group celerity $\vec{c}_g = \partial\sigma / \partial\vec{k}$, where $\vec{k}$ is the wave number vector. The third term represents the effect of shifts of the radian frequency due to variations in depth and currents. The fourth term represents depth- and current-induced refraction. The quantities c_σ and c_θ are the propagation velocities in spectral space (σ,θ). On the right-hand side S_{tot} is the source/sink term that represents all physical processes which generate, dissipate, or redistribute wave energy. They are defined for the energy density $E(\sigma,\theta)$. S_{tot} is expressed as:

$$S_{tot} = S_{in} + S_{nl3} + S_{nl4} + S_{ds,w} + S_{ds,b} + S_{ds.br} \quad (2\text{-}2)$$

where the terms on the right-hand side represent wind-induced wave growth, non-linear transfer of wave energy through three-wave and four-wave interactions, and wave decay due to white capping, bottom friction and depth-induced wave breaking.

Sediment Transport Model

The sediment transport model in LTFATE is the SEDZLJ sediment transport model (Jones and Lick, 2001; James *et al.*, 2010). In LTFATE SEDZLJ is dynamically linked to EFDC in that the hydrodynamics and sediment transport modules are run during each model time step.

One of the first steps in performing sediment transport modeling is to use grain size distribution data from sediment samples collected at different locations throughout the model domain to determine how many discrete sediment size classes are needed to adequately represent the full range of sediment sizes. Typically, three to eight size classes are used. For example, for the current modeling study, two size classes are used to represent sediment in the cohesive sediment size range, *i.e.*, less than 63 μm, and three size classes are used to represent noncohesive sediment size range, *i.e.*, greater than 63 μm. Each sediment size class is represented in SEDZLJ using the median or mean diameter within that size range.

EFDC simulates the transport of each of the sediment classes to determine the suspension concentration for each size class in every water column layer in each grid cell. The transport of suspended sediment is determined through the solution of Equation A-17, where $C = S_j$, where S_j represents the concentration of the *jth* sediment class, and Q_{ci} = source/sink term for the *ith* sediment size class that accounts for erosion/deposition.

The settling velocities for noncohesive sediments are calculated in SEDZLJ using the following equation by Cheng (1997).

$$W_s = \frac{\mu}{d}\left(\sqrt{25+1.2d_*^2}-5\right)^{\frac{3}{2}} \qquad (2\text{-}3)$$

where μ = dynamic viscosity of water; d = sediment diameter; and d_* = non-dimensional particle diameter given by:

$$d_* = d\left[\left(\rho_s/\rho_w - 1\right)g/\nu^2\right]^{1/3} \qquad (2\text{-}4)$$

where ρ_w = water density, ρ_s = sediment particle density, g = acceleration due to gravity, and ν = kinematic fluid viscosity. Cheng's formula is based on measured settling speeds of real sediments. As a result it produces slower settling speeds than those given by Stokes' Law because real sediments have irregular shapes and thus a greater hydrodynamic resistance than perfect spheres as assumed in Stokes' law.

The erosion and deposition of each of the sediment size classes, *i.e.*, the source/sink term in the 3D transport equation given above, and the subsequent change in the composition and thickness of the sediment bed in each grid cell are calculated by SEDZLJ at each time step.

SEDZLJ is an advanced sediment bed model that represents the dynamic processes of erosion, bedload transport, bed sorting, armoring, consolidation of fine-grain sediment dominated sediment beds, settling of flocculated cohesive sediment, settling of individual noncohesive sediment particles, and deposition. An active layer formulation is used to describe sediment bed interactions during simultaneous erosion and deposition. The active layer facilitates coarsening during the bed armoring process. The SEDZLJ model was designed to directly use the results obtained from a Sedflume study.

Figure 2-1 shows the simulated sediment transport processes in SEDZLJ. In this figure, U = near bed flow velocity, δ_{bl} = thickness of layer in which bedload occurs, U_{bl} = average bedload transport velocity, D_{bl} = sediment deposition rate for the sediment being transported as bedload, E_{bl} = sediment erosion rate for the sediment being transported as bedload, E_{sus} = sediment erosion rate for the sediment that is eroded and entrained into suspension, and D_{sus} = sediment deposition rate for suspended sediment. Specific capabilities of SEDZLJ are listed below.

- Whereas a hydrodynamic model is calibrated to account for the total bed shear stress, which is the sum of the form drag due to bed forms and other large-scale physical features (*e.g.*, boulder size particles) and the skin friction (also called the surface friction), the correct component of the bed shear stress to use in predicting sediment resuspension and deposition is the skin friction. The skin friction is calculated in SEDZLJ as a function of the near-bed current velocity and the effective bed roughness. The latter is specified in SEDZLJ as a linear function of the mean particle diameter in the active layer.

- Multiple size classes of both fine-grain (*i.e.*, cohesive) and noncohesive sediments can be represented in the sediment bed. This capability is necessary in order to simulate coarsening and subsequent armoring of the surficial sediment bed surface during high flow events.

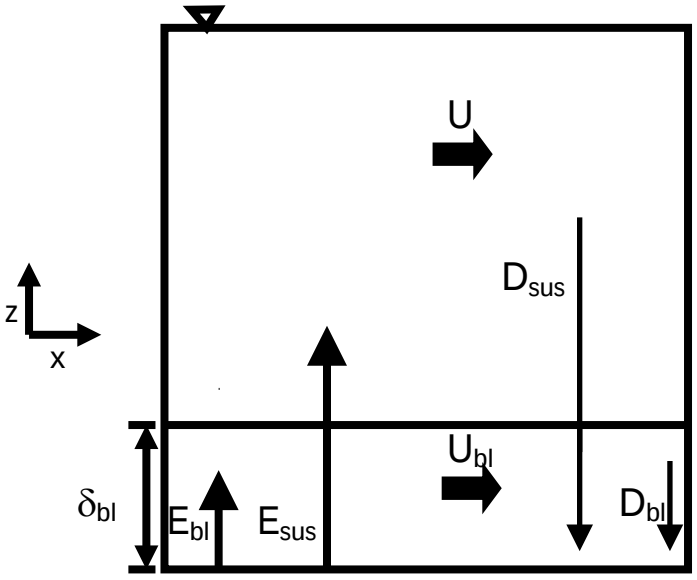

Figure 2-1 Sediment Transport Processes Simulated in SEDZLJ (terms defined in text above)

- To correctly represent the processes of erosion and deposition, the sediment bed in SEDZLJ can be divided into multiple layers, some of which are used to represent the existing sediment bed and others that are used to represent new bed layers that form due to deposition during model simulations. Figure 2-2 shows a schematic diagram of this multiple bed layer structure. The graph on the right hand side of this figure shows the variation in the measured gross erosion rate (in units of cm/s) with depth into the sediment bed as a function of the applied skin friction. A SEDFLUME study is normally used to measure these erosion rates.

- Erosion from both cohesive and non-cohesive beds is affected by bed armoring, which is a process that limits the amount of bed erosion that occurs during a high-flow event. Bed armoring occurs in a bed that contains a range of particle sizes (*e.g.*, clay, silt, sand). During a high- flow event when erosion is occurring, finer particles (*i.e.*, clay and silt, and fine sand) tend to be eroded at a faster rate than coarser particles (*i.e.*, medium to coarse sand). The differences in erosion rates of the various sediment particle sizes creates a thin layer at the surface of the sediment bed, referred to as the active layer, that is depleted of finer particles and enriched with coarser particles. This depletion-enrichment process can lead to bed armoring, where the active layer is primarily composed of coarse particles that have limited mobility. The multiple bed model in SEDZLJ accounts for the exchange of sediment through and the change in composition of this active layer. The thickness of the active layer is normally calculated as a time varying function of the mean sediment particle diameter in the active layer, the critical shear stress for resuspension corresponding to the mean particle diameter, and the bed shear stress. Figure 2-3 shows a schematic of the active layer at the top of the multi-bed layer model used in SEDZLJ.

  SEDZLJ was designed to use the results obtained with SEDFLUME, which is a straight, closed conduit rectangular cross-section flume in which detailed measurements of critical shear stress of erosion and erosion rate as a function of sediment depth are made using sediment cores dominated by cohesive sediment collected at the site to be modeled (McNeil *et al.*, 1996). However, when SEDFLUME results are not available, it is possible to use a combination of literature values for these parameters as well as the results of SEDFLUME tests performed at other similar sites. In this case, a detailed sensitivity

analysis should be performed to assist in quantifying the uncertainty that results from the use of these non-site specific erosion parameters.

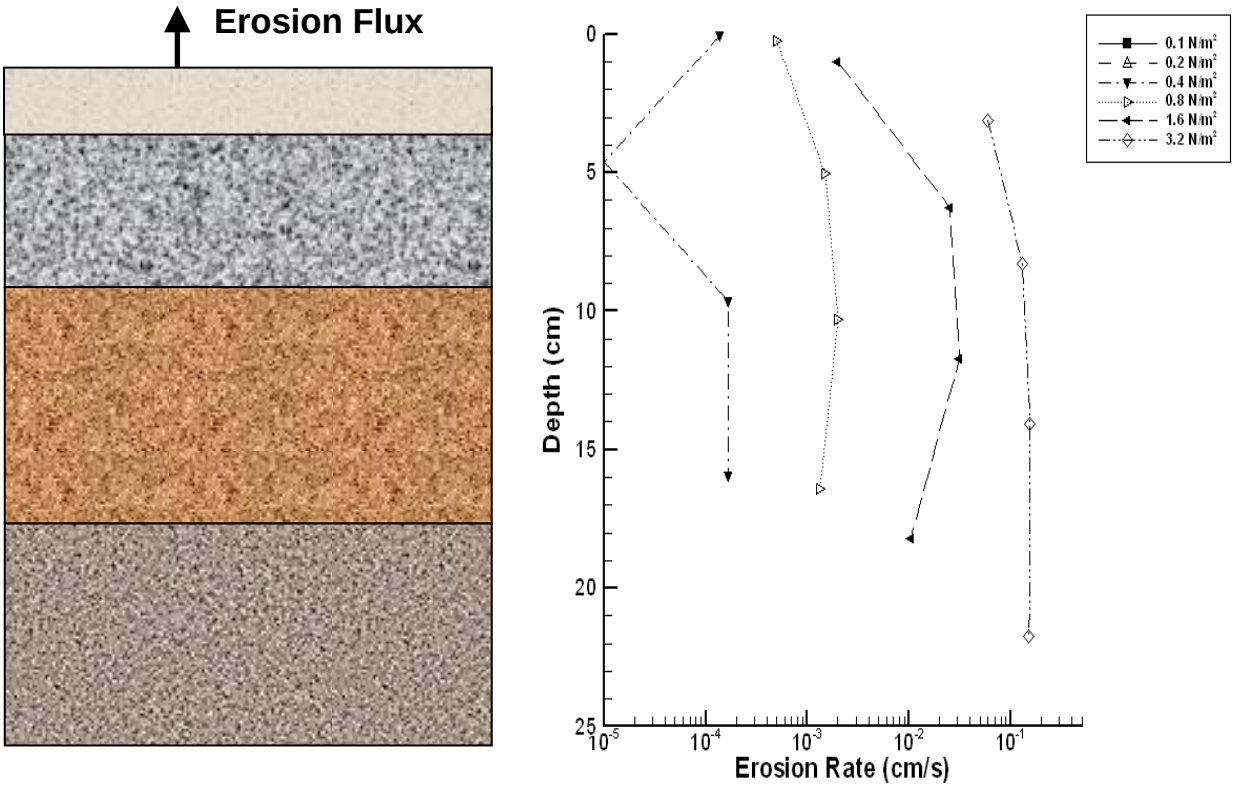

Figure 2-2 Multi-Bed Layer Model Used in SEDZLJ

SEDZLJ can simulate overburden-induced consolidation of cohesive sediments. An algorithm that simulates the process of primary consolidation, which is caused by the expulsion of pore water from the sediment, of a fine-grained, *i.e.*, cohesive, dominated sediment bed is included in SEDZLJ. The consolidation algorithm in SEDZLJ accounts for the following changes in two important bed parameters: 1) increase in bed bulk density with time due to the expulsion of pore water, and 2) increase in the bed shear strength (also referred to as the critical shear stress for resuspension) with time. The latter parameter is the minimum value of the bed shear stress at which measurable resuspension of cohesive sediment occurs. As such, the process of consolidation typically results in reduced erosion for a given excess bed shear stress (defined as the difference between the bed shear stress and bed shear strength) due to the increase in the bed shear strength. In addition, the increase in bulk density needs to be represented to accurately account for the

mass of sediment (per unit bed area) that resuspends when the bed surface is subjected to a flow-induced excess bed shear stress. Models that represent

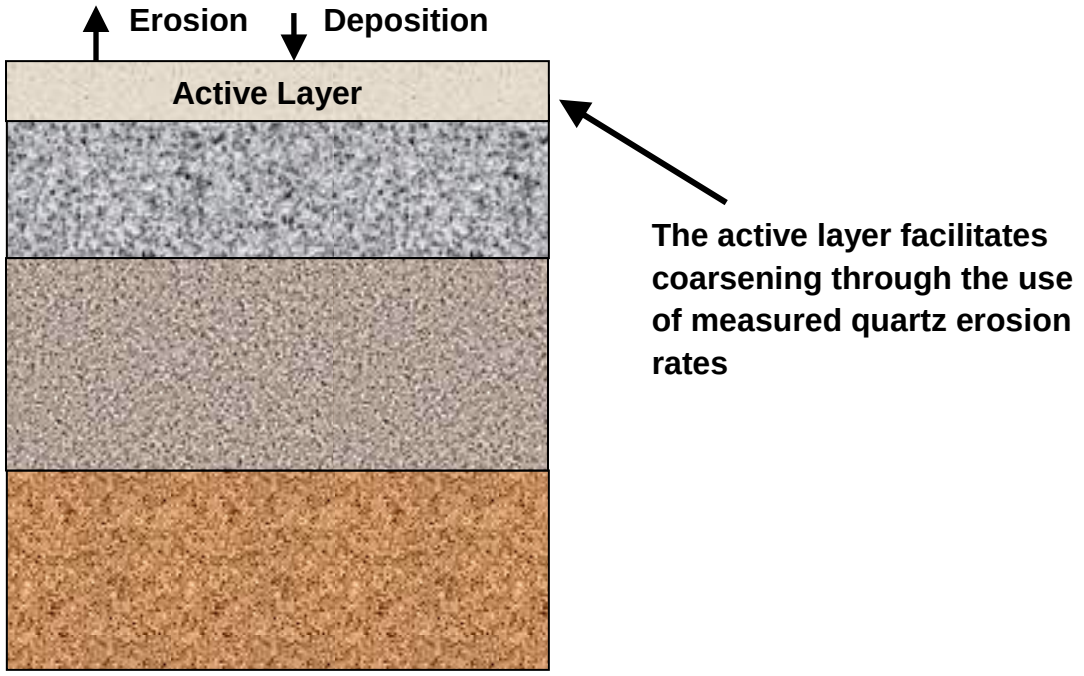

Figure 2-3 Schematic of Active Layer Used in SEDZLJ

primary consolidation range from empirical equations that approximate the increases in bed bulk density and critical shear stress for resuspension due to porewater expulsion (Sanford, 2008) to finite difference models that solve the non-linear finite strain consolidation equation that governs primary consolidation in saturated porous media (*e.g.*, Arega and Hayter, 2008). An empirical-based consolidation algorithm is included in SEDZLJ. Simulation of consolidation requires performing specialized consolidation experiments to quantify the rate of consolidation. These experiments were not conducted as a component of this modeling study, and as such, consolidation was not simulated.

- SEDZLJ contains a morphologic algorithm that, when enabled by the model user, will adjust the bed elevation of grid cells to account for erosion and deposition of sediment. Changes in grid cells' bed elevations are used by the hydrodynamic model in LTFATE during the next time step to update the flow field.

- SEDZLJ accounts for the effect of bed slope on erosion rates and bedload transport. The bed slopes in both the x- and y-directions are calculated, and scaling factors are applied to the bed shear stress, erosion rate, and bedload transport equations. A maximum adverse bed slope is specified that prevents bedload transport from occurring up too steep a slope.

- The approach used by Van Rijn (1984) to simulate bedload transport is used in SEDZLJ. The 2D mass balance equation for the concentration of sediment moving as bedload is given by:

$$\frac{\partial(\delta_{bl} C_b)}{\partial t} = \frac{\partial q_{b,x}}{\partial x} + \frac{\partial q_{b,y}}{\partial y} + Q_b \qquad (2\text{-}5)$$

where δ_{bl} = bedload thickness; C_b = bedload concentration; $q_{b,x}$ and $q_{b,y}$ = x- and y-components of the bedload sediment flux, respectively; and Q_b = sediment flux from the bed. Van Rijn (1984) gives the following equation for the thickness of the layer in which bedload is occurring:

$$\delta_{bl} = 0.3 d d_*^{0.7} (\Delta\tau)^{0.5} \qquad (2\text{-}6)$$

where $\Delta\tau = \tau_b - \tau_{ce}$; τ_b = bed shear stress, and τ_{ce} = critical shear stress for erosion.

The bedload fluxes in the x- and y-directions are given by:

$q_{b,x} = \delta_{bl} u_{b,x} C_b$

$q_{b,y} = \delta_{bl} u_{b,y} C_b$

where $u_{b,x}$ and $u_{b,y}$ = x- and y-components of the bedload velocity, u_b, which van Rijn (1984) gave as

$$u_b = 1.5 \tau_*^{0.6} \left[\left(\frac{\rho_s}{\rho_w} - 1 \right) g d \right]^{0.5} \qquad (2\text{-}7)$$

with the dimensionless parameter τ_* given as

$$\tau_* = \frac{\tau_b - \tau_{ce}}{\tau_{ce}} \qquad (2\text{-}8)$$

The x- and y-components of u_b are calculated as the ratios of u and v to the total hydrodynamic velocity times u_b, respectively.

The sediment flux from the bed due to bedload, Q_b, is equal to

$$Q_b = E_b - D_b \quad (2\text{-}9)$$

where E_b is the erosion of sediment into bedload, and D_b is the deposition of sediment from bedload onto the sediment bed.

Contaminant Transport Model

The contaminant transport model in LTFATE is a three-phase partitioning model in EFDC that is used to simulate the transport of one or more contaminants during a single model simulation. It can be used to simulate the transport of organic chemicals (*e.g.*, PCBs), metalloids (*e.g.*, Arsenic), and metals (*e.g.*, Copper, Zinc). Use of a three-phase partitioning model explicitly accounts for the freely dissolved contaminant, the phase (or fraction) that is bioavailable via waterborne exposures, and is a better representation of the bioavailable fraction than a two-phase partitioning model as is used in other contaminant fate models such as HSCTM-2D (Hayter *et al.*, 1999). Since the model simulation described in this report is of PCB transport in New Bedford Harbor, the remainder of this chapter concentrates on the specifics of representing the transport and fate of a hydrophobic organic chemical.

Nonionic organic chemicals, such as PCBs, can be distributed in various phases in aquatic ecosystems. One representation of this distribution is that the chemicals are partitioned among the particulate organic matter (POM), the dissolved organic matter (DOM), and also the freely dissolved form (USEPA, 1998). The degree of partitioning, as characterized by the dissolved, *i.e.*, free plus dissolved organic carbon (DOC) complexed, and particulate fractions, f_d and f_p, respectively, is an important parameter that controls the fate of chemicals. This is because the transport of both the dissolved and particulate chemical phases is related to this phase distribution (USEPA, 1998).

In EFDC it is assumed that the total PCB (tPCB) load is distributed among the three phases, *i.e.*, freely dissolved PCBs, DOC-complexed PCBs, and sorbed or particulate organic carbon (POC) bound PCBs, and that the PCBs are in equilibrium across all these phases. While the actual time it takes to reach complete equilibrium can be very long, it is often assumed that equilibrium

between the dissolved and particulate phases occurs over a time scale of only a few hours to a day (Jepsen *et al.*, 1995). This is the basis of the equilibrium partitioning assumption that is commonly used in contaminant transport modeling. Transport processes that affect the fate of PCBs, and that are represented in the EFDC model, are discussed next. The transport equations solved by the contaminant transport model are given in Appendix A.

Both dissolved and particulate-bound PCBs are advected by the predominately tide-driven flow in Buzzards Bay and New Bedford Harbor. Adsorbed PCBs are transported with sediment particles as the latter are moved as a result of bed load, suspended load, deposition and resuspension as simulated by the sediment transport model. There is also a vertical diffusive flux of PCBs that occurs in proportion to the gradient between the dissolved concentration in the water column and that in the pore water. This diffusive flux is due to molecular diffusion and bioturbation. In addition, advective transport due to groundwater flow may also result in a significant mass flux of other, less hydrophobic contaminants. Another PCB transport process, volatilization, is also simulated in EFDC. Volatilization is the loss of freely dissolved chemicals via transfer from the water column to the atmosphere.

The following change was made to the contaminant transport routine for this modeling study. A minimum contaminant concentration in the sediment bed can be set for each contaminant modeled by the model user. The value of the minimum concentration should correspond to the background concentration of that contaminant in the water body being modeled. This option prevents the simulated concentration from decreasing below the background value, and thus results in a more realistic representation of actual conditions, in this case at NBH. A value of 5 ppb was used for the background concentration in this modeling study. During the OU3 Remedial Investigation (RI), an average concentration of 8.4 ppb was found at 13 reference locations sampled in the Outer Harbor. The concentration at one of the locations (80 ppb) was more than 16 times higher than that of the next largest value (4.8 ppb). Excluding the 80 ppb value, the average concentration at the other 12 locations was 1.9 ppb. As such, the value of 5 ppb, which lies between these two average concentrations, was a reasonable value to use for this parameter.

3 Field Data Collection and Analyses

Objectives

The objectives of the field experiments performed by ERDC at NBH were to: 1) provide hydrodynamic data (tides and currents) for calibration and/or validation of the hydrodynamic model, and 2) provide data to parameterize cohesive sediment processes (erosion and settling) in SEDZLJ. Field experiments were conducted 3-14 November 2008 by the ERDC Coastal and Hydraulics Laboratory (CHL), with logistical and vessel support provided by the USEPA ORD Narragansett Laboratory. Hydrodynamic data measured included two tide gages with temperature and salinity record, Acoustic Doppler Current Profiler (ADCP) surveys, and Conductivity, Temperature, and Depth (CTD) profiles within the harbor. Physical cohesive sediment processes of settling and erosion were defined with the Particle Imaging Camera System (PICS) (for settling velocity) and SEDFLUME (for cohesive sediment erosion). This chapter describes the experimental and analyses methods used in this study and provides the physical process descriptions that were used to parameterize the hydrodynamic and sediment transport models.

Cohesive Sediment Transport Processes

The sediments of interest at New Bedford Harbor are generally classified as cohesive sediment. Non-cohesive sediment (sand and gravel) erosion and settling can be generally estimated as a function of grain size distribution and mineral density. Cohesive sediment transport processes are dominated by other factors. Cohesive sediments are generally a mixture of sand, silt, and clay sized particles and usually a relatively small fraction of organic matter.

Erosion

A general definition for cohesive sediment is sediment for which the erosion rate cannot be estimated by standard sand transport methods. In these cases, cohesive forces are equivalent to or are greater than the gravitational forces that dominate sand transport. Cohesive sediment erosion characteristics are highly dependent upon factors such as particle size distribution, particle coatings, fine sediment mineralogy, organic content, bulk density, gas content, pore-water chemistry, and biological activity. Erosion rate and critical shear stress for

erosion can vary significantly with small changes in only one of these inter-dependent parameters. It has been demonstrated that critical stress and erosion rates for cohesive sediment can vary over several orders of magnitude for sediments with only slightly differing properties. Thus, the influence of cohesion on sediment processes is significant. While it is understood which properties most significantly influence erosion, there are no quantitative methods available to determine erosion rates from cohesive sediment properties. Therefore, due to the wide range of influencing parameters, erosion characteristics of cohesive sediments are determined by site-specific measurements of erosion.

Several flumes are available to parameterize site-specific cohesive sediment erosion algorithms. Most of these devices operate over a range of low shear stress (<2 Pa) and are consequently capable of measuring surface sediment erosion. SEDFLUME is an erosion device with capability to impose bed stresses in the range of 0.1 to 12 Pa and measures erosion rates from sediment cores taken from the field (for in-situ or stratified bed conditions) or prepared in the laboratory (for assessing disturbed sediments such as dredged material). SEDFLUME is designed to quantify erosion rates for surface and sub-surface sediments. These measurements permit description of the vertical variation of erosion rate within the bed. It should be noted that even if sediments are well mixed, cohesive sediment bed erosion will change with depth due to the influence of consolidation (bed density) on erosion rate. Erosion rate can vary by several orders of magnitude between surficial sediments and sediment buried less than 30 cm below the surface. SEDFLUME was selected to quantify erosion rate and erosion rate variation with depth (density) for this study.

Settling Velocity

Settling of cohesive sediments is also governed by processes that are difficult to estimate from fundamental sediment properties. Cohesive sediments are known to aggregate (or stick together) to form flocs, composed of fine-grained sediments and organic matter. Floc size is governed by the balance between aggregation and disaggregation processes. Aggregation is influenced by processes causing particles to collide and the efficiency with which these particle stick together. Particle collisions are influenced by turbulence, differential settling, and Brownian motion; whereas aggregation efficiency is largely associated with surface characteristics of the particles (mineralogy, surface coatings, biological polymers, and water chemistry). Disaggregation is influenced by turbulent shear and interparticle bonding strength of the floc.

Flocs formed in suspension have large porosities, and a large fraction of floc volume is occupied by water. After flocs have settled to the sediment bed, the weight of overlying sediments collapses the floc structure and expels pore water. This process, known as consolidation, results in increased bed density and increased interparticle bond strength. If the consolidated bed is later exposed by erosion, a portion of the eroded sediment may not be completely disaggregated and instead is suspended as small fragments of the consolidated bed. The bed aggregates are different from the flocs formed in the water column as they have larger particle densities and have stronger interparticle bonds.

Understanding of how these various factors impact floc growth and settling velocity is incomplete. As is the case with cohesive sediment erosion, site-specific experiments are required to determine cohesive sediment settling velocities. This study employed a digital video settling column to measure settling velocities.

Methods and Results

The field experiments consisted of in-situ and field laboratory components. The in-situ experiments consisted of: a) short-term, point measurements of tide, temperature, and salinity, b) vessel-mounted, roving surveys of currents, c) vertical profiles of temperature and salinity, d) settling velocity measurements of suspended particulates, and e) collection of sediment cores for field laboratory analysis. The field laboratory experiments included: a) physical sub-sampling of sediment cores, b) quantification of cohesive sediment erosion properties, and c) settling velocity measurements on material eroded from sediment cores. Each of these experiments and the resulting data are described in greater detail below. Samples and data collected from the harbor are referenced to stations as indicated in Figure 3-1. Actual sampling positions are provided with the tabulated data, but are generally within 100 m of the indicated positions in this figure.

Tide

Tide data were obtained from existing gages maintained by the U.S. Army Engineer District, New England (NAE) at the New Bedford Harbor hurricane barrier. Additionally, two YSI-6000 multi-parameter instruments were deployed at the SEDFLUME Lab Site (T1) and Slocum St bridge (T2) to record water level, water temperature, and salinity (Figure 3-1). The YSI-6000 recorded water level, temperature, and salinity at 5-minute intervals during the study period. The

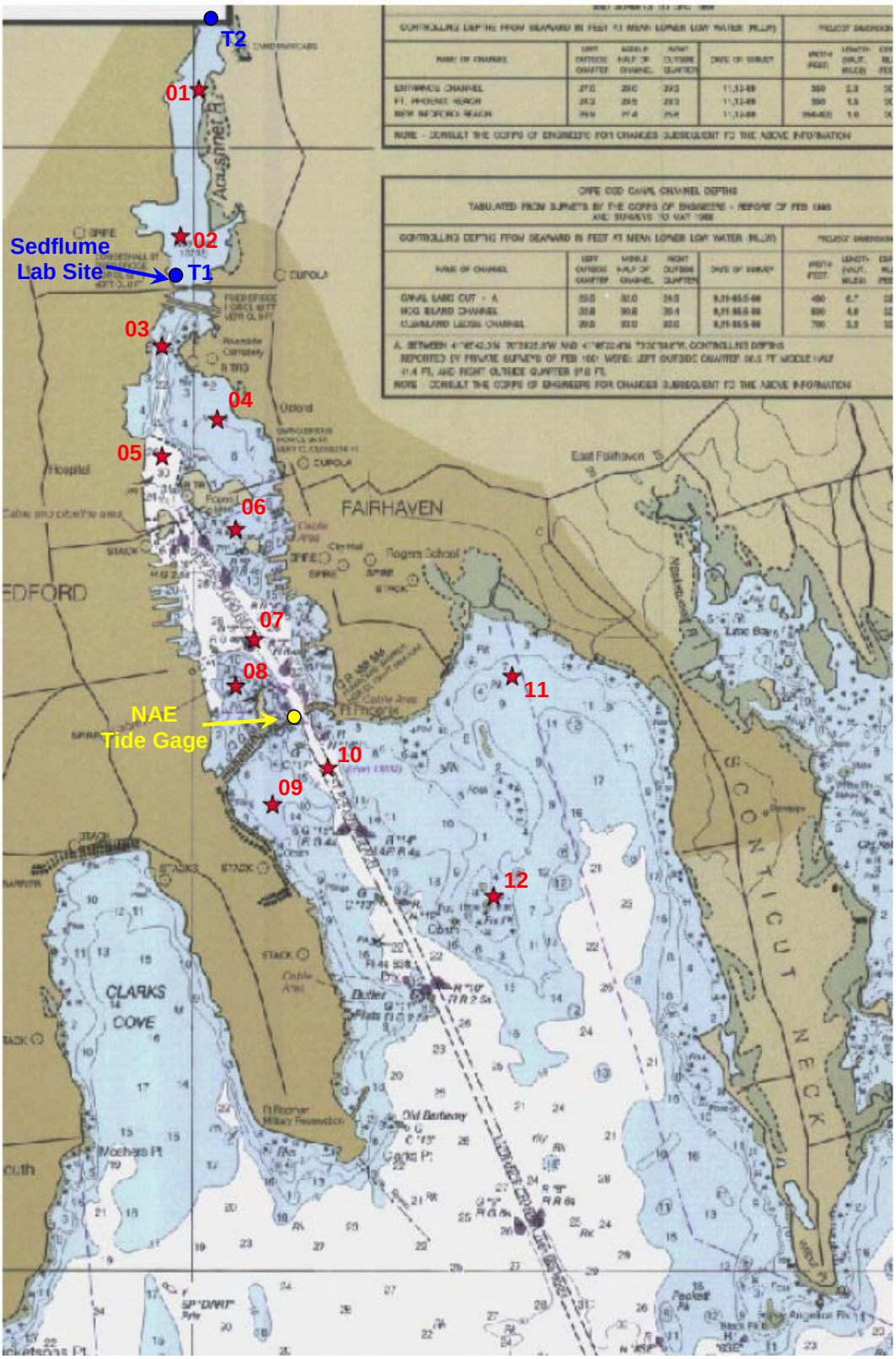

Figure 3-1. New Bedford Harbor sampling stations. Numbered stations associated with stars indicate sampling stations, circles indicate fixed tide stations. NOAA navigation chart 13230 (6/1999).

recorded tide at each tide station is presented in Figure 3-2. Tide gages T1 and T2 were not surveyed to vertical control, and the vertical datum presented in Figure 3-2 is the Mean Tide Level (MTL) over the period of record. The tide range at gage T1 is essentially the same as at the hurricane barrier, but the tide range at gage T2 is on the order of 0.1 to 0.2 m less.

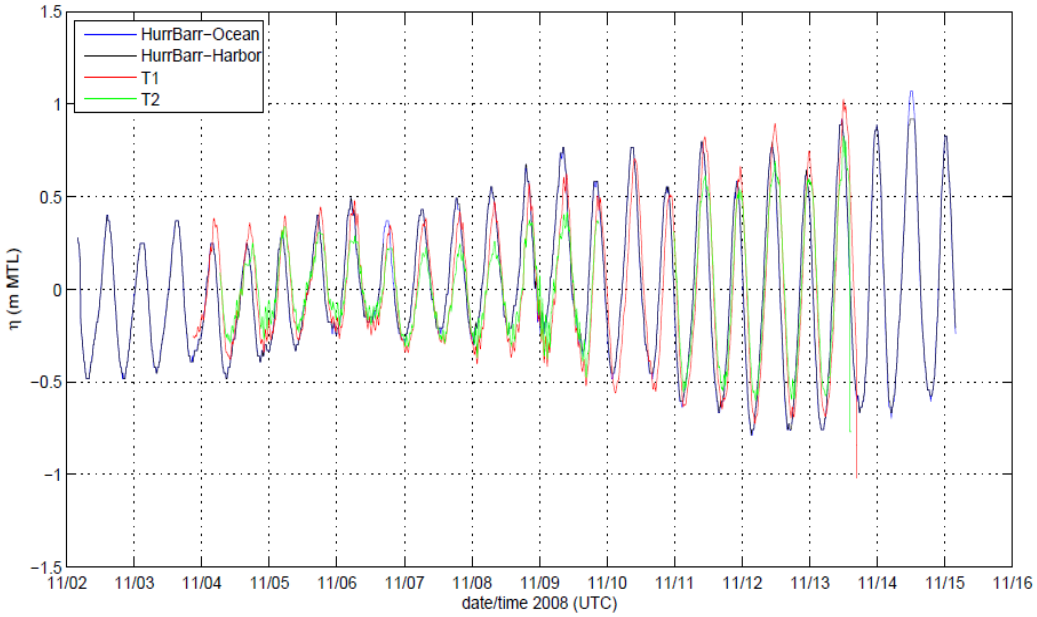

Figure 3-2. Tide record during study period.

Salinity and Temperature

Salinity and temperature were recorded at tide stations T1 and T2 and also during casts at the 12 stations (Figure 3-1) from 04-06 November 2008. Tide, temperature, and salinity recorded at stations T1 and T2 are presented in Figure 3-3. Gage T2 stopped recording for approximately 26 hours on 09 November, for unknown reasons.

Conductivity, Temperature, and Depth (CTD) casts were performed at Stations 03 through 12 for both flood and ebb conditions on 04-06 November 2008. (Measurements were not possible from Stations 01 and 02 due to draft limitations of the survey vessel.) An example of temperature and salinity profiles is provided in Figure 3-4. Temperature and salinity profiles were generally well-mixed at depths deeper than 2 m, but a thin surface layer was often observed that was both warmer and fresher than the underlying water. Temperature and salinity profiles for all stations are provided in Appendix B.

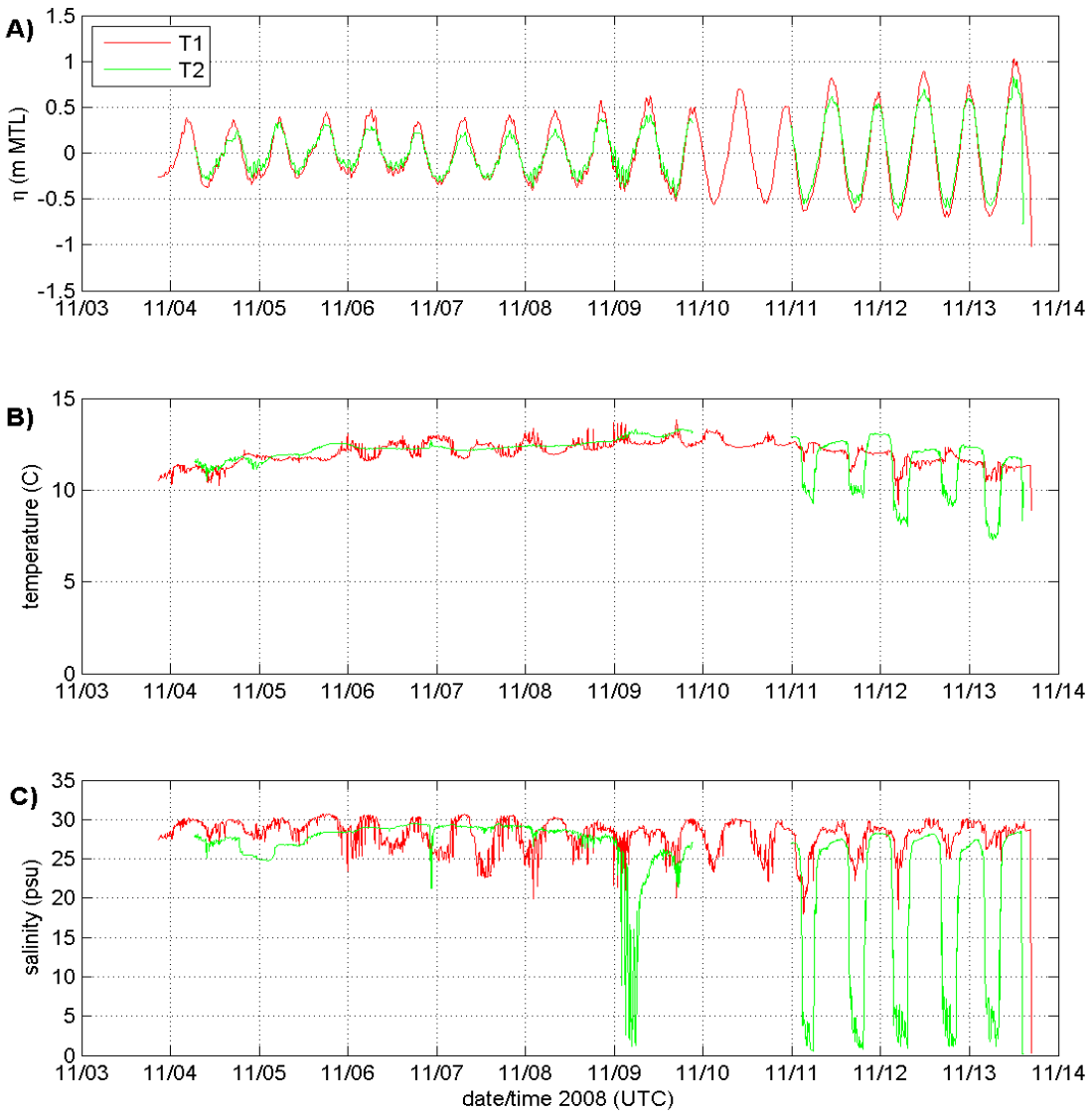

Figure 3-3. Tide, temperature, and salinity recorded at Stations T1 and T2.

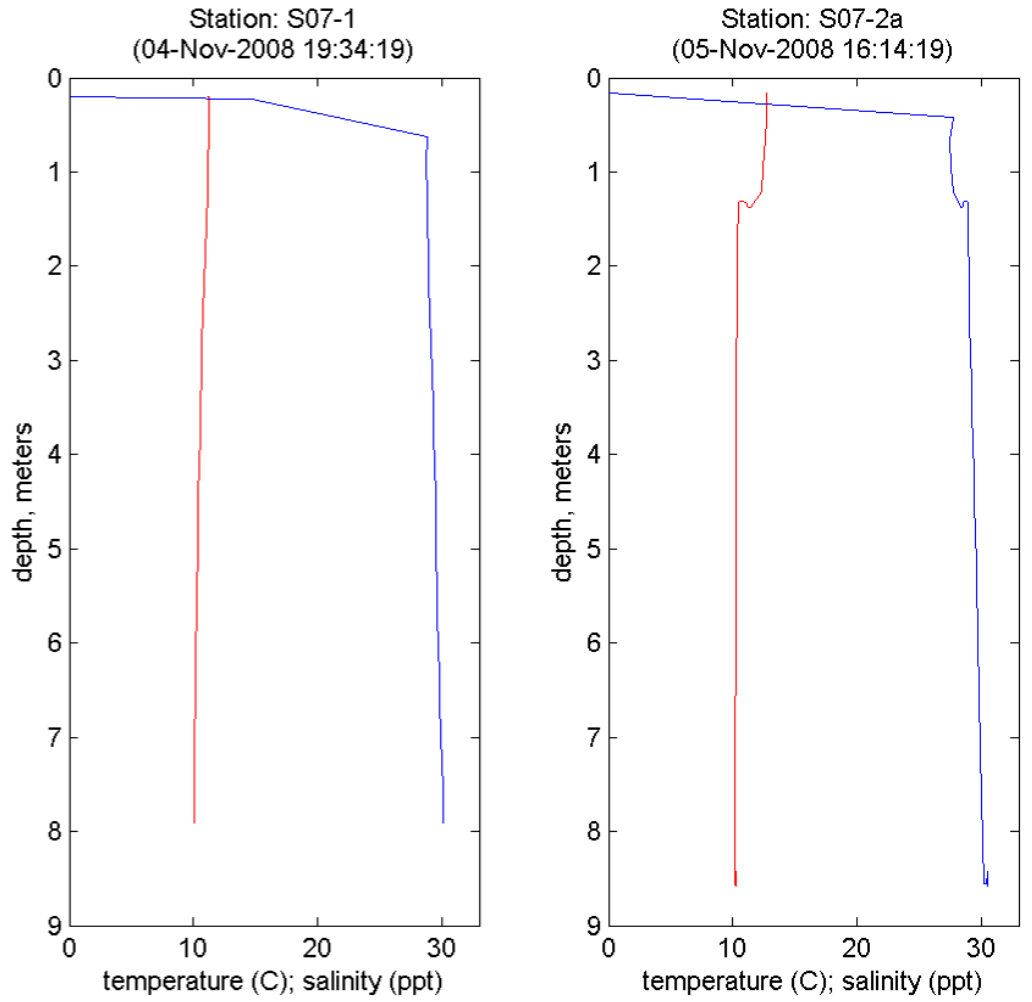

Figure 3-4. Temperature (red) and salinity (blue) profiles at Station 07 for two tidal conditions. Depth is indicated from the water surface.

ADCP Surveys

Vessel-mounted Acoustic Doppler Current Profiler (ADCP) surveys were conducted while traveling between stations during 04-06 November. A 1200 kHz RDI ADCP was configured with 0.25-m bin spacing. For this type of application, vessel speed is customarily logged with kinematic GPS and bottom tracking (from acoustic reflections from the bed). In this experiment, technical issues prevented logging of the GPS position to the data stream. GPS position at the starting and ending point of each transect segment was manually logged, and positioning

within each survey segment was determined by dead reckoning (from the bottom-track velocity) and distribution of errors between the known starting and ending positions. Vessel tracks for November 05 are presented in Figure 3-5.

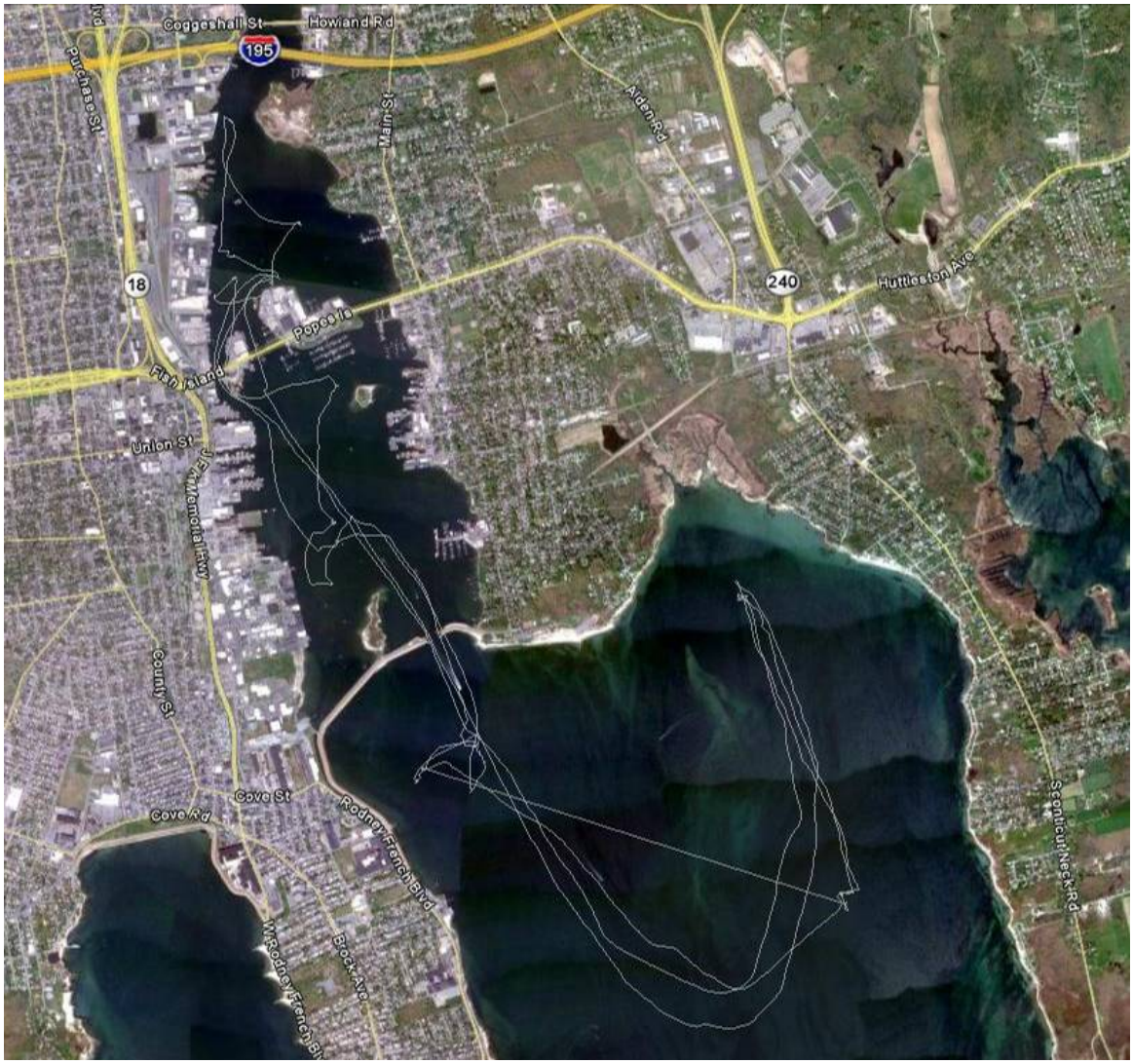

Figure 3-5. Vessel track for roving ADCP surveys of 05 Nov 2008. Track segments run between settling velocity sampling stations in lower and outer New Bedford Harbor (Figure 3-1).

Figure 3-6. Vessel track for roving ADCP surveys of 05 Nov 2008. Track segments run between settling velocity sampling stations in lower and outer New Bedford Harbor (Figure 3-1). Velocity vectors presented are depth-averaged.

Velocities from the ADCP were depth-averaged and provided for model comparison. An example segment of depth-averaged velocities from the 05 November 2008 survey is provided in Figure 3-6. This survey segment was collected during a flooding tide near Popes Island. During these measurements the suspended sediment concentrations (SSC) were very low (mostly less than 10 mg/L), so it was not possible to develop a correlation between SSC and ADCP signal.

Sediment Samples

Sediment cores for SEDFLUME erosion experiments were collected with gravity and push coring methods. Cores were collected by push coring in water depths less than approximately 3-4 m, and gravity coring at deeper locations. Cores were collected at 11 of the 12 sites indicated in Figure 3-1 (the sediment bed at Site 12 was too rocky to collect a core). Photographs of the gravity and push coring devices are shown in Figures 3-7A and 3-7B. Each device is designed to accept a

A) Gravity Corer

B) Push Corer

C) Plungers with Bentonite slurry

D) Core with plunger inserted.

Figure 3-7. Coring devices and core collection.

10-cm (4-inch) outer diameter polycarbonate coring sleeve, which is later inserted into SEDFLUME. Each coring device is equipped with a flapper-style check valve to ensure core recovery in soft sediments. Push coring is achieved by pressing the coring device into the sediment bed and lifting the core to the surface. Gravity coring is achieved by lowering the 32-kg gravity corer to bed, where the coring device will penetrate the bed under its own weight. If this is insufficient to obtain a suitable length of sample, the gravity corer is raised above the bed in varying increments and allowed to fall to the bed, utilizing momentum to achieve greater depth of penetration.

Upon sample recovery, a plunger with Bentonite paste (for sealing and lubrication) is inserted into the bottom of the recovered core (Figures 3-7C and 3-7D). Target recovery for this study was 15 to 30 cm of sediment bed, and actual sediment recovery ranged from 15 to 45 cm. Cores were transported by vessel to the SEDFLUME laboratory site, and stored in a drum filled with site water until the erosion experiment.

Cohesive Sediment Erosion

Sedflume is a field- or laboratory-deployable flume for quantifying cohesive sediment erosion. The USACE-developed SEDFLUME is a derivative of the flume developed by researchers at the University of California at Santa Barbara (McNeil *et al.*, 1996). The flume includes an 80 cm long inlet section (Figure 3-8) with cross-sectional area of 2 × 10 cm for uniform, fully developed, smooth-turbulent flow. The inlet section is followed by a 15 cm long test section with a 10 × 15 cm open bottom (the open bottom can accept cores with rectangular cross-section (10 × 15 cm) or circular cross-section (10 cm diameter)). Coring tubes and flume test section, inlet section, and exit sections are constructed of clear polycarbonate materials to permit observation of sediment-water interactions during the course of erosion experiments. The flume includes a port over the test section to provide access to the core surface for physical sampling. The flume accepts sediment cores up to 80 cm in length.

Erosion experiments

Prior to the erosion experiment, descriptions of the core are recorded, including length, condition of the core surface, biological activity, and any visual evidence of layering. Cores are inserted into the testing section of SEDFLUME and a screw jack is used to advance the plunger such that the core surface becomes flush with the bottom wall of the flume. Flow is directed over the sample by diverting flow from a 3-hp pump, through a 5-cm inner diameter stiff hose, into the flume. The flow through the flume produces shear stress on the surface of the core.

(Numerical, experimental, and analytical analyses have been performed to relate flow rate to bottom shear stress.) Erosion of the surface sediment is initiated as the shear stress is increased beyond the critical stress for erosion, τ_{cr}. As sediment erodes from the core surface, the operator advances the screw jack to maintain the sediment surface flush with the bottom wall of the erosion flume. Figure 3-8 includes a photograph of the flume, a close-up photograph of the test section, and a table of flow rate/shear stress relationships.

Erosion rate is determined from the displacement of the core surface over the elapsed time of the experiment. Generally, erosion experiments are performed in repeating sequences of increasing shear stress. Operator experience permits sequencing of erosion tests to allow greater vertical resolution of shear stress/erosion rate data where required. The duration of each erosion experiment at a specified shear stress is dependent on the rate of erosion and generally is between 0.25 and 15 minutes. Shear stresses that induce no measurable erosion are also recorded. The range of shear stress for each cycle is determined by the operator based on the previous erosion sequences and erosion behavior during the ongoing sequence.

Sediment bulk properties

Physical samples for bulk sediment property measurements are taken at approximately 3-5 cm intervals during erosion experiments, generally at the end of each shear stress cycle. Physical samples are collected by draining the flume channel, opening the port over the test section, and extracting a sample from the

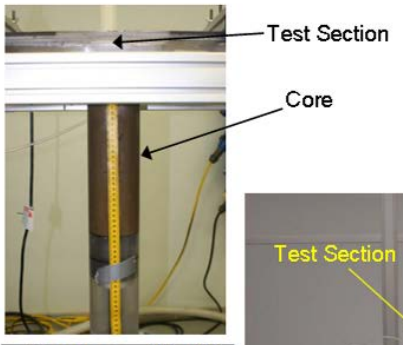

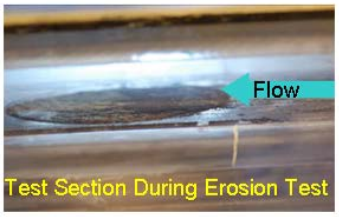

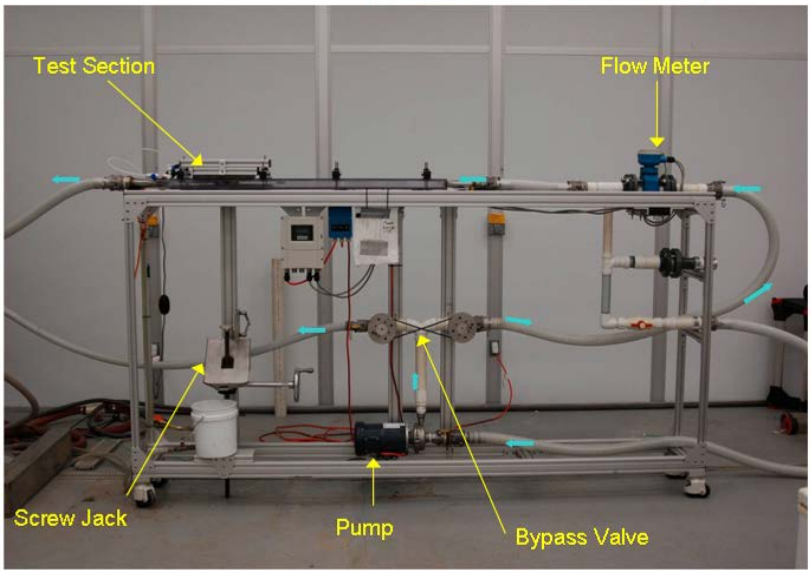

Shear stress t (Pa)	Flow Rate (GPM)
0.1	6.1
0.2	9.1
0.4	13.5
0.6	17.0
0.8	20.1
1.2	25.3
1.6	29.8
2.4	37.4
3.2	44.0
4	49.9
5	56.6
6.4	65.0
8	73.7
10	83.5
12	92.5
13	96.7
14	100.8

Figure 3-8. Sedflume erosion flume (lower right). Core inserted into test section (upper left). Core surface flush with bottom of flume (upper right). Table of shear stresses associated with channel flow rates (lower left).

sediment bed. Properties measured include bulk density and grain-size distribution, and separate samples were collected from the core surface for these analyses. These properties strongly influence erosion; therefore, understanding their variation with depth is important in interpreting the erosion data.

Bulk Density: Bulk sediment density of physical samples is determined by a wet-dry weight analysis. Physical samples are extracted from the saturated core surface and placed in a pre-weighed aluminum tray. Sample weight is recorded immediately after collection and again after a minimum of 12 hours in a 90° C (194° F) drying oven. Wet weight of the sample was calculated by subtracting tare weight from the weight of the sample. The dry weight of the sample was calculated as the tare weight subtracted from the weight after drying. The water content w is then given by

$$w = \left(\frac{m_w - m_d}{m_d} \right) \tag{3-1}$$

where m_w and m_d are the wet and dry weights, respectively. A volume of saturated sediment, V, consists of both solid particles and water and can be written as

$$V = V_s + V_w \tag{3-2}$$

where V_s is the volume of solid particles and V_w is the volume of water. If the sediment particles and water have density ρ_s and ρ_w, respectively, the water content of the sediment can be written as

$$w = \frac{\rho_w V_w}{\rho_s V_s} \tag{3-3}$$

A mass balance of the volume of sediment gives

$$\rho V = \rho_s V_s + \rho_w V_w \tag{3-4}$$

where ρ is the bulk density of the sediment sample.

Equations 3-1 through 3-4 are used to derive an explicit expression for the bulk density of the sediment sample, ρ, as a function of the water content, w, and the densities of the sediment particles and water. This equation is

$$\rho = \rho_s + \frac{w\rho_s \left(\rho_w - \rho_s \right)}{\rho_w + w\rho_s} \tag{3-5}$$

For the purpose of these calculations, ρ_s = 2.65 g·cm^{-3} and ρ_w is calculated for measured pore water at core temperature.

Particle-Size Distribution: Samples collected during erosion experiments were transported to the Sediment Transport Processes Lab at ERDC for grain size analysis. A Beckman Coulter LS-120 laser particle-sizer was used to measure the particle-size distributions in sub-samples collected from the cores. The LS-120 measures particle size over the range 0.4 to 900 μm. The sample was added to a small volume of water (approximately 150 mL) and sonicated using a high-powered laboratory sonicator to disperse the sediment. The dispersed solution was placed in the particle-sizer fluid module. The sample is pumped and recirculated through the optical module. The optical module includes a spatial filter assembly containing a laser diode and laser beam collimator. The diffraction detector assembly contains a custom photo-detector array that is used for the measurement of light scattering by the suspended particles. The distribution of grain sizes and median grain sizes is derived from this light scattering measurement. Organic material was not oxidized before grain size analysis was performed; therefore grain size distributions include organic material. The bulk density and particle-size analyses results are presented in Appendix C.

Erosion thresholds and rates

Cohesive sediment transport algorithms rely on parameterization of the relative effects of first-order parameters such as applied shear stress and bed density to describe cohesive sediment erosion rates. As described previously, cohesive sediment erosion is influenced by many other parameters, which are generally included in the parameterization through empirical coefficients. The SEDFLUME erosion data were analyzed to assess erosion rate variation associated with the various bed properties. Given the variable bed composition and layering of cores, no unified relationship was found between erosion rate, bed density, and applied shear stress. The bed density term was removed from the best-fit algorithm, and reasonable trends emerged relating erosion rate to applied shear stress. The influence of bed density and sediment composition on erosion rate was included by grouping the erosion data by depth beneath the sediment surface and by segments of cores with similar erosion characteristics. The resulting grouping of erosion data resulted in three bed layers: upper (0 to 4 cm), middle (4 to 14 cm), and lower (14 to 35 cm below the sediment surface). Within each depth grouping, 3-4 different erosion responses were determined, resulting in data associations

for each core as presented in Table 3-1. For instance, the surface portion of Core 03-01 is associated with group U1, and the erosion data for this portion of the core is similar to the erosion responses of Cores 04-01, 04-02, 05-02, and 06-02.

Erosion relationships were determined by linear-transformed, least-squares regression to

$$E = A\tau^{n} \tag{3-6}$$

where E is erosion rate (cm/s), τ is bed stress (in $N \cdot m^{-2}$ or Pa), and A and n are empirical coefficients. The best fit to the erosion data for group M1 is provided in Figure 3-9. Best fits for all groups are provided in Appendix D. Critical stress for erosion (τ_{cr}) is defined as the applied bed stress at which a specified rate of erosion occurs. The critical erosion rate assigned here is 10^{-4} $cm \cdot s^{-1}$. Critical stress for erosion is determined by applying the critical erosion rate and the empirical coefficients determined for each group to Equation 3-6 and solving for critical bed stress. The resulting erosion rate algorithm for the numerical model is:

$$\begin{aligned} E &= A\tau^{n} \quad (\tau \geq \tau_{cr}) \\ E &= 0 \quad (\tau < \tau_{cr}) \end{aligned} \tag{3-7}$$

Empirical terms and critical bed shears for all sediments are given in Table 3-2.

Table 3-1 Sediment Grouping by Erosion Characteristics

Core ID	Upper (0 to 4 cm)	Middle (4 to 14 cm)	Lower (14 to 35 cm)
01-01	U3	M2	L1
02-01	-	M2	L2
02-02	U2	M3	L3
03-01	U1	M3	L3
04-01	U1	M2	L1
04-02	U1	M1	L2
05-01	U2	M1	L1
05-02	U1	M1	-
06-01	U2	M4	L3
06-02	U1	-	-
07-01	U3	M2	L1
08-01	U2	M1	-
09-01	U4	M1	L3

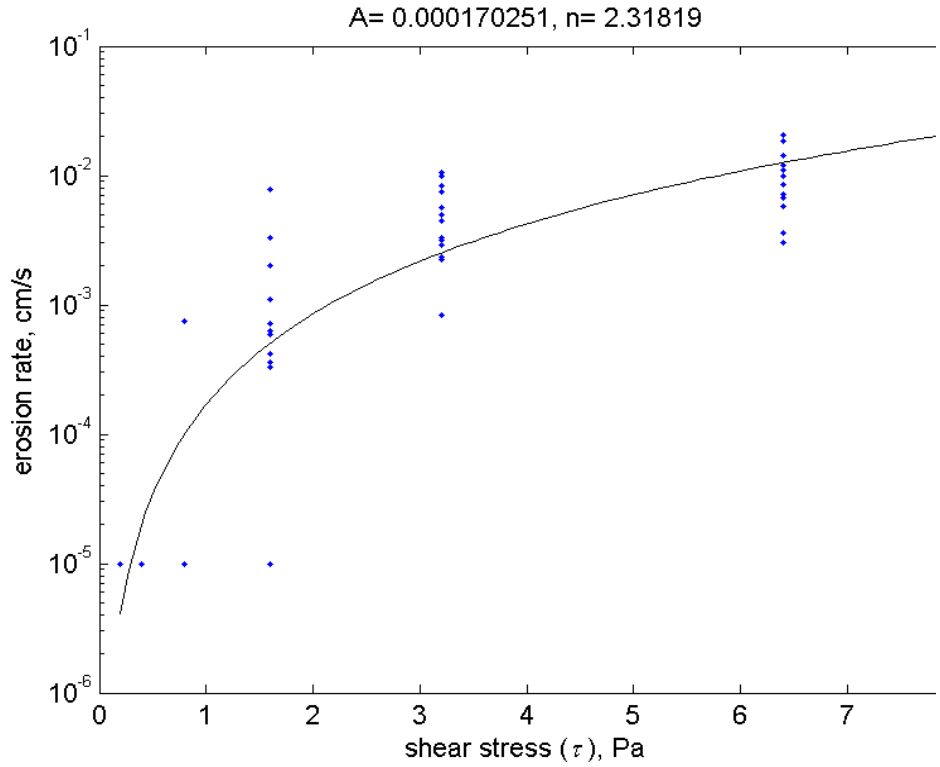

Figure 3-9 Erosion data and best-fit relationship ($E = A\tau^n$) for sediment group M1.

Table 3-2 Erosion parameters for Eq. 3-7 for each sediment group

Group	τ_{cr} (Pa)	A	n
U1	0.22	1.73×10^{-3}	1.88
U2	0.36	9.55×10^{-5}	2.23
U3	0.14	8.65×10^{-3}	2.27
U4	0.13	7.21×10^{-3}	2.09
M1	0.79	1.70×10^{-4}	2.32
M2	0.32	1.05×10^{-3}	2.08
M3	1.55	3.96×10^{-5}	2.11
M4	1.25	4.85×10^{-5}	3.27
L1	0.70	2.10×10^{-4}	2.06
L2	1.77	2.14×10^{-5}	2.69
L3	2.56	4.69×10^{-6}	3.25

Settling Velocity

The Particle Imaging Camera System (PICS) is an ERDC-developed system for *in-situ* and laboratory measurements of cohesive sediment settling velocities. PICS collects digital video of particle settling within a small settling column and can be deployed in the water column or in a laboratory setting. Sample collection, optical and lighting design, and image acquisition were designed to produce high-quality, *in-situ* image sequences. PICS consists of a 1-m long, 5-cm inner diameter settling column with a mega-pixel digital video camera and strobed LED lighting (Figure 3-10). The settling column is equipped with two pneumatically controlled ball valves at the column ends which permit sample capture and a third pneumatic actuator for rotating the column from horizontal to vertical orientation for image acquisition. Image sequences collected by PICS are analyzed with automated particle tracking software to produce size, settling velocity, and density (inferred) distributions of particles suspended at the sampling location. Additional instrumentation may be deployed with PICS, such as: Laser in-Situ Scattering and Transmissometry (LISST-floc), Conductivity-Temperature-Depth (CTD), Acoustic Doppler Velocimeter (ADV), and pump sampler. For the present study, PICS was deployed with a YSI-6000 CTD. Additional details of PICS, including system configuration and measurement uncertainty are provided by Smith and Friedrichs (2010).

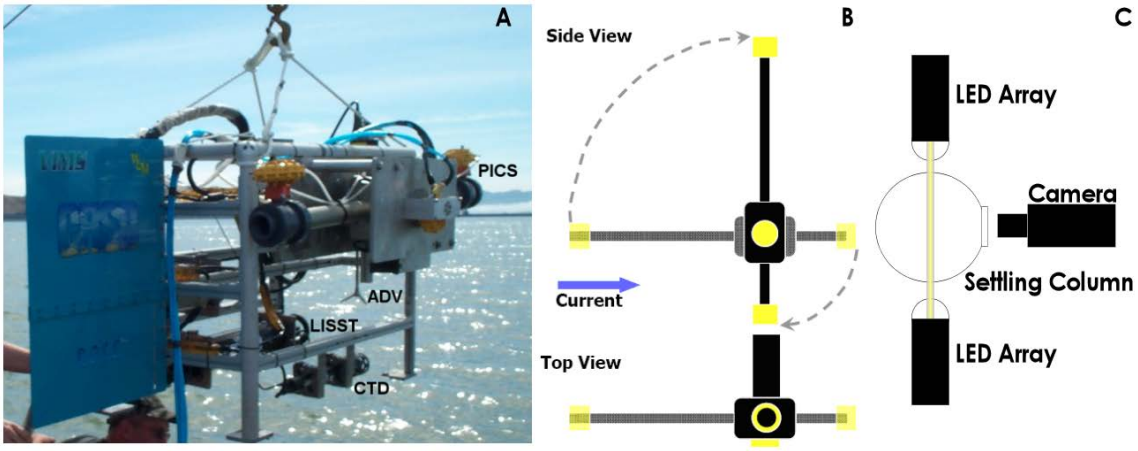

Figure 3-10. A) Instrumentation frame indicating positioning of PICS with optional deployment of additional instrumentation such as ADV, LISST, and CTD B) Schematic of settling column indicating horizontal and vertical orientations, C) Schematic of camera, settling column cross section, and LED lighting.

Image analysis

Image analysis is accomplished with a combination of Particle Tracking Velocimetry (PTV) and Particle Image Velocimetry (PIV) methods. PTV is applied to particles larger than 30 μm and results in estimates of large particle motion relative to the focal plane. PIV is applied to particles smaller than 20 μm and the motion of these small particles is treated as a surrogate for fluid motions within the column relative to the focal plane. Vector subtraction of the fluid and particle velocities results in individual particle settling velocity (relative to the suspending fluid). Additional details of the image processing and analysis methods are provided in Smith and Friedrichs (2010b).

Particle density and aggregation state

Image analysis results in simultaneous measurement of particle size and settling velocity. Using these two measured parameters permits estimation of individual particle densities. This is accomplished by solving the settling balance for spherical particles with the Schiller-Naumann (1933) (Graf, 1971) drag approximation:

$$w_s = \frac{gd^2}{18\mu}\frac{\left(\rho_p - \rho\right)}{\left(1+0.15Re_p^{0.687}\right)} \tag{3-8}$$

for particle density:

$$\rho_p = \rho + \frac{18\mu w_s}{gd^2}\left(1+0.15Re_p^{0.687}\right) \tag{3-9}$$

where w_s is particle settling velocity, d is particle diameter, μ is fluid dynamic viscosity, ρ_p is particle density, ρ is fluid density, Re_p is particle Reynolds Number ($Re_p = w_s d/\nu$), and ν is fluid kinematic viscosity. The Schiller-Naumann drag approximation essentially extends Stokes Law (which is limited to $Re_p \leq 0.5$) to $Re_p < 800$.

The estimated individual particle densities are used to classify particles by their aggregation state. Aggregation states include primary particles (individual mineral grains), bed aggregates (aggregations with density approximating that of the sediment bed), and flocs (lower-density aggregations formed in the water column). Flocs are associated with density between 1010-1200 kg m^{-3} (excess density: 0-180 kg m^{-3}), bed aggregates: 1200-1800 kg m^{-3} (excess density: 180-

780 kg m^{-3}), primary particles: 1800-3000 kg m^{-3} (excess density: 780-2000 kg m^{-3}). Density range for flocs was determined from published data (Krone, 1963; Krank *et al.*, 1993; van Leussen, 1994). The density range for bed aggregates extends from the upper limit of flocs to 1800 kg m^{-3} (an upper limit based on saturated bulk density of densely consolidated cohesive and mixed sediment beds and supported by published data: Torfs *et al.*, 2001; Winterwerp and van Kesteren, 2004). Density range for primary particles was set from the upper limit of bed aggregates to the maximum expected mineral density.

In-Situ settling velocity experiments

In-situ settling experiments were conducted 04-06 November 2008 with PICS. The optical configuration of PICS for the present study included a monochrome Prosilica GE1380 camera with pixel resolution of 1380 x 1024 focused with a 25mm Pentax C-mount lens to a field of view of 13.8 x 10.2 mm and a depth of focus of 1.0 mm. Video at each measurement position was collected for 30 sec at 8 fps. PICS was deployed from the EPA R/V *Coastal Explorer*, a 27-ft Boston Whaler Challenger. PICS target sampling positions are provided in Figure 3-1. During the field experiment, data were collected at Stations 03 through 12 (Stations 01 and 02 were inaccessible due to draft limitations of the research vessel). At each station PICS was lowered to within 5 ft (1.5 m) above the sediment bed (as indicated by the shipboard fathometer and pressure sensor on PICS). After collecting data near the bed, PICS was raised by approximately 5-ft (1.5-m) increments to near the water surface.

During the PICS *in-situ* experiments, surface conditions were extremely calm and water clarity was exceptionally high, and very little suspended sediments were observed. Most suspended matter observed was organic in nature, including centric diatoms, various zooplanktons, and other low-density organic matter. These visual observations were later confirmed with image analysis in that there was insufficient suspended sediment to determine settling velocity of suspended sediment from the *in-situ* experiments.

Settling velocity of eroded aggregates

A second objective of settling velocity experiments was to determine settling velocities of sediment eroded from the bed. This was accomplished by coupling PICS with SEDFLUME to measure size and settling velocity of sediments eroded from the collected cores. By this method, the eroded effluent from SEDFLUME is

passed through PICS, and periodically the PICS valves are closed to isolate the sediment suspension and to record particle settling. The New Bedford Harbor field experiment was the first application of SEDFLUME and PICS in which the settling velocity of eroded sediments was quantified.

The settling velocity measurements were grouped according to the classification determined in the erosion experiments (Table 3-1). From this grouping, a subset of settling images with good imaging characteristics was selected for size, settling velocity, and aggregate class analysis. For each video sequence included in the analysis, all particles larger than 30 μm were tracked and their size and settling velocity recorded. From the set of tracked particles (ranging from 200 to 2000 particles per 20-sec video), distributions of size, settling velocity, and estimated particle density were determined. Each particle was classified as a single mineral grain, bed aggregate, or floc based on its estimated density. The fraction of sediment mass in the floc and bed aggregate classes is presented in Figure 3-11. The fraction of particles eroded as flocs was occasionally as large as 50 percent, but was generally in the range of 10-40 percent. Conversely, the fraction of bed aggregates was generally in the range of 60-75 percent of the eroded sediment mass. These data agree with visual SEDFLUME observations, where fragments of the core surface were observed to release and transport intact as either bed or suspended load in a wide range of particle sizes.

The median settling velocity of each particle class was determined based on the set of particle sizes, densities, and settling velocities within that particle class. Figure 3-12 presents the median settling velocities for the floc and bed aggregate particle classes. The floc settling velocities were generally in the range of 0.2 to 0.6 mm/s. Median settling velocities for the bed aggregate class were generally larger, in the range of 0.4 to 1.4 mm/s.

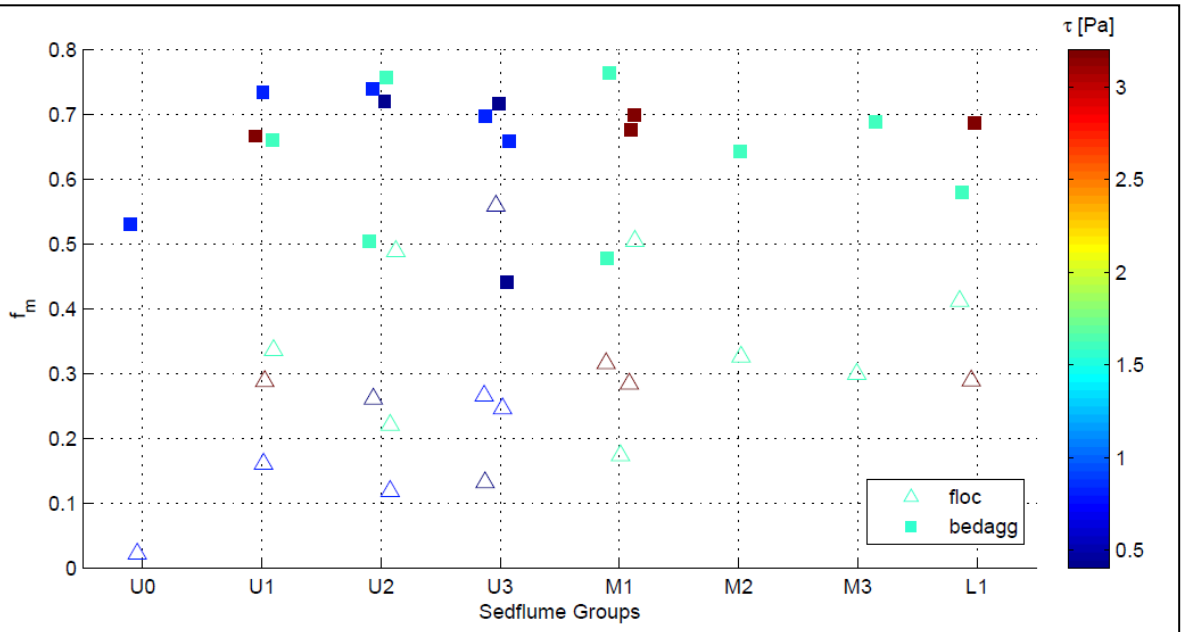

Figure 3-11. Fraction of sediment mass eroded as flocs and bed aggregates. Sedflume group designations correspond to Table 3-1. Symbol color is associated with applied shear stress (τ). The remaining fraction of sediment mass is associated with primary particles (individual mineral grains).

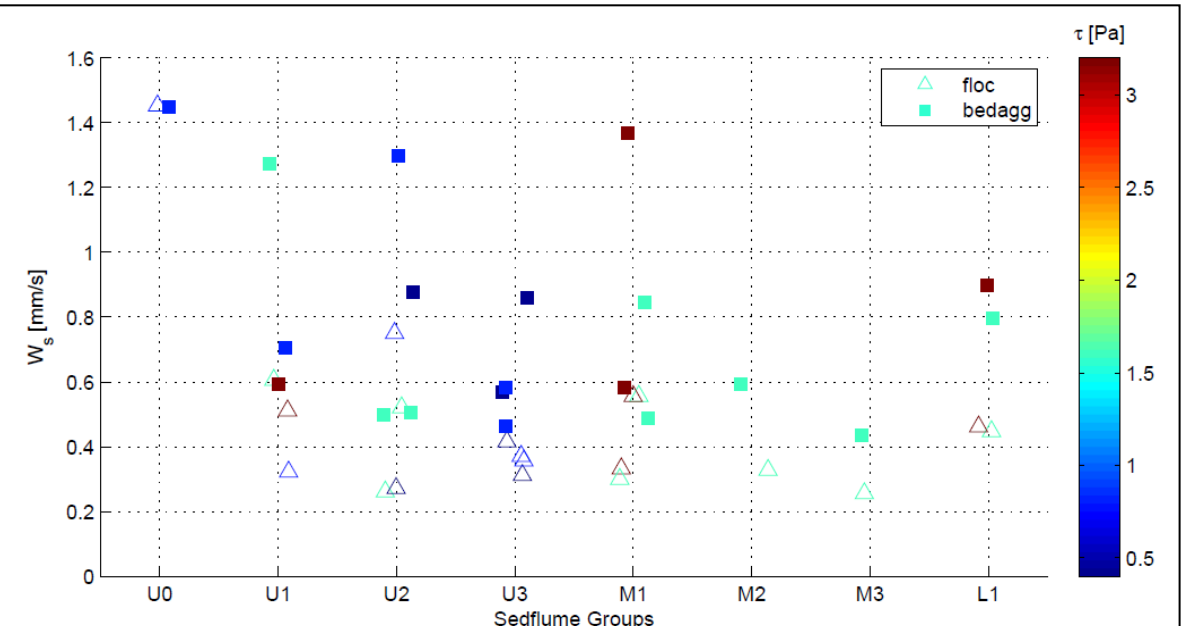

Figure 3-12. Median settling velocities for the floc and bed aggregate particle classes. Sedflume group designations correspond to Table 3-1. Symbol color is associated with applied shear stress (τ).

4 Setup of Models

Introduction

The setup of the models described in the previous chapter to simulate the transport and fate of sediments and PCBs in the New Bedford Harbor estuarine system is described in this chapter. First, the data sources as well as processing that were used in setting up the models are described.

Data Sources and Processing

PCB Data

The primary source of data used in this modeling study was the Battelle database. These data were either long-term monitoring (LTM) data from EPA's Office of Research and Development (EPA ORD) or from other site investigations ("non-LTM" data). LTM data were collected using consistent protocols over time at set stations in the upper, lower, and outer harbor established to be representative of those areas (Nelson *et al.* 2009; Nelson 2009; Nelson and Bergen 2012). Data from this effort were collected in 1993, 1995, 1999, 2004, 2009, and 2014. The non-LTM data stem from the Superfund remedial investigation and post-remediation monitoring efforts. That sampling, which started in 1999, focused on particular study objectives such as evaluating shoreline areas or contamination remaining following dredging. Both the LTM and non-LTM data are in the Battelle database.

The decision was made by the modeling team in concert with the EPA RPMs to model the NOAA 18 congeners for the following reasons:

- These congeners have been most frequently chosen for assessment in New Bedford Harbor water, sediments, and biota;
- They are analyzed in EPA's long-term monitoring program and included in the State of Massachusetts seafood sampling as well as other programs that assess individual congeners.
- There is a strong, well-studied, site-specific relationship between these congeners and total PCBs (Foster Wheeler 2001). If needed, that

relationship permits extrapolation between the NOAA 18 congeners and total PCBs using a multiplication factor of 2.5.

The LTM data were downloaded and not further processed (except as described below for "non-detect" congener values). The initial non-LTM query from the Battelle database designated:

- sediment as the matrix;
- collection from 1999-2007, excluding LTM efforts (1999 is the first non-LTM data collection effort, 2007 is the end of the modeling calibration and validation time period);
- surface ("Depth Top" = 0); and
- analysis for the NOAA 18 congeners[2].

All the data were processed to derive the sum of the NOAA 18 congeners. The data stemmed from many sampling efforts that reported "non-detects" differently; for example, as the method detection limit, half the method detection limit, or the reporting limit. The Battelle database also provides a "sum of congeners" that converts congener results below the MDL (designated with a "U" as a "Final Qualifier") to zero. This procedure ensures consistent processing among sampling efforts. That procedure was maintained in this study. Thus, all congener values with "U" qualifiers were converted to zero, and then the total PCB value was determined by summing the congeners. These processed PCB data were used to establish initial conditions for the modeling as described later in this section. The data sets used for establishing the initial conditions are described in Table 4-1. Four geographic areas are presented: North of Wood Street (NWS); Upper Harbor; Lower Harbor; and Outer Harbor. For the initial conditions, the 1993 LTM chemistry data were combined with the "Phase I" chemistry data set to represent initial conditions. This was done because the 1993 LTM data set did not provide coverage of nearshore areas, while the "Phase 1" data set (collected in 1999 and 2000) focused extensively on these areas. The Phase 1 data expanded the geographic coverage of measured data points used to represent the initial conditions. Chemistry or bathymetric data sets were sometimes available for only one particular area.

[2]The data download also included 65 "Phase I" samples that were analyzed for Aroclors, not congeners. These samples were removed from the modeling database (n=65).

Table 4-1 Data description and source for initial conditions

Area	PCB Concentrations	Organic Carbon Concentrations	Bathymetry
NWS[3]	Pre-remediation (1999-April 2003) sediment samples provided by *WH Group*.	WH Group	Electronic bathymetry not available. Estimated from design drawings (Tetra Tech FW 2005).
Upper Harbor[2]	EPA ORD Long-term monitoring data set from 1993 combined with 1999-2000 "Phase I" data set.	EPA ORD Long-term monitoring data set	1999 Bathymetry provided by Jacobs Engineering (orgbathy_ngvd.txt)
Lower Harbor[2]	EPA ORD Long-term monitoring data set from 1993 combined with 1999-2000 "Phase I" data set.	EPA ORD Long-term monitoring data set	Bathymetry from approx 1999-2000, provided by Apex Companies, LLC (USACE_Bathy_MLLW.xls
Outer Harbor[2]	EPA ORD long-term monitoring data set from 1993 combined with 1999-2000 "Phase I" data set.	EPA ORD Long-term monitoring data set	NOAA NOS Bathymetry, downloaded from their website.[2]

Hydrodynamic Model

A coarse curvilinear-orthogonal grid of Buzzards Bay and New Bedford Harbor with 5,662 cells was used to construct the water surface elevation boundary conditions to drive a finer non-uniform Cartesian grid with 7,882 cells of New Bedford Harbor and a portion of Buzzards Bay. The finer grid model was used to simulate the transport of sediments and PCBs. Figures 4-1 and 4-3 show the coarse grid and fine grid, respectively.

Time series of wind velocity, water surface elevations at the open water boundaries in Buzzards Bay, and river discharges into Buzzards Bay and New Bedford Harbor were used for the boundary conditions for the coarse grid model.

[3] http://egisws01.nos.noaa.gov/servlet/BuildPage?template=bathy.txt&parm1=M010

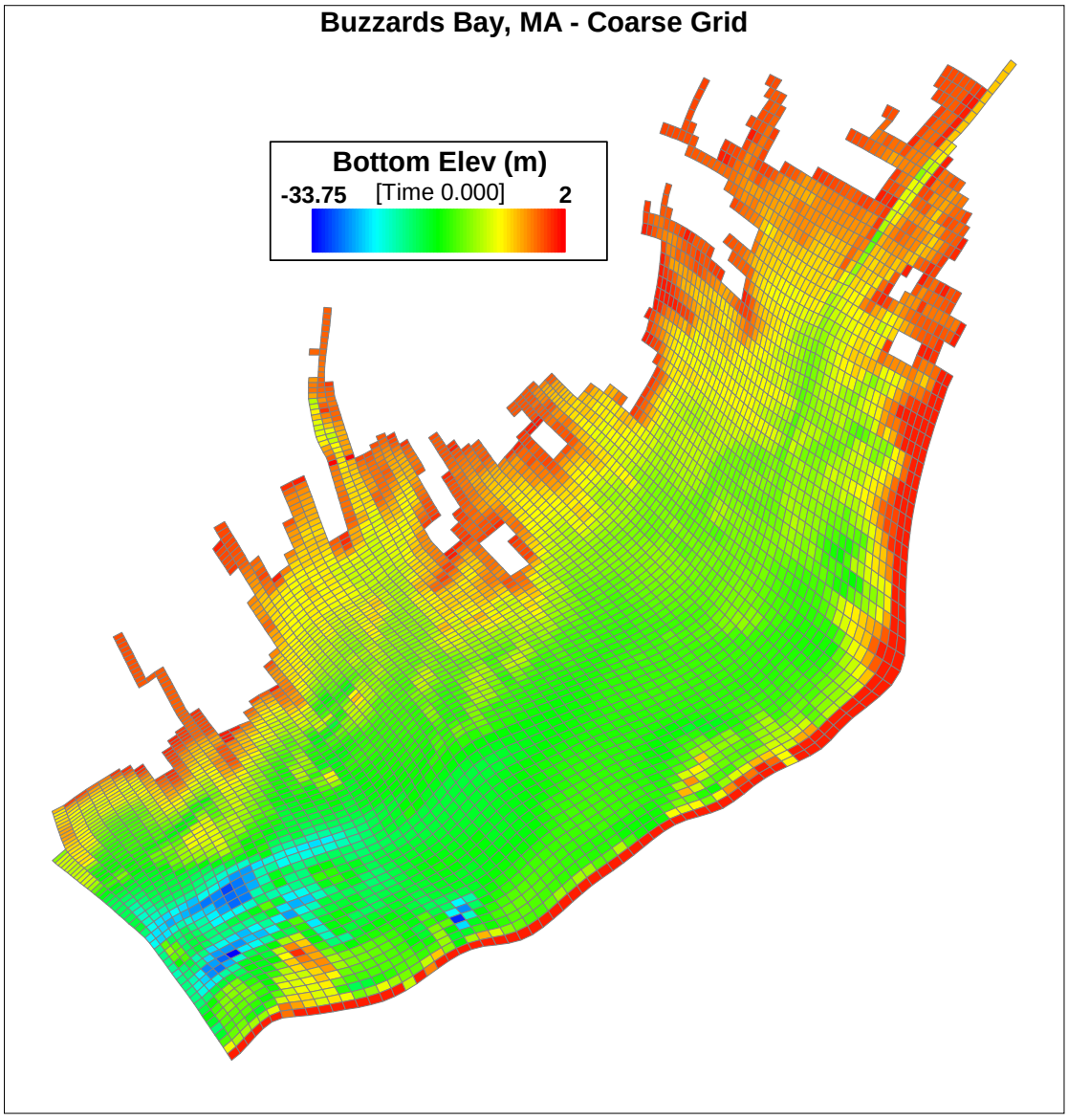

Figure 4-1 Coarse curvilinear-orthogonal grid for Buzzards Bay and New Bedford Harbor.

Figure 4-2 shows the grid of the coarse model and the locations of the open water boundaries. Water surface elevation time series were applied at the labels that begin with “Head”. The time series were computed by EFDC using interpolated harmonic constituents for those locations from the tidal constituent database for the western North Atlantic (Mukai *et al.*, 2002). For example, the location

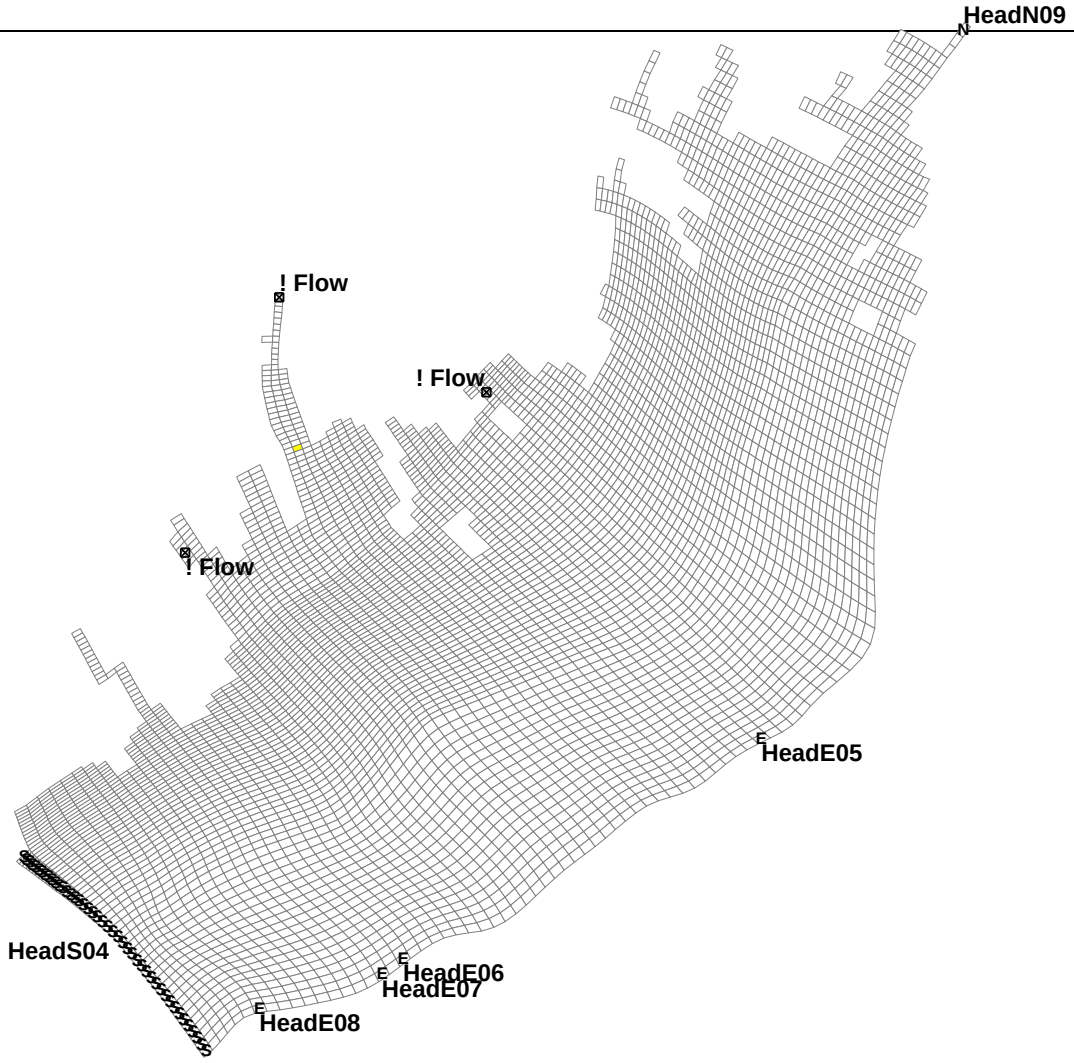

Figure 4-2 Grid outline for coarse grid model that shows locations where open water boundary conditions were applied.

Labeled HeadE05 is the open water boundary at Woods Hole, MA, and the location labeled HeadN09 is the Cape Cod canal that connects Buzzard Bay to Cape Cod. Measured discharge time series were applied at the locations with labels “Flow”. The three rivers are the Mattapoisett, the Paskamanset, and the Acushnet.

In Figure 4-3, the grey areas within the harbor and in the vertical band south of the hurricane barrier and in the horizontal band east of the harbor represent are caused by the finest of the grid used in those portions of the model domain.

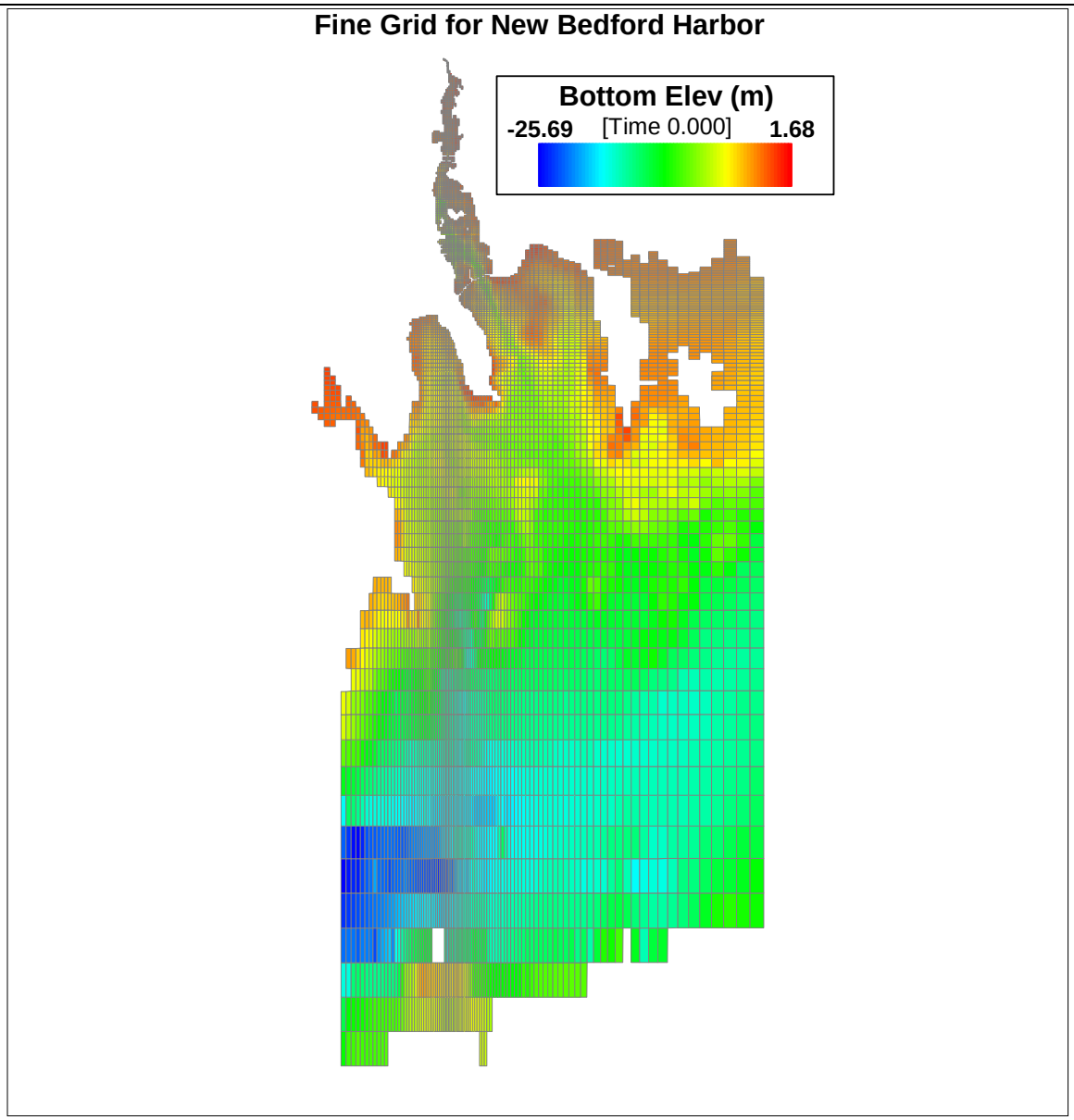

Figure 4-3 Fine non-uniform Cartesian grid for New Bedford Harbor and a portion of Buzzards Bay.

Figure 4-4 shows a portion of the fine grid in the Upper Harbor and shows how the grid approximates the complex shoreline in that portion of the harbor. Figure 4-5 shows the bathymetry of the fine grid model.

Time series of wind velocity, water surface elevations at the open water boundaries in Buzzards Bay, and river discharges into New Bedford Harbor and the portion Buzzards Bay included in the model domain were used for the boundary conditions for the fine grid model. Figure 4-6 shows the grid of the fine

Figure 4-4 Fine non-uniform Cartesian grid is overlain on this Google photo of a portion of New Bedford Harbor

grid model and the locations of the open water boundaries. Water surface elevation time series were applied at the locations with labels that begin with “W”, “S”, and “E”. The water surface elevation time series at the indicated locations were extracted from the output of a 30-year model run of the coarse grid model. Measured discharge time series were applied at the locations with labels “Flow”. The calibration of the hydrodynamic model is described in Section 5.

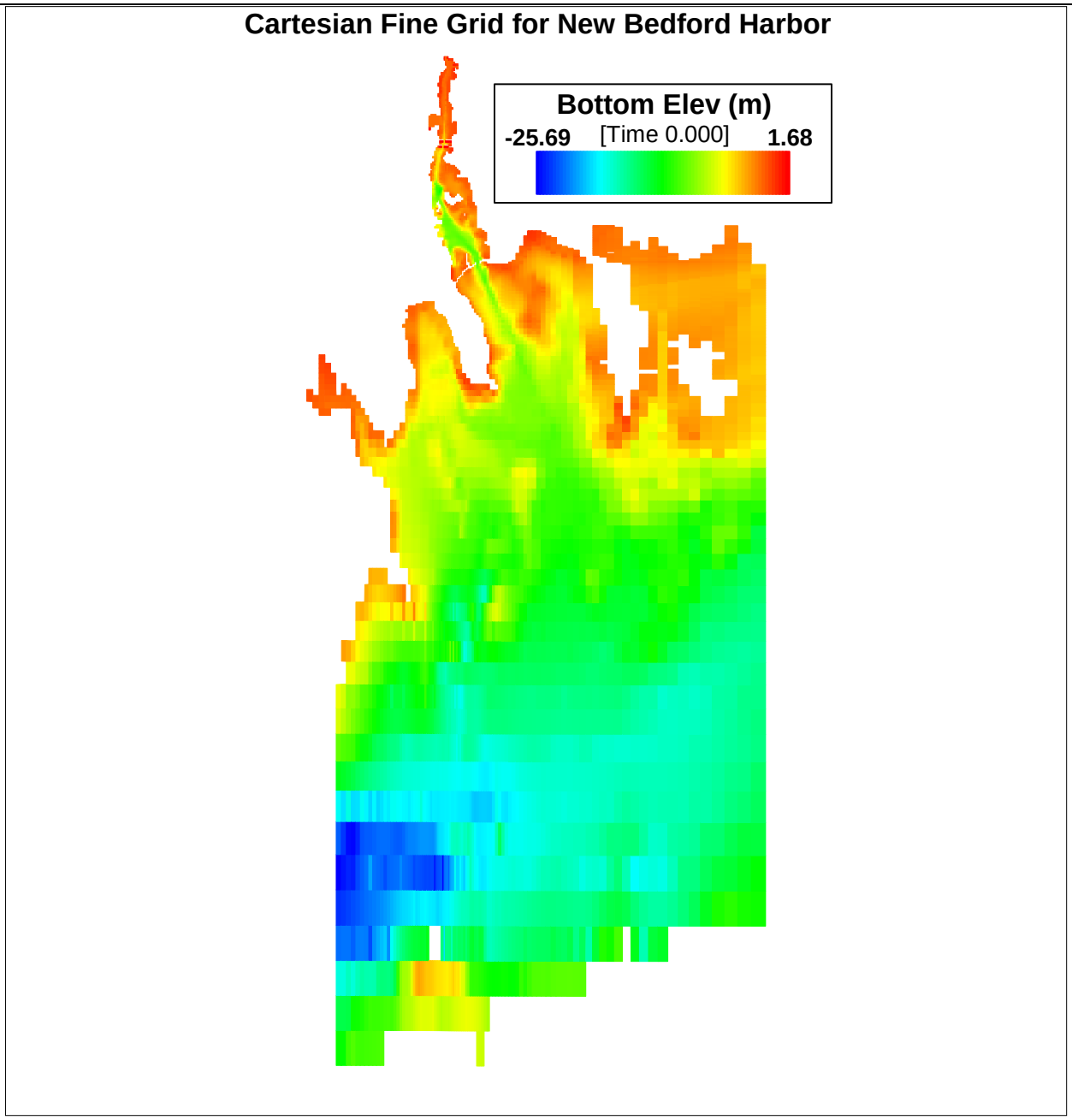

Figure 4-5 Bathymetry in the model domain for the fine non-uniform Cartesian grid for New Bedford Harbor and a portion of Buzzards Bay.

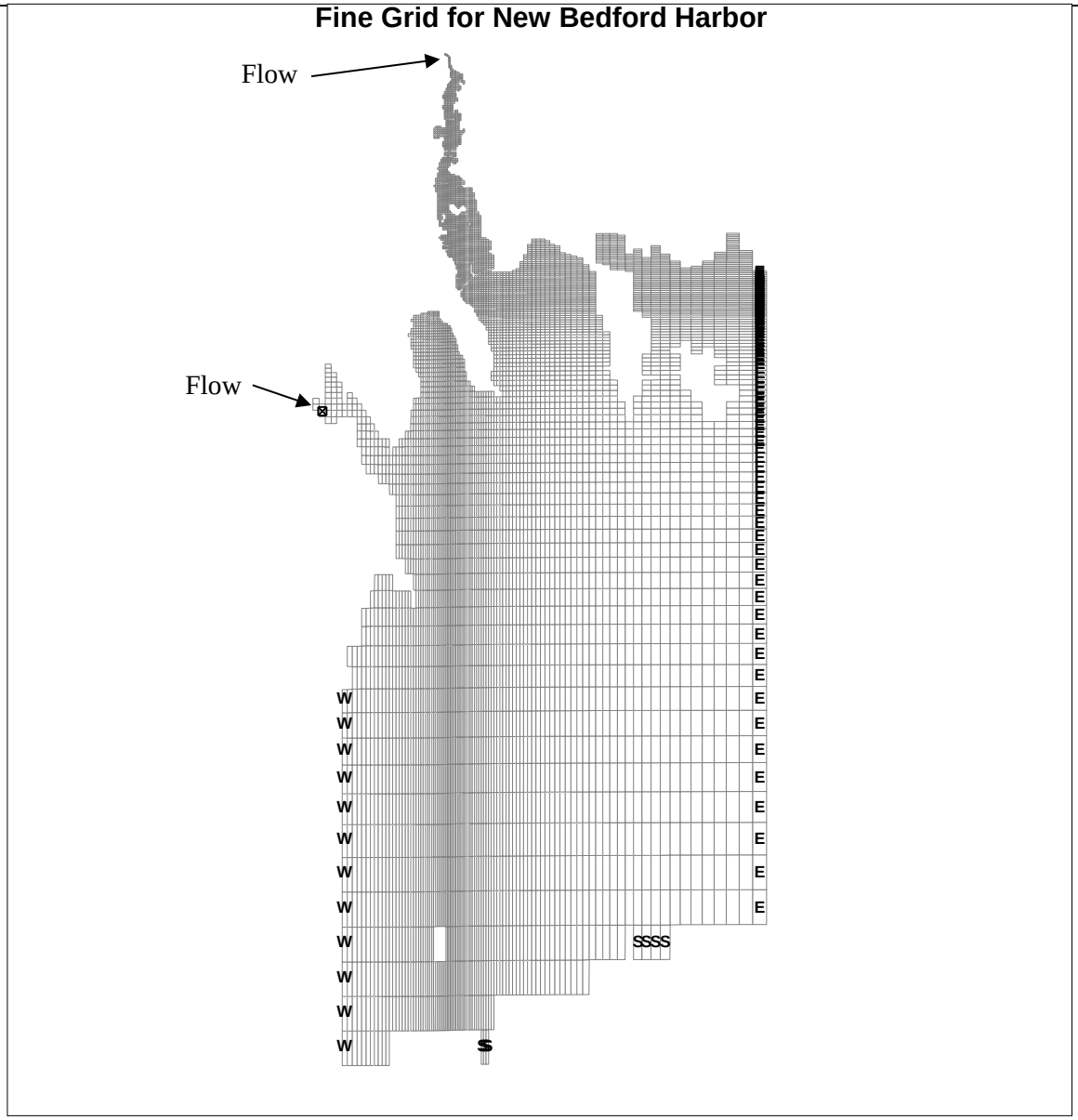

Figure 4-6 Grid outline for coarse grid model that shows locations where open water boundary conditions were applied. Water surface elevations were applied at the locations labeled “W”, “S”, and “E”. Discharge time series were applied at the two locations labeled “Flow”.

Wave Model

The SWAN wave transformation model was used to simulate the formation of wind-generated surface waves in the fine grid model domain. Measured wind speeds and directions at a NOAA buoy near the entrance to Buzzards Bay were used to construct a time series of three-hour average wind speeds and directions.

This three-hour average time series was used to drive the SWAN model. Time series of predicted wave heights, wave periods and propagation directions were used to calculate the combined current- and wave-induced bed shear stress in the SEDZLJ sediment transport model. The SWAN model was setup using the fine non-uniform Cartesian grid, so there was no need for any interpolation of wave properties onto the grid used for LTFATE. The wave processes that were simulated in this modeling were the following: wave generation using the wave growth term of Cavaleri and Malanotte (1981), refraction, diffraction, shoaling, breaking, and bottom friction. The importance of including waves in this modeling system is that shallow water wind waves can increase the bed shear stress, and thus potentially increase the erosion rate of contaminated sediments. During the model simulation, the bed shear stress due to both currents and waves is calculated in each grid cell during each time step to better represent the total shear stress that acts on the bed surface, and thus the mass of sediment that is resuspended.

Sediment Transport Model

The SEDZLJ model was setup to simulate sediment transport in the New Bedford Harbor fine grid model domain using the following information:

- Mean settling velocities for flocs of 0.4 mm/s, and mean settling velocities of bed aggregates of 0.9 mm/s.
- SEDFLUME determined erosion rate versus bed shear stress given by Equation 8-7 along with the results shown in Figure 3-9 and in Table 3-2, and the critical shear stresses for erosion given in Table 3-2 were used to parameterize the erosional characteristics of the analyzed Sedflume cores.

Based on the SEDFLUME and PICS studies performed along with existing grain-size distribution data for the harbor and Buzzards Bay, it was decided that five sediment grain sizes were needed to adequately represent the wide range of sediment from clay to gravel. The diameters of the five sediment size classes used are 3, 25, 222 (fine sand), 432 (medium sand), and 2,000 μm (gravel). It was assumed that the specific gravity of all five size classes was 2.65. The 3 μm size class was used to represent the flocs whose settling speeds were measured in the PICs experiment, whereas the 25 μm size class was used to represent the bed aggregates eroded in the SEDFLUME experiments. These two cohesive size classes are used to represent the erosion, transport and settling of the fine-grain sediment deposited. They are not treated as individual sediment particles with

the specified diameters. In fact, the specified diameters for these two cohesive size classes are not used in SEDZLJ. During the model simulation, the sorbed PCB concentration on sediment eroded from a particular grid cell is the PCB concentration in the surface layer of the sediment bed in that grid cell, which varies spatially and temporally throughout the model domain.

Six bed layers were used for each SEDFLUME core. The first (top) layer is the active layer through which depositing and eroding sediment passes. The second layer is the layer in which new sediment deposits are placed. This layer is subdivided into a user-specified number of sublayers that are used to represent consolidating fine-grain dominated sediment. The third through fifth bed layer are used to represent the existing sediment bed in each grid cell at the start of the model simulation. The sixth bed layer is an unerodible layer and was added to prevent the number of bed layers from ever going to zero if layers two through five were eroded during a significant hydrologic/meteorologic event. The grain size distribution in each bed layer in each SEDFLUME core was assumed to be the same, but the critical shear stress and bed density was increased for the lower layers for the cores in which cohesive sediment (*i.e.*, clay and silt size sediment) made up at least 20 percent by mass of the sediment.

Because LTFATE was run in a depth-averaged mode, a Rouse profile was assumed for the vertical suspended sediment concentration profiles for the three noncohesive sediment size classes. This is a normal assumption that is made in modeling the transport of noncohesive sediments and represents the fact that the highest suspended sediment concentration occurs immediately above the bed. This nearbed concentration used in defining the Rouse profile was calculated for each noncohesive sediment size class in each grid cell at each timestep as a function of the settling velocity for that sediment size class, and the time-variable depth-averaged suspended sediment concentration, flow depth, and shear velocity. The deposition rate for each noncohesive sediment size class was calculated as the product of the nearbed concentration, the settling velocity, and the probability of deposition for noncohesive sediment.

No measurements of suspended sediment concentrations (SSC) or total suspended solids (TSS) were found for the two rivers that flow into the fine grid model domain. For the suspended sediment boundary condition, a regional discharge-SSC relationship was used to calculate the SSC time series of the finest cohesive sediment size class as a function of the discharge time series. These SSC values were used as the boundary conditions at the two cells shown in Figure 4-6.

Contaminant Transport Model

3-phase equilibrium partitioning of PCBs between particulate (sorbed), freely dissolved, and DOC-bound phase was simulated using EFDC. Additional transport processes simulated in EFDC included volatilization of PCBs, diffusion of freely dissolved PCBs from the water column to the top sediment bed layer (and vice-versa), and diffusion of freely dissolved PCBs within the layered sediment bed in each grid cell.

Chemical Partitioning Values for New Bedford Harbor

In order to predict the fate and transports of the PCBs in New Bedford Harbor, the chemical partitioning values (K_{ow}) need to be selected. As described previously, the modeling was performed using the sum total of the NOAA 18 PCB congeners (Table 4-2). K_{ow} values for these congeners exist in the literature (*e.g.*, Hawker and Connell, 1988); however, those values are derived from laboratory studies using distilled water at 25°C, and hydrophobicity is known to change as a function of temperature and salinity. In addition, there are not equal amounts of each of the 18 PCBs in the mixture sampled at the site. Therefore, to correctly estimate the K_{ow} of the PCB mixture in New Bedford Harbor, the relative proportions of each congener in the mixture need to be appropriately weighted in the derivation of the K_{ow} value.

The goals of the analysis performed was to 1) estimate K_{ow} values at the salinity and temperature found in New Bedford Harbor for the NOAA 18 PCB mixture, and 2) develop the weight-averaged chemical partition coefficients for the PCB mixture on the basis of observed contaminant concentrations.

Salinity- and temperature-corrected K_{ow}s

n-Octanol-water partition coefficients were obtained from Hawker and Connell (1988) and were adjusted to the average NBH temperature of 11.7°C using the method of Li *et al.* (2003):

$$\log K_{ow}(T_{NBH}) = \log K_{ow,25} + \Delta H_{ow}/R/\ln(10)\times(1/298.15-1/T_{NBH})$$

where T_{NBH} is the average temperature in NBH (°K), K_{ow} (T_{NBH}) is the temperature adjusted K_{ow} for NBH, $K_{ow,25}$ is the n-octanol water partition coefficient at 25°C from Hawker and Connell (1988), R is the ideal gas constant (8.314472E-3 (kJ/K/mol)), and ΔH_{ow} is the internal energy of phase transfer between n-octanol and water. Internal energies of transfer were taken from Li *et*

al. (2003) for PCB congeners with measured values, and for the other PCB congeners, the average value from Li *et al.* (2003) was applied, *i.e.*, -26.3 kJ/mol. The average NBH temperature of 11.7°C was derived by averaging the predicted daily temperatures for Fish Closure Areas 1, 2 and 3. The temperature adjusted values are provided in Table 4-3.

To adjust for salinity, the method of Xie *et al.* (1997) was used.

$$\log(S_{sw}/S_{fw}) = k_s C_s = 0.0018 \times V_H \times C_s$$

$$\log\left(K_{ow,seawater}\right) = \log\left(K_{ow,freshwater}\right) + \log\left(S_{sw}/S_{fw}\right)$$

Table 4-2 NOAA 18 PCB Congeners

IUPAC No.	Compound	Melting Point (°C)	Molecular Weight (g/mol)
8	2,4'-dichlorobiphenyl	44.5	223.1
18	2,2',5-trichlorobiphenyl	45	257.5
28	2,4,4'-trichlorobiphenyl	58	257.5
44	2,2',3,5'-tetrachlorobiphenyl	48	292.0
52	2,2',5,5'-tetrachlorobiphenyl	86	292.0
66	2,3',4,4'-tetrachlorobiphenyl	125	292.0
101	2,2',4,5,5'-pentachlorobiphenyl	78.5	326.4
105	2,3,3',4,4'-pentachlorobiphenyl	117	326.4
118	2,3',4,4',5-pentachlorobiphenyl	112	326.4
128	2,2',3,3',4,4'-hexachlorobiphenyl	151	360.9
138	2,2',3,4,4',5'-hexachlorobiphenyl	79.5	360.9
153	2,2',4,4',5,5'-hexachlorobiphenyl	103	360.9
170	2,2',3,3',4,4',5-heptachlorobiphenyl	137.5	395.3
180	2,2',3,4,4',5,5'-heptachlorobiphenyl	113.5	395.3
187	2,2',3,4',5,5',6-heptachlorobiphenyl	104.5	395.3
195	2,2',3,3',4,4',5,6-octachlorobiphenyl	171	429.8
206	2,2',3,3',4,4',5,5',6-nonachlorobiphenyl	203	464.2
209	Decachlorobiphenyl	319	498.7

where k_s is the Setschenow constant, V_H is the LeBas molar volume (cm^3/mol) (Mackay *et al.*, 2002), C_s is the molar concentration of the salt solution, seawater

= 0.5 mol/L, S_{sw} is the solubility in seawater/salt solution, and S_{fw} is the solubility in freshwater.

Based upon salinity measurements in October 1999 and August 2004 (associated with the long term monitoring program in Battelle's NBH database), Fish Closure Areas 1 and 2&3 had average salinities of 32.1 (n=114) and 33.1 (n=42) psu, respectively. Similar results were observed in the USACE mooring studies, Ellis *et al.*, (1977), and Geyer and Dragos (1988). In the NBH-ROD, the harbor (above the hurricane barrier) was concluded to be vertically well mixed below the Coggeshell Street Bridge, with salinities typically ranging from 26 to 30 psu. In this effort, the salinities in all three Fish Closure Areas were set equal to that of seawater. The salinity corrected $K_{ow}s$ are shown in Table 4-4.

Derivation of the weight-averaged $K_{ow's}$ from empirical data

To determine the weight-averaged K_{ow} for the NOAA 18 PCB mixture in New Bedford Harbor sediments, surface sediment data were downloaded from the Battelle NBH database for the 2004 field season. Using the data points for the long term monitoring program (samples with station ids ending with "LTM"), the composition of the NOAA 18 PCB congeners was computed for samples above (Area 1) and below (Areas 2 and 3) the hurricane barrier (Table 4-5).

Using the $K_{ow}s$ (Table 4-4) and prevalence information (Table 4-5), the weight-averaged log $K_{ow}s$ for the NOAA 18 PCB mixture at 11.7°C in Fish Closure Area 1 and Areas 2&3 are 6.67 and 6.88, respectively. The relationships of Burkhard (2000), US-EPA (2000), and Seth *et al.* (1999) were used to derive K_{doc}, K_{poc}, and K_{soc}, respectively, for the NOAA 18 PCB mixture (Table 4-6). The values in Table 4-6 were used in the modeling effort for the NOAA 18 PCB mixture.

The contaminant transport module in EFDC was modified to include the ability to specify spatially variable n-Octanol-Water Partition Coefficients (K_{ow}) for both the water column and the sediment bed for the NOAA 18 PCB congener mixture. Analysis of existing data yielded spatially averaged log K_{ow} values for both the water column and sediment for Fish Closure Area 1 and for Areas 2 and 3.

The initial concentrations of PCBs in the sediment bed in each of the grid cells were determined using LTM data set from 1993 combined with 1999-2000 "Phase I" data set for the upper, lower and outer harbor portions of the model

domain. For the NWS portion, the pre-remediation (1999- April 2003) in-water sediment samples were used for the initial conditions (see Table 4-1).

Table 4-3 n-Octanol/Water Partition Coefficients for NOAA 18 PCB Congeners

IUPAC No.	Log K_{ow}[a] at 25°C	ΔH_{ow}[b] (kJ/mol)	Log K_{ow} 11.7°C
8	5.07	-22.7	5.26
18	5.24	**-26.3**	5.45
28	5.67	-26.3	5.89
44	5.75	**-26.3**	5.96
52	5.84	-27.3	6.06
66	6.20	**-26.3**	6.41
101	6.38	-23.8	6.57
105	6.65	-28.6	6.88
118	6.74	-28.5	6.97
128	6.74	**-26.3**	6.95
138	6.83	-25.0	7.03
153	6.92	-31.1	7.17
170	7.27	**-26.3**	7.48
180	7.36	-29.1	7.60
187	7.17	**-26.3**	7.38
195	7.56	**-26.3**	7.77
206	8.09	**-26.3**	8.30
209	8.18	**-26.3**	8.39

[a]Hawker and Connell (1988). [b]Li *et al.* (2003). Bold values are an average value from Li *et al.* (2003).

Table 4-4 Salinity corrected n-octanol/water partition coefficients for the NOAA 18 PCB congeners

IUPAC No.	log K_{ow} at 11.7°C	LeBas Volume[a] (cm^3/mol)	Seawater Adjustment Factor $log(S_{sw}/S_{fw})$	Log $K_{ow,sw}$ 11.7 °C
8	5.26	226.4	0.20	5.46
18	5.45	247.4	0.22	5.68
28	5.89	247.4	0.22	6.11
44	5.96	268.4	0.24	6.21
52	6.06	268.4	0.24	6.30
66	6.41	268.4	0.24	6.66
101	6.57	289.4	0.26	6.84
105	6.88	289.4	0.26	7.14
118	6.97	289.4	0.26	7.23
128	6.95	310.4	0.28	7.23
138	7.03	310.4	0.28	7.31
153	7.17	310.4	0.28	7.45
170	7.48	331.4	0.30	7.78
180	7.60	331.4	0.30	7.90
187	7.38	331.4	0.30	7.68
195	7.77	352.4	0.32	8.09
206	8.30	372.7	0.34	8.64
209	8.39	393.6	0.35	8.75

[a]Mackay *et al.* (2000)

Table 4-5 Prevalence of NOAA 18 PCB congeners in sediment samples from the 2004 field season for the long term monitoring program

Fish Closure Area 1			Fish Closure Areas 2 & 3		
Average	Standard deviation	Count	Average	Standard deviation	Count
2.136%	1.398%	58	3.191%	3.529%	24
6.899%	4.531%	58	3.397%	2.568%	24
16.023%	4.181%	58	10.419%	2.275%	24
5.168%	1.059%	58	3.897%	0.754%	24
17.926%	6.704%	58	8.164%	1.647%	24
5.566%	2.557%	58	7.843%	0.760%	24
10.097%	2.905%	58	11.346%	1.210%	24
2.335%	1.457%	58	3.726%	0.809%	24
10.302%	3.418%	58	13.626%	1.852%	24
1.374%	0.840%	58	2.708%	0.518%	24
7.879%	2.798%	58	12.175%	2.931%	24
10.511%	2.409%	58	12.642%	1.667%	24
0.965%	0.354%	58	2.168%	1.871%	24
1.276%	0.363%	58	1.865%	0.320%	24
1.141%	0.206%	58	1.334%	0.276%	24
0.157%	0.076%	58	0.601%	0.449%	24
0.147%	0.152%	58	0.433%	0.322%	24
0.098%	0.076%	58	0.467%	0.258%	24

Table 4-6 n-Octanol-water and organic carbon partition coefficients for NOAA 18 PCB congener mixture for NBH, 11.7°C and seawater salinity

	Fish Closure Area 1	Fish Closure Areas 2&3
Weighted Average log K_{ow}	6.67	6.88
Water Column		
Weighted Average log K_{doc}	5.57	5.79
Weighted Average log K_{poc}	6.67	6.88
Sediment		
Weighted Average log K_{doc}	5.57	5.79
Weighted Average log K_{soc}	6.21	6.43

$K_{doc} = 0.08 \times K_{ow}$ (Burkhard, 2000)

$K_{poc} = 1.00 \times K_{ow}$ (US-EPA, 2000)

$K_{soc} = 0.35 \times K_{ow}$ (Seth *et al.*, 1999)

5 Calibration and Validation of Models

Hydrodynamic Model

As described in Chapter 3 and seen in the vertical profiles given in Appendix B, the vertical temperature and salinity profiles measured throughout the harbor during ERDC's field study verified that the water column in New Bedford Harbor is well mixed under normal conditions due to the low flow of freshwater in the Acushnet River. This justifies the use of a depth-averaged model in this study.

Time series of water surface elevations and current velocities measured at different locations throughout the model domain were used in calibrating the hydrodynamic model. Figure 5-1 shows the comparison between the measured and simulated water surface time series at the hurricane barrier during the first 12 days of the November 2008 field study. The comparison during the remaining 12 days was similar.

Good quality comparison was obtained between the simulated Eulerian velocity fields and the ADCP moving transects measured during the field study. Appendix E contains plots (Figures E-1 – E21) from Dragos (2009) that show comparisons of the measured and simulated horizontal velocity fields in the northern half of the lower harbor at different stages of a tidal cycle. The velocities were measured with a downward pointing ADCP attached to a boat along the plotted transect lines. For easier viewing, the velocity vector in every fifth grid cell (in both horizontal directions) is plotted in these figures. In general, good comparisons are seen in the measured and simulated circulation patterns. In addition, the simulated current speeds were an average of five percent higher along the grid cells that fell along the transect lines. There is always a fair amount of noise in the signal recorded by an ADCP, so filtering of the measured velocities is usually necessary. This introduces more uncertainty into the measurements which needs to be taken into consideration when comparing measure velocities to simulated ones. No additional data existed to validate the hydrodynamic model.

Wave Model

There were no wave measurements in NBH, so it was not possible to validate the SWAN generated wave fields. The predicted wave heights, periods and directions

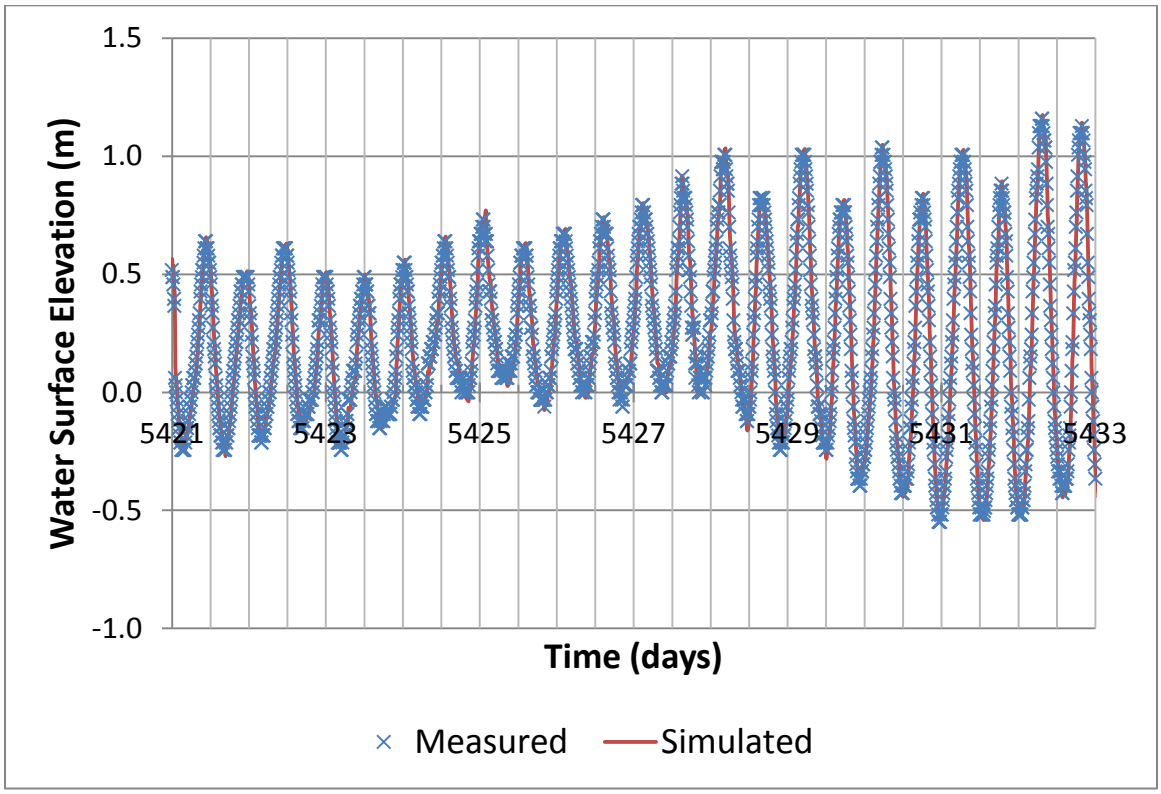

Figure 5-1 Comparison of measured and simulated water surface elevations at hurricane barrier entrance during the November 2008 field study.

under a variety of wind conditions, *i.e.*, during average to extreme weather conditions, were closely examined to insure that the predicted waves had reasonable heights, periods and directions for the given winds. In addition, a quantitative check was made by comparing the SWAN predicted wave heights and periods at different locations throughout the model domain (both inside and outside the harbor) with those computed using the fetch-limited wave procedure recommended in the Coastal Engineering Manual – Part II (USACE, 2002). None of the predicted values by SWAN were either 25% higher or 25% lower than the calculated values. This comparison of computed values gave more confidence in the SWAN predicted wave fields.

Sediment Transport Model

There were no data to use to calibrate or validate the sediment transport model in LTFATE. Suspended sediment concentrations were scheduled to be measured during the field study conducted in November 2008, but the conditions were relatively calm. No high winds or waves occurred during the measurement

periods, so the concentration of suspended sediment was very small – less than 10 mg/L. However, the sediment transport model was constrained using the measured erosion rates, bulk densities, and grain size distributions during the SEDFLUME study, and the mean floc and bed aggregate settling velocities determined from the PICS study. No adjustments were made to these parameters as is commonly done during a formal calibration of a sediment transport model. Thus, the amount of erosion, transport and deposition of sediment simulated by the sediment transport model was constrained by the measured values of these parameters.

The net sedimentation rates (NSR) in the Upper Harbor and in the Middle Harbor (in proximity to Core NBH5C061098) calculated from a 30 year No Action scenario model run were equal to 0.2 cm/year and 0.4 cm/year, respectively. These values are in close agreement with the sedimentation rates seen in Figure 5-2. This serves as an important check that the sediment transport model is well constrained and predicts realistic values for the NSR. Accurate prediction of the NSR is essential for prediction of the transport and fate of particulate contaminants, especially to be able to accurately access No Action or MNR remedial alternatives.

Contaminant Transport Model

The PCB transport and fate model was partially calibrated and validated using the data in the Battelle database described in the Data Sources and Processing section in Section 4. The start date for model runs for calibration and validation purposes was January 1, 1993 which predates any remedial actions in the harbor. Data from the database were used to construct the initial conditions (*e.g.*, spatially varying concentrations of the total of the NOAA 18 PCB congeners in the sediment bed) for the start of the calibration and validation simulation periods.

Calibration of the PCB transport and fate model in LTFATE was performed in two stages. First the model was run for two years (1993 – 1994) to perform a short-term calibration, and then it was run for three years (1993-1995) to perform a longer-term calibration using the appropriate tide, wind and wave forcings for these two periods. For the short-term calibration, time series of the predicted water column dissolved and particulate PCB concentrations were outputted from the model grid cells at the locations of Stations 1, 2 and 7 for which data exists in the Battelle database from April – December 1994. As shown in Figure 5-3, Station 1 was in the upper harbor, near Aerovox; Station 2 was at

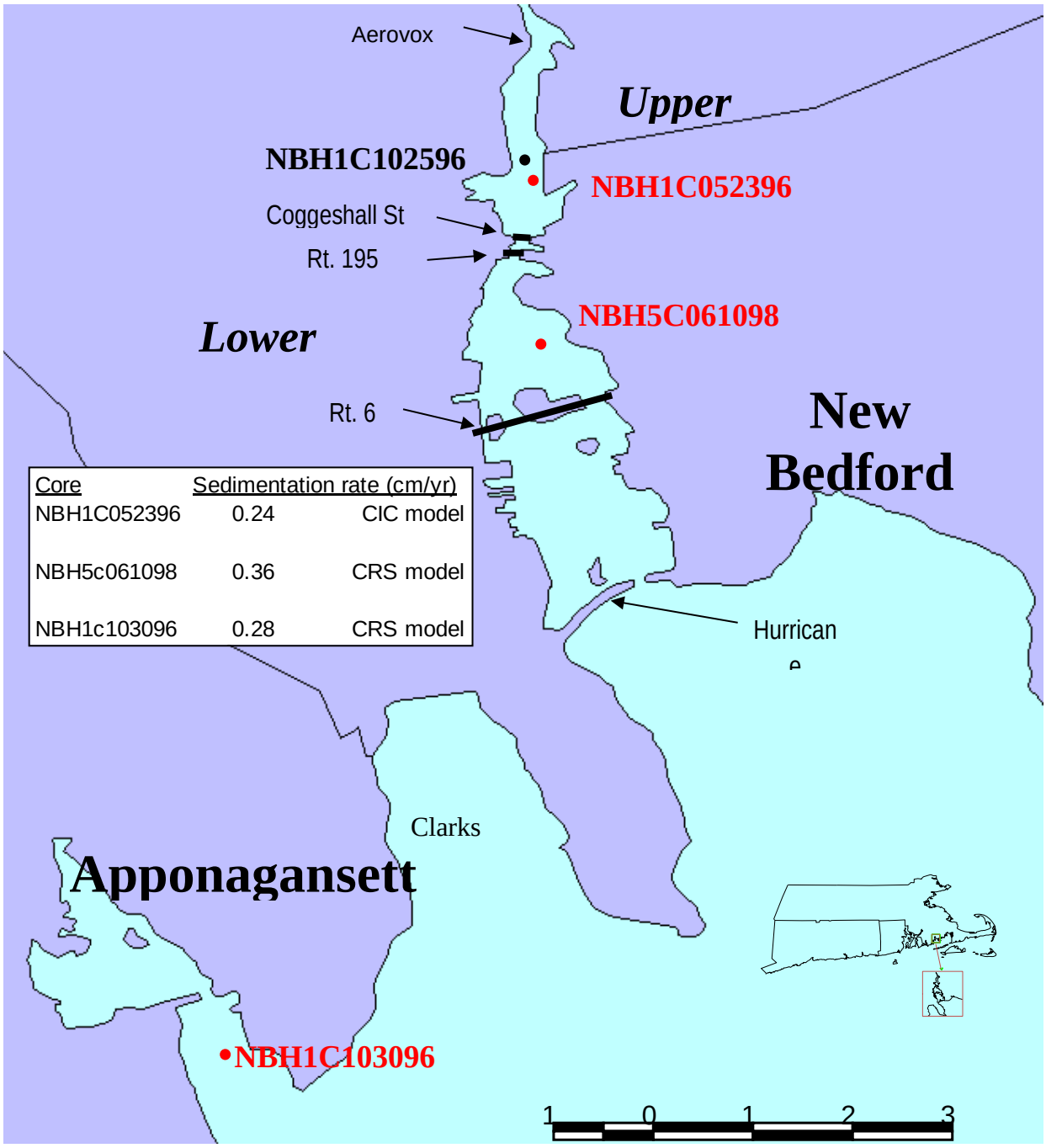

Figure 5-2 Net sedimentation rates in New Bedford Harbor

the Coggeshall St. Bridge; Station 7 was in the pilot study cove, just above Coggeshall Street. The diffusion coefficient that quantifies the diffusive flux of PCBs between the surface bed layer and the overlying water column was adjusted until the model gave the best overall agreement with the measured and predicted

Figure 5-3 Locations of Sampling Stations 1, 2 and 7.

dissolved and particulate concentrations. The best agreement was obtained using a spatially constant diffusion coefficient of $2*10^{-6}$ cm^2/s. The range of values typically measured for this parameter (that is proportional to the sediment porosity, among other factors) is $1*10^{-6}$ cm^2/s to $4*10^{-6}$ cm^2/s, so the value obtained through calibration of the contaminant transport model is a realistic one.

The importance of this calibration is understood in that the diffusive flux of PCBs from the sediment bed into the water column has a significant impact on the long-term (*i.e.*, decadal) change in PCB concentrations in NBH. The reason for this is that there is only a very small load of clean sediment that is transported into Upper NBH by the Acushnet River, and as such, there is very little burial, *i.e.*, natural remediation, of the contaminated sediments. So the diffusive flux of

PCBs from the surface of the sediment bed into the over lying water is a very slow process that will, over the long-term, result in the gradual decrease of the sediment concentrations (as is reflected in EPA's long-term database). The PCB mass that is diffused into the water column is subject to losses due to volatilization and the net tide-induced transport out of NBH into Buzzards Bay.

Next, LTFATE was run to simulate PCB transport and fate for the years 1993 – 1995 using the adjusted diffusion coefficient. The sediment bed PCB concentrations measured in the harbor in October 1995 at the long-term monitoring stations (Nelson and Bergen 2012) were compared to the predicted PCB concentrations in the grid cells in which the monitoring stations are located. The percentages of organic matter adsorbed to the different sediment size classes (for which there were not much data) were adjusted during this second stage of model calibration to decrease the relative differences in the measured and predicted PCB concentrations. The best results yielded relative differences between the measured and predicted PCB concentrations that fell within a ± 10 percent envelope. These relative differences are considered to be acceptable.

Next, the PCB transport and fate model in LTFATE was partially validated, again using a two phase approach. First, the calibrated LTFATE model was run to simulate PCB transport and fate for the years 1993 – 1999, and the PCB concentrations collected in the harbor as part of the Phase 1 sampling and the long term monitoring effort during 1999 were compared to the predicted concentrations. As before, model predicted PCB concentrations for each grid cell were compared to data within a cell; when multiple data points exist within a single cell, the arithmetic mean was used for comparison. The comparison yielded relative differences between these concentrations that fell within a ± 50 percent envelope. Considering that some of the changes in measured concentrations were probably caused by processes not represented by the model, *e.g.*, prop scour, these relative differences are considered to be acceptable, and are comparable to the accuracy of contaminant transport models performed at other Superfund Sites, *e.g.*, Upper Hudson River, Housatonic River, and the San Jacinto River Waste Pits.

The partially validated model was then run for the years 1993 – 2006 for the second phase of model validation. Over this extended validation period there were a number of dredging activities that needed to be depicted in the model. In the dredged areas, the dredging activities obviously modified the surface PCB concentration and changed the bathymetry. A description of these modifications

and their schedule is provided in Table 5.1. LTFATE was modified so that these changes in bathymetry in the dredging footprints and changes in surface layer PCB concentrations could be made during a model run, *i.e.*, without having to stop the model run, make the changes, and then restart the model. Having to stop and then restart the model several times over this model run would have increased the model runtimes by at least 50 percent. Not surprisingly, the comparison made for this 14 year model simulation between the measured 2005 long-term monitoring data and the Post-2006 data and the predicted PCB concentrations yielded larger relative differences – within a ± 350 percent envelope. The increase in the uncertainty envelope from ± 50 percent over the 1993 - 1999 time period to ± 350 percent over the 1993 – 2006 time period was not unexpected due, at least in part, to: a) the simulation period being more than twice as long, and b) the extremely simplistic representation of the dredging activities that occurred in NBH between 1999 and 2006. Based on experience gained from performing contaminant transport modeling studies at other sites, the latter factor increased the uncertainty much more than the first factor. As such, considering the complexity of the natural, *e.g.*, nor'easters, and anthropogenic processes, *e.g.*, removal of contaminated sediment by dredging, being simulated over such a long time period, and the uncertainty associated with collection and analyses of all chemistry data and that of the model itself, having the relative differences be within a factor of 3.5 is considered acceptable.

As discussed previously, the impact of the described data limitations on this modeling study did result in only a partially calibrated and validated sediment transport and contaminant transport models. As another check on at least the partial validity of the modeling system, the predicted flux of PCBs at the entrance to NBH was within 20 percent of the measured flux (see Figure 5-4). Since the PCB flux was calculated using predictions by the hydrodynamic model, the sediment transport model, and the contaminant transport model, this indicates that the performance of the combined modeling system was at least representative of the actual conditions at NBH. In conclusion, considering the described validation checks for both the sediment and contaminant transport models, LTFATE was determined to be robust enough to use in simulating the planned post remediation scenario.

Table 5-1 Dredging activities accounted for during the 1993 – 2006 model validation period

Year	Area	Description	Change
2002	Lower Harbor	City navigation "State Pier Expedited Dredging" completed October 2002	Input updated bathymetry; no post-dredging chemistry. Will change concentration to 1 PPM based on direction from D. Dickerson.
2003	NWS	NWS excavated in the "dry"	New sediment surface concentration in NWS area of 7.0 PPM, per confirmation sampling average, Table 1-2 of the NWS completion report.
2004	Upper Harbor	Remedial Dredging.	New bathymetry and new surface sediment concentration in dredge outline.
2005	Upper Harbor	Remedial Dredging	Input updated bathymetry; no post.
	Lower Harbor	F1 area, completed February 2005; SR1, completed October 2005	Input updated bathymetry; no post-dredging chemistry. Concentration changed 1 ppm based on direction from D. Dickerson.
2006	Upper Harbor	Remedial Dredging.	New bathymetry and new surface sediment concentration in dredge outline.
2007	Upper Harbor	Remedial Dredging.	New bathymetry and new sediment concentration in dredge outline.

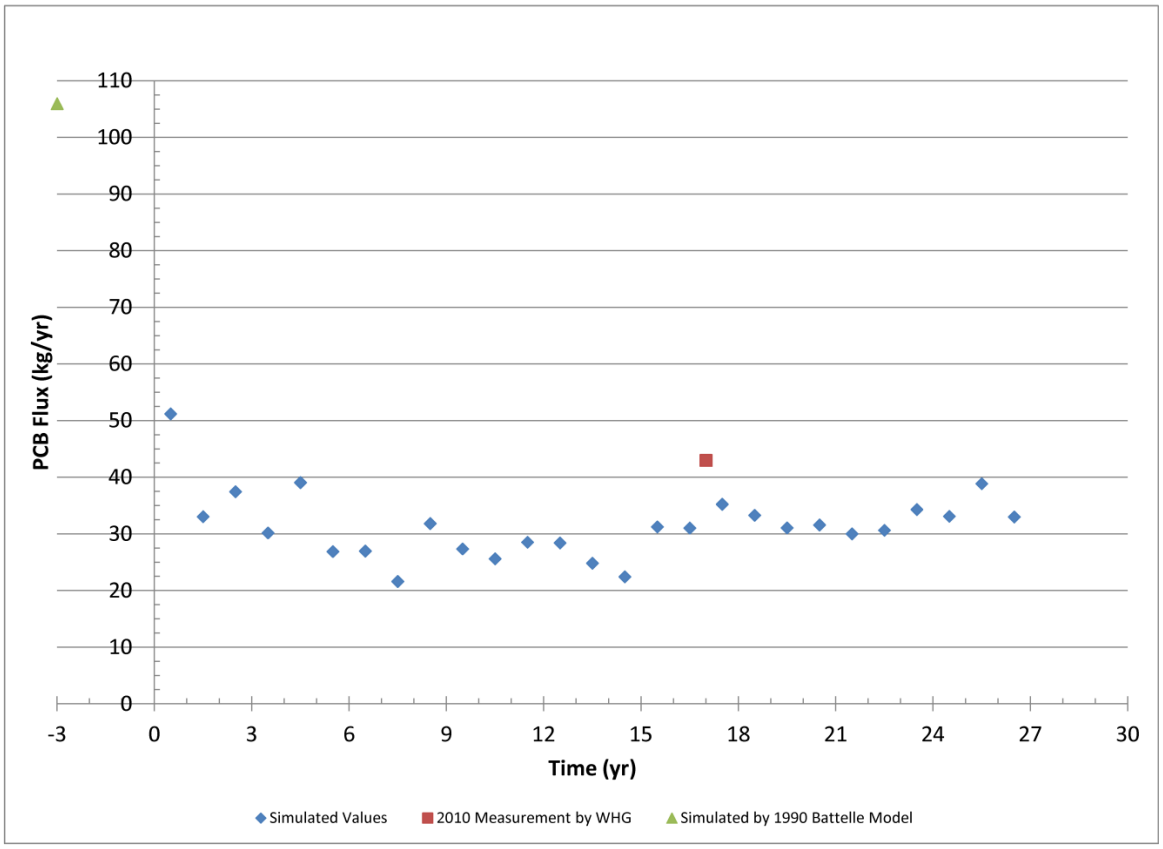

Figure 5-4 Predicted Annual PCB Net Flux to Buzzards Bay at the Hurricane Barrier Prior to Remediation, as compared to measured value by Woods Hole Group (2010) Flux Study.

6 Modeling Results

Using the partially validated LTFATE model of New Bedford Harbor, a 30 year simulation of the selected post-remediation condition in New Bedford Harbor was performed. A description of this scenario, followed by a description of how the model simulation was performed, and the results from this model run are given in this section.

Description of Modeling Scenario

EPA's Project Team chose the following post-remediation scenario to be simulated by LTFATE and run for 30 years. The results from this model simulation was post-processed so that daily averaged water column and bed surface PCB concentrations calculated during the model simulations are spatially averaged over six areas that the three fish closure areas shown in Figure 1-5 as well as the area in the model domain in Buzzards Bay outside of fish closure area 3 were divided into. The six areas are shown in Figure 6-1. These averaged time series for each of the six areas were written to an external data file. The post-remediation scenario was constructed in LTFATE as follows.

a) The bathymetry in the NBH portion of the model domain was updated using the latest bathymetric survey provided by EPA.

b) In the Upper harbor, the concentration of total PCBs in the bottom sediment in the subtidal and mudflat areas was set equal to 10 ppm.

c) In the Outer harbor, the concentration of total PCBs in the bottom sediment was set equal to 1 ppm.

d) The sediment PCB initial concentrations in the non-remediated areas of the NBH was re-interpreted using the 2014 LTM PCB data provided by EPA. The average concentration in these areas has been set to 8 ppm in the Lower Harbor based on the average of the 2014 LTM sampling data from that area of the Harbor.

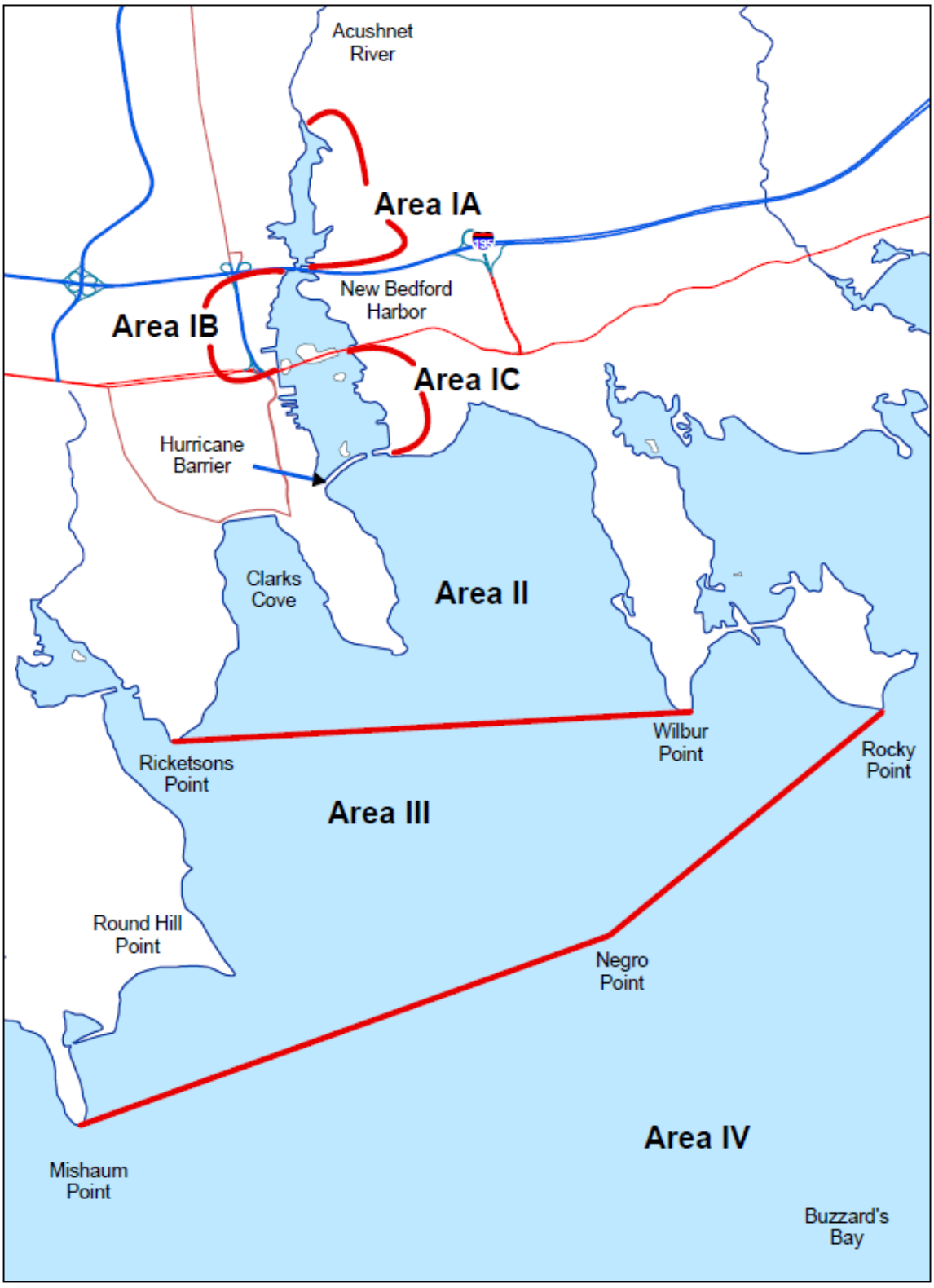

Figure 6-1 Foodchain Model Areas (after Burkhard 2014)

e) In the Lower Harbor, the PCB bed concentrations was set to 15 ppm in the areas where dredging has been performed.

f) The concentration of total PCBs in the cap material covering the LHCC was set equal to 1 ppm.

g) LTFATE was run for eight years to "spin-up" the sediment bed properties specified in the initial sediment bed conditions. This process is commonly used in sediment transport modeling studies as this allows the initially specified sediment bed properties to adjust to the hydrodynamic conditions present in the model domain. The sediment properties in each grid cell at the end of the spin-up model run are written out to a hot-start file. The latter was read at the beginning of the post-remediation model simulation, the results of which are described below.

Model Simulation of the Post-Remediation Scenario

The 30-year model simulation for the chosen post-remediation scenario was driven by the following forcing conditions:

- Tidal boundary conditions around the open water boundaries of the fine grid model in Buzzards Bay (see Figure 4-6) that were extracted from the 30-year simulation of the coarse grid model described in Section 4.

- The 30-year wind speed and direction time series.

- The 30-year of wave conditions as predicted by SWAN.

This model simulation was run on a SGI Linux server. The output files from this simulation were downloaded to a Windows computer for post-processing. The post-processing included a thorough QA/QC check of all the results to insure the following:

- No NaNs (Not a Number) were generated during the simulations. NaNs are usually generated by a computer program when dividing a value by zero, and indicate that something in the model input files is not setup correctly.

- The mass of water and PCBs in the entire model domain were adequately conserved (less than 2 percent loss) over the duration of the 30-year simulation.

- The values of specified state variables (*e.g.*, concentration of suspended sediment of the simulated sediment size classes) were checked to insure none of the outputted values exceeded specified limits. For example, the suspended sediment concentrations were checked to insure the values were no less than 0 mg/L and no higher than 3,000 mg/L. All of the concentrations that were checked were inside these limits.

The following expands on the comment given above that the mass of water and PCBs in the entire model domain were adequately conserved over the duration of the model simulation. LTFATE has an internal mass balance routine that calculates the loss or gain of water mass and that of other model constituents (*i.e.*, PCBs) during a model simulation. Mass loss or gain can occur because the model solves, using the finite volume method, an approximate, *i.e.*, discrete, form of the conservation of mass equations that are numerically solved for water and for PCBs. Mass loss or gain can occur due to numerical dispersion and numerical roundoff. In addition, the cell wetting and drying algorithms in hydrodynamic models are not totally mass conserving because they do not solve the conservation of mass equation. The algorithms consist of an algebraic representation of the actual wetting and drying processes. This necessitates using the mass balance routine to calculate the loss (or main) of water and constituent mass in models where wetting and drying is simulated as it is in the NBH model.

Results of the Post-Remediation Scenarios

The result from the 30-year simulation is shown in Figure 6-2. As seen, the model predicts that the flux of PCBs out of NBH, starting with the conditions in the harbor at the end of remediation, will decline by approximately an order of magnitude over the simulated 30 years following the completion of remediation. Also shown in this figure are the +350 percent and the -350 percent uncertainty envelope about the simulation results. This uncertainty is assumed to be constant over the 30-year simulation, and thus represents a conservative estimate of the uncertainty in the model results.

The relatively smooth nature of this plot is due to the use of annual average flux values. The relatively small increase in the average annual PCB flux from the first year to the second year is due to a large storm event that occurred in the second year of the simulation. This resulted in more erosion in shallower areas of NBH, which increased the concentrations (and mass) of PCBs in the water column. This resulted in the higher flux of PCBs out of the harbor during the second year. The gradual decline in the flux after the second year reflects the very slow loss of PCBs due to the diffusive transport of PCBs from the sediment bed to the water column as well as the loss due to volatilization.

Combining the results shown in Figures 5-4 and 6-2, it is seen that the estimated average annual flux of PCBs to Buzzards Bay 30 years after the completion of remediation is approximately two orders of magnitude less than that before remediation. Considering the remediation of the entire harbor is represented in this simulation, this is at least qualitatively the expected result.

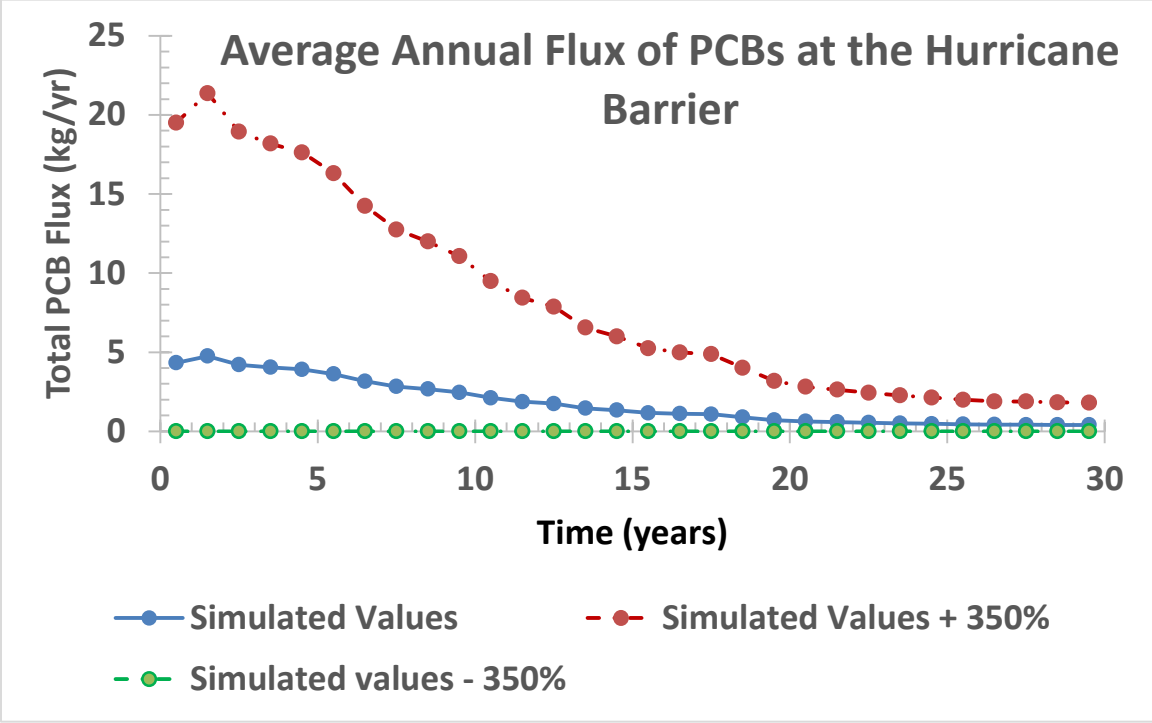

Figure 6-2 Predicted average annual flux of PCBs to Buzzards Bay at the Hurricane Barrier, beginning at the completion of dredging remedy in the Inner Harbor. Positive values indicate flux to the south (out of the harbor).

7 Conclusions

The following conclusions have been formulated from this modeling study.

- The 30-year post-remediation scenario that was run for New Bedford Harbor using LTFATE revealed very slowly changing PCB concentrations in the harbor. Considering the relatively low energy environment inside the harbor as well as the very small load of clean sediment that is transported into the harbor by the Acushnet River, this is not too surprising.

- Resuspension of sediment in the shallower areas of NBH only occurs during simulated nor'easters. This results in the transfer of more PCBs from the sediment bed to the water column due to the release of dissolved PCBs in the porewater of the sediment bed as well as particulate PCBs that are adsorbed onto the sediment that is resuspended.

- The diffusive flux of PCBs from the sediment bed to the overlying water column occurs at a very slow rate. This, in combination to a small loss of PCB mass due to volatilization, contribute to the very slow decrease in PCB concentrations, as reflected by the decreasing flux of PCBs out of the harbor, as seen in the model simulation.

- The simulated average annual flux of PCBs to Buzzards Bay at the Hurricane Barrier 30 years after remediation is complete is approximately two orders of magnitude less than that before remediation.

References

Arega, F., and E.J. Hayter. 2008. "Coupled Consolidation and Contaminant Transport Model for Simulating Migration of Contaminants through Sediment and a Cap," *Journal of Applied Mathematical Modelling*, 32:2413–2428.

Battelle. 1990. Modeling of the transport, distribution and fate of PCBs and heavy metals in the Acushnet River / New Bedford Harbor / Buzzards Bay system. Battelle Memorial Institute, Duxbury, MA.

Battelle Ocean Services. 1991. Overview of the New Bedford Harbor Physical/Chemical Modeling Program, Duxbury, MA.

Bergen B.J., K.A. Rahn, W.G. Nelson. 1998. "Remediation at a Marine Superfund Site: Surficial Sediment PCB Congener Concentration, Composition, and Redistribution," *Environmental Science & Technology* 32:3496-3501.

Booij, N., R.C. Ris and L.H. Holthuijsen, 1999, A third-generation wave model for coastal regions, Part I, Model description and validation, *J. Geophysical Research,* 104(C4): 7649-7666.

Brylawski, B. J., and T.J. Miller. 2006. "Temperature-dependent growth of the blue crab (Callinectes sapidus): a molt process approach," *Canadian Journal of Fisheries and Aquatic Sciences*, 63(6):1298-1308.

Burkhard, L. 2014. "Polychlorinated Biphenyl Food Web Modeling at the New Bedford Harbor Superfund Site," Technical Report, USEPA Environmental Effects Research Laboratory, Duluth, MN. (in preparation).

Cadman, L.R., and M.P. Weinstein. 1985. "Size-Weight Relationships of Postecdysial Juvenile Blue Crabs (Callinectes sapidus Rathbun) from the Lower Chesapeake Bay," *Journal of Crustacean Biology*, 306-310.

Cheng, N.S. 1997. "Simplified settling velocity formula for sediment particles." *Journal of Hydraulic Engineering*, 123(2):149-152.

Dragos, P.M. 2009. Turbidity Monitoring and Plume Sampling Results for City Dredge Disposal at the New Bedford Harbor CAD Cell # 2. Prepared under Contract No. DACW33-03-D-0004, Delivery Order No. 22 by Battelle for the U.S. Army Corps of Engineers. September 2009. 14 pp + Appendices.

EBASCO. 1990. Draft Final Baseline Ecological Risk Assessment New Bedford Harbor Site Feasibility Study. APRIL 1990. EPA Work Assignment Number: 04-1L43. EPA Contract Number: 68-01-7250.

Eldridge Tide and Pilot Book, 1994.

EPA (U.S. Environmental Protection Agency), State of Massachusetts. 2004. Contaminant Monitoring Report for Seafood Harvested in 2002 from the New Bedford Harbor Superfund Site. U.S. Environmental Protection Agency (EPA), Massachusetts Department of Marine Fisheries (DMF), Massachusetts Department of Environmental Protection (DEP).

Fennessy, M.J., K.R. Dyer, and D.A. Huntley. 1994. "INSSEV: an instrument to measure the size and settling velocity of flocs in situ." *Marine Geology*, 117:107-117.

Foster Wheeler Environmental Corporation. 2001. Technical Memorandum Comparison of PCB NOAA Congener with Total Homologue Group Concentrations New Bedford Harbor Superfund Site. Bristol County, Massachusetts. May 2001. Prepared for U.S. Army Corps of Engineers New England District Concord, Massachusetts. USACE Contract NO. DACW33-94-D-0002. Task Order NO. 017. Total Environmental Restoration Contract.

Gailani, J.Z., S.J. Smith, and N.C. Kraus. 2003. Monitoring dredged material disposal at the mouth of the Columbia River, Washington/Oregon, USA. *ERDC/CHL TR-03-5*, U.S. Army Engineer Research and Development Center, Vicksburg, MS.

Galperin, B., L.H. Kantha, S. Hassid, and A. Rosati, 1988. "A quasi-equilibrium turbulent energy model for geophysical flows," *J. Atmos. Sci.*, 45:55-62.

Geyer, W.R. and P. Dragos. 1988. Hydrodynamic Baseline Measurements in New Bedford Harbor prepared for Camp Dresser & McKee Inc., Boston, Mass., by Woods Hole Oceanographic Institution, Woods Hole, MA.

Graf, W.H. 1971. Hydraulics of Sediment Transport. McGraw-Hill, New York.

Hall J., Delorenzo D., S. Sandberg, G. Hunt. 1983. New Bedford Environmental Investigation--Sampling and Analysis of Harbor Bottom Sediment for Polychlorinated Biphenyls (PCBs). Final Report. Volume I. January 1983. Prepared for U.S. Environmental Protection Agency Research Triangle Park, N.C. Contract No. 68-02-3168. Work Assignment No. 79.

Hamrick, J.M. 2007a. "The Environmental Fluid Dynamics Code User Manual: US EPA Version 1.01," Tetra Tech, Inc., Fairfax, VA.

Hamrick, J.M. 2007b. "The Environmental Fluid Dynamics Code Theory and Computation. Volume 1: Hydrodynamics and Mass Transport," Tetra Tech, Inc., Fairfax, VA.

Hamrick, J.M. 2007c. "The Environmental Fluid Dynamics Code Theory and Computation. Volume 2: Sediment and Contaminant Transport and Fate," Tetra Tech, Inc., Fairfax, VA.

Hawker, , Connell, .1988

James, S.C., C.A. Jones, M.D. Grace, and J.D. Roberts. 2010. "Advances in sediment transport modelling." *Journal of Hydraulic Research*, 48: 6, 754-763.

Jepsen, R., J. Roberts, W. Lick. 1997a. "Effects of bulk density on sediment erosion rates," *Water, Air, and Soil Pollution*, 99:21-31.

Johnson, B.H., and M.T. Fong. 1995. "Development and Verification of Numerical Models for Predicting the Initial Fate of Dredged Material Disposed in Open Water, Report 2: Theoretical Developments and Verification Results," Technical Report DRP-93-1, U.S. Engineer Waterways Experiment Station, Vicksburg, MS.

Johnson, B.H. 1990. "User's guide for models of dredged material disposal in open water," *Technical Report D-90-5*, U.S. Army Engineer Waterways Experiment Station, Vicksburg, MS.

Jones, C.A., and W. Lick. 2001. "SEDZLJ: A Sediment Transport Model." *Final Report*. University of California, Santa Barbara, California.

Krank, K., E. Petticrew, T.G. Milligan, and I.G. Droppo. 1993. "In situ particle size distributions resulting from flocculation of suspended sediment," In: Mehta, A.J. (Ed.), *Nearshore and Estuarine Cohesive Sediment Transport*, American Geophysical Union, 60-74.

Krone, R.B. 1963. "A study of rheological properties of estuarial sediments," *Technical Bulletin No. 7*, Committee on Tidal Hydraulics, U.S. Army Engineer Waterways Experiment Station, Vicksburg, Mississippi.

Larsen B.R. 1995. "HRGC separation of PCB congeners," *Journal of High Resolution Chromatography* 18:141-151.

Lick, W.L. 1982. "The transport of contaminants in the Great Lakes," *Annual Review of Earth and Planetary Science*, 10: 327-353.

Madsen, O.S., and P.N. Wikramanayake. 1991. "Simple models for turbulent wave-current bottom boundary layer flow." *Contract Report DRP-91-1*. U.S. Army Engineer Waterways Experiment Station, Vicksburg, MS.

Mase, H. 1989. "Random wave runup height on gentle slope." ASCE, *Journal of Waterway, Port, Coastal, and Ocean Engineering* 85(3): 123-152.

Mase, H. 2001. "Multidirectional random wave transformation model based on energy balance equation." *Coastal Engineering Journal*, 43(4): 317-337.

Mase, H., and T. Kitano. 2000. "Spectrum-based prediction model for random wave transformation over arbitrary bottom topography." *Coastal Engineering Journal*, 42(1): 111-151.

Mase, H., and Y. Iwagaki. 1984. "Runup of random waves on gentle slopes," *Proceeding 19th International Conference on Coastal Engineering*, ASCE, 593-609.

Mase, H., H. Amamori, and T. Takayama. 2005a. “Wave prediction model in wave-current coexisting field.” *Proceedings 12th Canadian Coastal Conference* (CD-ROM).

Mase, H., K. Oki, T.S. Hedges, and H.J. Li. 2005b. “Extended energy-balance-equation wave model for multidirectional random wave transformation.” *Ocean Engineering*, 32(8-9): 961-985.

MA Department of Environmental Protection and MA Div of Marine Fisheries. 2016. “Monitoring Report for Seafood Harvested in 2015 from the New Bedford Harbor Superfund Site.”

Mei, C.C. 1983. The applied dynamics of ocean surface waves, Wiley, New York, 740 p.

McFarland V.A., and J.U. Clarke. 1989. Environmental occurrence, abundance, and potential toxicity of polychlorinated biphenyl congeners: considerations for a congener-specific analysis. *Environmental Health Perspectives*, 81:225.

McNeil, J., C. Taylor, and W. Lick. 1996. “Measurements of erosion of undisturbed bottom sediments with depth.” ASCE, *J. Hydr. Engr.*, 122(6): 316-324.

Mellor, G.L., and T. Yamada. 1982. “Development of a turbulence closure model for geophysical fluid problems.” *Rev. Geophys. Space Phys.*, 20: 851-875.

Meyer-Peter, E., and R. Müller. 1948. “Formulas for bed-load transport.” *Second International Association of Hydraulic Engineering and Research (IAHR) Congress*, Stockholm, Sweden. Delft, Netherlands: IAHR.

Mikkelsen, O.A., Milligan, T.G., Hill, P.S., and Moffatt, D. 2004. “INSSECT—an instrumented platform for investigating floc properties close to the seabed.” *Limnol. Oceanogr. Methods*, 2: 226-236.

Mukai, A.Y., J.J. Westerink, R.A. Luettich, Jr., and D. Mark. 2002. “Eastcoast 2001, A Tidal Constituent Database for the Western North Atlantic, Gulf of Mexico, and Caribbean Sea,” ERDC/CHL TR-02-24, U.S. Army Engineer Research and Development Center, Vicksburg, MS.

Myrhaug, D. 1989. "A rational approach to wave friction coefficients for rough, smooth, and transitional turbulent flow," *Coastal Engineering*, 13:11-21.

Nelson, W. 2009. "The New Bedford Harbor Superfund Site Long-Term Monitoring Program," Fifth international conference on remediation of contaminated sediments, Battelle Inc., Jacksonville, FL.

Nelson, W.G., B.J. Bergen, S.J. Benyi, G. Morrison, R.A. Voyer, C.J. Strobel, S. Rego, G. Thursby, and C.E. Pesch. 1996. "New Bedford Harbor long-term monitoring assessment report: Baseline sampling," U.S. Environmental Protection Agency. National Health and Environmental Effects Research Laboratory, Atlantic Ecology Division. *Research Report 600/R-96/097*.

Nelson, W.G., and B.J. Bergen. 2012. "The New Bedford Harbor Superfund Site long-term monitoring program (1993-2009)," *Environmental Monitoring and Assessment*, 184: 7531-7550.

New Bedford Harbor Trustee Council. 1998. New Bedford Harbor Draft Restoration Plan/Environmental Impact Statement. Available at: http://www.darrp.noaa.gov/northeast/new_bedford/admin.html.

Nielsen, P. 1992. "Coastal Bottom Boundary Layers and Sediment Transport," World Scientific Publishing, Singapore, *Advanced Series on Ocean Engineering*, 4.

NOAA. 1984. NOAA Hazardous Waste Site Report. New Bedford Harbor (1-5). New Bedford, Massachusetts. April 13, 1984. Available at: http://response.restoration.noaa.gov/book_shelf/295_New_Bedford.pdf.

Oceanweather 2007. "Global reanalysis of ocean waves (GROW), Project Description." *Oceanweather Letter Report*, dated 2 October 2007. Oceanweather Inc., Cos Cob, CT, USA.

Partheniades, E. 1965. "Erosion and deposition of cohesive soils." *Journal of the Hydraulic Division*, 91(HY1):105-139.

Raudkivi, A.J. 1998. *Loose Boundary Hydraulics*, 4th ed., Taylor & Francis, London.

Risebrough R.W., P. Reiche, and H. S. Olcott. 1969. “Current progress in the determination of the polychlorinated biphenyls,” *Bulletin of Environmental Contamination and Toxicology*, 4:192-201.

Sanford, L.P. 2008. “Modeling a dynamically varying mixed sediment bed with erosion, deposition, bioturbation, consolidation, and armoring.” *Computers & Geosciences*, 34(10):1263-1283.

Sanford, L.P., P.J. Dickhudt, L. Rubiano-Gomez, M. Yates, S.E. Suttles, C.T. Friedrichs, D.D. Fugate, and H. Romine. 2005. “Variability of suspended particle concentrations, sizes, and settling velocities in the Chesapeake Bay turbidity maximum.” In: Droppo, I.G.; Leppard, G.G.; Liss, S.N.; and Milligan, T.G. (Eds.), *Flocculation in Natural and Engineered Environmental Systems*, CRC Press, Boca Raton, Florida, USA.

Schiller, L., and A. Naumann. 1933. Über die grundlegenden Berechnungen bei der Schwerkraftaufbereitung, Z. VDI, vol. 77.

Schlichting, H., and K. Gersten. 2000. *Boundary-Layer Theory*. Springer, Berlin.

Smith, S.J., and C.T. Friedrichs 2010. “Size and settling velocities of cohesive flocs and suspended sediment aggregates in a trailing suction hopper dredge plume. *Continental Shelf Research*, oi:10.1016/j.csr.2010.04.002.

Smith, S.J., and C.T. Friedrichs. (submitted, 2010). “Image processing methods for in-situ estimation of cohesive sediment floc size, settling velocity, and density,” Submitted to *Limnology and Oceanography: Methods*.

Soulsby, R.L., and R.J.S. Whitehouse. 1997. “Threshold of sediment motion in coastal environments,” *Proceedings Pacific Coasts and Ports '97*, Christchurch, 149 -1 54.

Soulsby, R.L. 1997. *Dynamics of Marine Sands*. Thomas Telford. London.

Summerhayes *et al*., 1977.

Ten Brinke, W.B.M. 1994. “Settling velocities of mud aggregates in the Oosterschelde tidal basin (The Netherlands), determined by a submersible video system,” *Estuar. Coast. Shelf S.*, 39:549-564.

Tetra Tech FW. 2005. After Action Report for North of Wood Street Remediation New Bedford Harbor Superfund Site, New Bedford, Massachusetts.

Torfs, H., J. Jiang, and A. J. Mehta. 2001. "Assessment of the erodibility of fine/coarse sediment mixtures," In: W. H. McAnally and A. J. Mehta (Eds.), *Coastal and Estuarine Fine Sediment Processes*, Elsevier, 109-124.

USACE. 2002. "Coastal Engineering Manual," Manual No. 1110-2-1100, Washington, DC.

USEPA. 1998. "Ambient Water Quality Criteria Derivation Methodology Human Health: Technical Support Document," *EPA-822-B-98-005*.

Van Leussen, W. 1994. "Estuarine Macroflocs and Their Role in Fine-Grained Sediment Transport." Ministry of Transport, Pubic Works and Water Management. Den Haag.

Van Leussen, W.V. and J.M. Cornelisse. 1993. "The determination of the sizes and settling velocities of estuarine flocs by underwater video system." *Neth. J. Sea Res.*, 31(3): 231-241.

Van Leussen, W. 1994. "Estuarine Macroflocs and Their Role in Fine-Grained Sediment Transport," Ministry of Transport, Pubic Works and Water Management. Den Haag.

Van Rijn, L.C. 1984. "Sediment Transport: part I: bedload transport; part ii: suspended load transport: part iii: bed forms and alluvial roughness." *Journal of Hydraulic Engineering* 110(10): 1431-1456; 110(11): 1613-1641, 110(12): 1733-1754.

Wikramanayake, P.N., and Madsen, O.S. 1994a. "Calculation of suspended sediment transport by combined wave-current flows." *Contract Report DRP-94-7*, U.S. Army Engineer Waterway Experiment Station, Vicksburg, MS, USA.

Wikramanayake, P.N., and Madsen, O.S., 1994b. "Calculation of movable bed friction factors." *Contract Report DRP-94-5*, U.S. Army Engineer Waterway Experiment Station, Vicksburg, MS, USA.

Winterwerp, J.C. 2002. “On the flocculation and settling velocity of estuarine mud,” *Cont. Shelf Res.*, 22: 1339-1360.

Winterwerp, J.C. 1998. “A simple model for turbulence induced flocculation of cohesive sediment.” IAHR, *J. Hydraul. Res.*, 36(3):309-326.

Winterwerp, J.C. and van Kesteren, W.G.M. 2004. “Introduction to the Physics of Cohesive Sediment in the Marine Environment,” *Developments in Sedimentology series*, 56, Elsevier. Amsterdam.

Zundel, A. 2006. “Surface-water modeling system reference manual – Version 9.2,” Brigham Young University Environmental Modeling Research Laboratory, Provo, UT.

Appendix A

Hydrodynamics and Transport Governing Equations

The governing equations that are solved by EFDC are the 3D Reynolds-averaged equations of continuity (Equation A-1), linear momentum (Equations A-2 and A-3), hydrostatic pressure (Equation A-4), equation of state (Equation A-5), and transport equations for salinity and temperature (Equations A-6 and A-7), written for curvilinear-orthogonal horizontal coordinates and a sigma vertical coordinate, are given by Hamrick (2007b) and repeated below:

$$\frac{\partial(m\varepsilon)}{\partial t}+\frac{\partial(m_y Hu)}{\partial x}+\frac{\partial(m_x Hv)}{\partial y}+\frac{\partial(mw)}{\partial z}=0 \tag{A-1}$$

$$\begin{aligned}&\frac{\partial(mHu)}{\partial t}+\frac{\partial(m_y Huu)}{\partial x}+\frac{\partial(m_x Hvu)}{\partial y}+\frac{\partial(mwu)}{\partial z}-\\&(mf+v\frac{\partial(m_y)}{\partial x}-u\frac{\partial m_x}{\partial y})Hv=m_y H\frac{\partial(g\varepsilon+p)}{\partial x}-\\&m_y(\frac{\partial H}{\partial x}-z\frac{\partial H}{\partial x})\frac{\partial p}{\partial z}+\frac{\partial(mH^{-1}A_v\frac{\partial u}{\partial z})}{\partial z}+Q_u\end{aligned} \tag{A-2}$$

$$\begin{aligned}&\frac{\partial(mHv)}{\partial t}+\frac{\partial(m_y Huv)}{\partial x}+\frac{\partial(m_x Hvv)}{\partial y}+\frac{\partial(mwv)}{\partial z}+\\&(mf+v\frac{\partial(m_y)}{\partial x}+u\frac{\partial m_x}{\partial y})Hu=m_x H\frac{\partial(g\varepsilon+p)}{\partial y}-\\&m_x(\frac{\partial H}{\partial y}-z\frac{\partial H}{\partial y})\frac{\partial p}{\partial z}+\frac{\partial(mH^{-1}A_v\frac{\partial v}{\partial z})}{\partial z}+Q_v\end{aligned} \tag{A-3}$$

$$\frac{\partial p}{\partial z}=\frac{gH(\rho-\rho_o)}{\rho_o}=gHb \tag{A-4}$$

$$\rho=\rho(p,S,T) \tag{A-5}$$

$$\frac{\partial(mHS)}{\partial t}+\frac{\partial(m_y HuS)}{\partial x}+\frac{\partial(m_x HvS)}{\partial y}+\frac{\partial(mwS)}{\partial z}=\frac{\partial(\frac{mA_b}{H}\frac{\partial S}{\partial z})}{\partial z}+Q_s \quad \text{(A-6)}$$

$$\frac{\partial(mHT)}{\partial t}+\frac{\partial(m_y HuT)}{\partial x}+\frac{\partial(m_x HvT)}{\partial y}+\frac{\partial(mwT)}{\partial z}=\frac{\partial(\frac{mA_b}{H}\frac{\partial T}{\partial z})}{\partial z}+Q_T \quad \text{(A-7)}$$

where *u* and *v* are the mean horizontal velocity components in (*x*,*y*) coordinates; m_x and m_y are the square roots of the diagonal components of the metric tensor, and $m = m_x m_y$ is the Jacobian or square root of the metric tensor determinant; *p* is the pressure in excess of the reference pressure, $\frac{\rho_o gH(1-z)}{\rho_o}$, where ρ_o is the reference density; *f* is the Coriolis parameter for latitudinal variation; A_v is the vertical turbulent viscosity; and A_b is the vertical turbulent diffusivity. The buoyancy *b* in Equation A-4 is the normalized deviation of density from the reference value. Equation A-5 is the equation of state that calculates water density (ρ) as functions of *p*, salinity (*S*) and temperature (*T*).

The sigma (stretching) transformation and mapping of the vertical coordinate is given as

$$z=\frac{(z^*+h)}{(\xi+h)} \quad \text{(A-8)}$$

where *z** is the physical vertical coordinate, and *h* and ξ are the depth below and the displacement about the undisturbed physical vertical coordinate origin, *z** = 0, respectively, and $H = h + \xi$ is the total depth. The vertical velocity in z coordinates, *w*, is related to the physical vertical velocity *w** by

$$w = w^* - z(\frac{\partial\xi}{\partial t}+\frac{u}{m_x}\frac{\partial\xi}{\partial x}+\frac{v}{m_y}\frac{\partial\xi}{\partial y})+(1-z)(\frac{u}{m_x}\frac{\partial h}{\partial x}+\frac{v}{m_y}\frac{\partial h}{\partial y}) \quad \text{(A-9)}$$

The solutions of Equations A-2, A-3, A-6 and A-7 require the values for the vertical turbulent viscosity and diffusivity and the source and sink terms. The vertical eddy viscosity and diffusivity, A_v and A_b, are parameterized according to the level 2.5 (second-order) turbulence closure model of Mellor and Yamada (1982), as modified by Galperin *et al.* (1988), in which the vertical eddy viscosities are calculated based on the turbulent kinetic energy and the turbulent

macroscale equations. The Mellor and Yamada level 2.5 (MY2.5) turbulence closure model is derived starting from the Reynolds stress and turbulent heat flux equations under the assumption of a nearly isotropic environment, where the Reynolds stress is generated due to the exchange of momentum in turbulent mixing. To make the turbulence equations closed, all empirical constants are obtained by assuming that turbulent heat production is primarily balanced by turbulent dissipation.

The vertical turbulent viscosity and diffusivity are related to the turbulent intensity, q^2, turbulent length scale, l and a Richardson number R_q as follows:

$$A_v = \Phi_v ql = 0.4(1+36R_q)^{-1}(1+6R_q)^{-1}(1+8R_q)ql \tag{A-10}$$

$$A_b = \Phi_b ql = 0.5(1+36R_q)^{-1}ql \tag{A-11}$$

where A_v and A_b are stability functions that account for reduced and enhanced vertical mixing or transport in stable and unstable vertical, density-stratified environments, respectively, and the local Richardson number is given as

$$R_q = \frac{gH\dfrac{\partial b}{\partial z}}{q^2}\frac{l^2}{H^2} \tag{A-12}$$

A critical Richardson number, R_q = 0.20, was found at which turbulence and mixing cease to exist (Mellor and Yamada, 1982). Galperin *et al.* (1988) introduced a length scale limitation by imposing an upper limit for the mixing length to account for the limitation of the vertical turbulent excursions in stably stratified flows. They also introduced stability functions that account for reduced or enhanced vertical mixing for different stratification regimes.

The turbulence intensity (q^2) and the turbulence length scale (l) are computed using the following two transport equations:

$$\frac{\partial(mHq^2)}{\partial t}+\frac{\partial(m_yHuq^2)}{\partial x}+\frac{\partial(m_xHvq^2)}{\partial y}+\frac{\partial(mwq^2)}{\partial z}=\frac{\partial(\dfrac{mA_q\dfrac{\partial q^2}{\partial z}}{H})}{\partial z}+Q_q$$
$$+2\frac{mA_v}{H}((\frac{\partial^2 u}{\partial z^2})+(\frac{\partial^2 v}{\partial z^2}))+2mgA_b\frac{\partial b}{\partial z}-2mH(\frac{q^3}{(B_1 l)}) \tag{A-13}$$

$$\frac{\partial(mHq^2l)}{\partial t}+\frac{\partial(m_yHuq^2l)}{\partial x}+\frac{\partial(m_xHvq^2l)}{\partial y}+\frac{\partial(mwq^2l)}{\partial z}=\frac{\partial(\frac{mA_q\frac{\partial q^2l}{\partial z}}{H})}{\partial z}+Q_l \qquad \text{(A-14)}$$
$$+2\frac{mE_1lA_v}{H}((\frac{\partial^2u}{\partial z^2})+(\frac{\partial^2v}{\partial z^2}))+mgE_1E_3lA_b\frac{\partial b}{\partial z}-H(\frac{q^3}{(B_1)})(1+E_2(\kappa L)^{-2}l^2)$$

The above two equations include a wall proximity function, $W=1+E_2l(\kappa L)^{-2}$, that assures a positive value of diffusion coefficient $L^{-1}=(H)^{-1}(z^{-1}+(1-z)^{-1}))$. B_1, E_1, E_2, and E_3 are empirical constants with values 16.6, 1.8, 1.33, and 0.53, respectively. All terms with *Q's* (Q_u, Q_v, Q_q, Q_l, Q_s, Q_T) are sub-grid scale sink-source terms that are modeled as sub-grid scale horizontal diffusion. The vertical diffusivity, A_q, is in general taken to be equal to the vertical turbulent viscosity, A_v (Hamrick, 2007b).

The vertical boundary conditions for the solutions of the momentum equations are based on specification of the kinematic shear stresses. At the bottom, the bed shear stresses are computed using the near bed velocity components (u_1,v_1) as:

$$(\tau_{bx},\tau_{by})=c_b\sqrt{u_1^2+v_1^2}(u_1,v_1) \qquad \text{(A-15)}$$

where the bottom drag coefficient $c_b=(\frac{\kappa}{\ln(\Delta_1/2z_o)})^2$, where κ is the von Karman constant, Δ_1 is the dimensionless thickness of the bottom layer, $z_o = z_o^*/H$ is the dimensionless roughness height, and z_o^* is roughness height in meters. At the surface layer, the shear stresses are computed using the *u*, *v* components of the wind velocity (u_w,v_w) above the water surface (usually measured at 10 m above the surface) and are given as:

$$(\tau_{sx},\tau_{sy})=c_s\sqrt{u_w^2+v_w^2}(u_w,v_w) \qquad \text{(A-16)}$$

where $c_s=0.001\frac{\rho_a}{\rho_w}(0.8+0.065\sqrt{u_w{}^2+v_w^2})$ and ρ_a and ρ_w are the air and water densities, respectively. Zero flux vertical boundary conditions are used for the transport equations.

The generic transport equation solved in EFDC for a dissolved (*e.g.*, chemical contaminant) or suspended (*e.g.*, sediment) constituent having a mass per unit volume concentration *C*, is

$$\frac{\partial m_x m_y HC}{\partial t}+\frac{\partial m_y HuC}{\partial_x}+\frac{\partial m_x HvC}{\partial y}+\frac{\partial m_x m_y wC}{\partial z}-\frac{\partial m_x m_y w_{sc} C}{\partial z}=$$
$$\frac{\partial}{\partial_x}\left(\frac{m_y}{m_x}HK_H\frac{\partial C}{\partial x}\right)+\frac{\partial}{\partial_y}\left(\frac{m_x}{m_y}HK_H\frac{\partial C}{\partial y}\right)+\frac{\partial}{\partial_z}\left(m_x m_y\frac{K_v}{H}\frac{\partial C}{\partial z}\right)+Q_c \qquad \text{(A-17)}$$

where K_V and K_H are the vertical and horizontal turbulent diffusion coefficients, respectively; w_{sc} is a positive settling velocity when C represents the mass concentration of suspended sediment; and Q_c represents external sources or sinks and reactive internal sources or sinks. For sediment, $C = S_j$, where S_j represents the concentration of the *jth* sediment class. The solution procedure is the same as that for the salinity and heat transport equations, which use a high-order upwind difference solution scheme for the advection terms (Hamrick, 2007b). Although the advection scheme is designed to minimize numerical diffusion, a small amount of horizontal diffusion remains inherent in the numerical scheme. As such, the horizontal diffusion terms in Equation 2-17 are omitted by setting K_H equal to zero.

The transport equations solved by the contaminant transport model are given below. The transport equation for the freely dissolved chemical is:

$$\partial_t\left(m_x m_y HC_w\right)+\partial_x\left(m_y HuC_w\right)+\partial_y\left(m_x HvC_w\right)+\partial_z\left(m_x m_y wC_w\right)$$
$$=\partial_z\left(m_x m_y\frac{A_b}{H}\partial_z C_w\right)+m_x m_y H\left(\sum_i\left(K_{dS}^i S^i\chi_S^i\right)+\sum_j\left(K_{dD}^j D^j\chi_D^j\right)\right)$$
$$-m_x m_y H\begin{pmatrix}\sum_i\left(K_{aS}^i S^i\right)\left(\psi_w\frac{C_w}{\phi}\right)\left(\hat{\chi}_S^i-\chi_S^i\right)\\+\sum_j\left(K_{aD}^j D^j\right)\left(\psi_w\frac{C_w}{\phi}\right)\left(\hat{\chi}_D^j-\chi_D^j\right)+\gamma C_w\end{pmatrix} \qquad \text{(A-18)}$$

where C_w is the mass of freely dissolved contaminant per unit total volume, C_S is the mass of contaminant sorbed to sediment class *i* per mass of sediment, C_D is the mass of contaminant sorbed to dissolved material *j* per unit mass of dissolved material, φ is the porosity, ψ_w is the fraction of the freely dissolved contaminant available for sorption, K_a is the adsorption rate, K_d is the desorption rate, and γ is a net linearized decay rate coefficient. Since equilibrium partitioning is assumed, the adsorption and desorption rates are both equal to zero.

The sorption kinetics are based on the Langmuir isotherm (Chapra, 1997) with $\hat{\chi}$ denoting the saturation adsorbed mass per carrier mass. The solids and dissolved material (*i.e.*, DOC) concentrations, *S* and *D*, respectively, are defined as mass per unit total volume. The index *j* is the number of contaminants, and the index *i* is the number of classes of solids, *i.e.*, organic particulate matter and inorganic sediment. The transport equation for the contaminant adsorbed to DOC is:

$$\begin{aligned}&\partial_t\left(m_x m_y H D^j \chi_D^j\right)+\partial_x\left(m_y H u D^j \chi_D^j\right)+\partial_y\left(m_x H v D^j \chi_D^j\right)+\partial_z\left(m_x m_y w D^j \chi_D^j\right)\\&\quad=\partial_z\left(m_x m_y \frac{A_b}{H}\partial_z\left(D^j \chi_D^j\right)\right)+m_x m_y H\left(K_{sD}^j D^j\right)\left(\psi_w \frac{C_w}{\phi}\right)\left(\hat{\chi}_D^j-\chi_D^j\right)\\&\qquad -m_x m_y H\left(K_{dD}^j+\gamma\right)\left(D^j \chi_D^j\right)\end{aligned} \tag{A-19}$$

The transport equation for the contaminant adsorbed to suspended solids is:

$$\begin{aligned}&\partial_t\left(m_x m_y H S^i \chi_S^i\right)+\partial_x\left(m_y H u S^i \chi_S^i\right)+\partial_y\left(m_x H v S^i \chi_S^i\right)+\partial_z\left(m_x m_y w S^i \chi_S^i\right)\\&\qquad +\partial_z\left(m_x m_y w_S^i S^i \chi_S^i\right)=\partial_z\left(m_x m_y \frac{A_b}{H}\partial_z\left(S^i \chi_S^i\right)\right)\\&+m_x m_y H\left(K_{aS}^i S^i\right)\left(\psi_w \frac{C_w}{\phi}\right)\left(\hat{\chi}_S^i-\chi_S^i\right)-m_x m_y H\left(K_{dS}^i+\gamma\right)\left(S^i \chi_S^i\right)\end{aligned} \tag{A-20}$$

The concentrations (in units of sorbed mass per unit total volume) of chemicals adsorbed to DOC and solids, C_D and C_S, respectively, are defined as:

$$C_D^j = D^j \chi_D^j \tag{A-21}$$

$$C_S^i = S^i \chi_S^i \tag{A-22}$$

Introducing Equations A.21 and A.22 into Equations A.18 – A.20 gives:

$$\begin{aligned}
&\partial_t\left(m_x m_y H C_w\right)+\partial_x\left(m_y H u C_w\right)+\partial_y\left(m_x H v C_w\right)+\partial_z\left(m_x m_y w C_w\right)\\
&=\partial_z\left(m_x m_y \frac{A_b}{H}\partial_z C_w\right)+m_x m_y H\left(\sum_i\left(K_{dS}^i C_S^i\right)+\sum_j\left(K_{dD}^j C_D^j\right)\right)\\
&\quad -m_x m_y H\left(\begin{array}{c}\sum_i\left(K_{aS}^i S^i\right)\left(\psi_w\frac{C_w}{\phi}\right)\left(\hat{\chi}_S^i-\chi_S^i\right)\\ +\sum_j\left(K_{aD}^j D^j\right)\left(\psi_w\frac{C_w}{\phi}\right)\left(\hat{\chi}_D^j-\chi_D^j\right)+\gamma C_w\end{array}\right)
\end{aligned} \tag{A-23}$$

$$\begin{aligned}
&\partial_t\left(m_x m_y H C_D^j\right)+\partial_x\left(m_y H u C_D^j\right)+\partial_y\left(m_x H v C_D^j\right)+\partial_z\left(m_x m_y w C_D^j\right)\\
&=\partial_z\left(m_x m_y \frac{A_b}{H}\partial_z C_D^j\right)+m_x m_y H\left(K_{sD}^j D^j\right)\left(\psi_w\frac{C_w}{\phi}\right)\left(\hat{\chi}_D^j-\chi_D^j\right)\\
&\quad -m_x m_y H\left(K_{dD}^j+\gamma\right)C_D^j
\end{aligned} \tag{A-24}$$

$$\begin{aligned}
&\partial_t\left(m_x m_y H C_S^i\right)+\partial_x\left(m_y H u C_S^i\right)+\partial_y\left(m_x H v C_S^i\right)+\partial_z\left(m_x m_y w C_S^i\right)\\
&\quad +\partial_z\left(m_x m_y w_S^i C_S^i\right)=\partial_z\left(m_x m_y \frac{A_b}{H}\partial_z C_S^i\right)\\
&+m_x m_y H\left(K_{aS}^i S^i\right)\left(\psi_w\frac{C_w}{\phi}\right)\left(\hat{\chi}_S^i-\chi_S^i\right)-m_x m_y H\left(K_{dS}^i+\gamma\right)C_S^i
\end{aligned} \tag{A-25}$$

The EFDC sorbed contaminant transport formulation currently assumes equilibrium partitioning with the adsorption and desorption terms in Equations A-24 and A-25 being equal, such that:

$$\left(K_{sD}^j D^j\right)\left(\psi_w\frac{C_w}{\phi}\right)\left(\hat{\chi}_D^j-\chi_D^j\right)=K_{dD}^j C_D^j \tag{A-26}$$

$$\left(K_{aS}^i S^i\right)\left(\psi_w\frac{C_w}{\phi}\right)\left(\hat{\chi}_S^i-\chi_S^i\right)=K_{dS}^i C_S^i \tag{A-27}$$

Solving Equations A-26 and A-27 for the ratio of C_D and C_S to C_w gives

$$\frac{C_D^j}{C_w}=\frac{f_D^j}{f_w}=P_D^j\frac{D^j}{\phi} \tag{A-28}$$

$$\frac{C_S^i}{C_w} = \frac{f_S^i}{f_w} = P_S^i \frac{S^i}{\phi} \tag{A-29}$$

where *P* is the partition coefficient. With the relationship between the mass fractions expressed as

$$f_w + \sum_i f_S^i + \sum_j f_D^j = 1 \tag{A-30}$$

the expressions for these three fractions are given by:

$$f_w = \frac{C_w}{C} = \frac{\phi}{\phi + \sum_i P_S^i S^i + \sum_j P_D^j D^j}$$

$$f_D^j = \frac{C_D^j}{C} = \frac{P_D^j D^j}{\phi + \sum_i P_S^i S^i + \sum_j P_D^j D^j} \tag{A-31}$$

$$f_S^i = \frac{C_S^i}{C} = \frac{P_S^i S^i}{\phi + \sum_i P_S^i S^i + \sum_j P_D^j D^j}$$

Adding Equations A-23, A-24, and A-25, and using the equilibrium partitioning relationships given by Equations A-26 and A-27 gives the following transport equation for the total contaminant concentration:

$$\begin{aligned} &\partial_t \left(m_x m_y HC \right) + \frac{1}{m_x m_y} \partial_x \left(m_y HuC \right) + \frac{1}{m_x m_y} \partial_y \left(m_x HvC \right) + \partial_z \left(m_x m_y wC \right) \\ &\quad -\partial_z \left(m_x m_y \sum_i w_s^i f_s^i C \right) = \partial_z \left(m_x m_y \frac{A_b}{H} \partial_z C \right) - m_x m_y H \gamma C \end{aligned} \tag{A-32}$$

Equation A-32 is solved for *C*, and then the concentrations for the three phases are solved for using the relationships given by Equation A-31. The bottom boundary condition for Equation A-32 is given by Hamrick (2007c). In addition, the one-dimensional (vertical) transport equation for C_w in the pore water in the sediment bed that is solved in each grid cell is given by Hamrick (2007c).

Appendix B

Temperature and Salinity Profiles

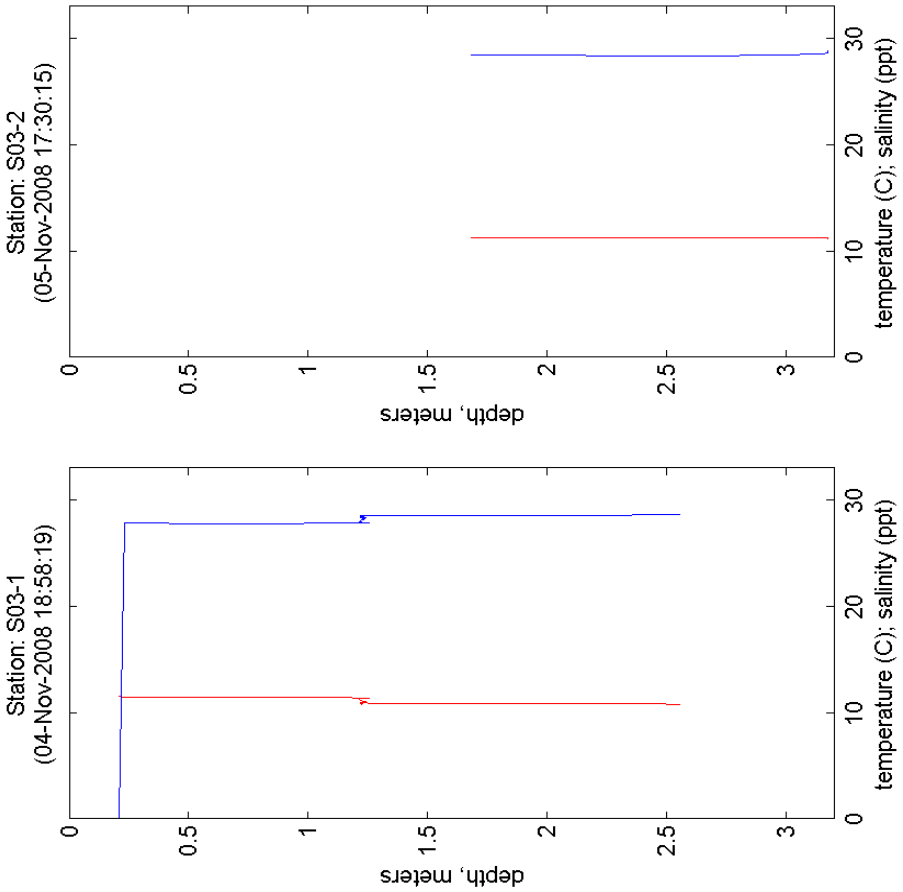

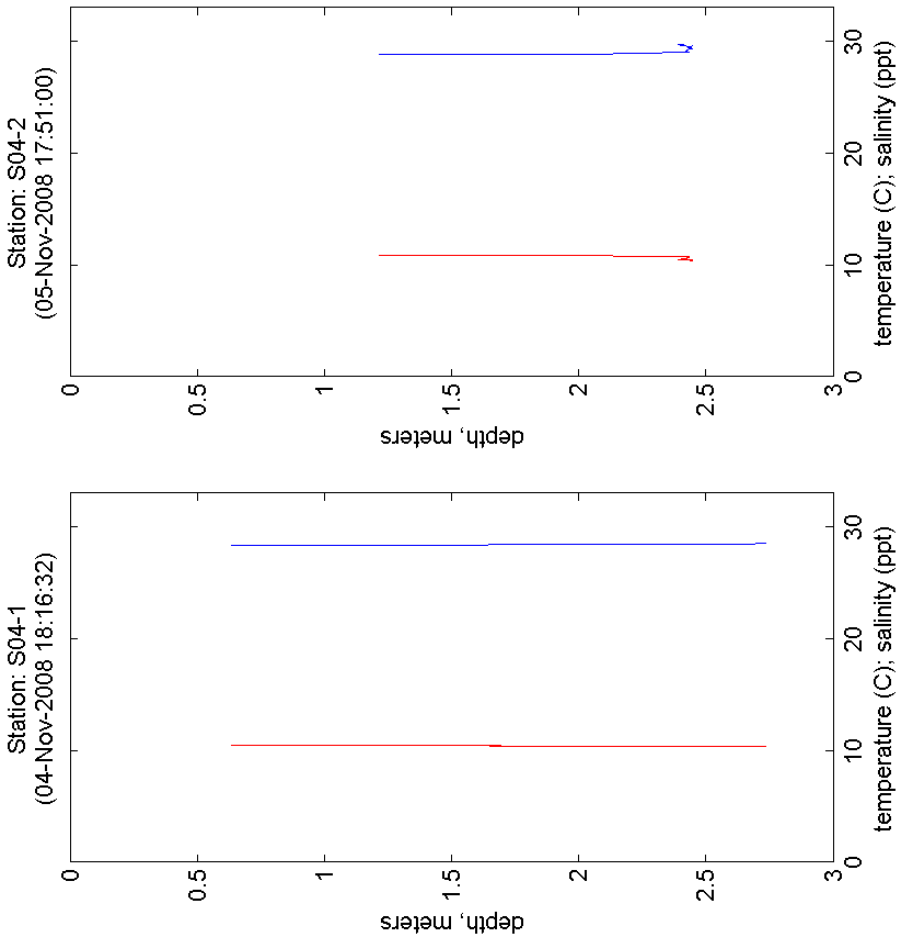
Station: S04-2
(05-Nov-2008 17:51:00)
depth, meters
temperature (C); salinity (ppt)
0
0.5
1
1.5
2
2.5
3
0
10
20
30
Station: S04-1
(04-Nov-2008 18:16:32)
depth, meters
temperature (C); salinity (ppt)

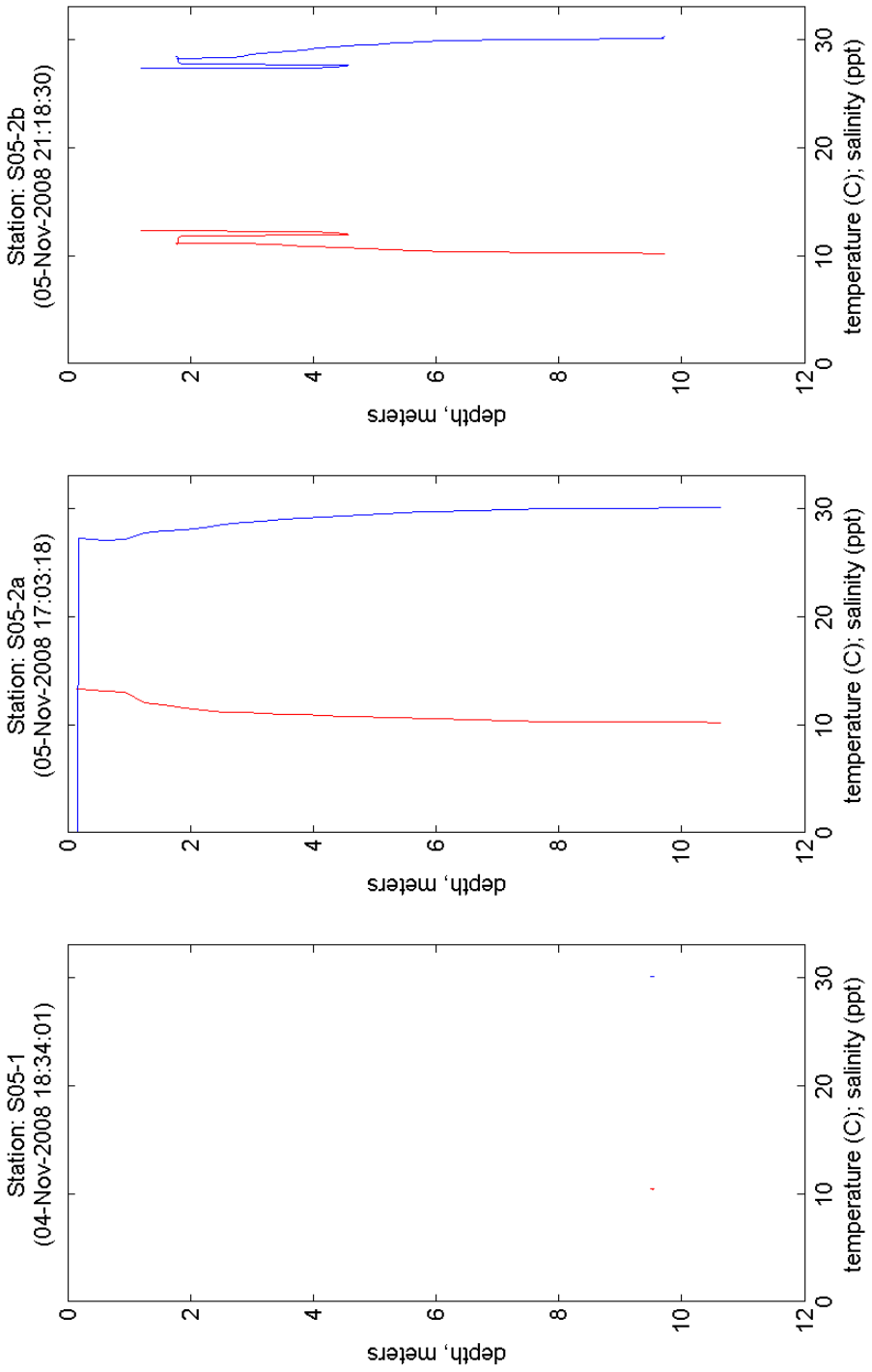
Station: S05-2b
(05-Nov-2008 21:18:30)
Station: S05-2a
(05-Nov-2008 17:03:18)
Station: S05-1
(04-Nov-2008 18:34:01)
depth, meters
temperature (C); salinity (ppt)
0
2
4
6
8
10
12
0
10
20
30

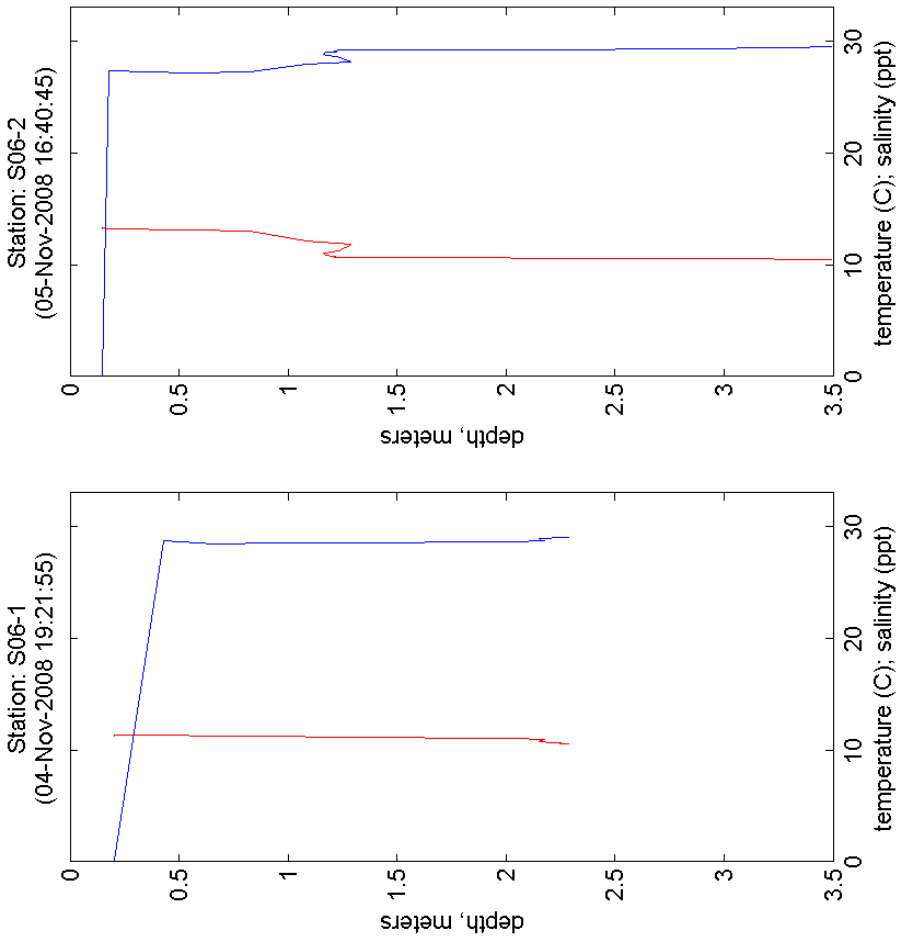
Station: S06-2
(05-Nov-2008 16:40:45)
depth, meters
temperature (C); salinity (ppt)
0
0.5
1
1.5
2
2.5
3
3.5
0
10
20
30
Station: S06-1
(04-Nov-2008 19:21:55)
depth, meters
temperature (C); salinity (ppt)

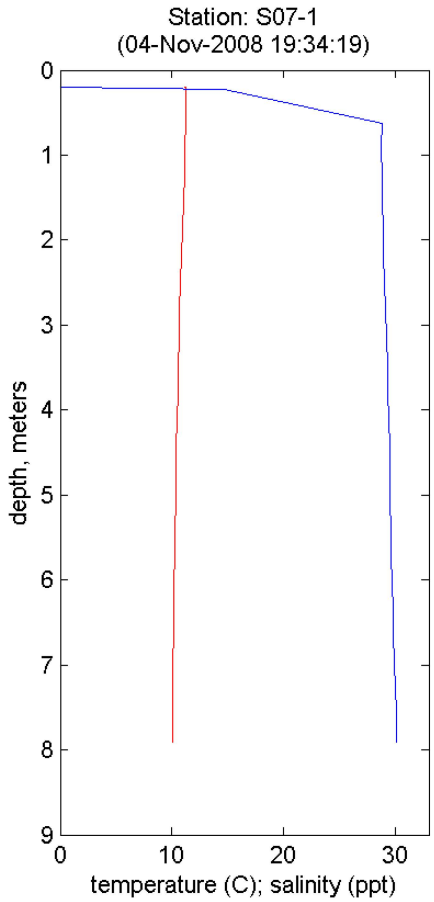
Station: S07-1
(04-Nov-2008 19:34:19)
depth, meters
temperature (C); salinity (ppt)
0
1
2
3
4
5
6
7
8
9
0
10
20
30

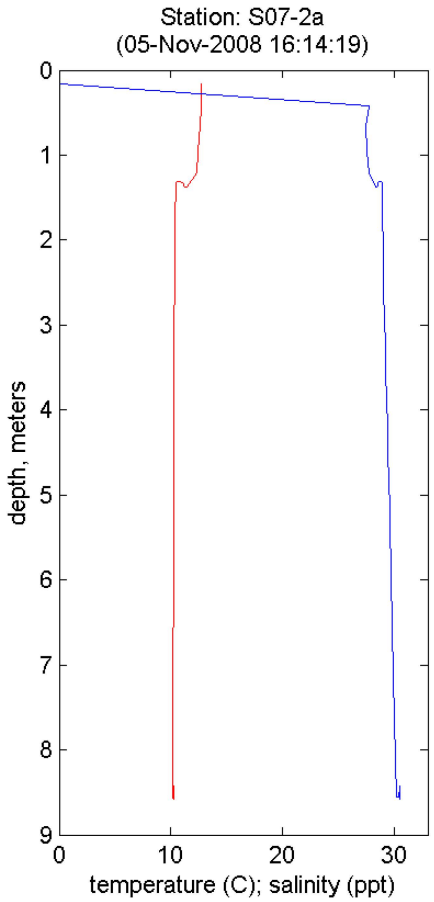
Station: S07-2a
(05-Nov-2008 16:14:19)
depth, meters
temperature (C); salinity (ppt)
0
1
2
3
4
5
6
7
8
9
0
10
20
30

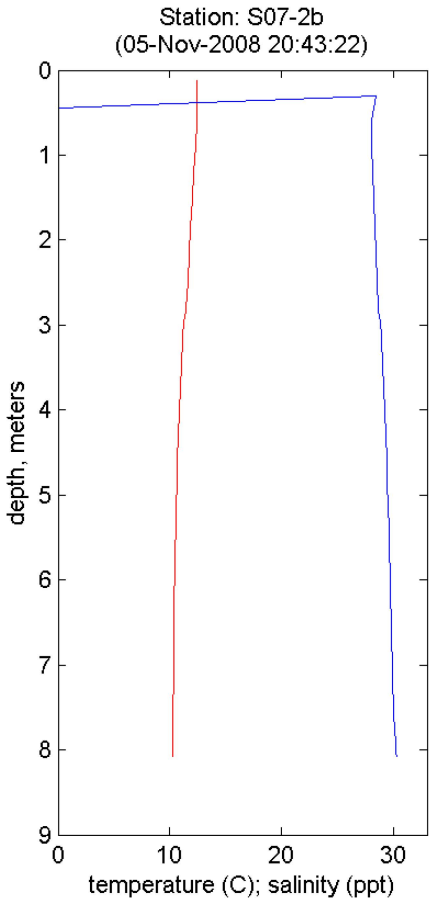
Station: S07-2b
(05-Nov-2008 20:43:22)
depth, meters
temperature (C); salinity (ppt)
0
1
2
3
4
5
6
7
8
9
0
10
20
30

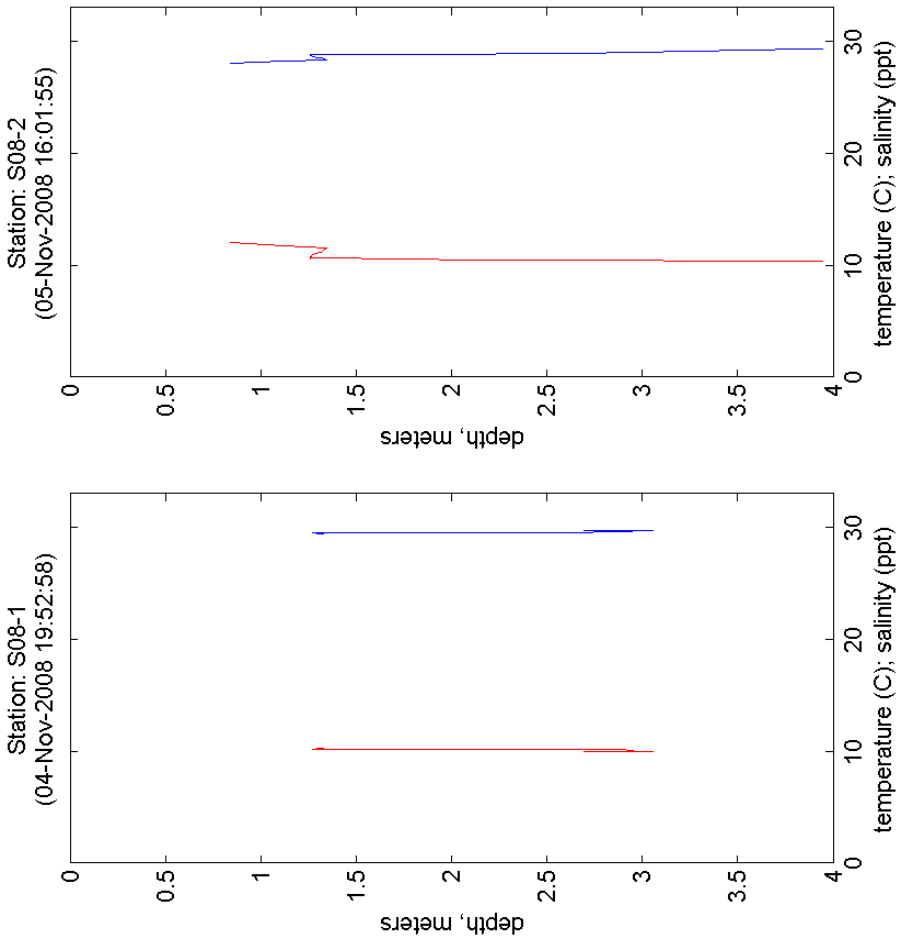
Station: S08-2
(05-Nov-2008 16:01:55)
depth, meters
temperature (C); salinity (ppt)
0
0.5
1
1.5
2
2.5
3
3.5
4
0
10
20
30
Station: S08-1
(04-Nov-2008 19:52:58)
depth, meters
temperature (C); salinity (ppt)

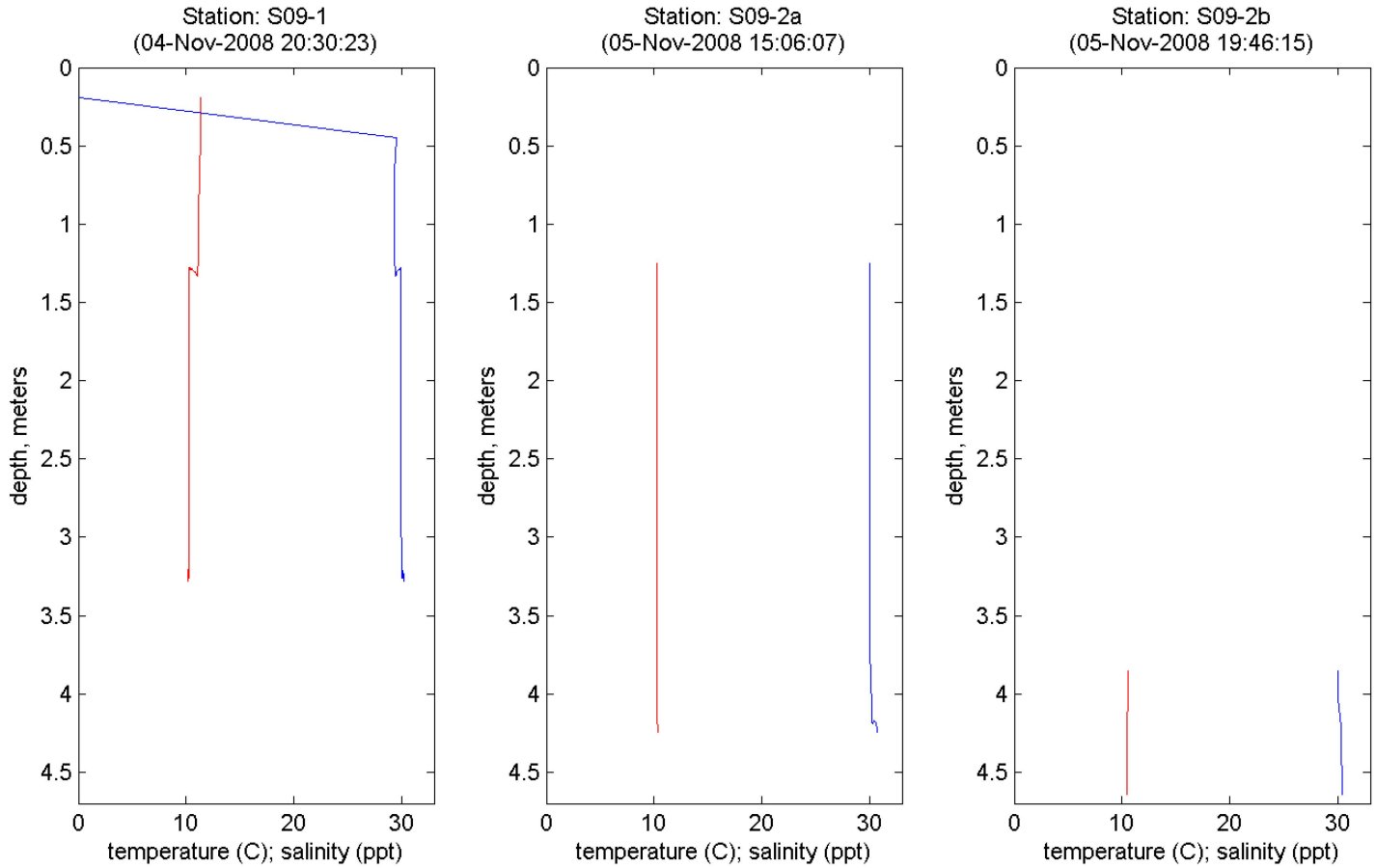
Station: S09-1
(04-Nov-2008 20:30:23)
depth, meters
temperature (C); salinity (ppt)
Station: S09-2a
(05-Nov-2008 15:06:07)
depth, meters
temperature (C); salinity (ppt)
Station: S09-2b
(05-Nov-2008 19:46:15)
depth, meters
temperature (C); salinity (ppt)

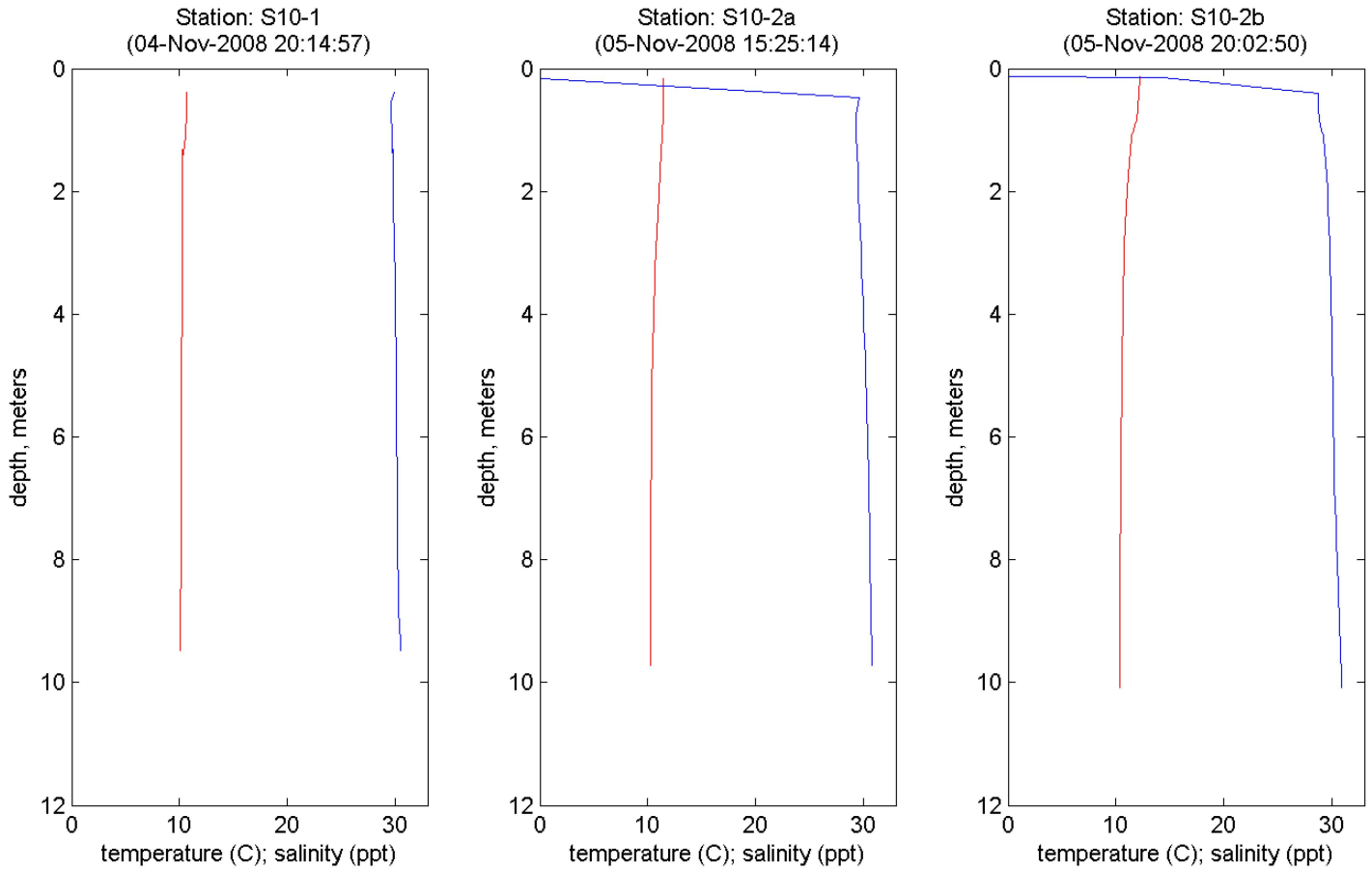
Station: S10-1
(04-Nov-2008 20:14:57)
depth, meters
temperature (C); salinity (ppt)
Station: S10-2a
(05-Nov-2008 15:25:14)
depth, meters
temperature (C); salinity (ppt)
Station: S10-2b
(05-Nov-2008 20:02:50)
depth, meters
temperature (C); salinity (ppt)

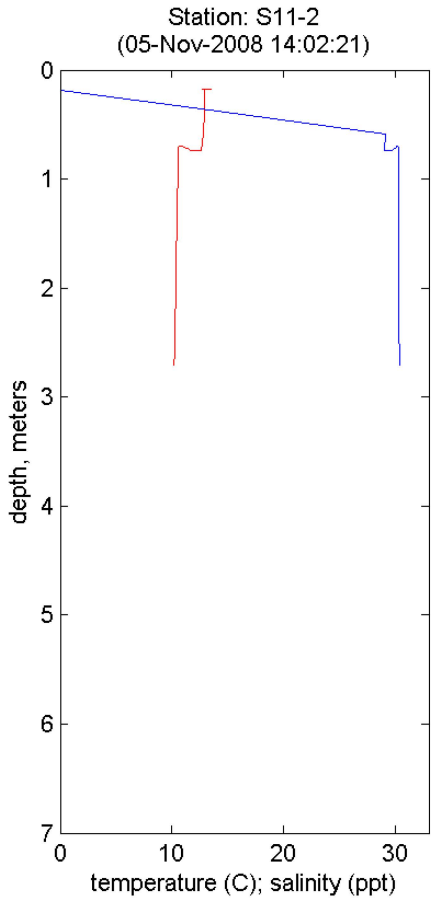
Station: S11-2
(05-Nov-2008 14:02:21)
depth, meters
temperature (C); salinity (ppt)
0
1
2
3
4
5
6
7
0
10
20
30

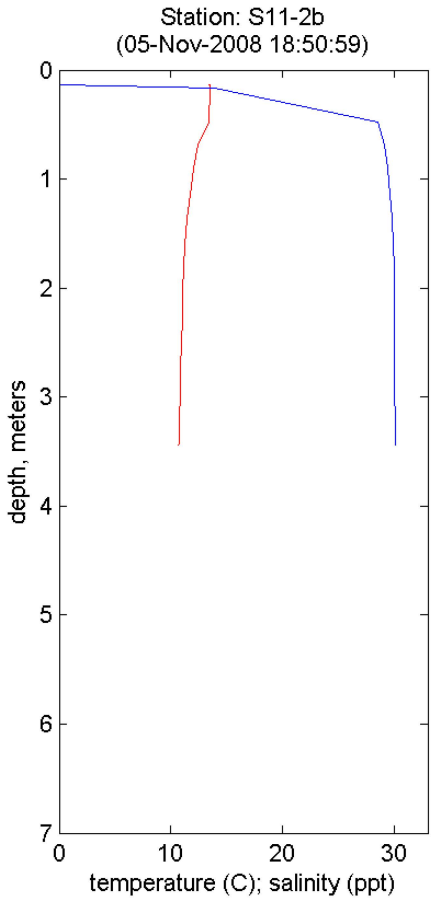
Station: S11-2b
(05-Nov-2008 18:50:59)
depth, meters
temperature (C); salinity (ppt)
0
1
2
3
4
5
6
7
0
10
20
30

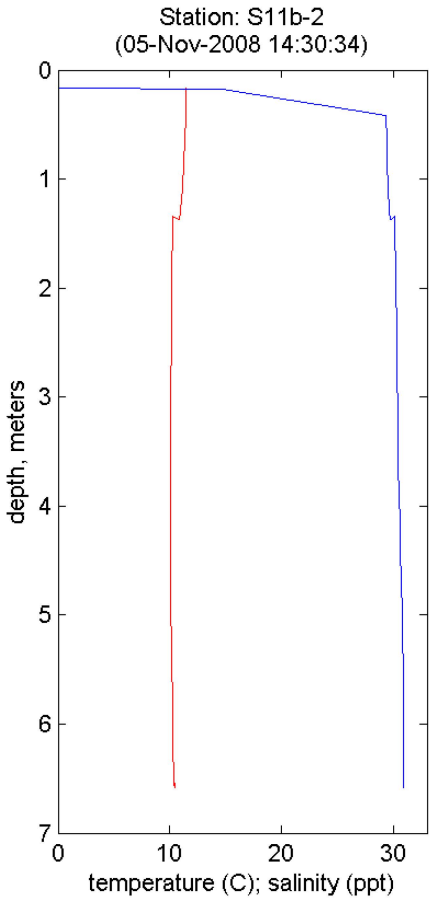
Station: S11b-2
(05-Nov-2008 14:30:34)
depth, meters
temperature (C); salinity (ppt)
0
1
2
3
4
5
6
7
0
10
20
30

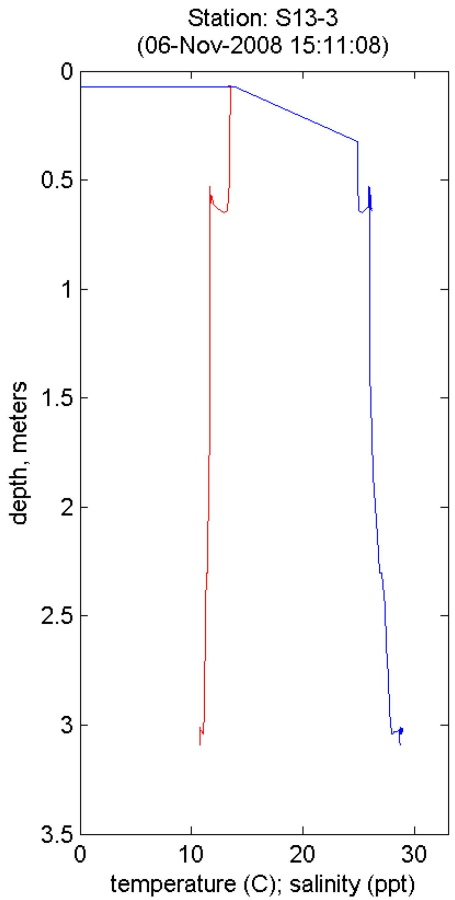
Station: S13-3
(06-Nov-2008 15:11:08)
depth, meters
temperature (C); salinity (ppt)
0
0.5
1
1.5
2
2.5
3
3.5
0
10
20
30

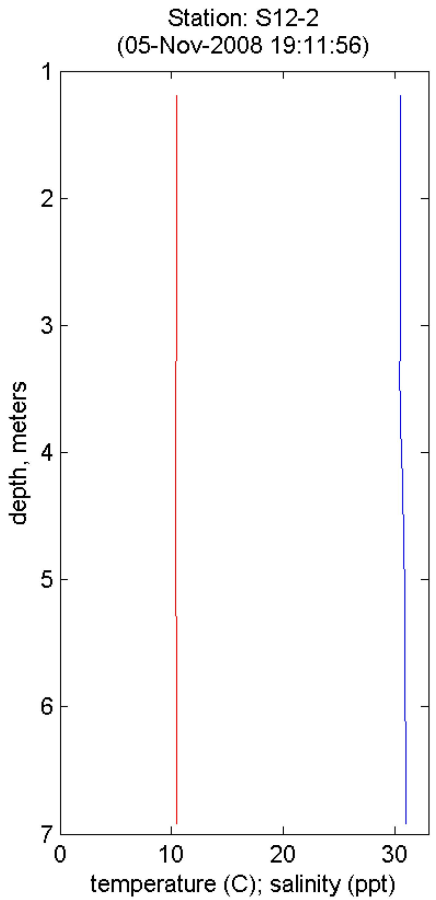
Station: S12-2
(05-Nov-2008 19:11:56)
depth, meters
temperature (C); salinity (ppt)
1
2
3
4
5
6
7
0
10
20
30

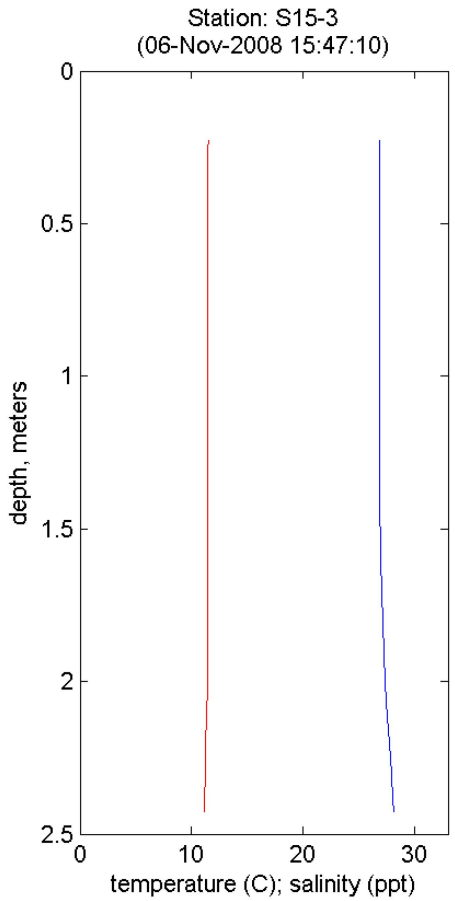
Station: S15-3
(06-Nov-2008 15:47:10)
depth, meters
temperature (C); salinity (ppt)
0
0.5
1
1.5
2
2.5
0
10
20
30

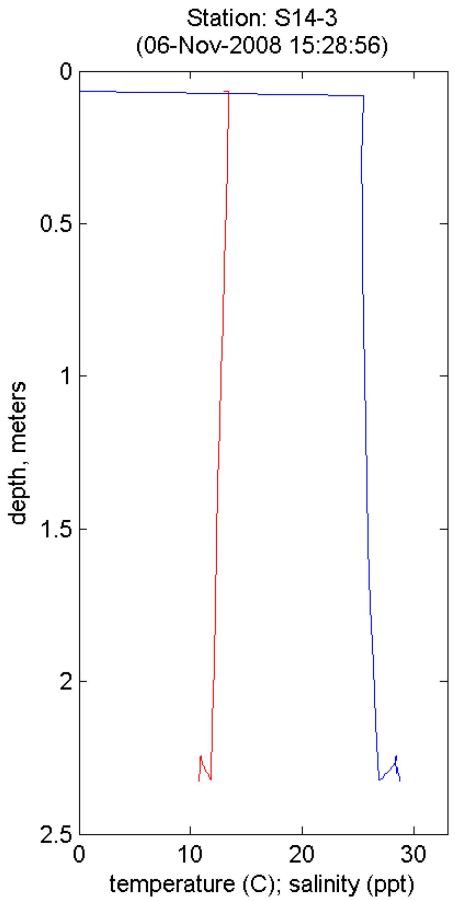
Station: S14-3
(06-Nov-2008 15:28:56)
depth, meters
temperature (C); salinity (ppt)
0
0.5
1
1.5
2
2.5
0
10
20
30

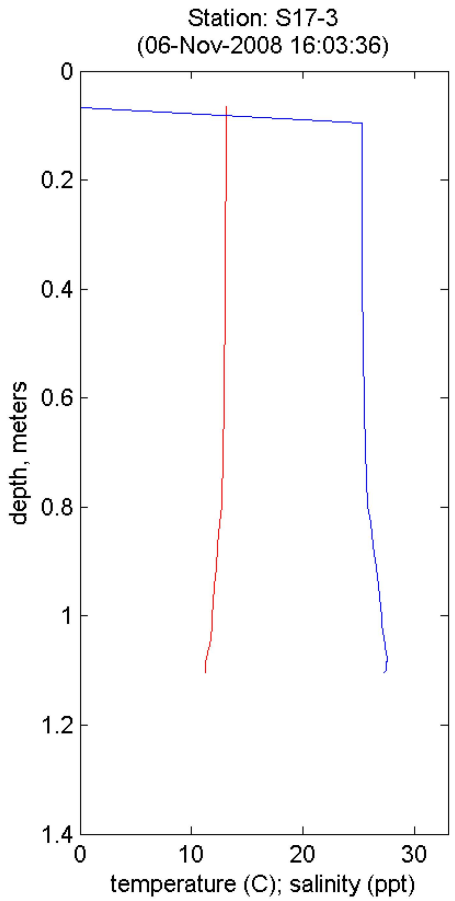
Station: S17-3
(06-Nov-2008 16:03:36)
depth, meters
temperature (C); salinity (ppt)
0
0.2
0.4
0.6
0.8
1
1.2
1.4
0
10
20
30

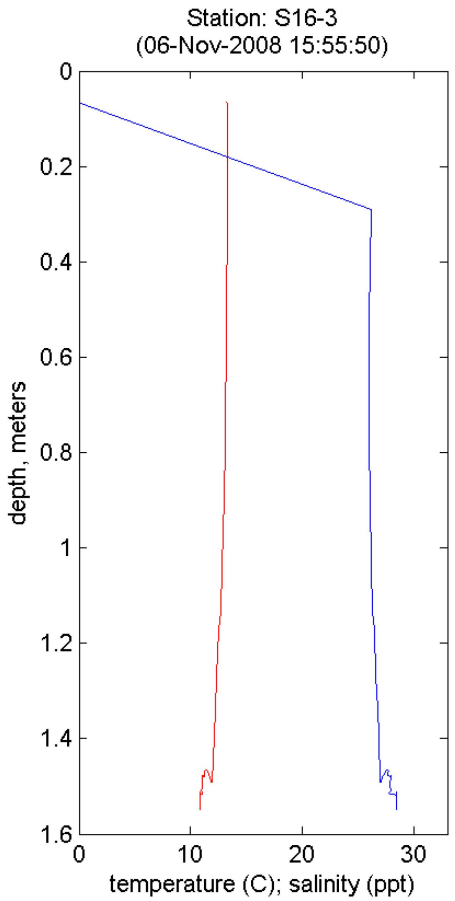
Station: S16-3
(06-Nov-2008 15:55:50)
depth, meters
temperature (C); salinity (ppt)
0
0.2
0.4
0.6
0.8
1
1.2
1.4
1.6
0
10
20
30

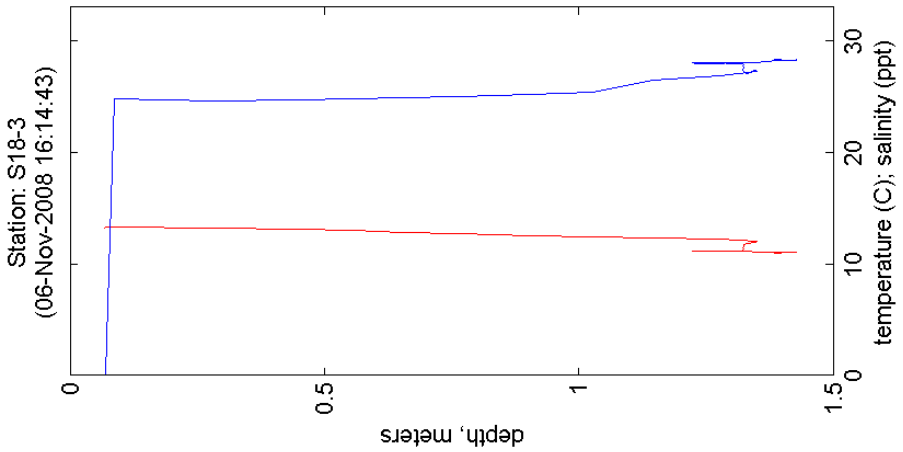
Station: S18-3
(06-Nov-2008 16:14:43)
depth, meters
temperature (C); salinity (ppt)
0
0.5
1
1.5
0
10
20
30

Appendix C

Physical Samples

This appendix provides the results of physical sample processing from the Sedflume cores. Depths are indicated from the sediment surface.

Table C-1 Physical properties of Core 01-01

Sample No.	Depth (cm)	Bulk density (g/cm^3)	% sand	% silt	%clay	D10 (μm)	D50 (μm)	D90 (μm)
#1	1.4	1.198	9.51	78.67	11.83	3.4	16.0	57.3
#2	4.0	1.232	13.06	73.41	13.53	3.1	17.0	86.1
#3	8.5	1.270	13.87	66.43	19.70	2.2	13.0	82.5
#4	13.7	1.282	20.54	62.87	16.59	2.5	17.0	130.4
#5	21.0	1.309	16.11	62.74	21.15	2.0	12.0	92.0
#6	27.4	1.311	20.98	64.01	15.01	2.7	18.8	133.8
#7	30.7	1.276	20.78	63.13	16.10	2.5	16.7	126.0

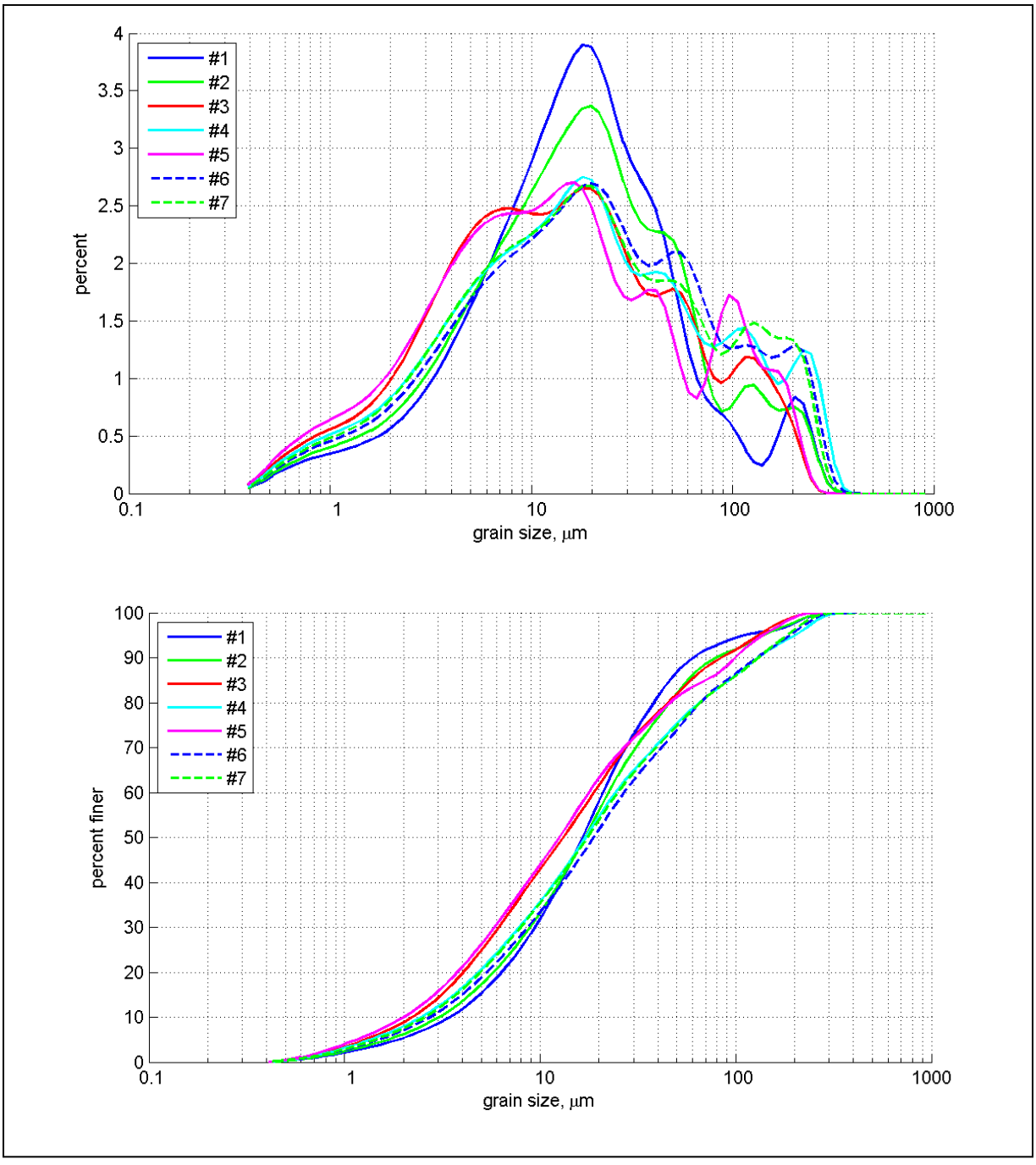
#1
#2
#3
#4
#5
#6
#7
percent
grain size, μm
0
0.5
1
1.5
2
2.5
3
3.5
4
0.1
1
10
100
1000
#1
#2
#3
#4
#5
#6
#7
percent finer
grain size, μm
0
10
20
30
40
50
60
70
80
90
100
0.1
1
10
100
1000

Table C-2. Physical properties of Core 02-01								
Sample Number	Depth (cm)	Bulk density (g/cm^3)	% sand	% silt	%clay	D10 (μm)	D50 (μm)	D90 (μm)
#1	2.5	1.416	11.90	63.44	24.66	1.8	9.6	85.3
#2	8.9	1.430	18.63	60.39	20.98	2.0	12.0	115.5
#3	13.2	1.439	24.53	58.36	17.11	2.5	16.4	145.5
#4	17.6	1.341	12.64	62.57	24.79	1.8	9.7	89.8
#5	23.1	1.350	3.77	68.17	28.06	1.5	8.1	34.7

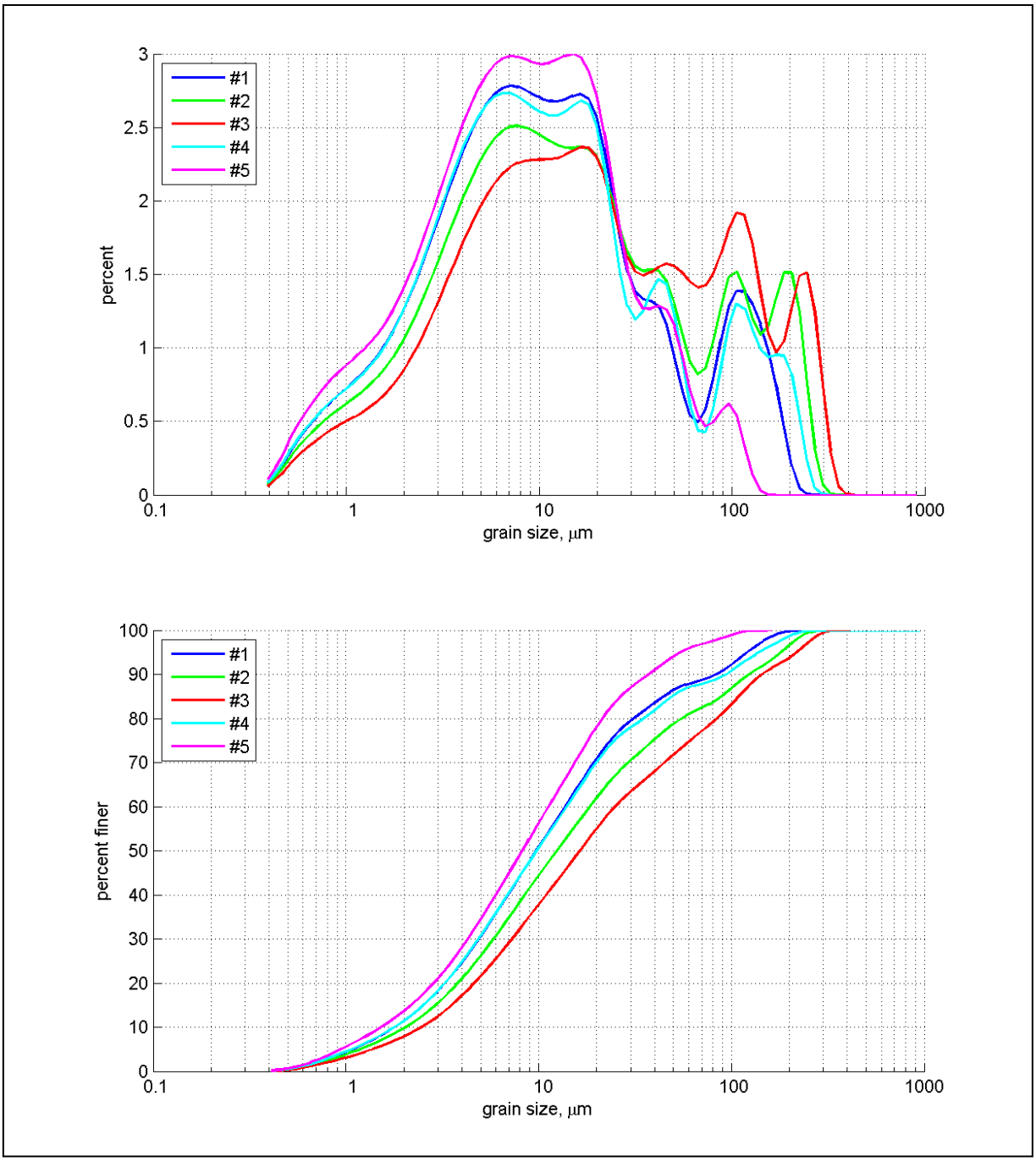
#1
#2
#3
#4
#5
percent
grain size, μm
0
0.5
1
1.5
2
2.5
3
0.1
1
10
100
1000
#1
#2
#3
#4
#5
percent finer
grain size, μm
0
10
20
30
40
50
60
70
80
90
100
0.1
1
10
100
1000

Table C-3 Physical properties of Core 02-02								
Sample Number	Depth (cm)	Bulk density (g/cm^3)	% sand	% silt	%clay	D10 (μm)	D50 (μm)	D90 (μm)
#1	0.0	1.354	28.59	54.80	16.61	2.5	19.5	160.4
#2	3.5	1.462	38.17	49.46	12.38	3.2	27.7	288.0
#3	7.5	1.410	25.54	58.64	15.82	2.6	18.6	180.6
#4	10.0	1.368	16.55	63.73	19.72	2.2	12.4	105.3
#5	12.3	1.351	14.13	63.68	22.18	1.9	10.8	97.0
#6	18.6	1.377	15.07	62.61	22.32	1.9	11.3	109.4
#7	23.1	1.368	12.69	65.52	21.79	2.0	10.6	87.1

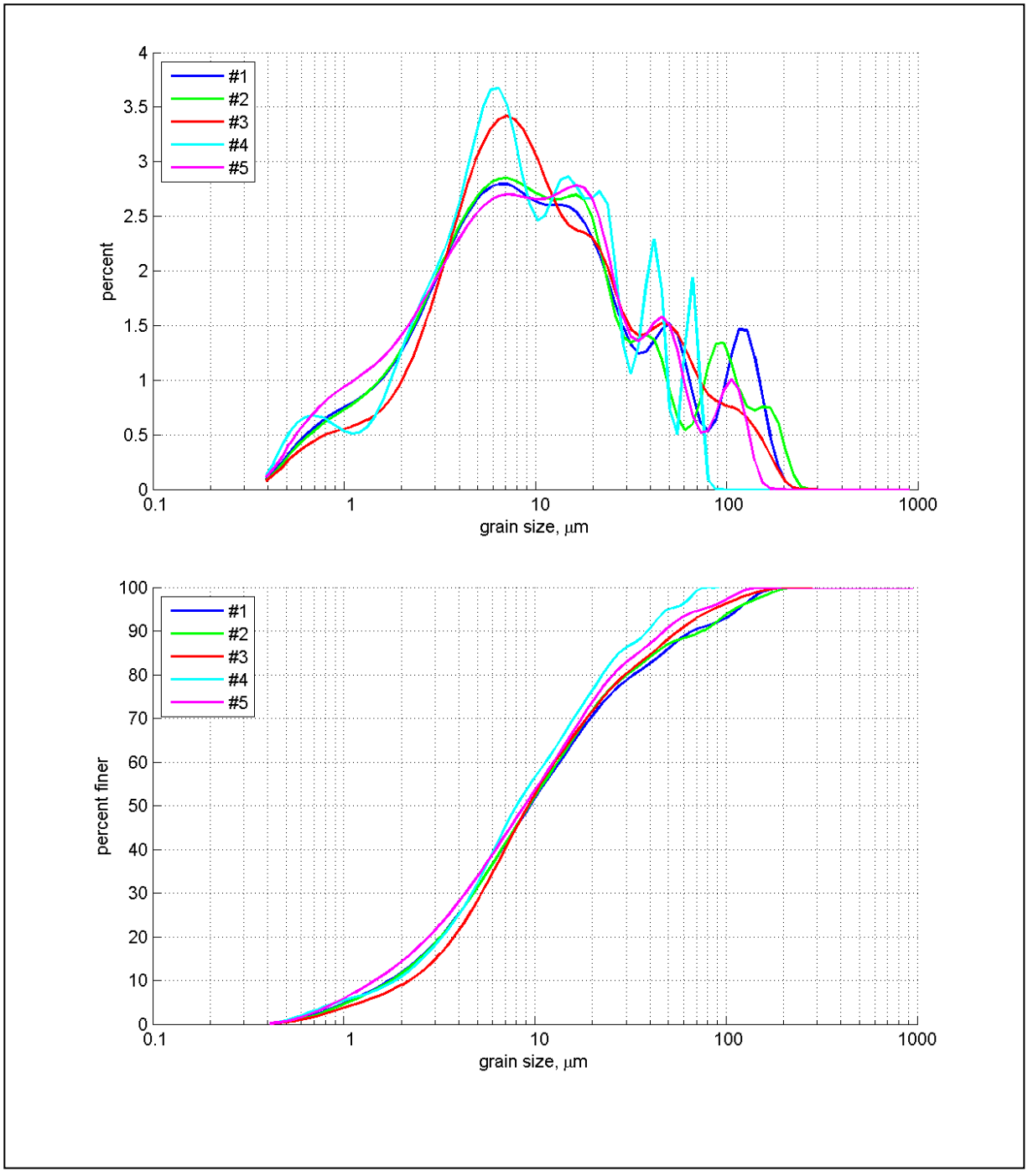
#1
#2
#3
#4
#5
percent
grain size, μm
percent finer
grain size, μm

Table C-4. Physical properties of Core 03-01								
Sample Number	Depth (cm)	Bulk density (g/cm^3)	% sand	% silt	%clay	D10 (μm)	D50 (μm)	D90 (μm)
#1	1.9	1.380	10.62	64.15	25.23	1.7	9.3	62.4
#2	6.7	1.401	11.40	63.42	25.18	1.8	9.3	76.5
#3	10.7	1.810	8.38	70.16	21.46	2.2	9.1	57.5
#4	13.1	1.373	3.04	71.91	25.05	1.8	7.9	38.4
#5	18.7	1.432	6.23	65.77	28.00	1.5	8.8	47.7

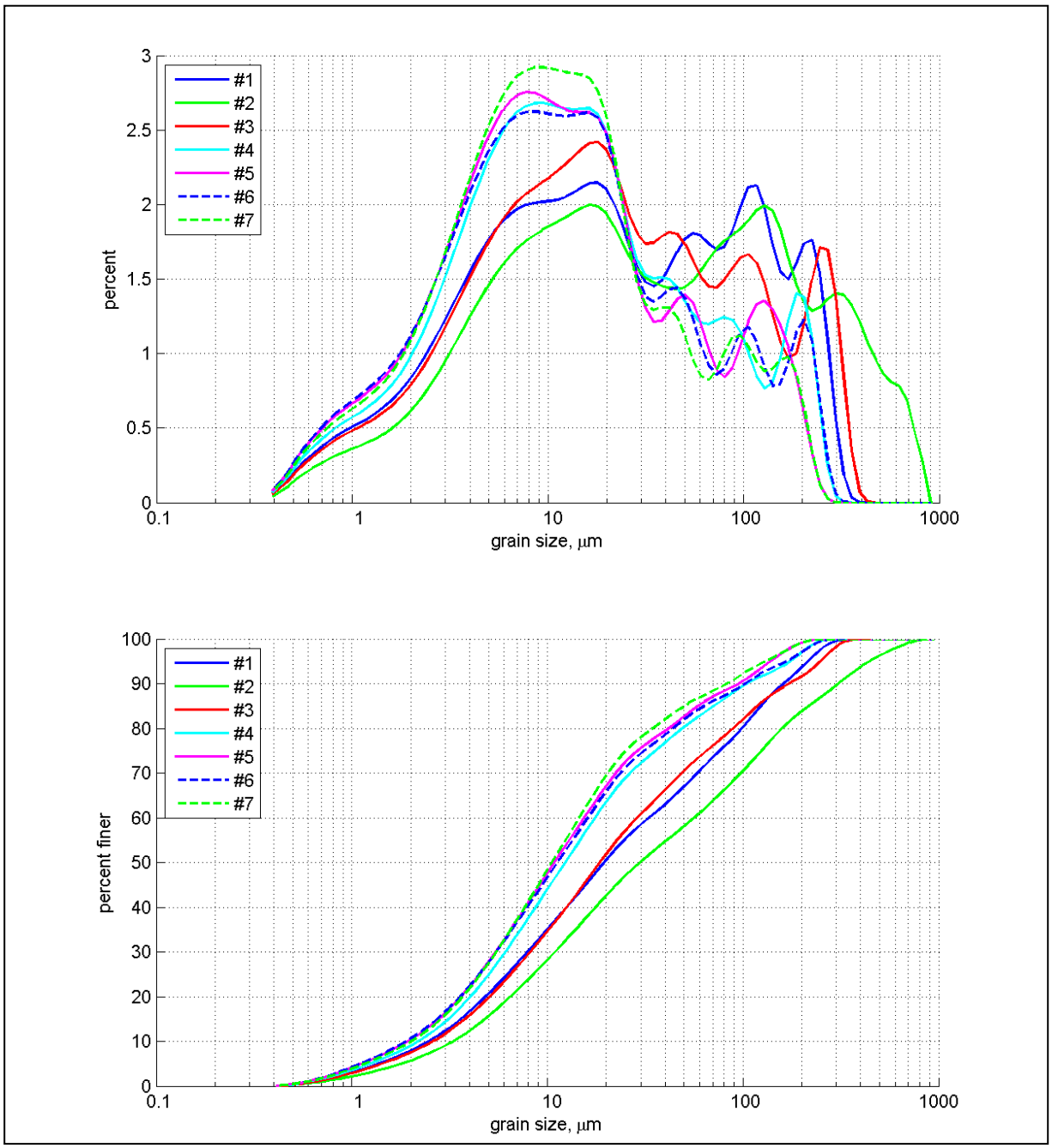
#1
#2
#3
#4
#5
#6
#7
percent
grain size, μm
percent finer
grain size, μm

Table C-5. Physical properties of Core 04-01								
Sample Number	Depth (cm)	Bulk density (g/cm^3)	% sand	% silt	%clay	D10 (μm)	D50 (μm)	D90 (μm)
#1	1.5	1.254	4.96	73.10	21.94	2.2	7.9	39.6
#2	7.3	1.322	15.97	64.30	19.73	2.1	13.3	113.1
#3	11.4	1.348	5.41	68.61	25.99	1.8	8.4	44.3
#4	16.5	1.382	4.40	67.27	28.34	1.5	8.0	39.7
#5	21.8	1.372	11.82	62.41	25.77	1.5	10.0	75.9
#6	31.0	1.386	-	-	-	-	-	-

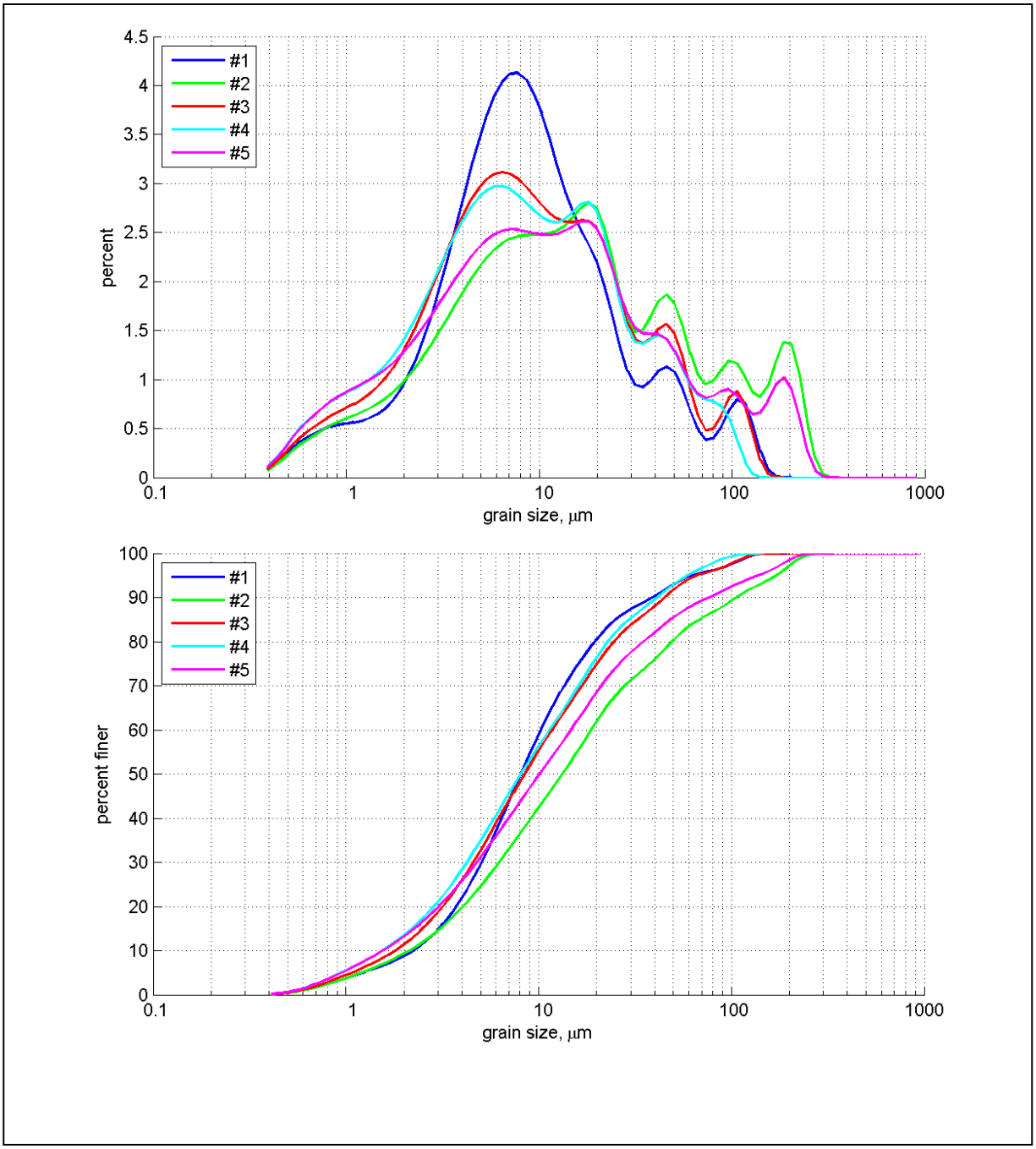
#1
#2
#3
#4
#5
percent
grain size, μm
percent finer
grain size, μm

Table C-6. Physical properties of Core 06-01								
Sample Number	Depth (cm)	Bulk density (g/cm^3)	% sand	% silt	%clay	D10 (μm)	D50 (μm)	D90 (μm)
#1	2.9	1.342	10.46	63.71	25.83	1.6	9.8	60.0
#2	8.7	1.342	12.97	63.01	24.02	1.9	10.4	84.9
#3	13.3	1.324	11.68	64.90	23.42	1.9	10.3	74.6
#4	15.8	1.355	3.24	70.39	26.37	1.7	8.6	40.3
#5	23.3	1.357	14.90	65.59	19.51	2.2	13.6	94.3
#6	25.6	1.363	9.21	62.66	28.13	1.4	8.9	57.6

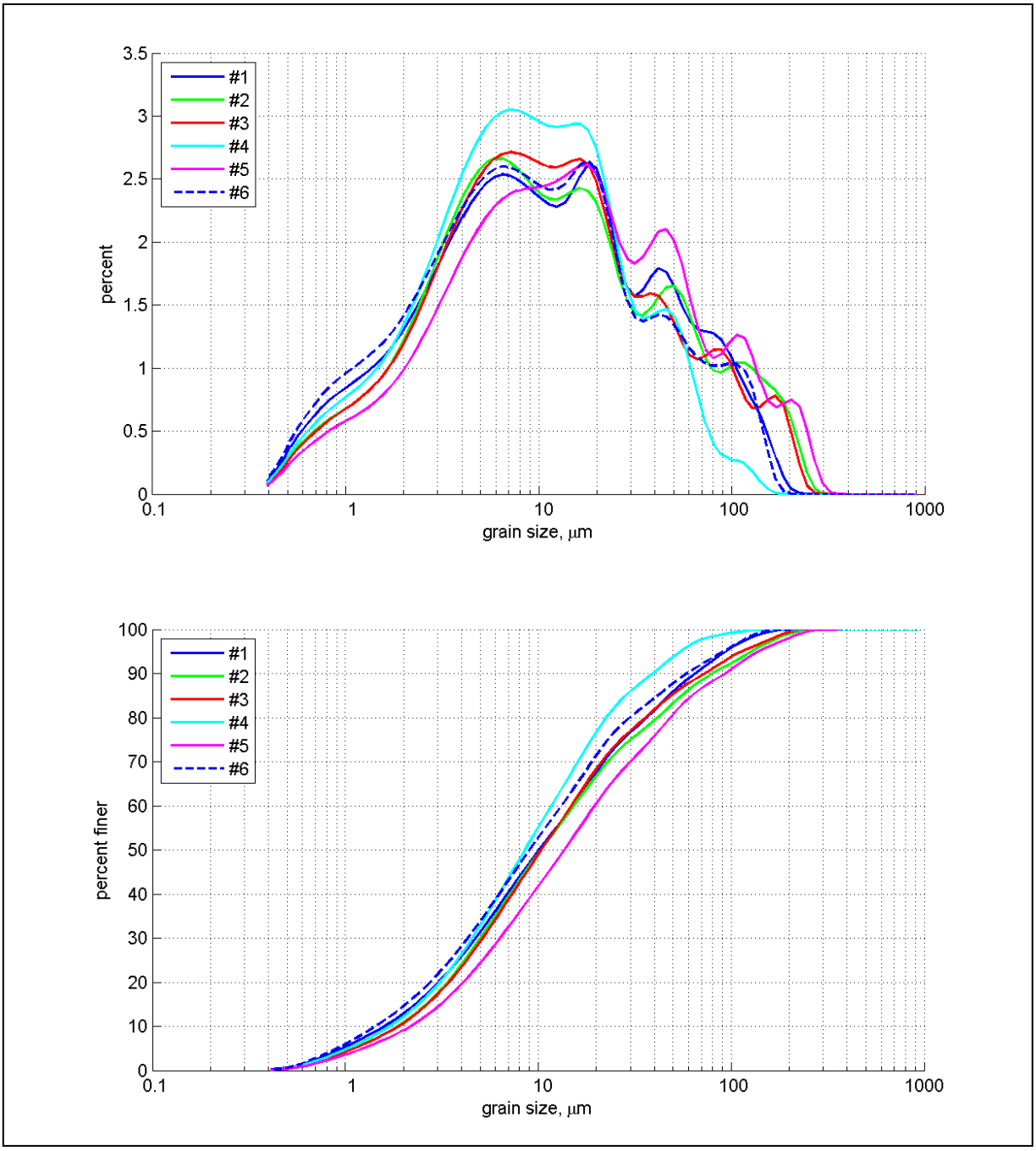
#1
#2
#3
#4
#5
#6
percent
grain size, μm
0
0.5
1
1.5
2
2.5
3
3.5
0.1
1
10
100
1000
#1
#2
#3
#4
#5
#6
percent finer
grain size, μm
0
10
20
30
40
50
60
70
80
90
100
0.1
1
10
100
1000

Table C-7. Physical properties of Core 07-01								
Sample Number	Depth (cm)	Bulk density (g/cm^3)	% sand	% silt	%clay	D10 (μm)	D50 (μm)	D90 (μm)
#1	3.8	1.214	6.03	66.18	27.78	1.6	7.6	34.5
#2	8.7	1.246	12.68	62.96	24.35	1.8	10.1	83.6
#3	14.0	1.251	4.36	71.31	24.33	1.8	9.2	39.1
#4	16.1	1.279	11.27	70.54	18.18	2.4	12.7	67.5
#5	21.6	1.323	10.60	68.05	21.35	2.1	10.6	69.2
#6	27.5	1.346	11.83	65.31	22.86	1.9	10.8	76.0

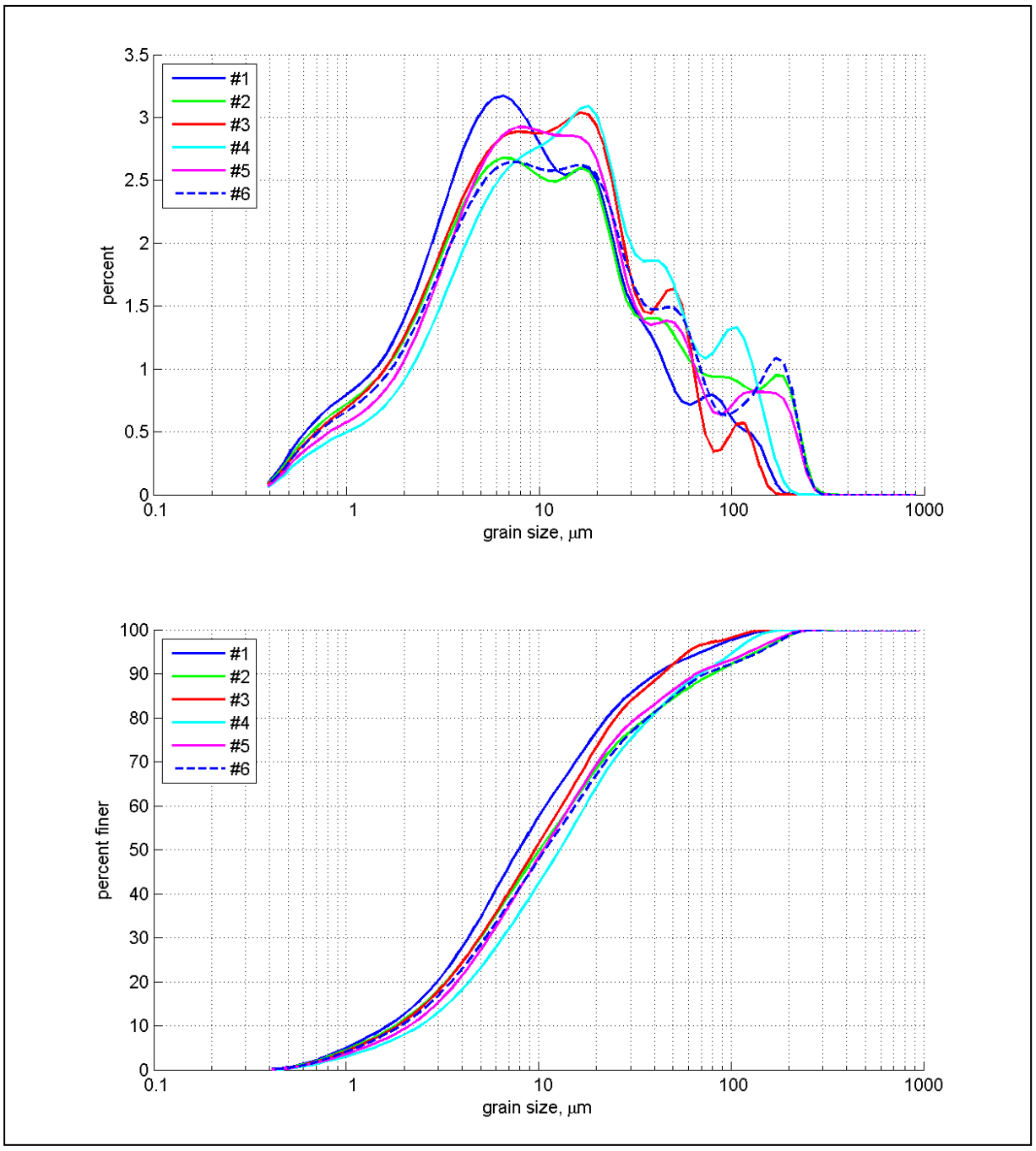
#1
#2
#3
#4
#5
#6
percent
grain size, μm
0
0.5
1
1.5
2
2.5
3
3.5
0.1
1
10
100
1000
#1
#2
#3
#4
#5
#6
percent finer
grain size, μm
0
10
20
30
40
50
60
70
80
90
100
0.1
1
10
100
1000

Table C-8. Physical properties of Core 08-01								
Sample Number	Depth (cm)	Bulk density (g/cm^3)	% sand	% silt	%clay	D10 (μm)	D50 (μm)	D90 (μm)
#1	3.2	1.462	38.06	47.98	13.96	3.0	24.7	260.9
#2	5.0	1.699	50.69	38.12	11.19	3.6	67.2	348.5
#3	8.6	1.548	44.00	43.20	12.80	3.2	38.1	287.0
#4	12.1	1.461	18.57	62.41	19.02	2.3	13.0	130.3

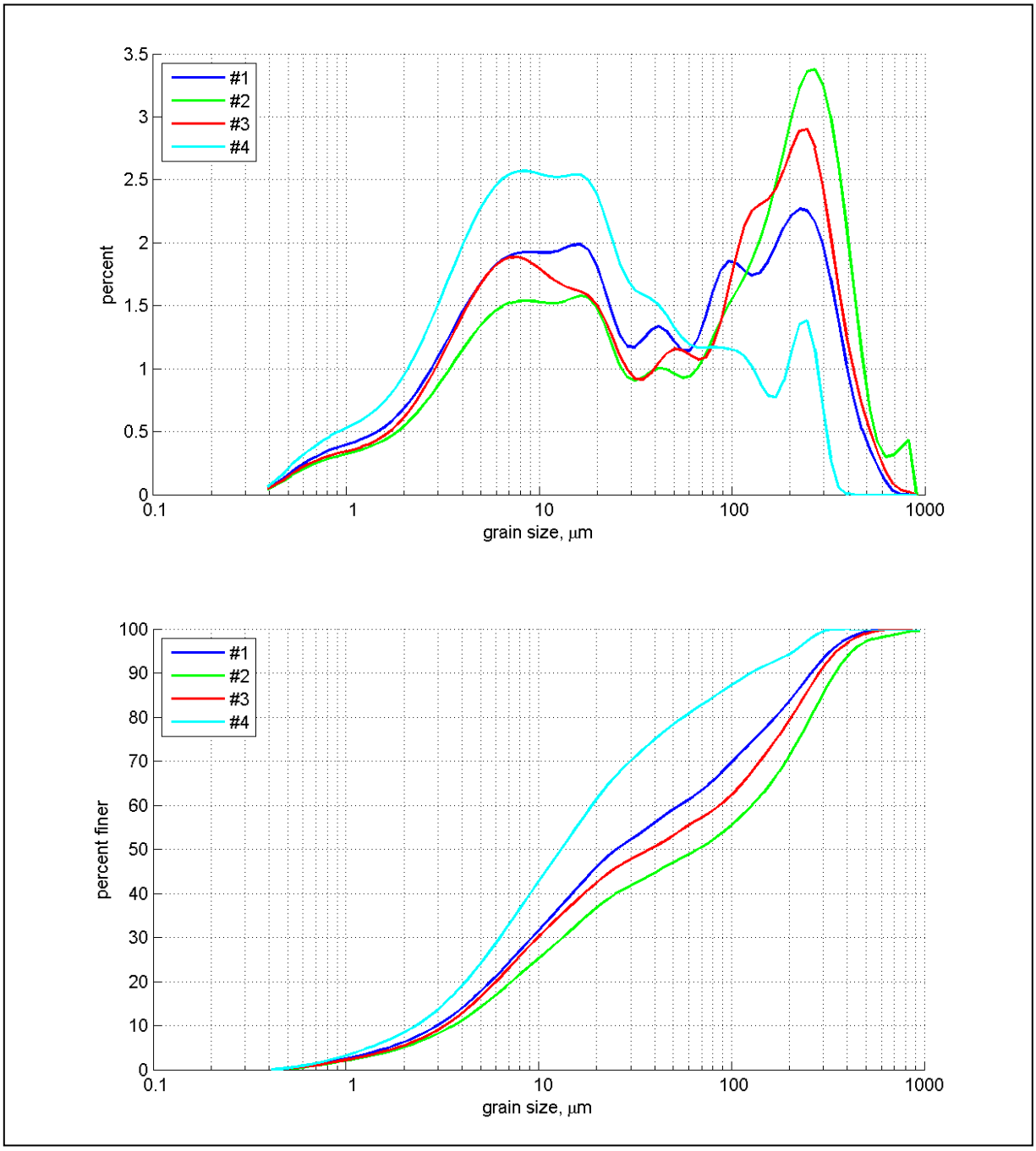
#1
#2
#3
#4
percent
grain size, μm
0.1
1
10
100
1000
0
0.5
1
1.5
2
2.5
3
3.5
#1
#2
#3
#4
percent finer
grain size, μm
0
10
20
30
40
50
60
70
80
90
100

Table C-9. Physical properties of Core 09-01								
Sample Number	Depth (cm)	Bulk density (g/cm^3)	% sand	% silt	%clay	D10 (μm)	D50 (μm)	D90 (μm)
#1	2.55	1.240	2.78	70.57	26.66	1.7	7.4	24.6
#2	5.5	1.340	38.51	43.84	17.65	2.4	21.5	395.3
#3	12.35	1.469	-	-	-	-	-	-
#4	16.65	1.431	-	-	-	-	-	-

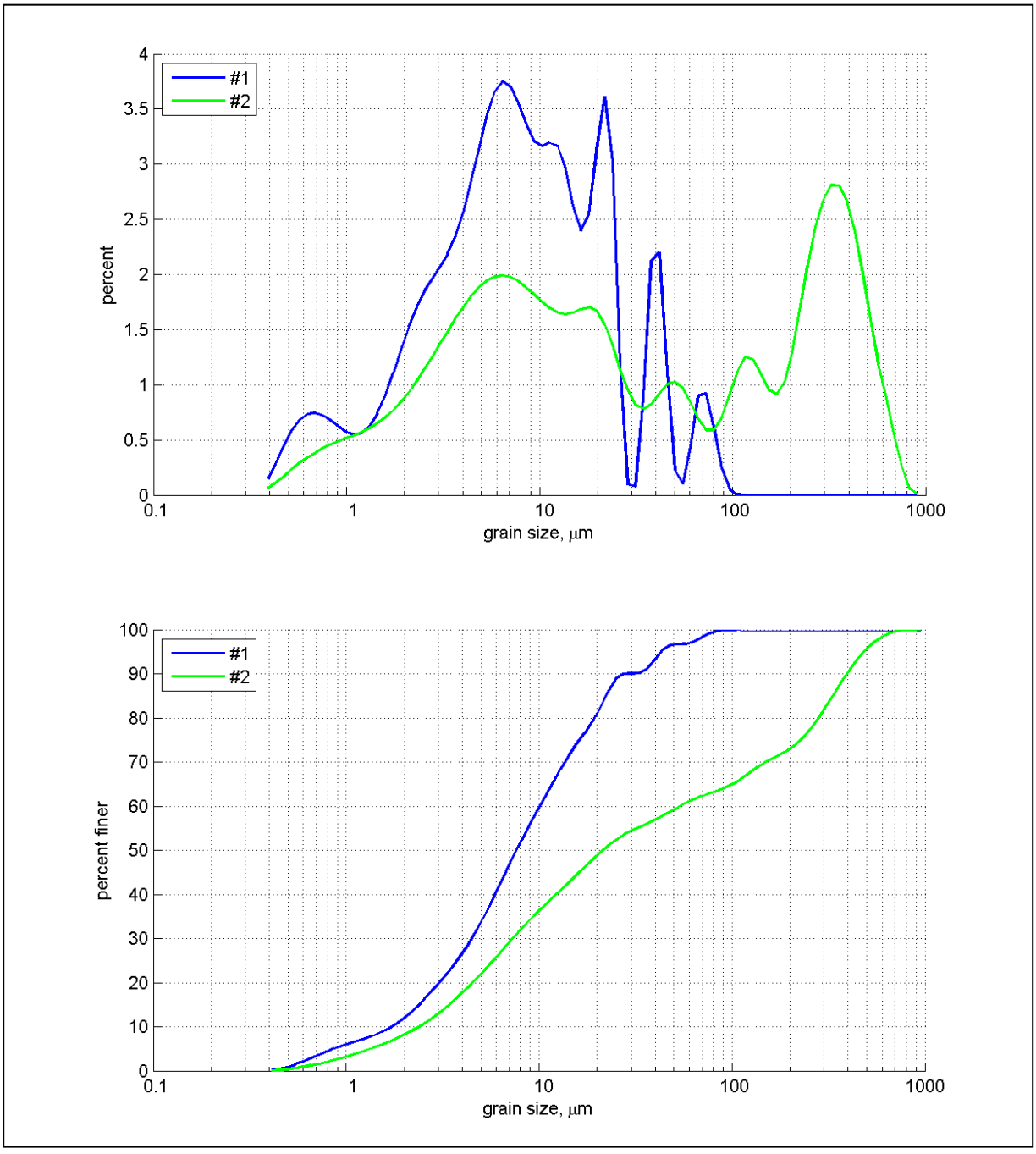
#1
#2
percent
grain size, μm
0
0.5
1
1.5
2
2.5
3
3.5
4
0.1
1
10
100
1000
#1
#2
percent finer
grain size, μm
0
10
20
30
40
50
60
70
80
90
100
0.1
1
10
100
1000

Appendix D

Erosion Rate Data

This Appendix contains erosion rate data and relationships associated with Table 3-2 in the main report. These data are the result of grouping layers of cores with similar erosion characteristics.

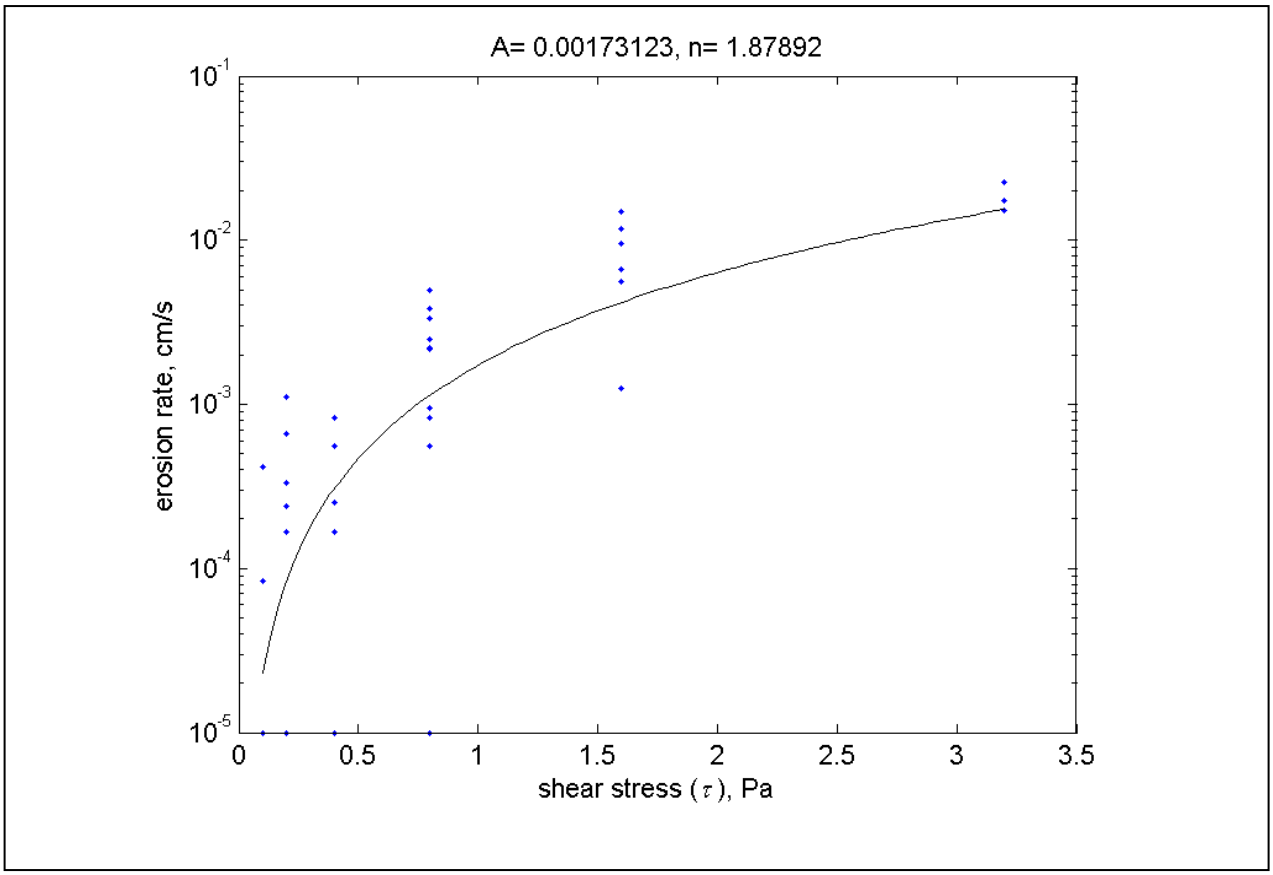

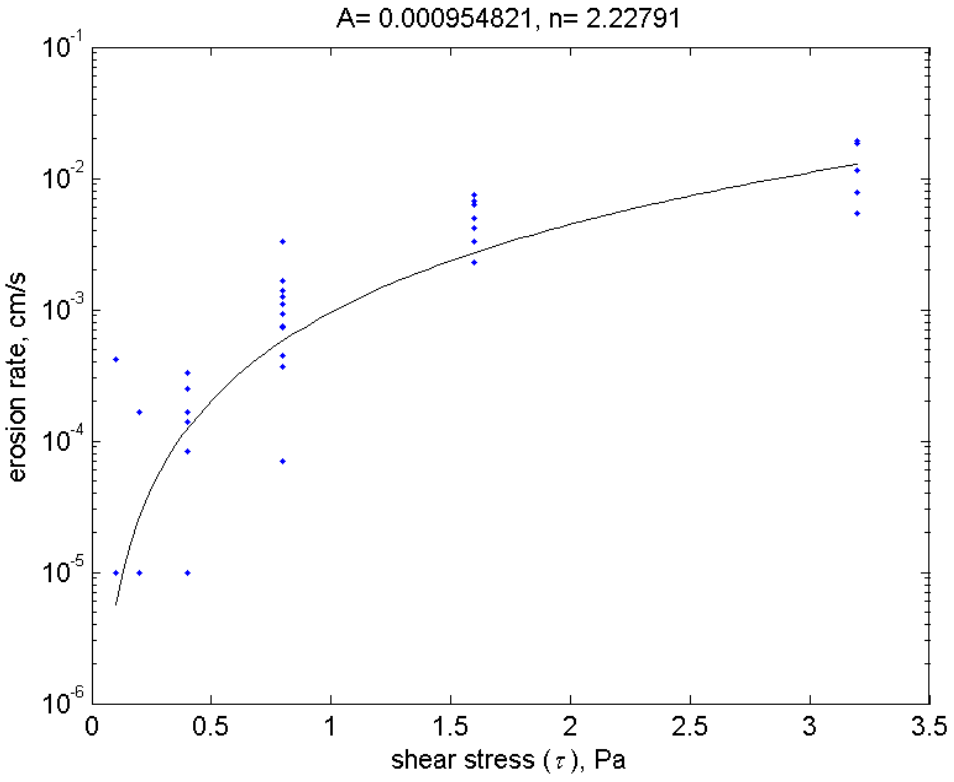
A= 0.000954821, n= 2.22791
erosion rate, cm/s
shear stress (τ), Pa

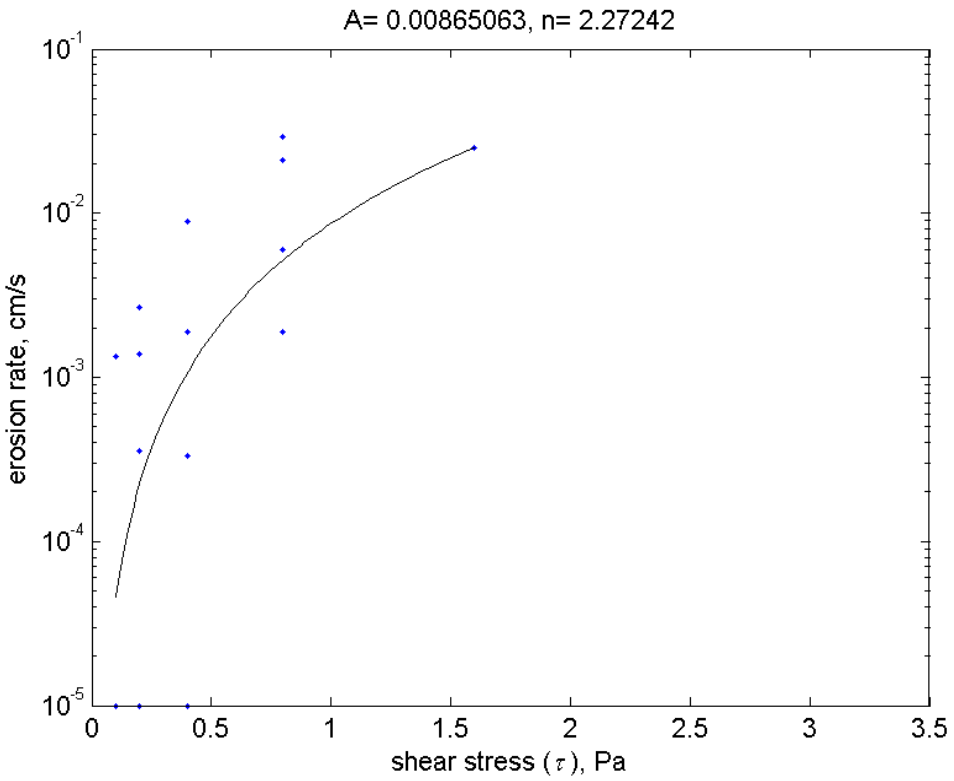
A= 0.00865063, n= 2.27242
erosion rate, cm/s
shear stress (τ), Pa

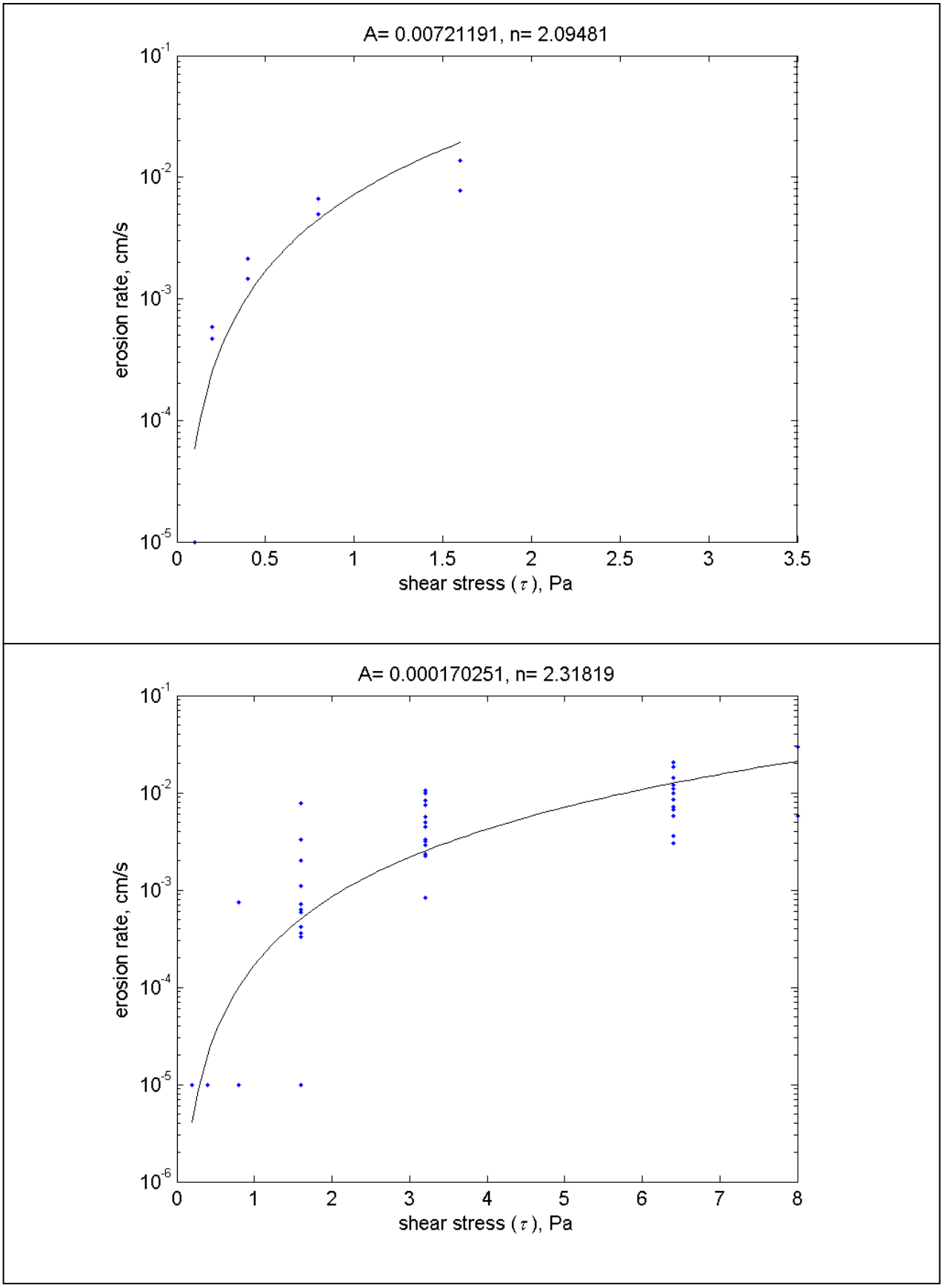
A= 0.00721191, n= 2.09481
erosion rate, cm/s
shear stress (τ), Pa
A= 0.000170251, n= 2.31819
erosion rate, cm/s
shear stress (τ), Pa

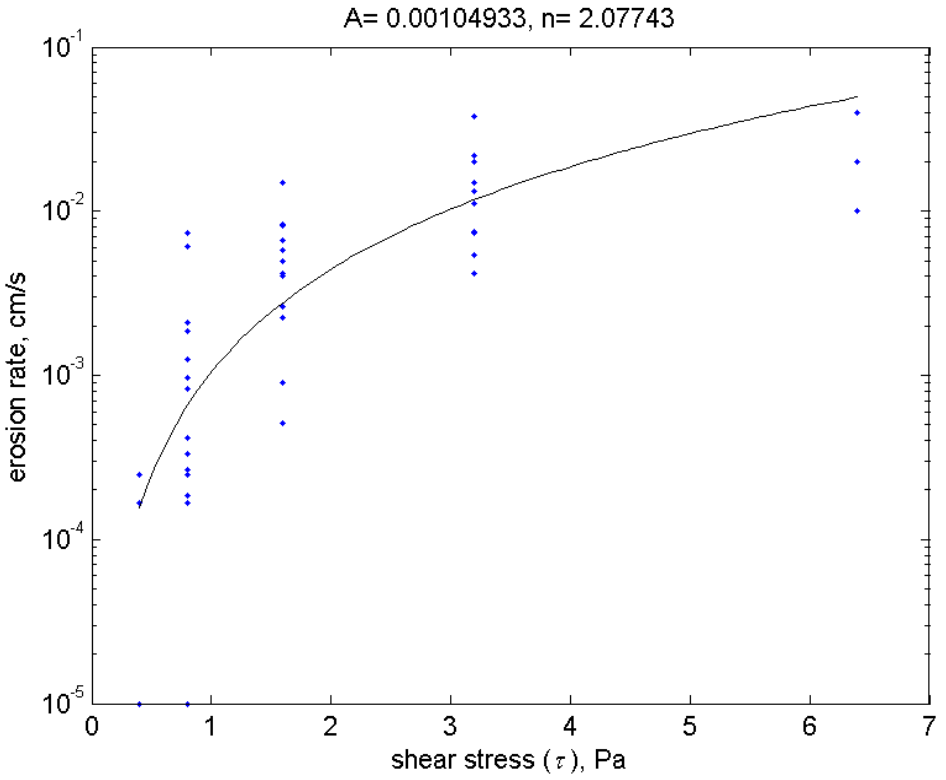
A= 0.00104933, n= 2.07743
erosion rate, cm/s
shear stress (τ), Pa

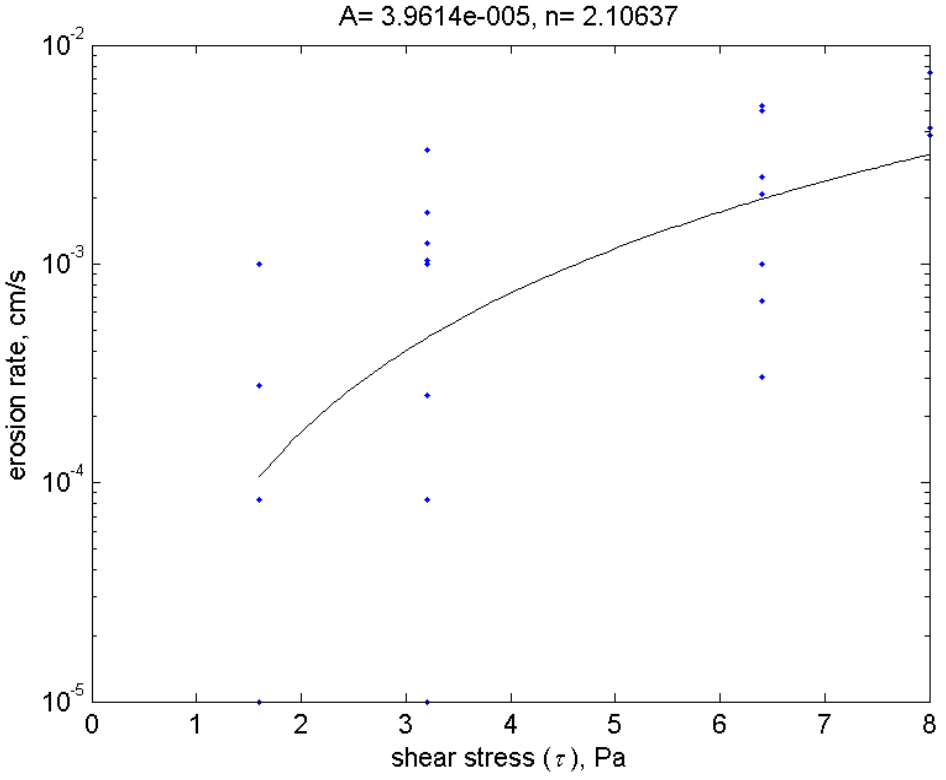
A= 3.9614e-005, n= 2.10637
erosion rate, cm/s
shear stress (τ), Pa

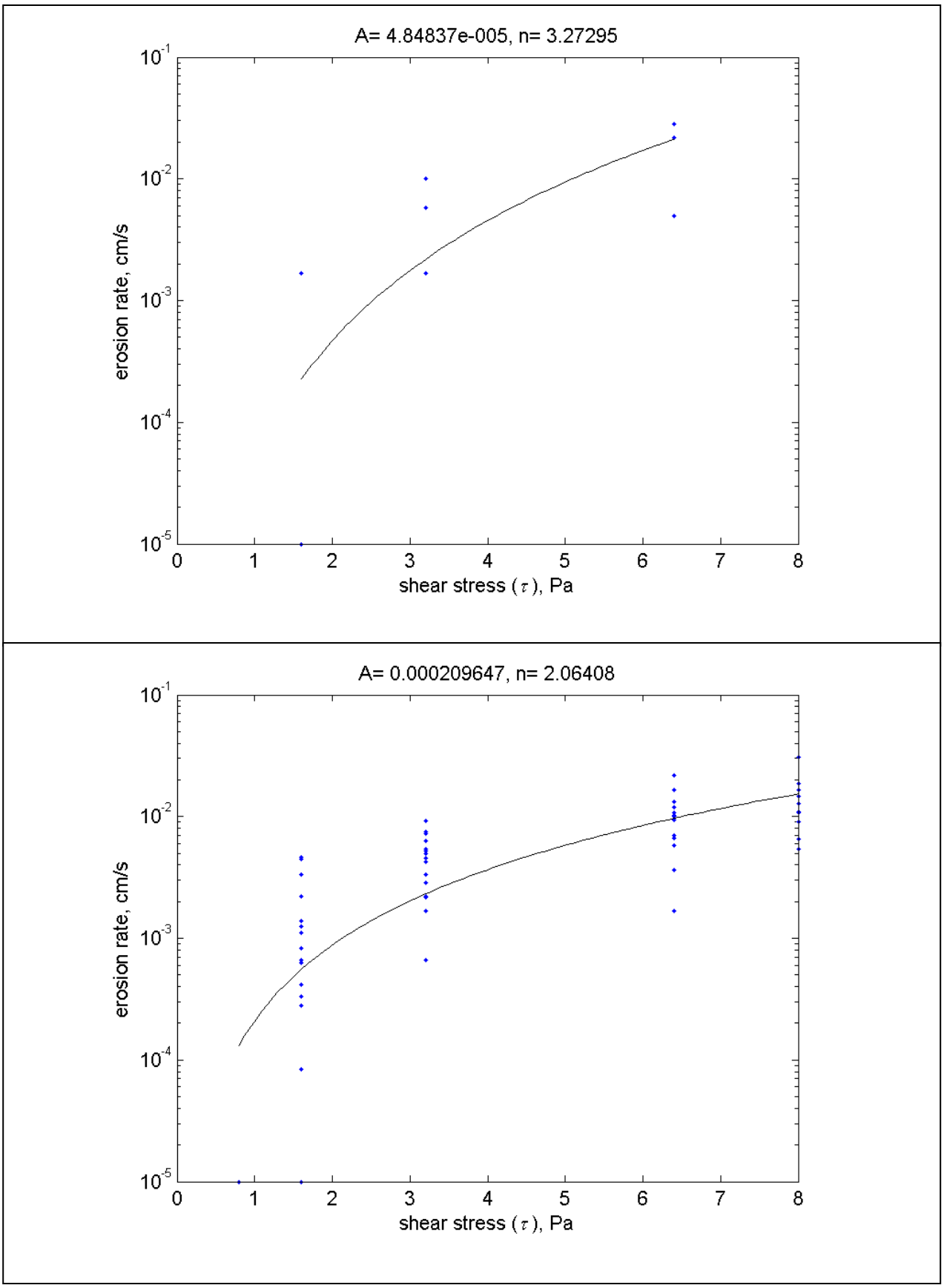
A= 4.84837e-005, n= 3.27295
erosion rate, cm/s
shear stress (τ), Pa
A= 0.000209647, n= 2.06408
erosion rate, cm/s
shear stress (τ), Pa

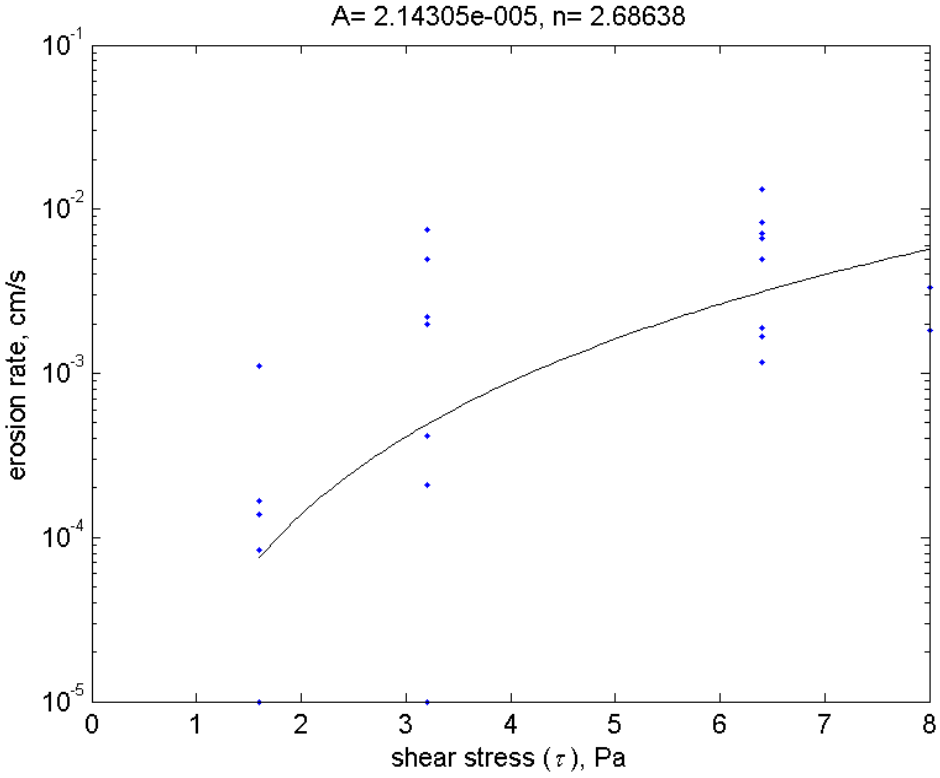
A= 2.14305e-005, n= 2.68638
erosion rate, cm/s
shear stress (τ), Pa

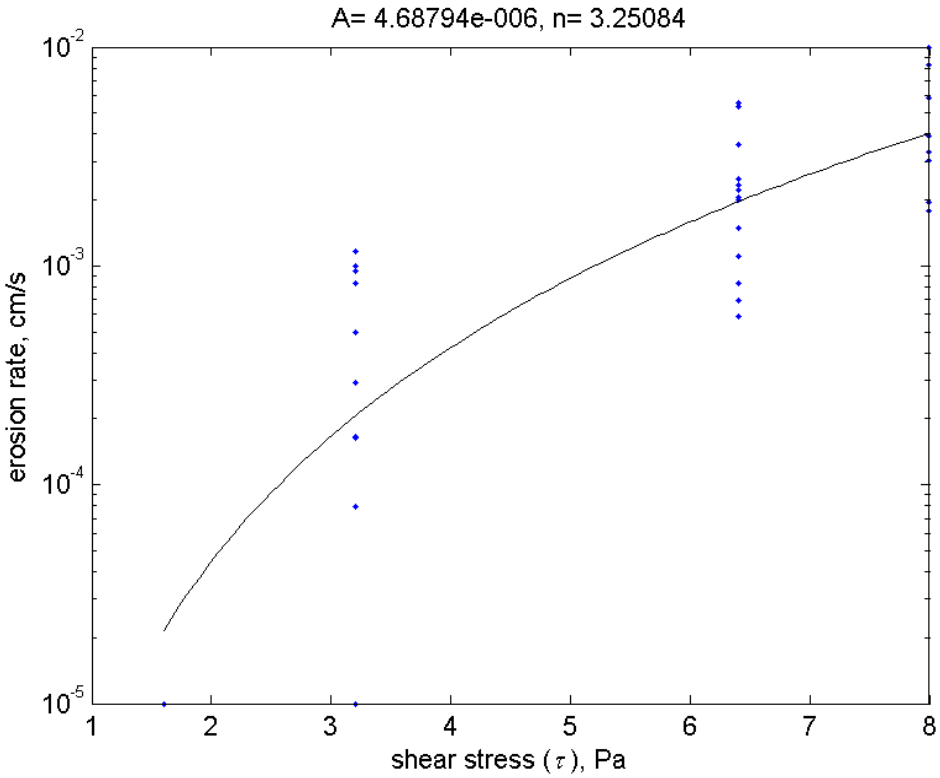
A= 4.68794e-006, n= 3.25084
erosion rate, cm/s
shear stress (τ), Pa

Appendix E

Comparison of Measured and Simulated Velocity Vectors

This Appendix contains plots showing measured and simulated velocity vectors in New Bedford Harbor at different times during a tidal cycle.

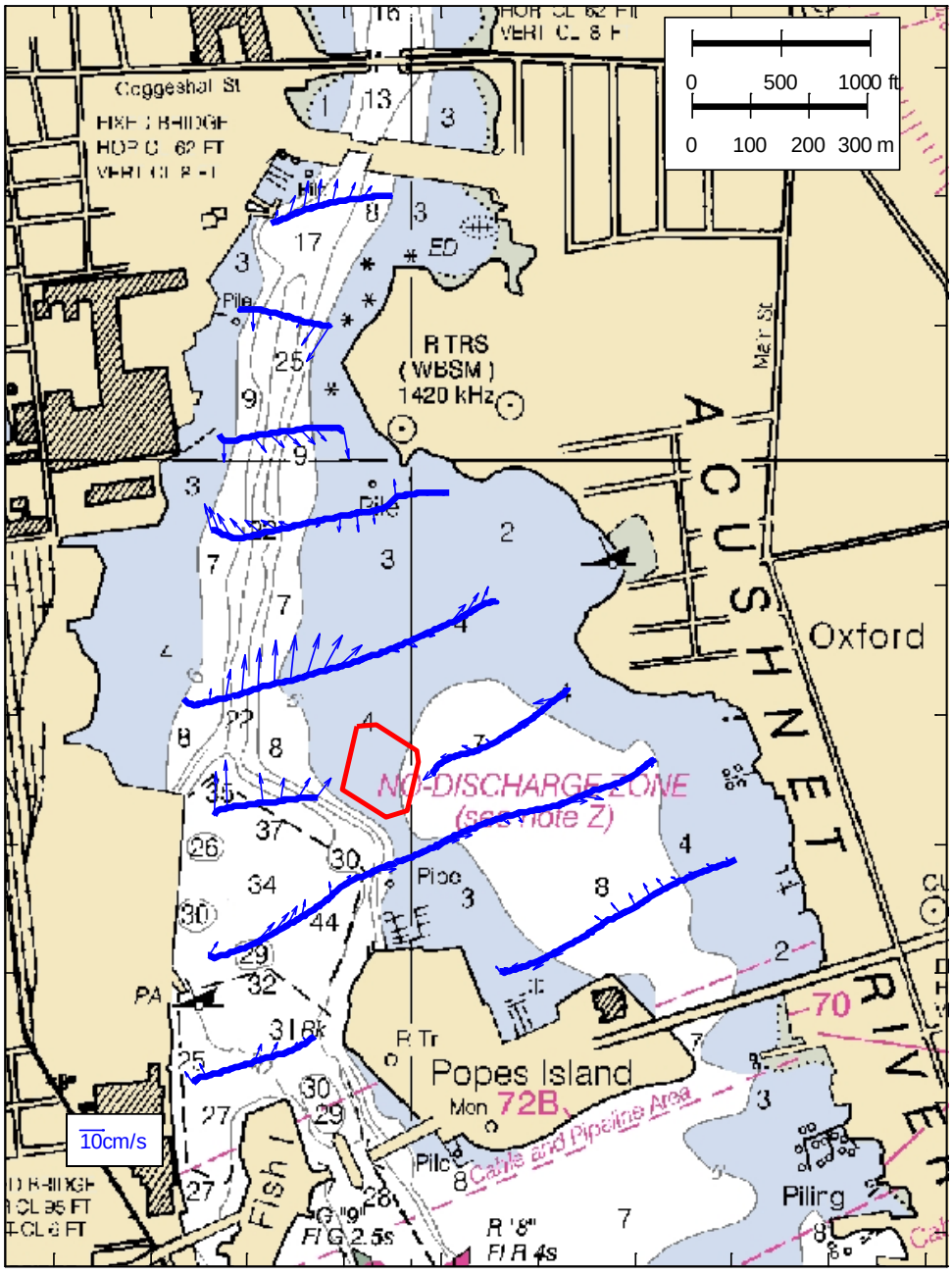

Figure E-1a Measured velocity vectors at 1 hrs before high water slack

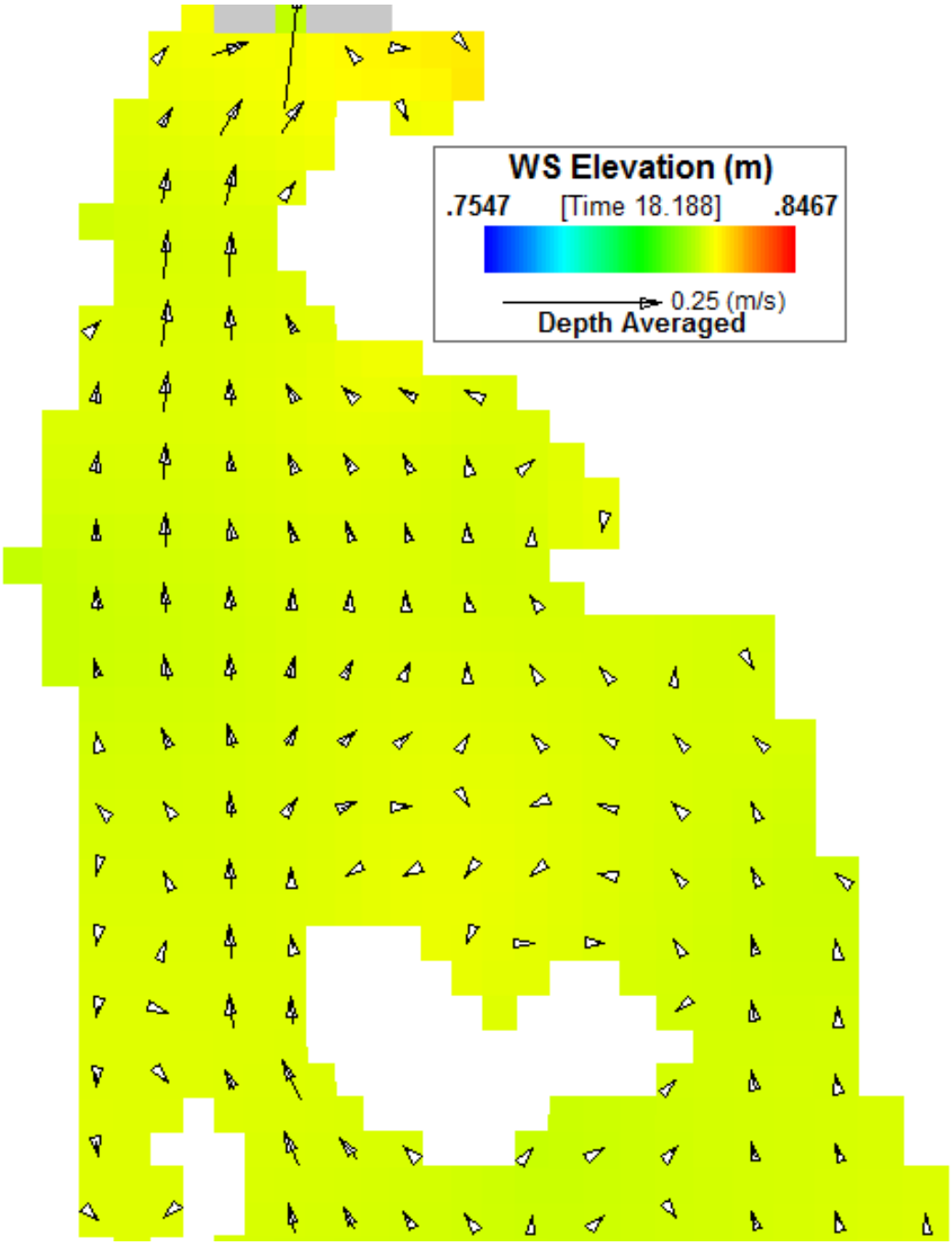

Figure E-1b Simulated vectors at 1 hrs before high water slack

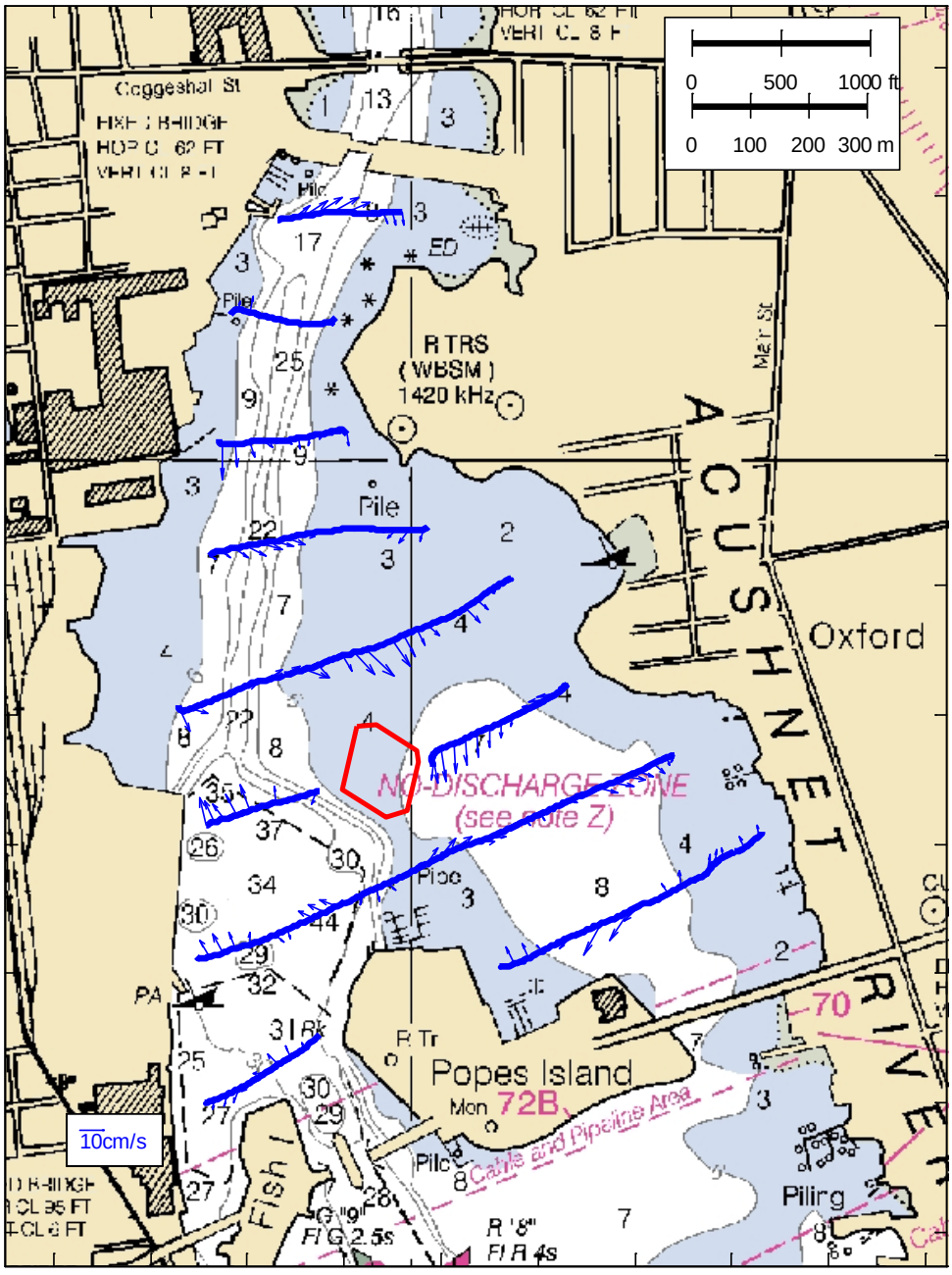

Figure E-2a Measured velocity vectors at high water slack

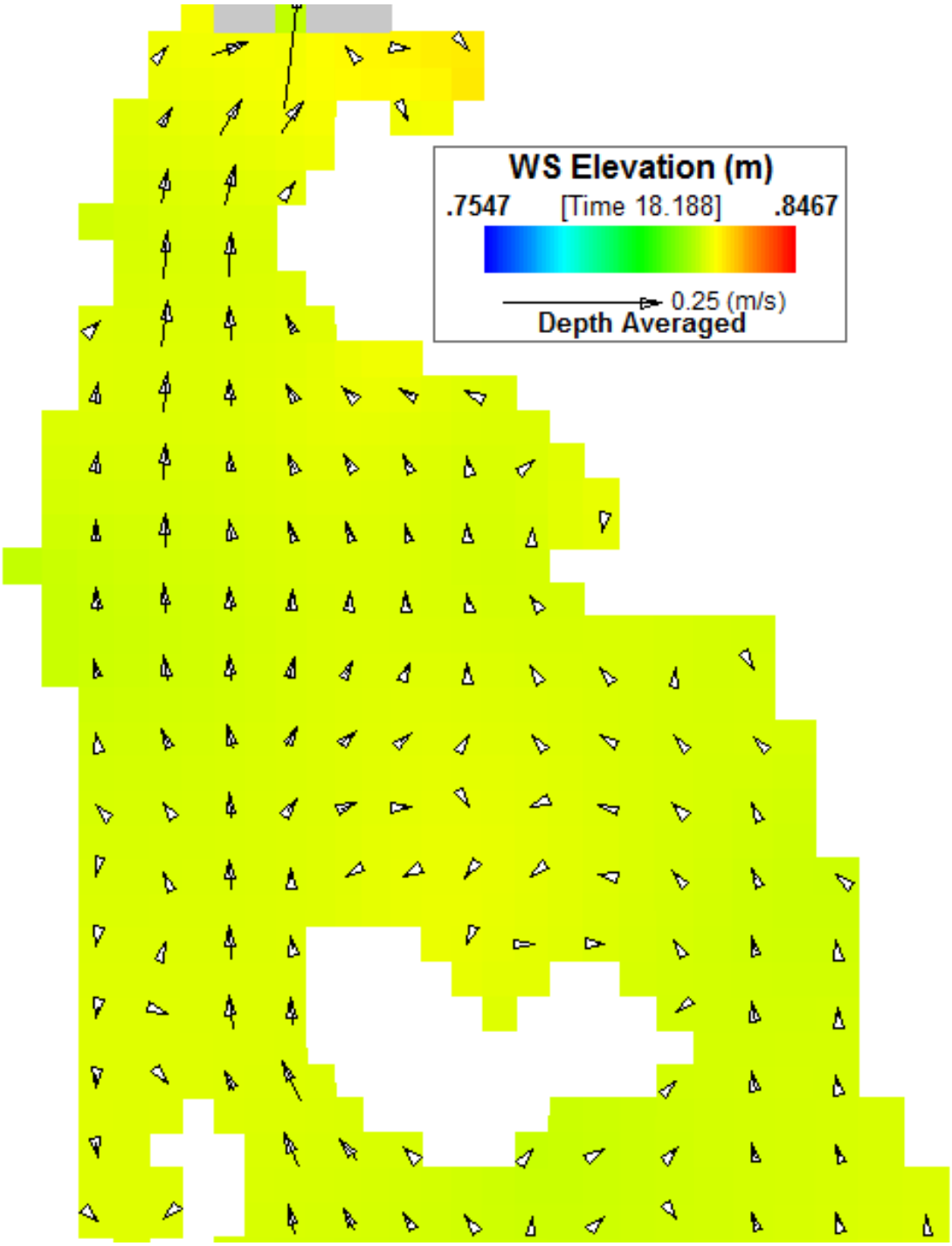

Figure E-2b Simulated velocity vectors at high water slack

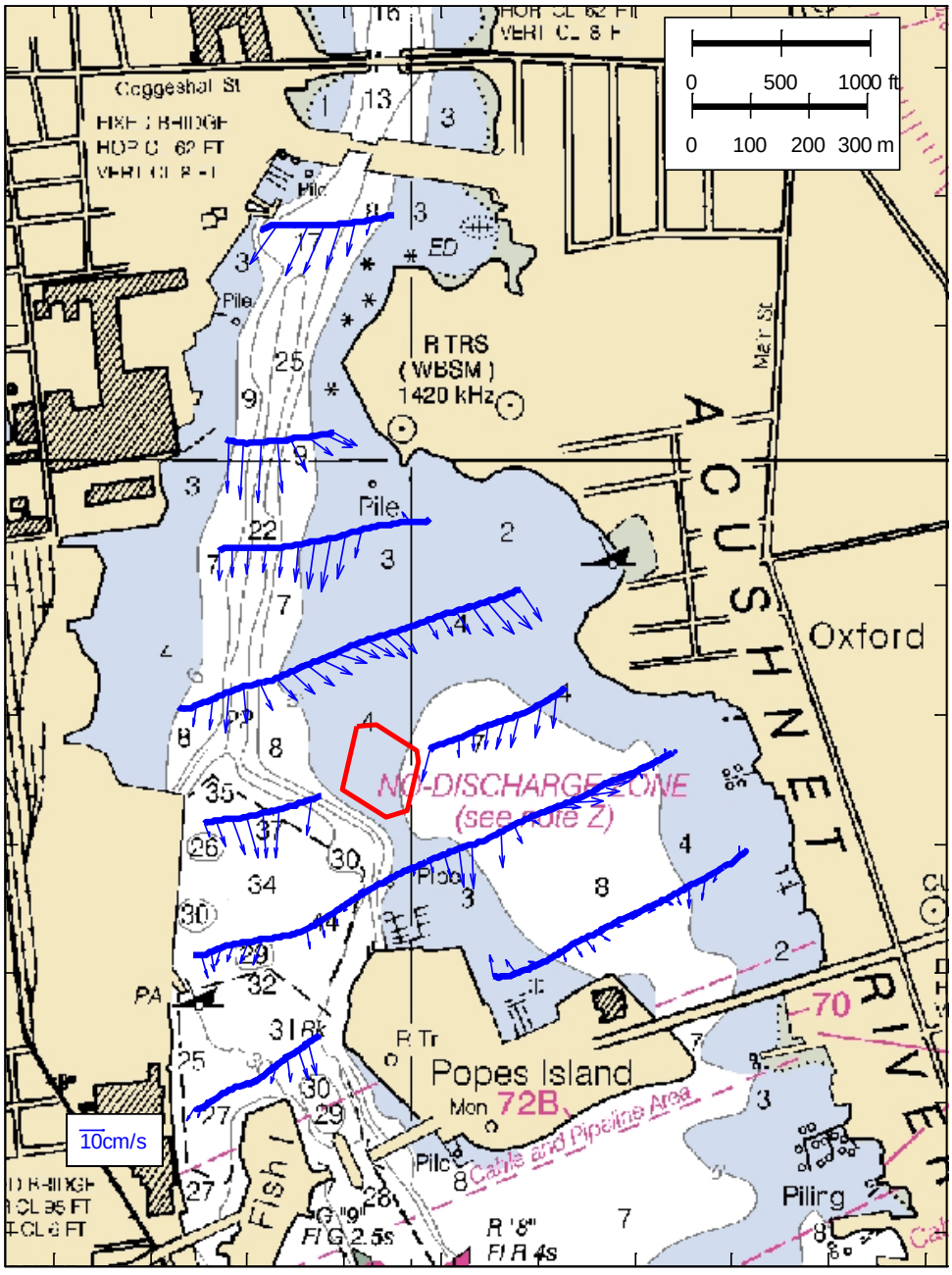

Figure E-3a Measured velocity vectors at 1 hr after high water slack

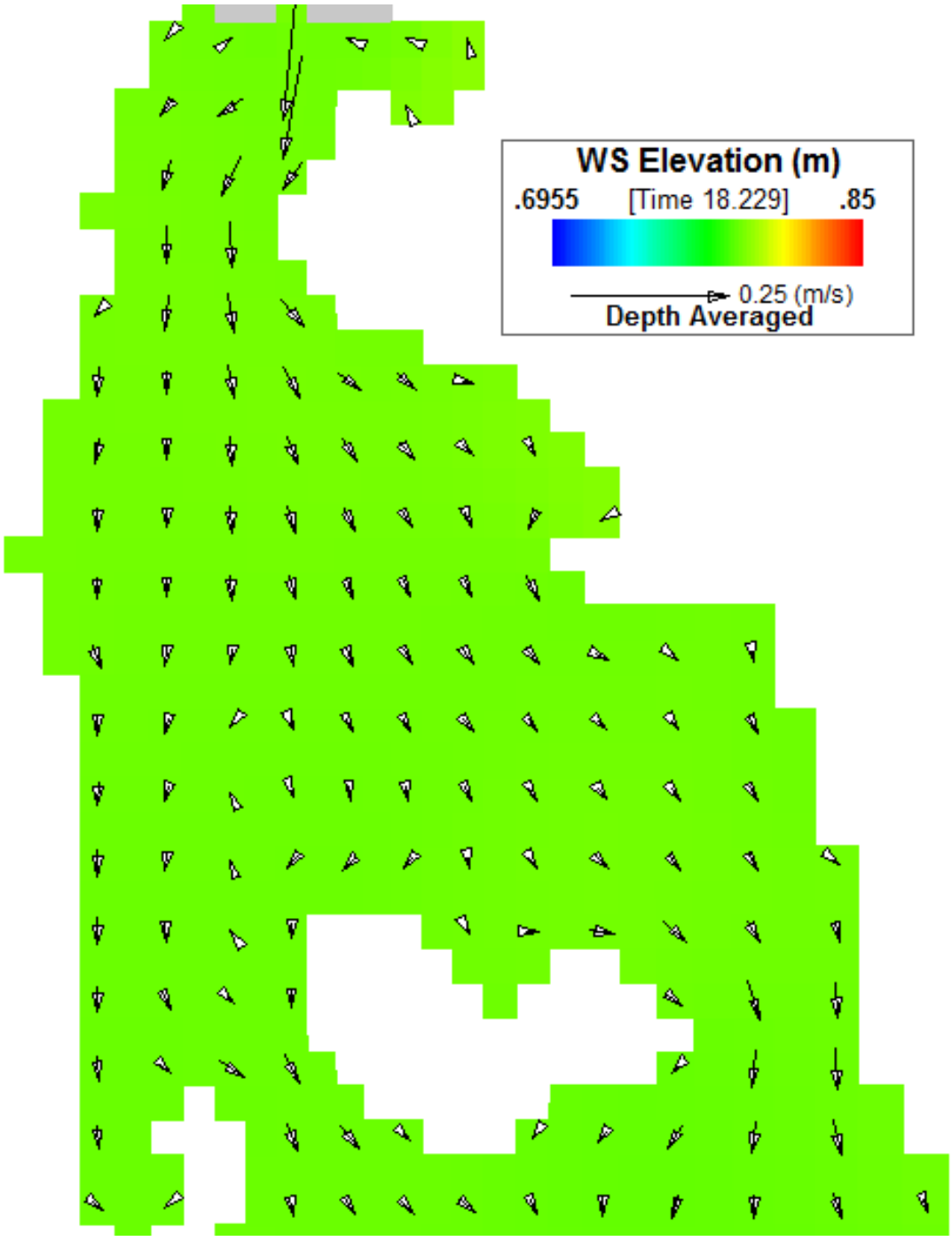

Figure E-3b Simulated velocity vectors at 1 hr after high water slack

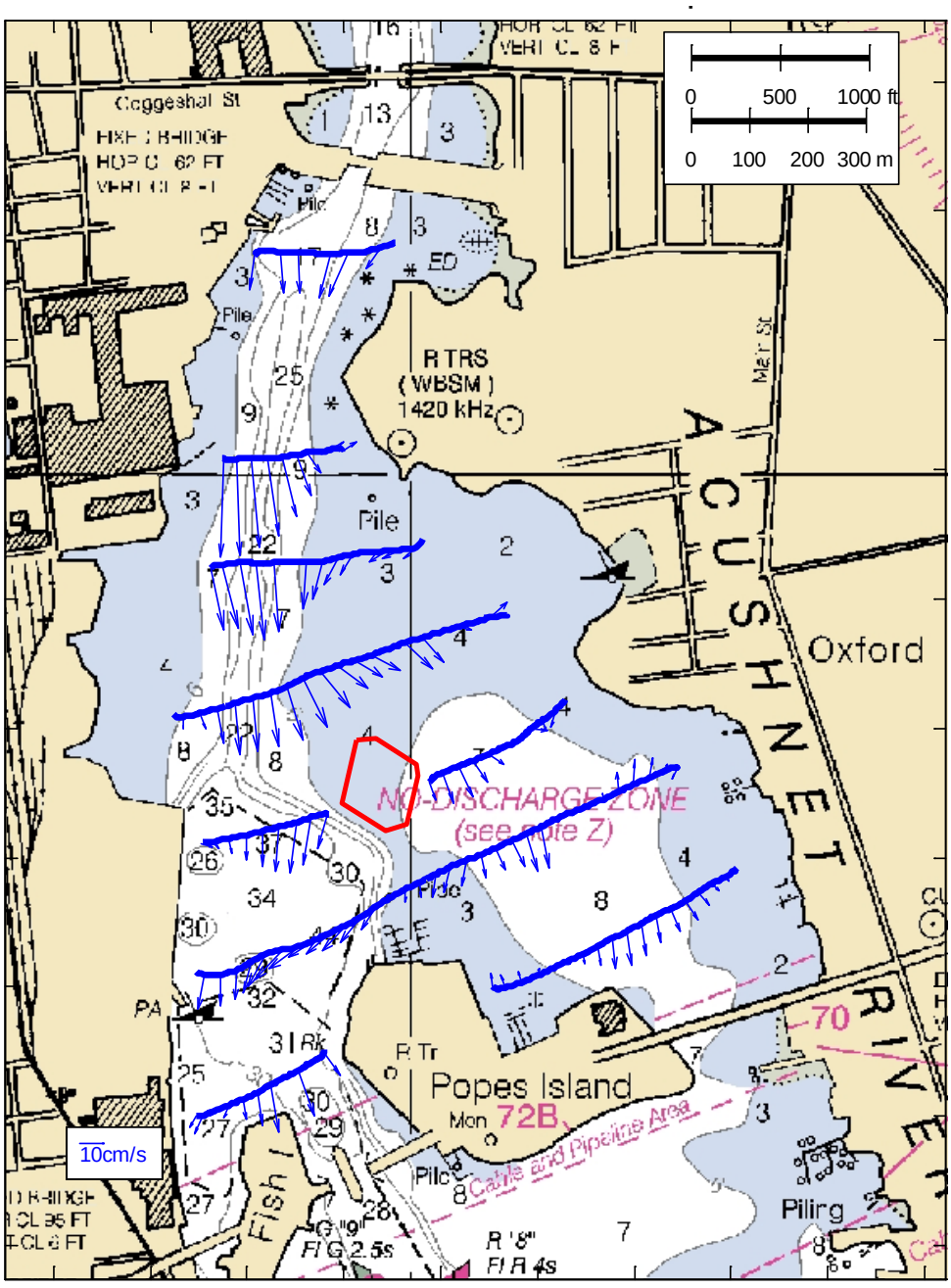

Figure E-4a Measured velocity vectors 2 hrs after high water slack

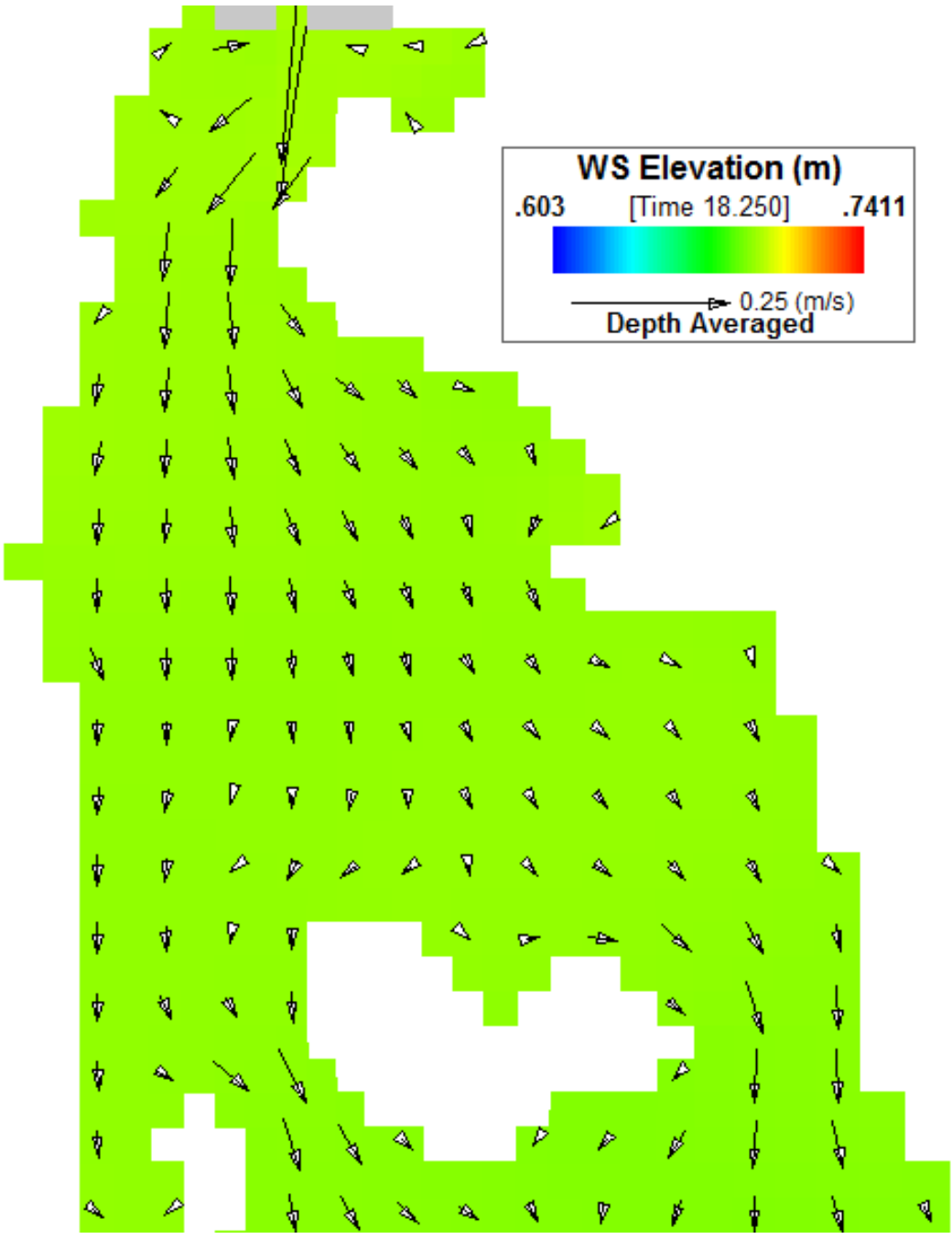

Figure E-4b Simulated velocity vectors 2 hrs after high water slack

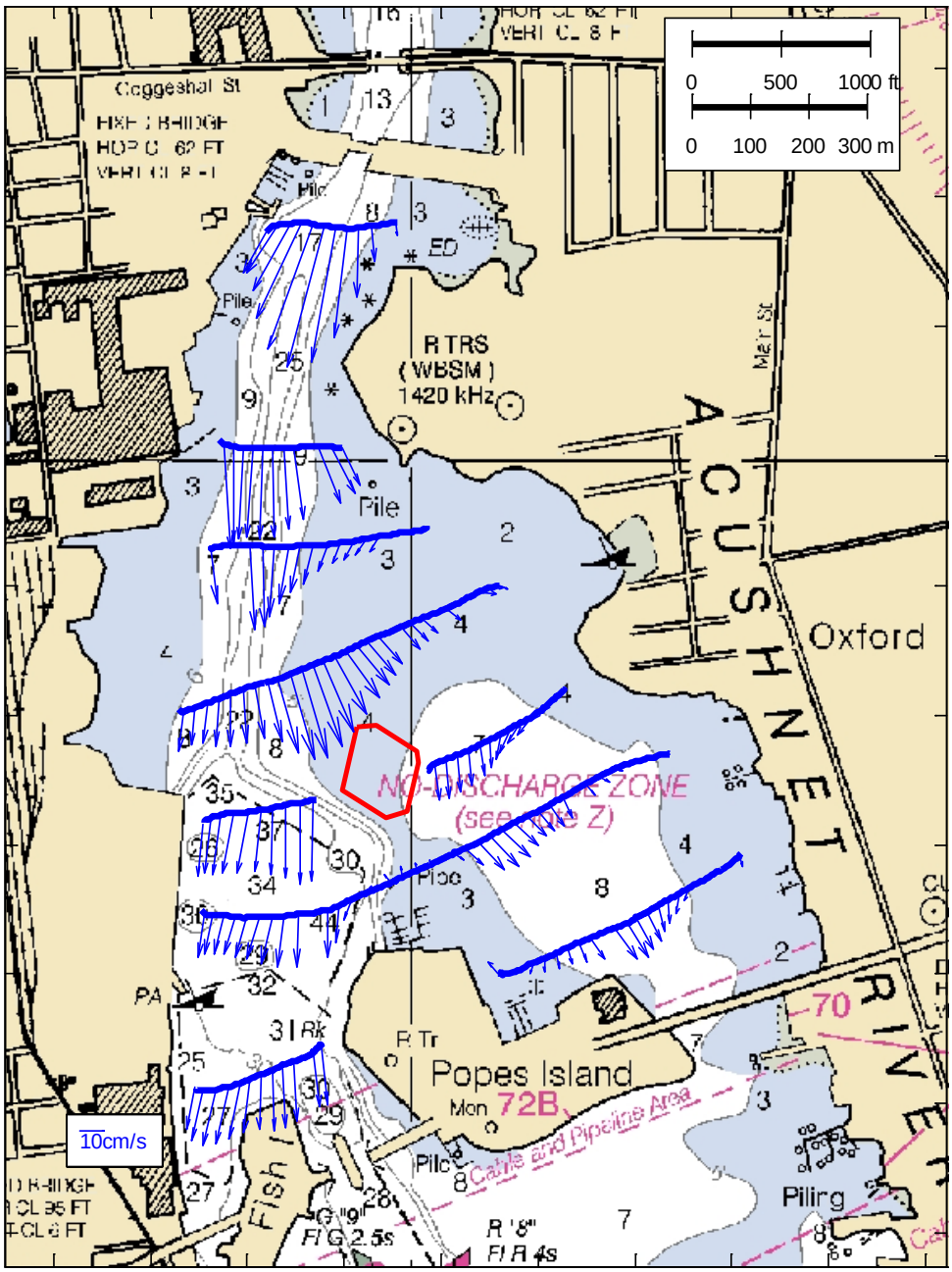

Figure E-5a Measured velocity vectors 3 hrs after high water slack

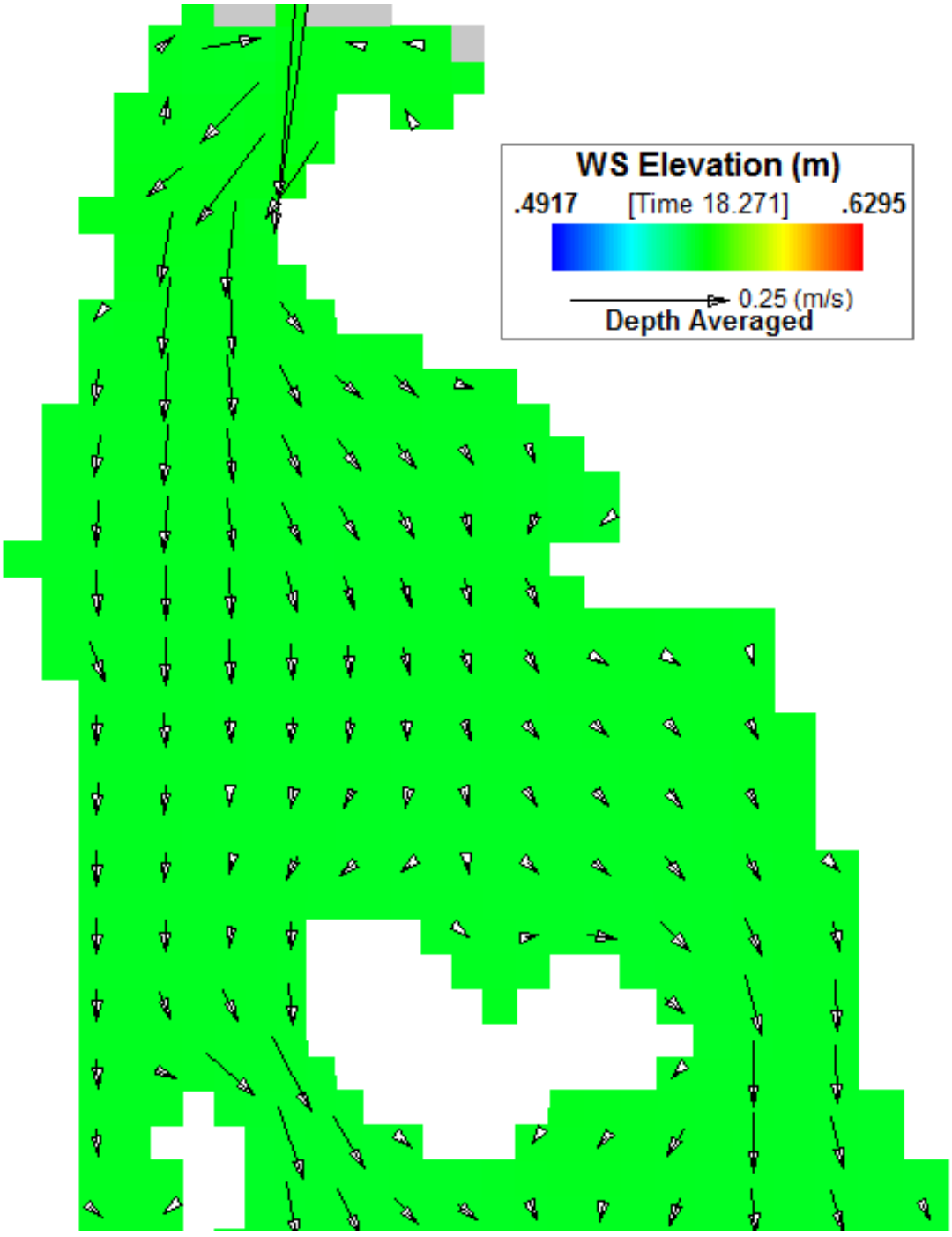

Figure E-5b Simulated velocity vectors 3 hrs after high water slack

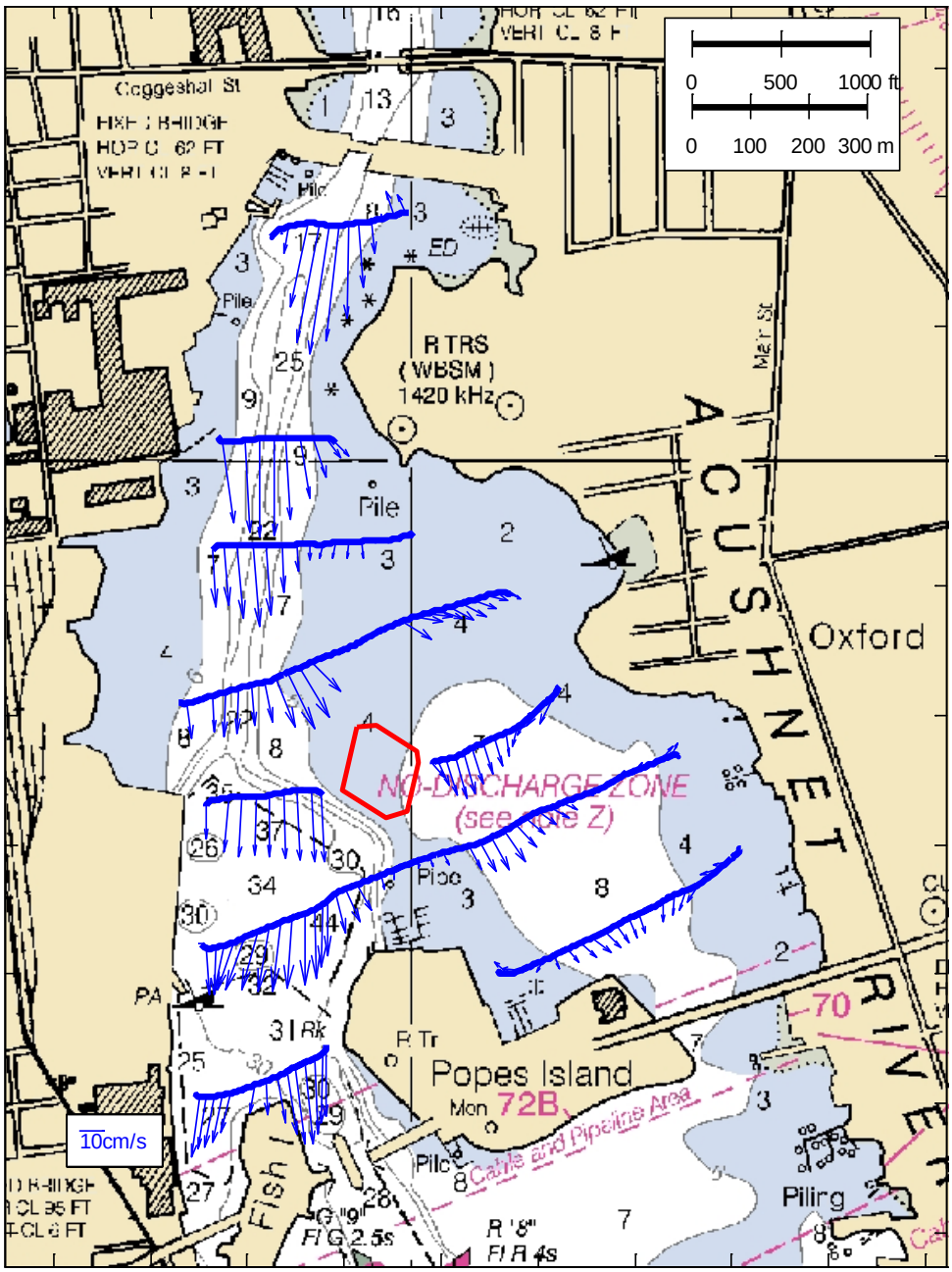

Figure E-6a Measured velocity vectors 4 hrs after high water slack

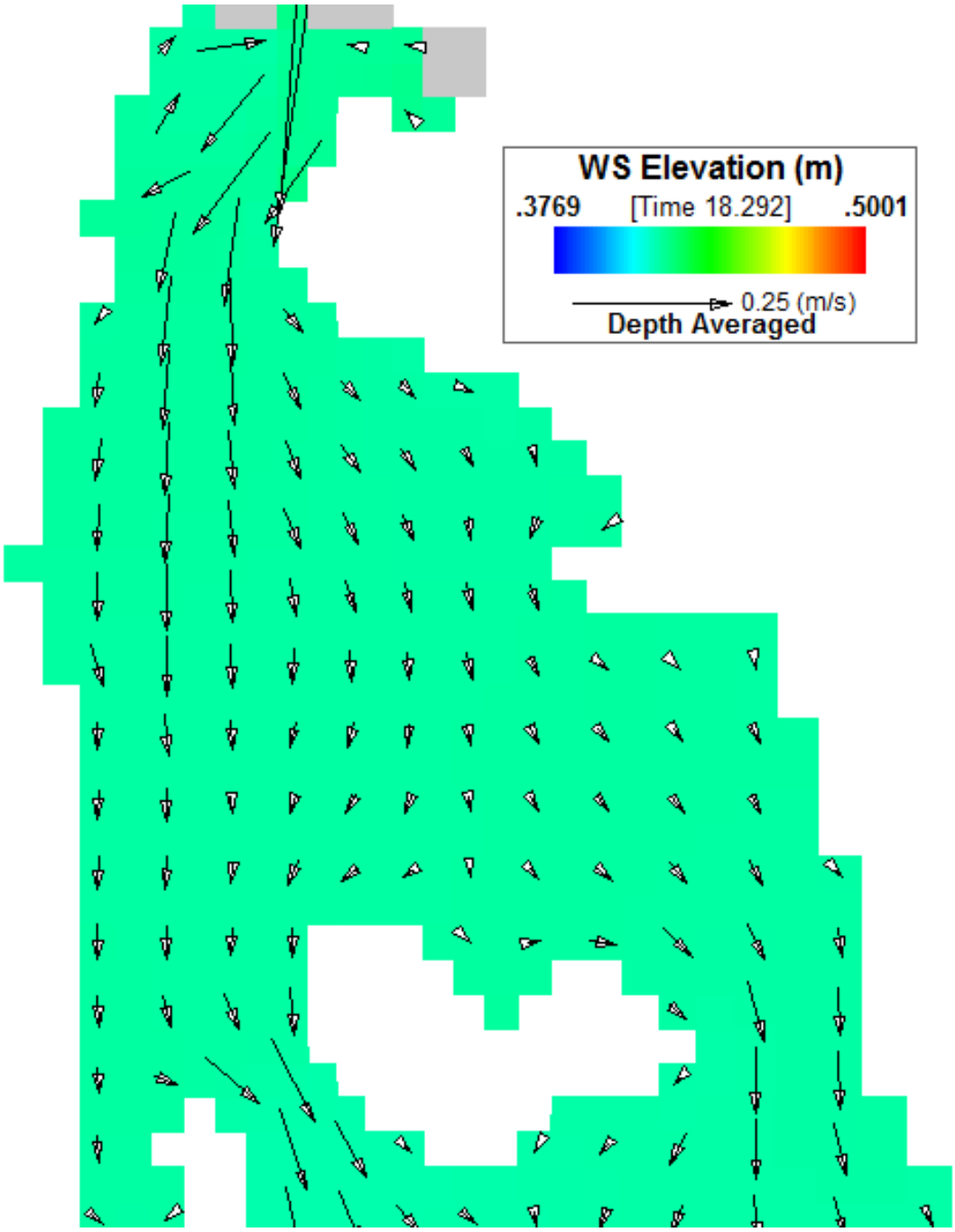

Figure E-6b Simulated velocity vectors 4 hrs after high water slack

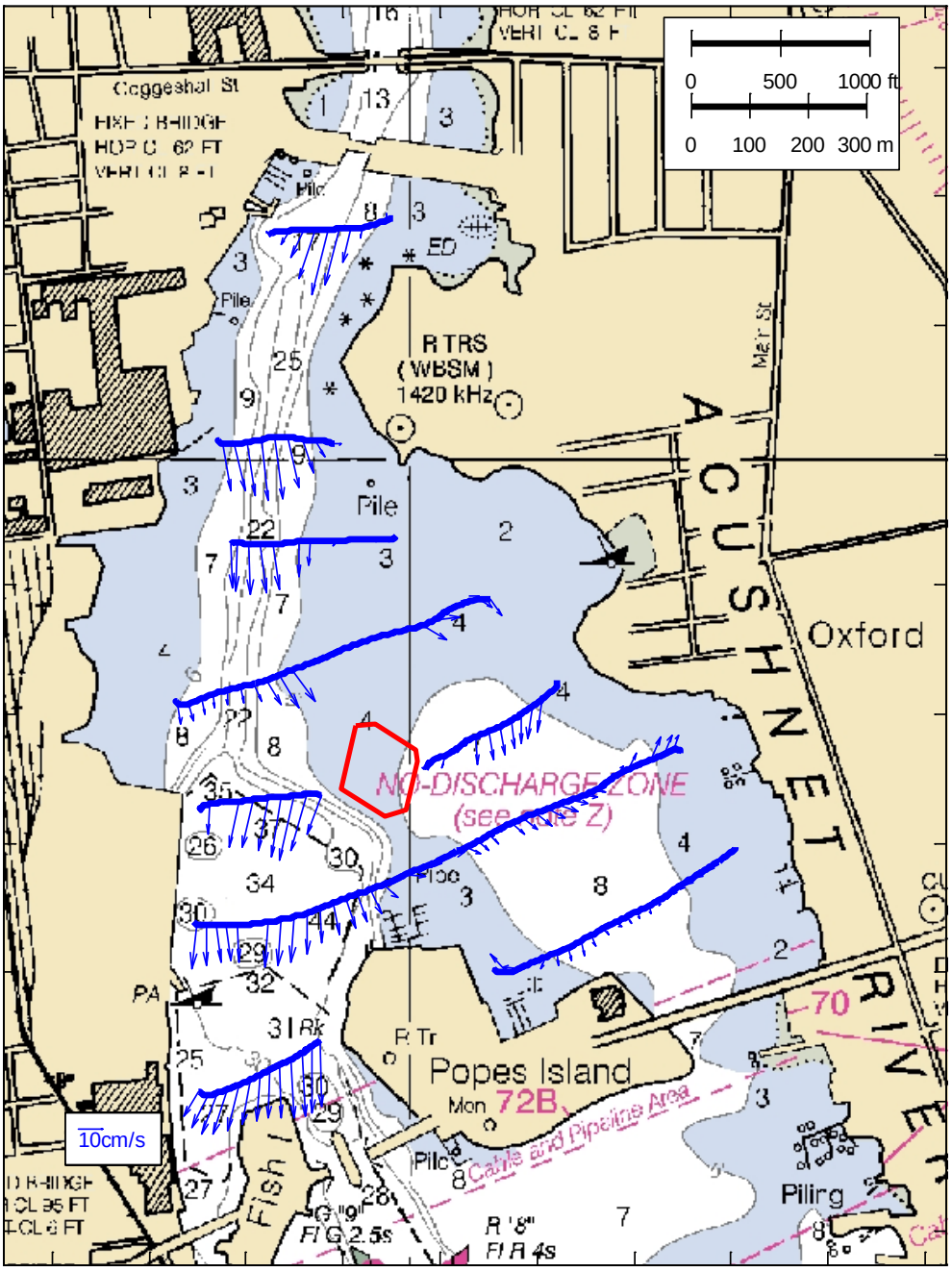

Figure E-7a Measured velocity vectors 5 hrs after high water slack

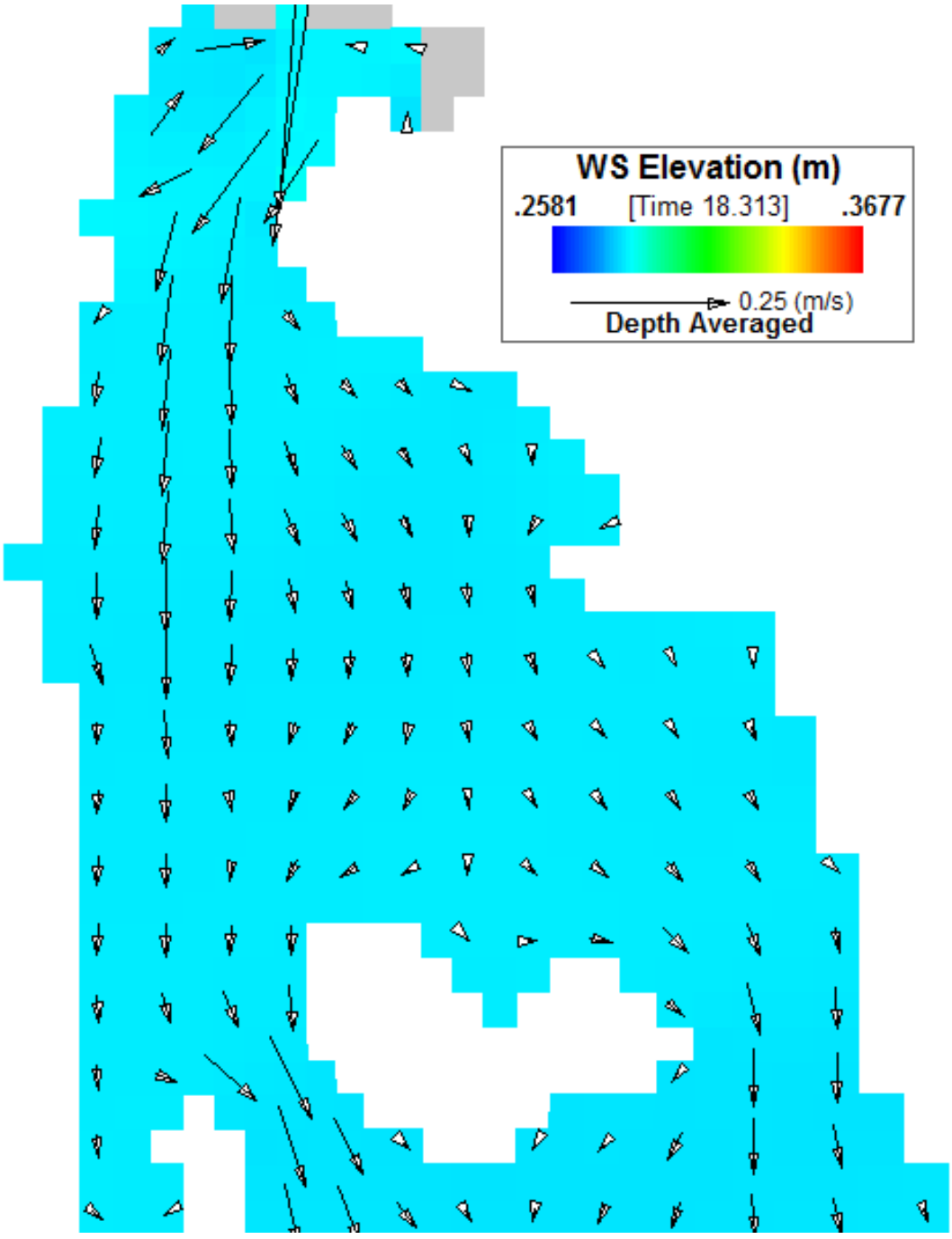

Figure E-7b Simulated velocity vectors 5 hrs after high water slack

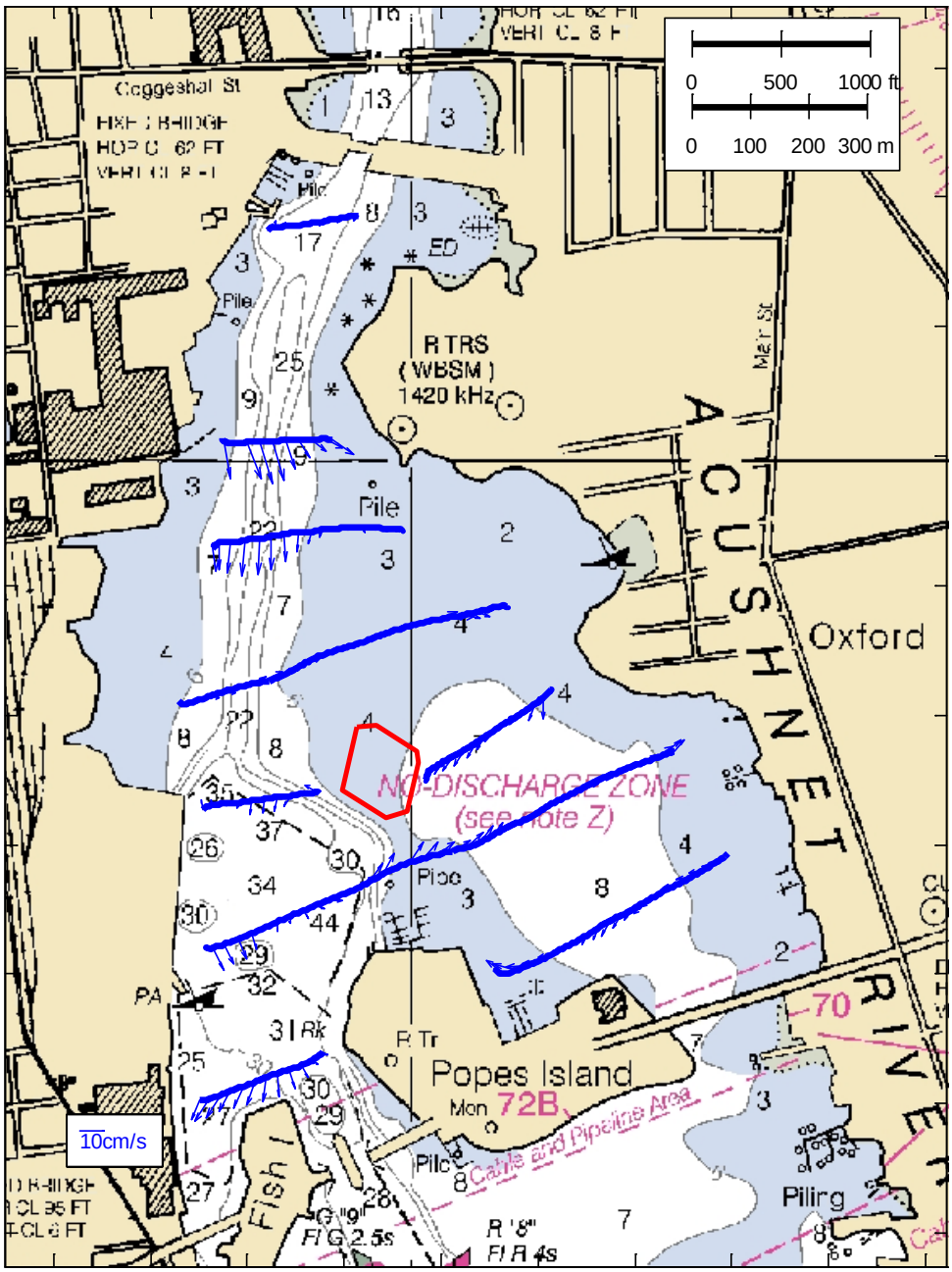

Figure E-8a Measured velocity vectors 6 hrs after high water slack

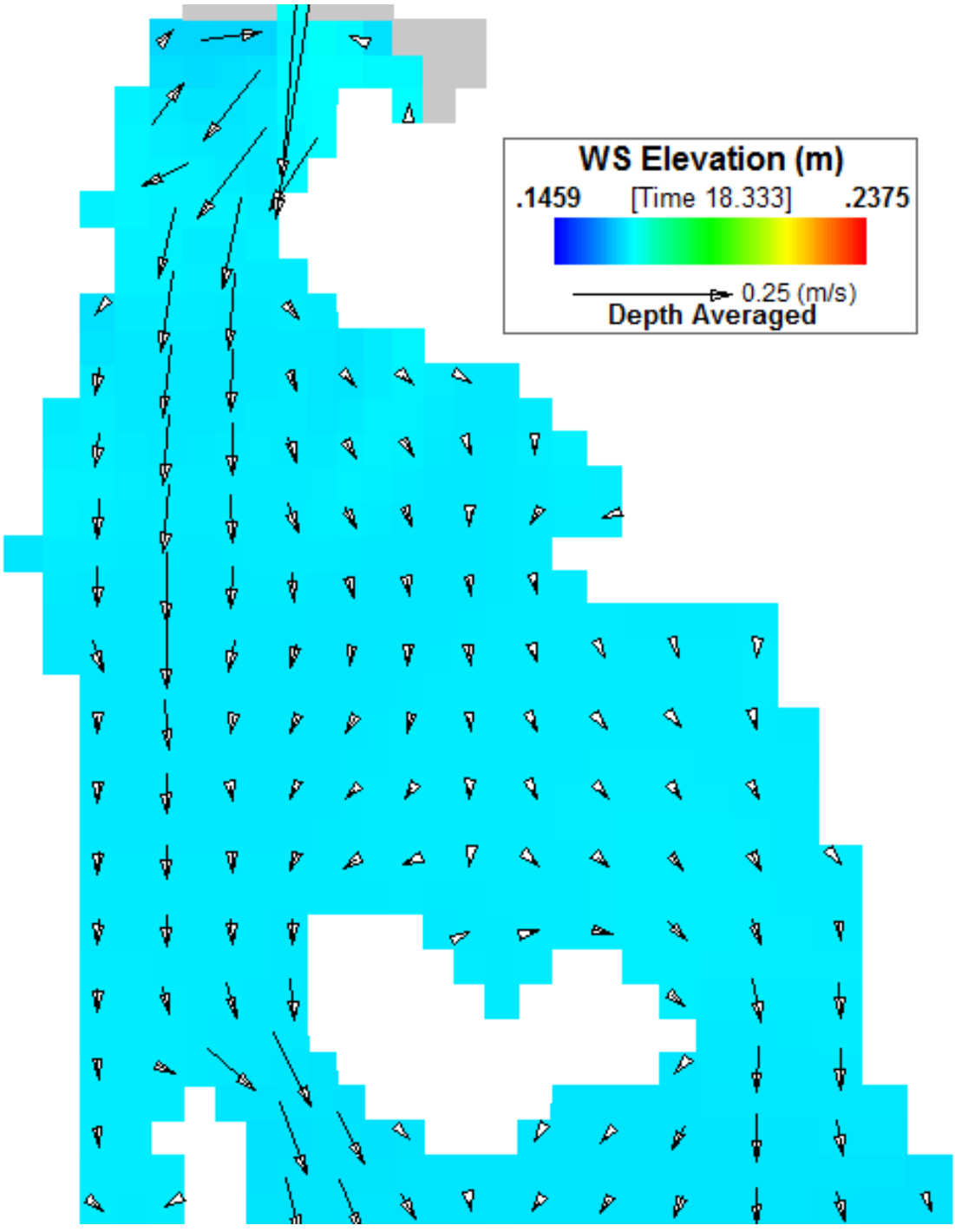

Figure E-8b Simulated velocity vectors 6 hrs after high water slack

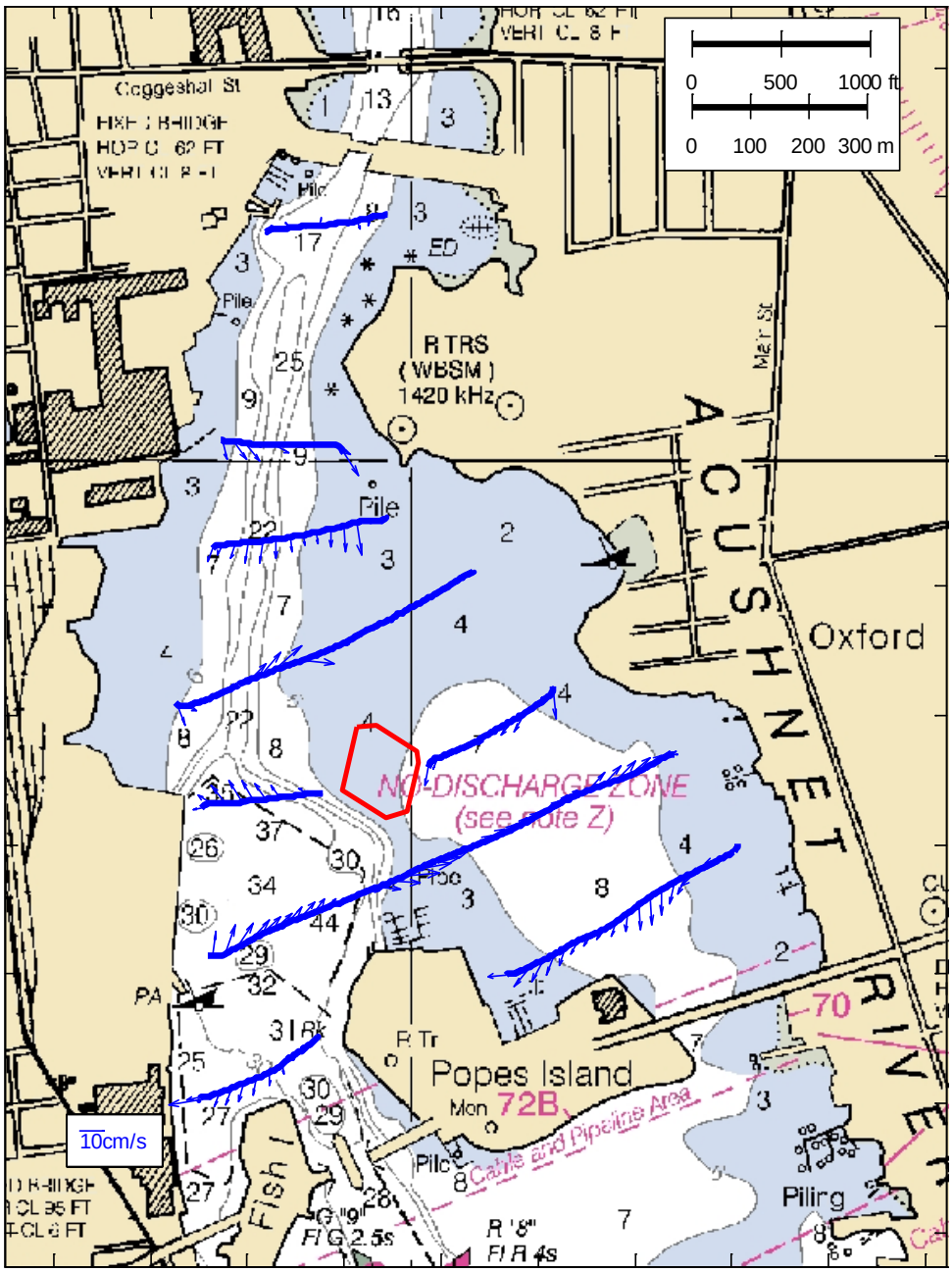

Figure E-9a Measured velocity vectors at low water slack

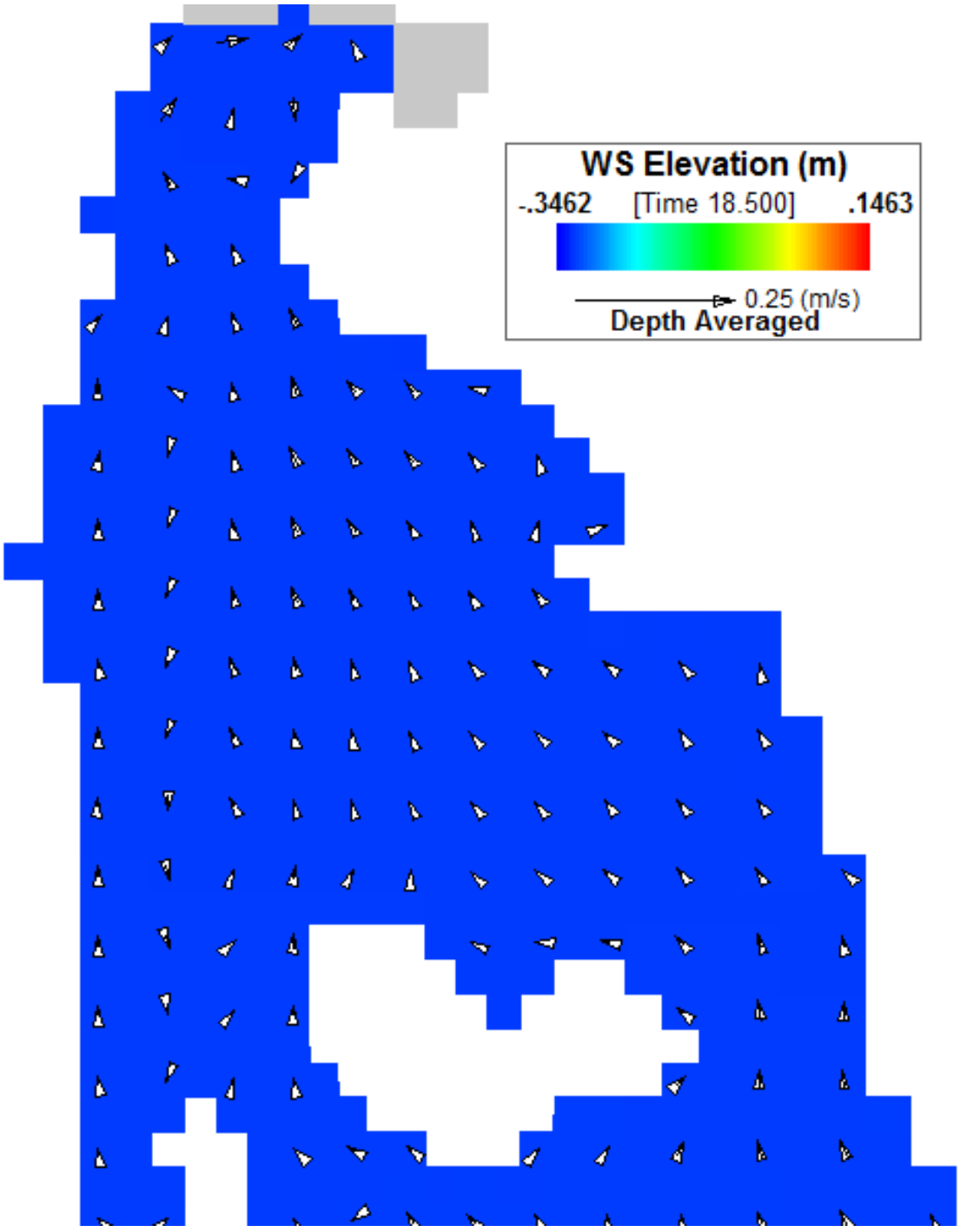

Figure E-9b Simulated velocity vectors at low water slack

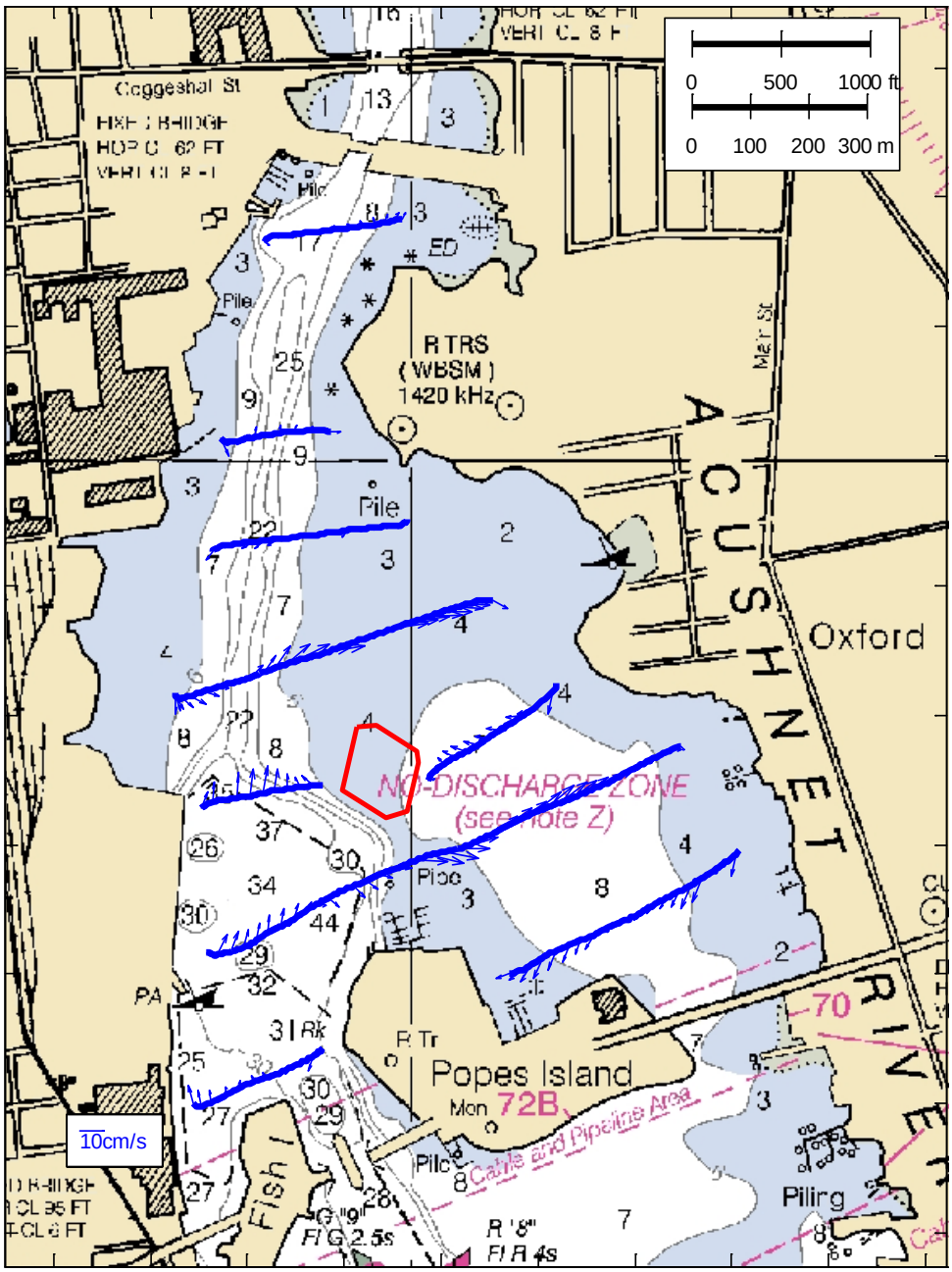

Figure E-10a Measured velocity vectors 0.5 hrs after low water slack

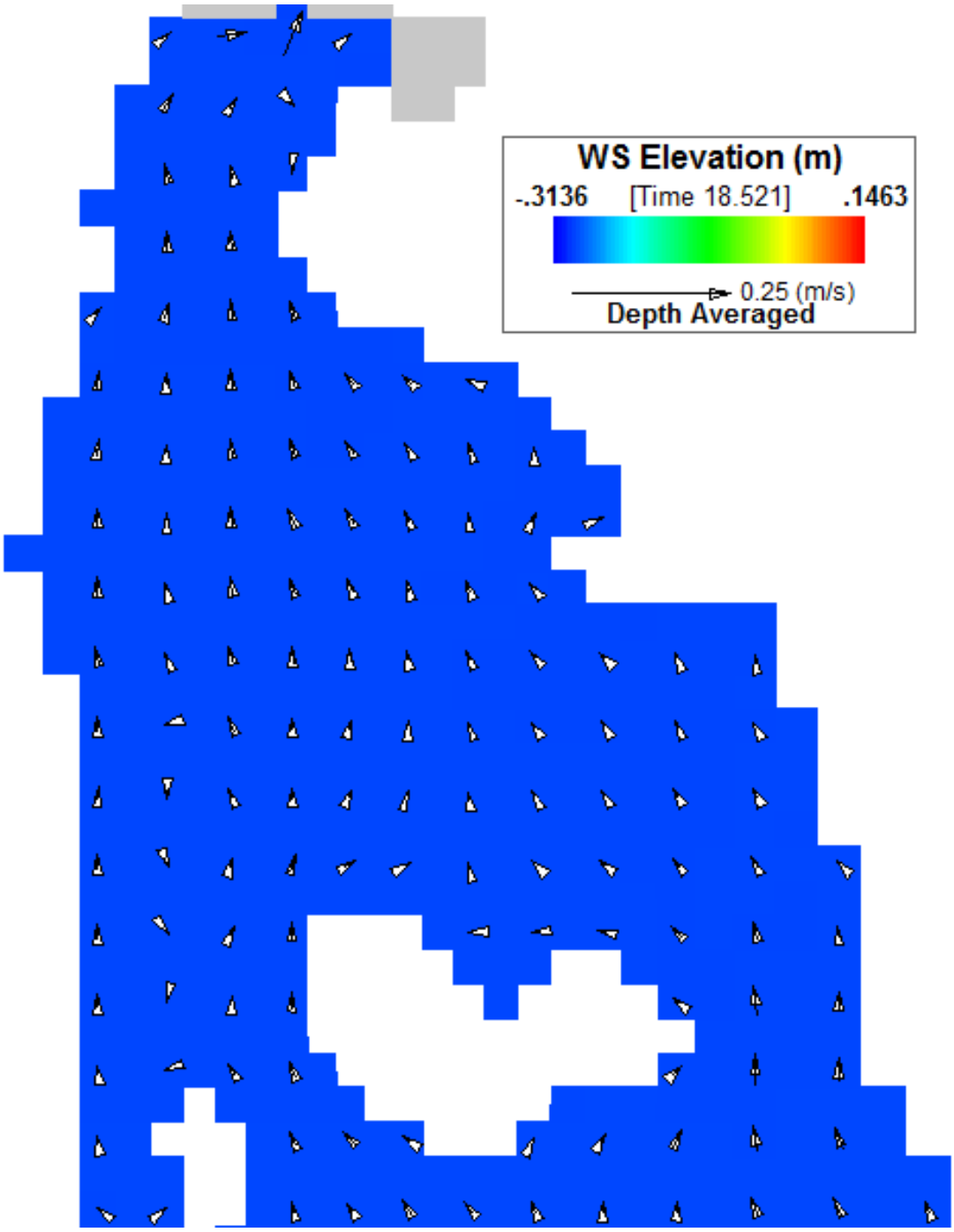

Figure E-10b Simulated velocity vectors 0.5 hrs after low water slack

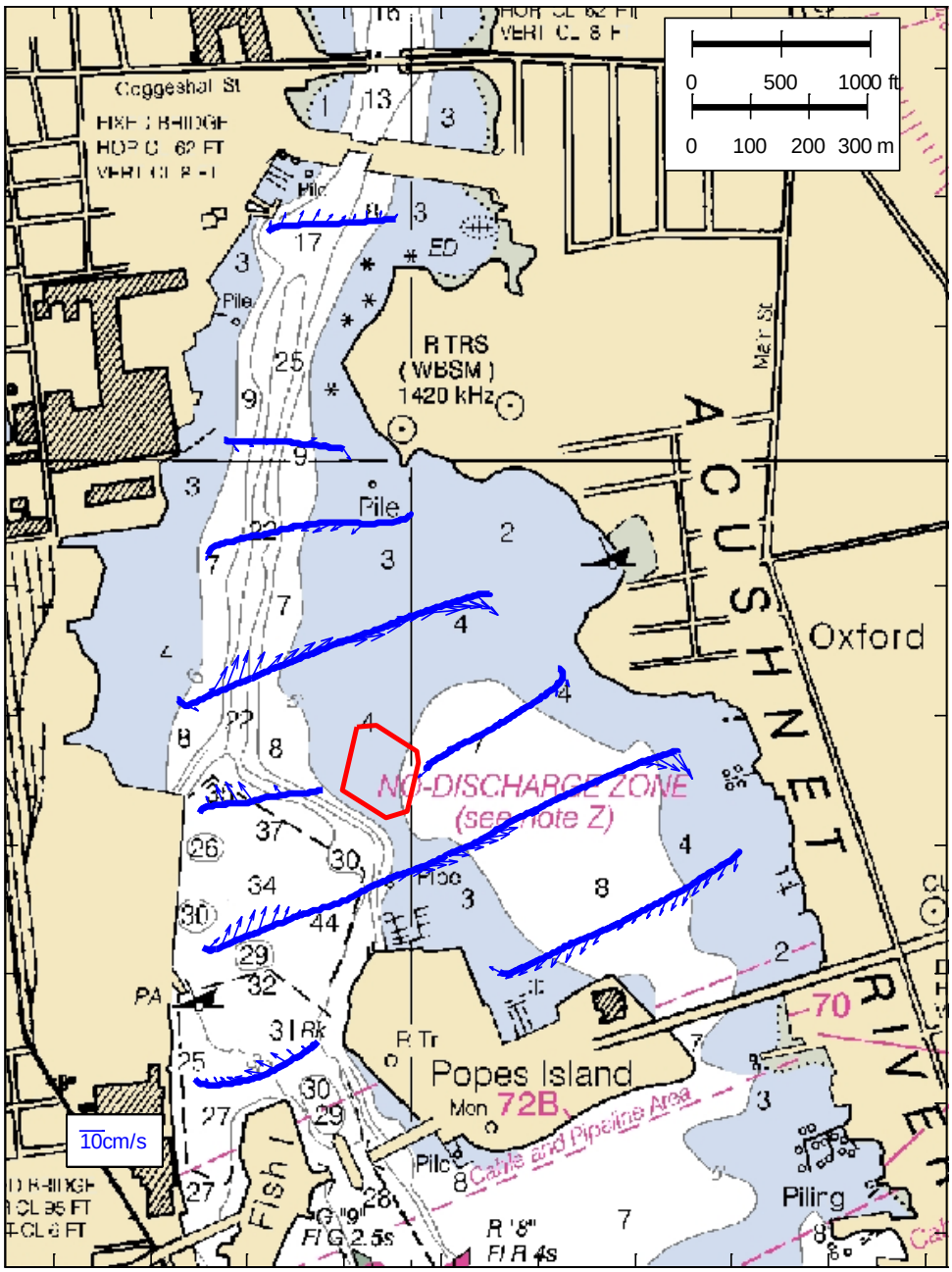

Figure E-11a Measured velocity vectors 1.5 hrs after low water slack

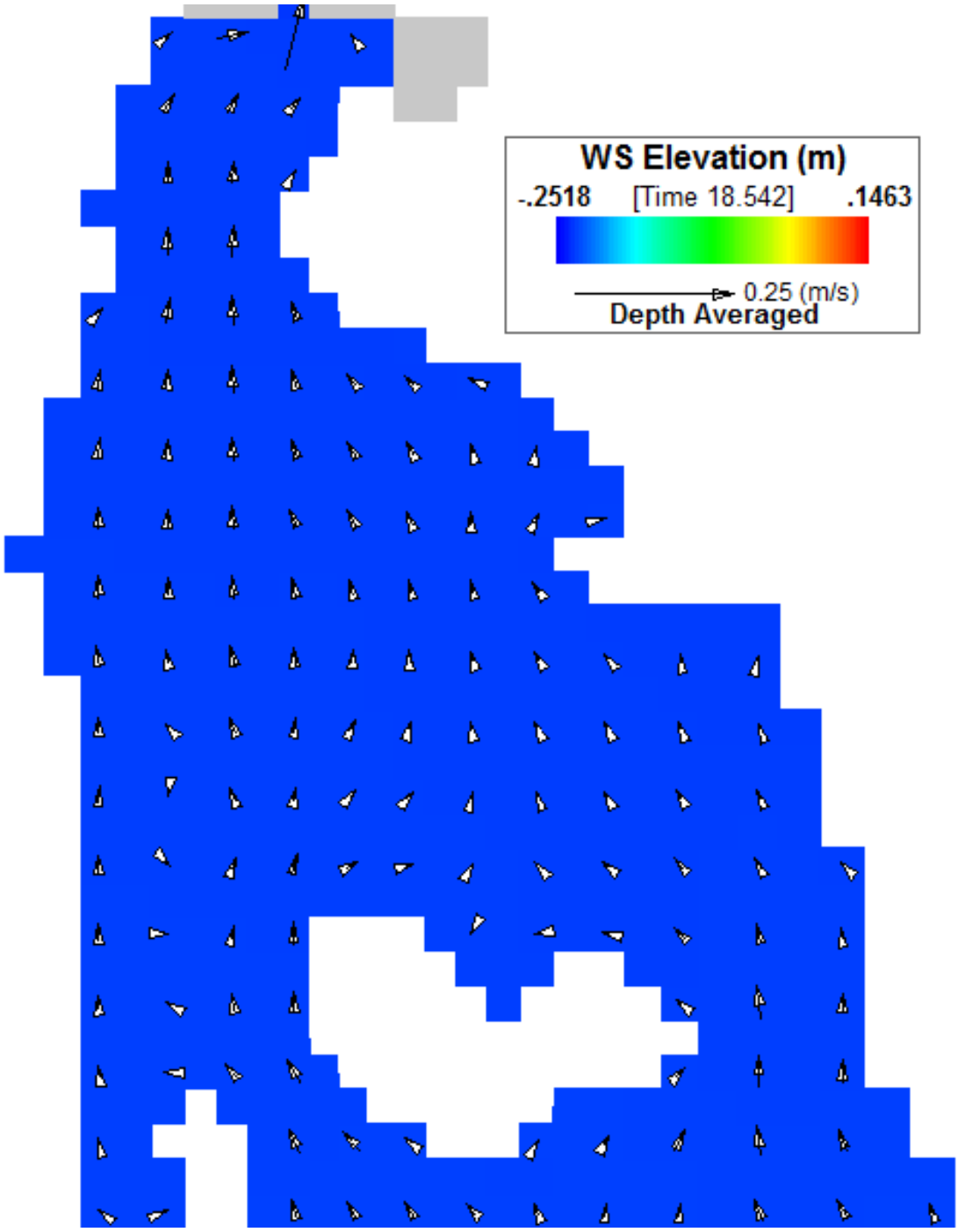

Figure E-11b Simulated velocity vectors 1.5 hrs after low water slack

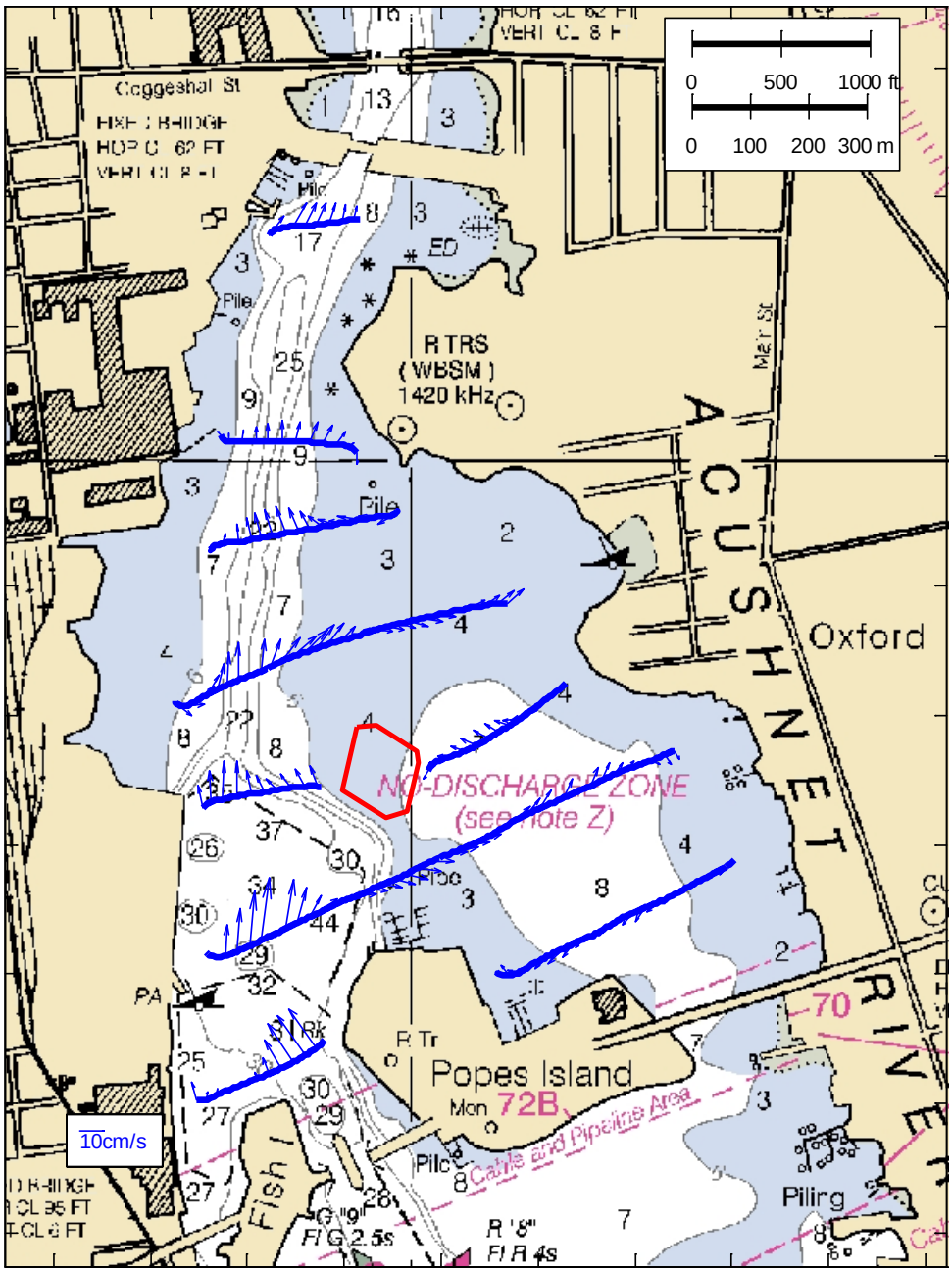

Figure E-12a Measured velocity vectors 2.5 hrs after low water slack

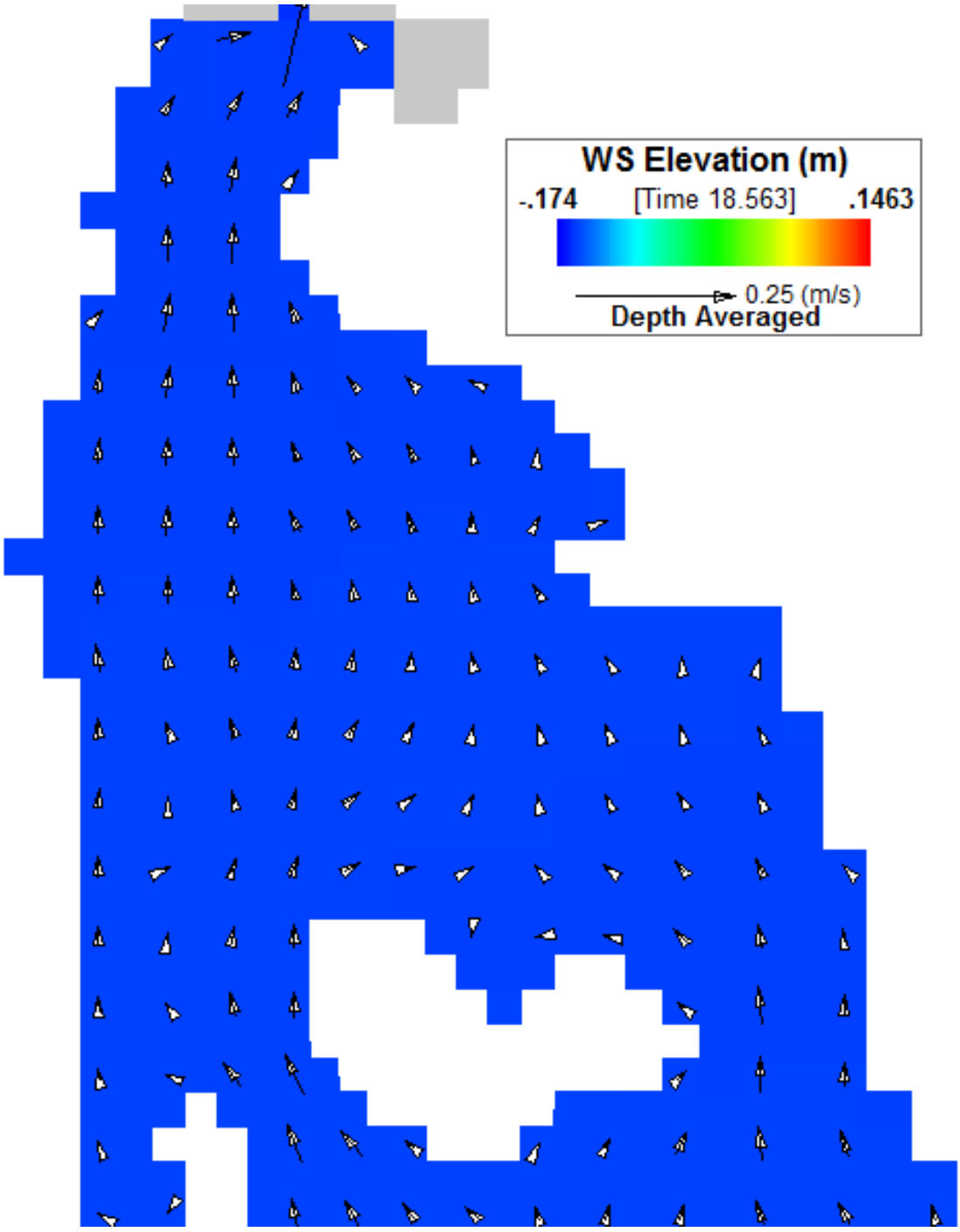

Figure E-12b Simulated velocity vectors 2.5 hrs after low water slack

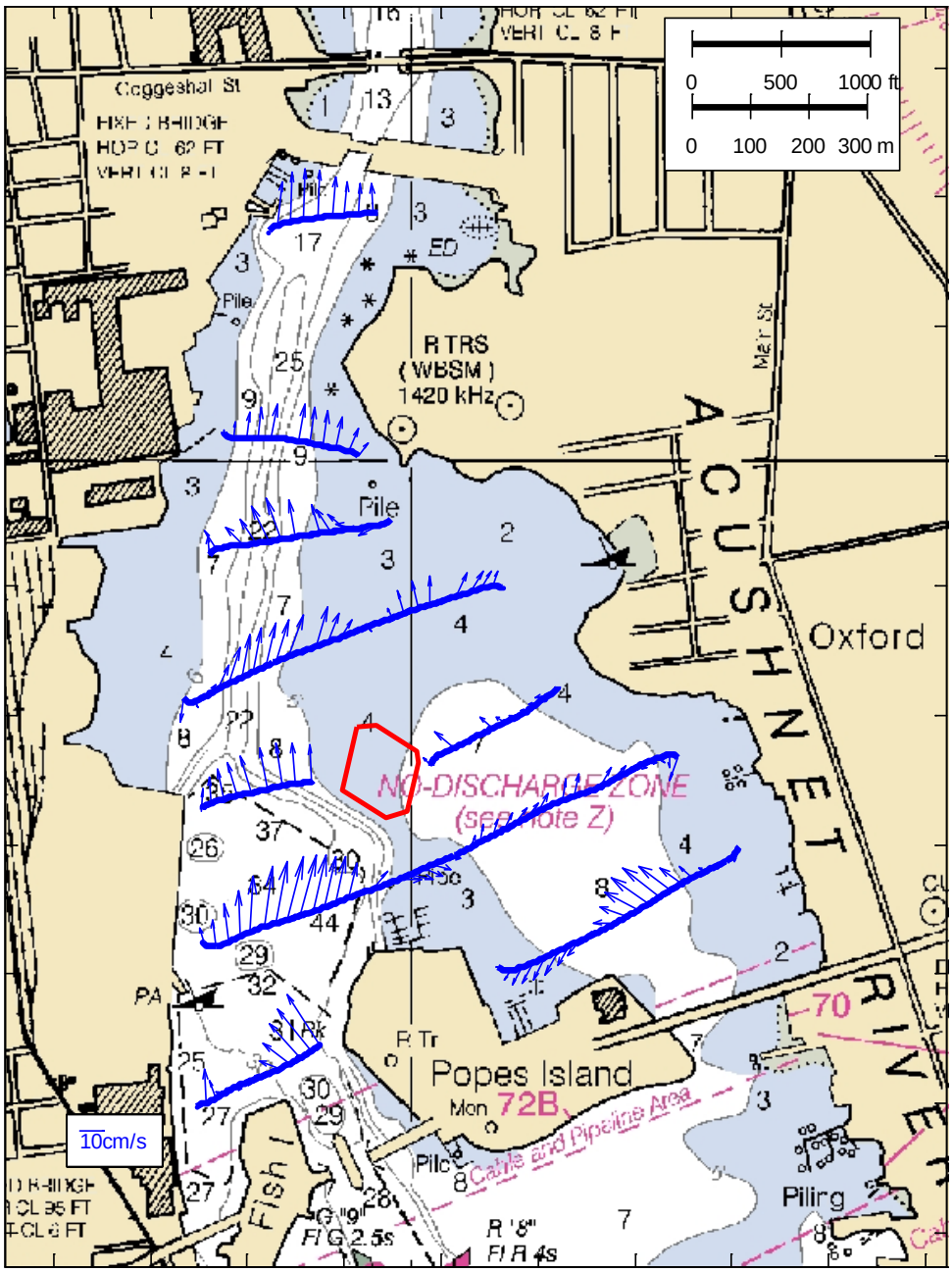

Figure E-13a Measured velocity vectors 3.5 hrs after low water slack

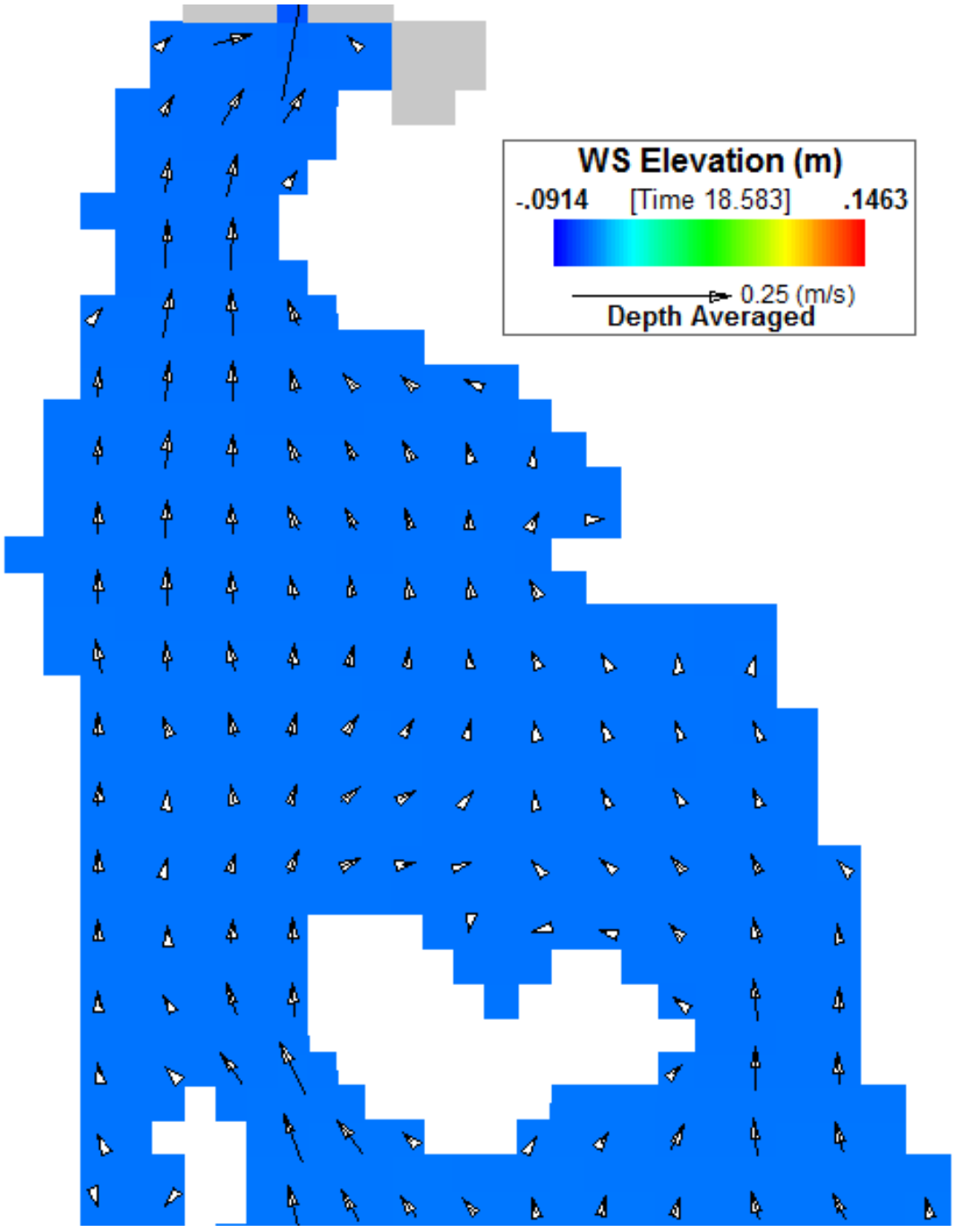

Figure E-13b Simulated velocity vectors 3.5 hrs after low water slack

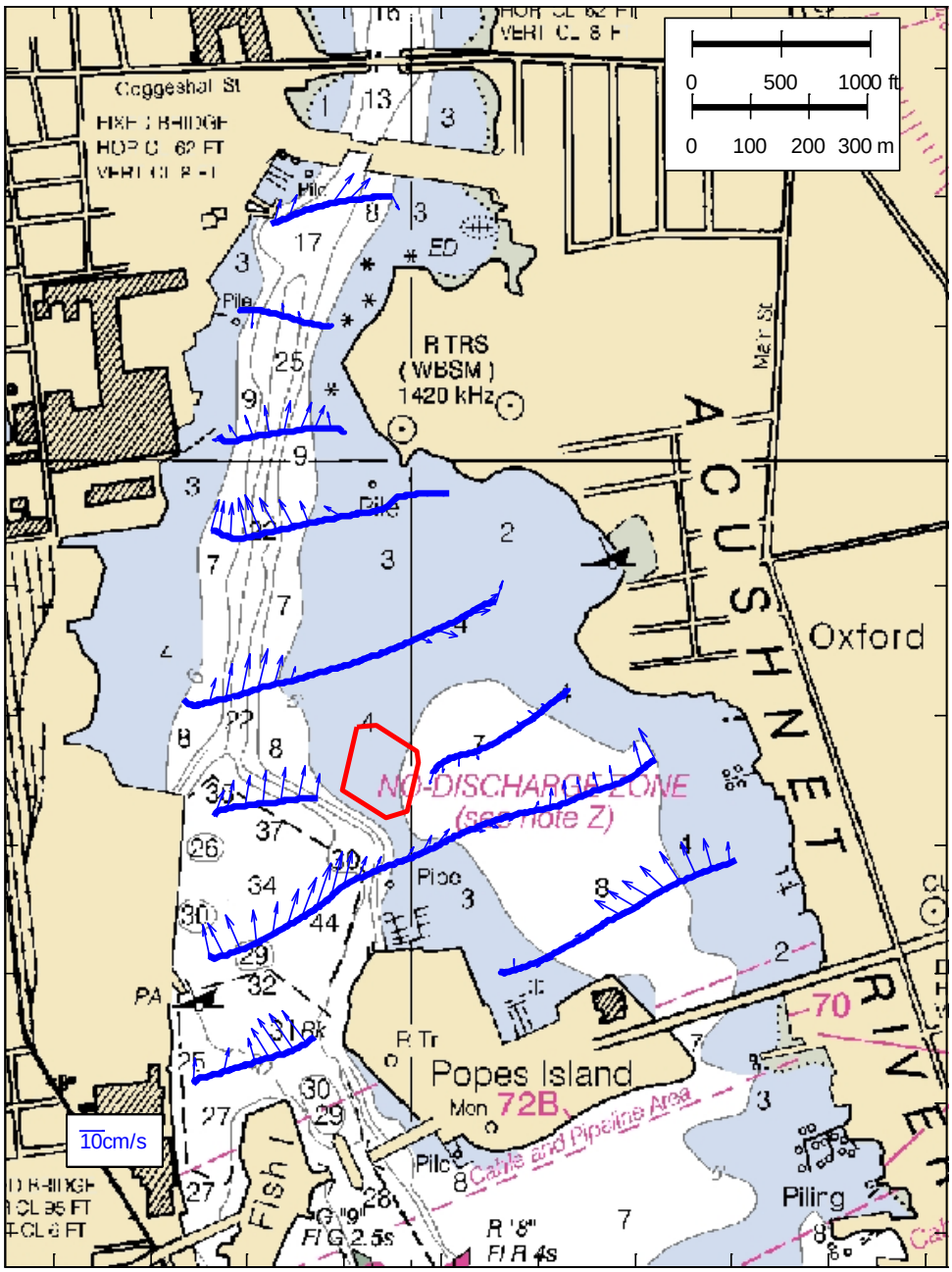

Figure E-14a Measured velocity vectors 2 hrs before high water slack

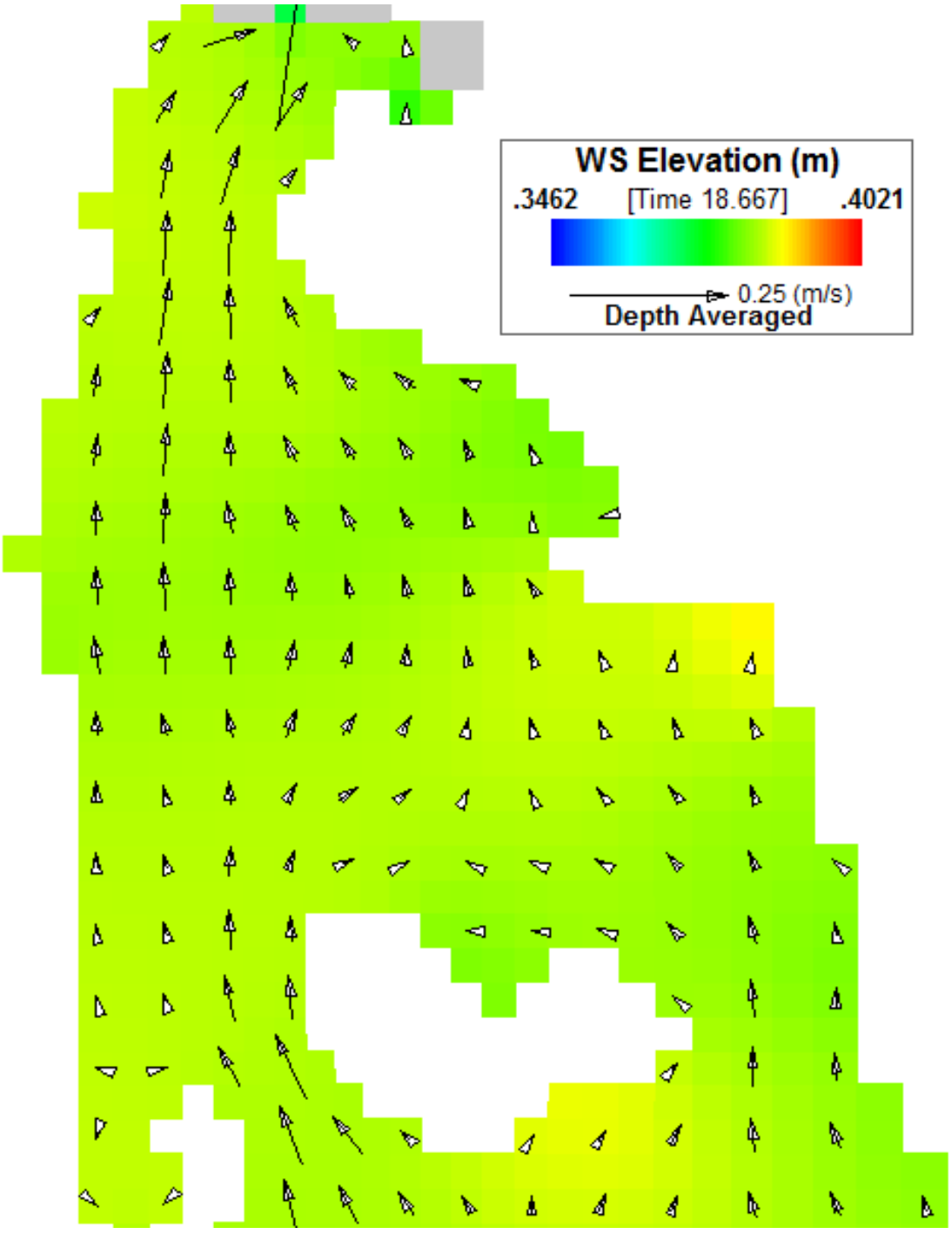

Figure E-14b Simulated velocity vectors 2 hrs before high water slack

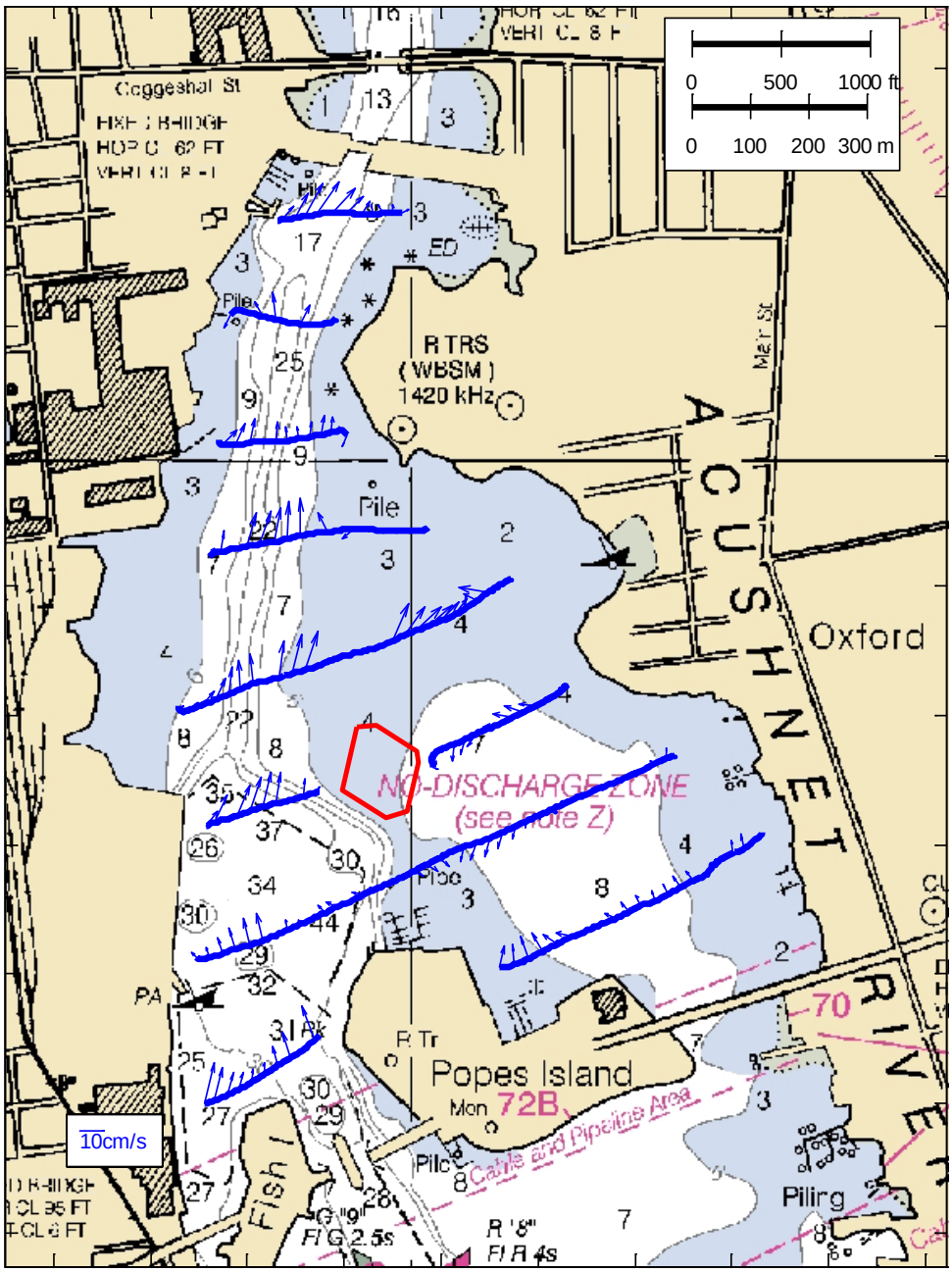

Figure E-15a Measured velocity vectors 1 hr before high water slack

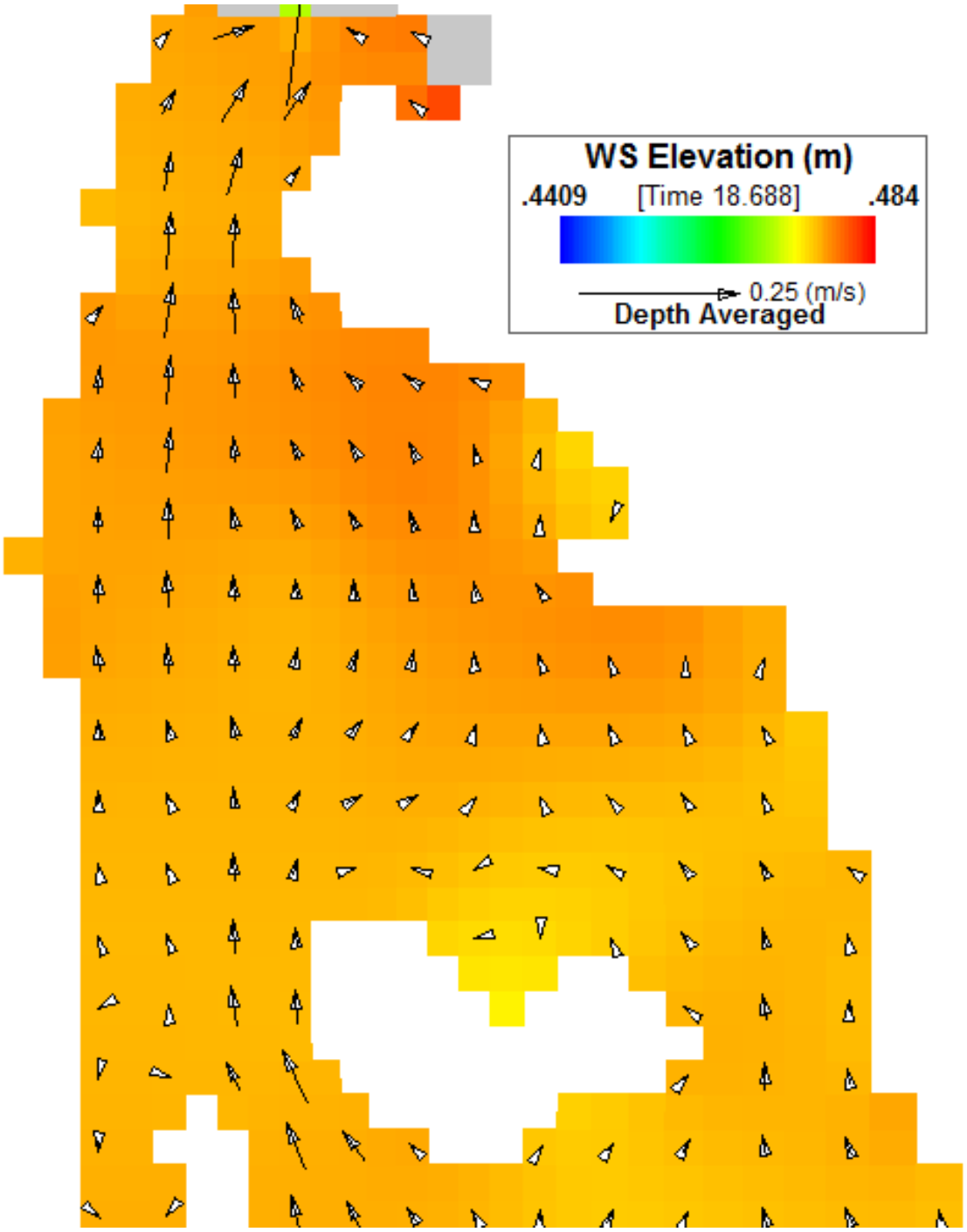

Figure E-15b Simulated velocity vectors 1 hr before high water slack

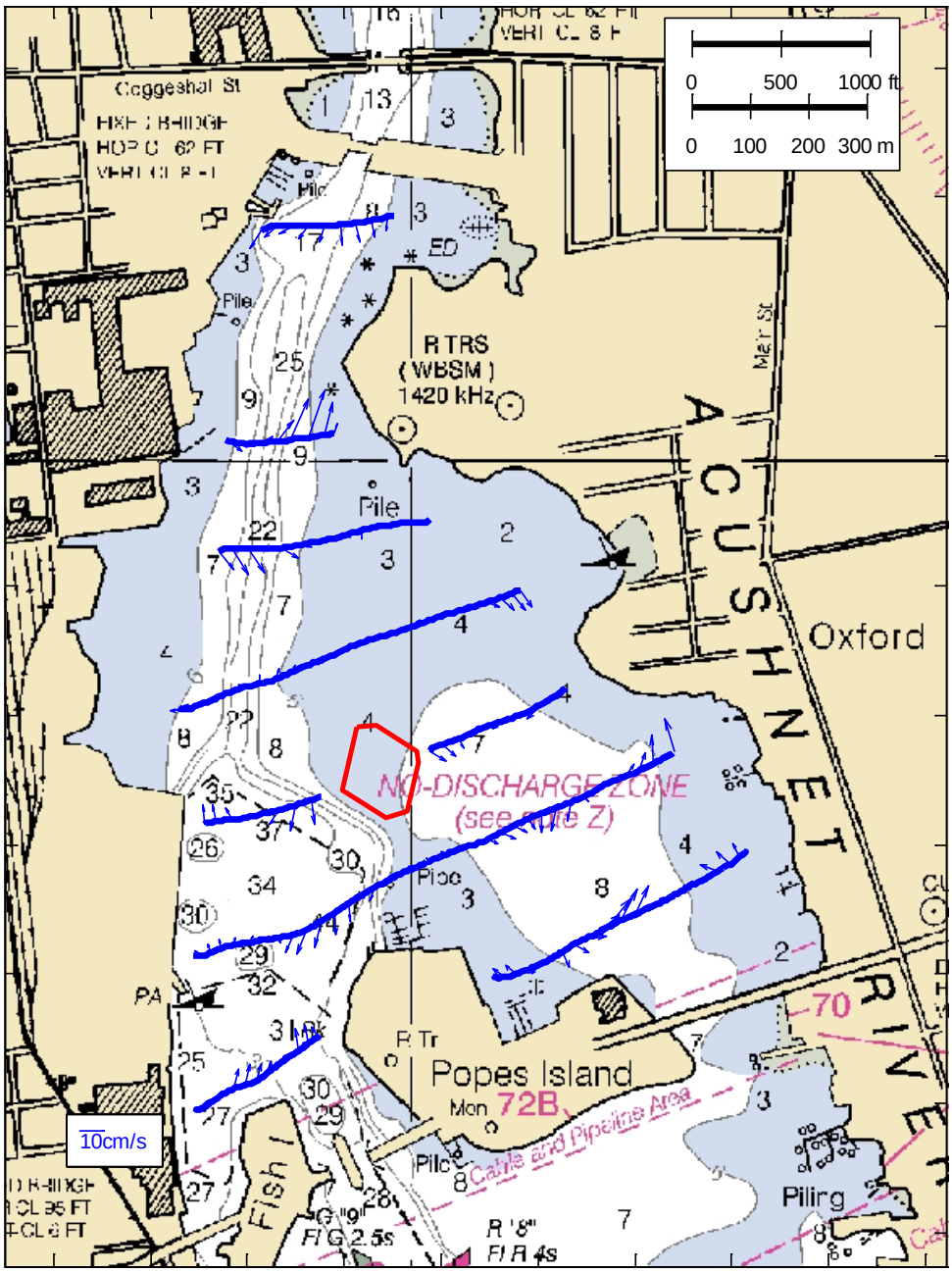

Figure E-16a Measured velocity vectors at high water slack

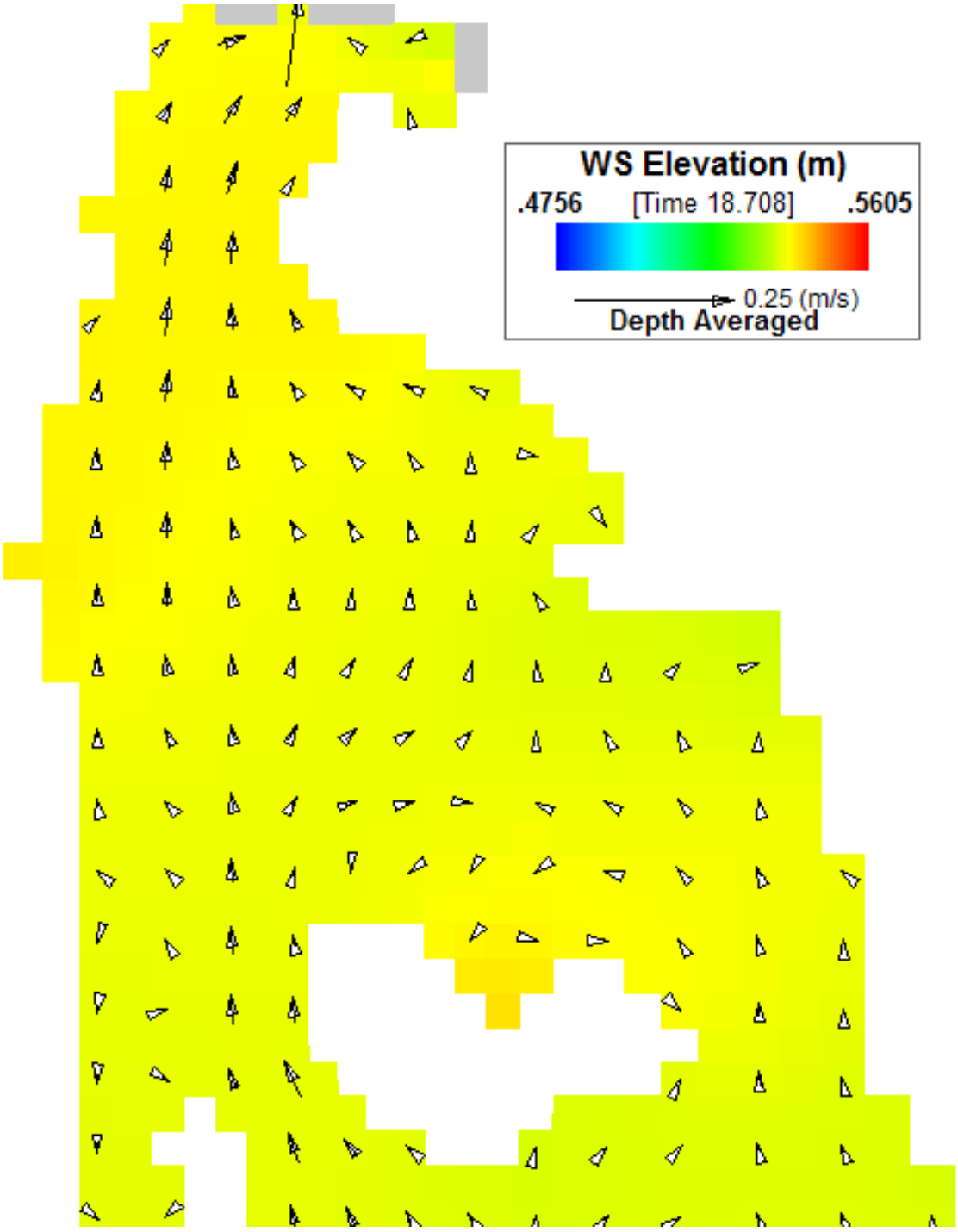

Figure E-16b Simulated velocity vectors at high water slack

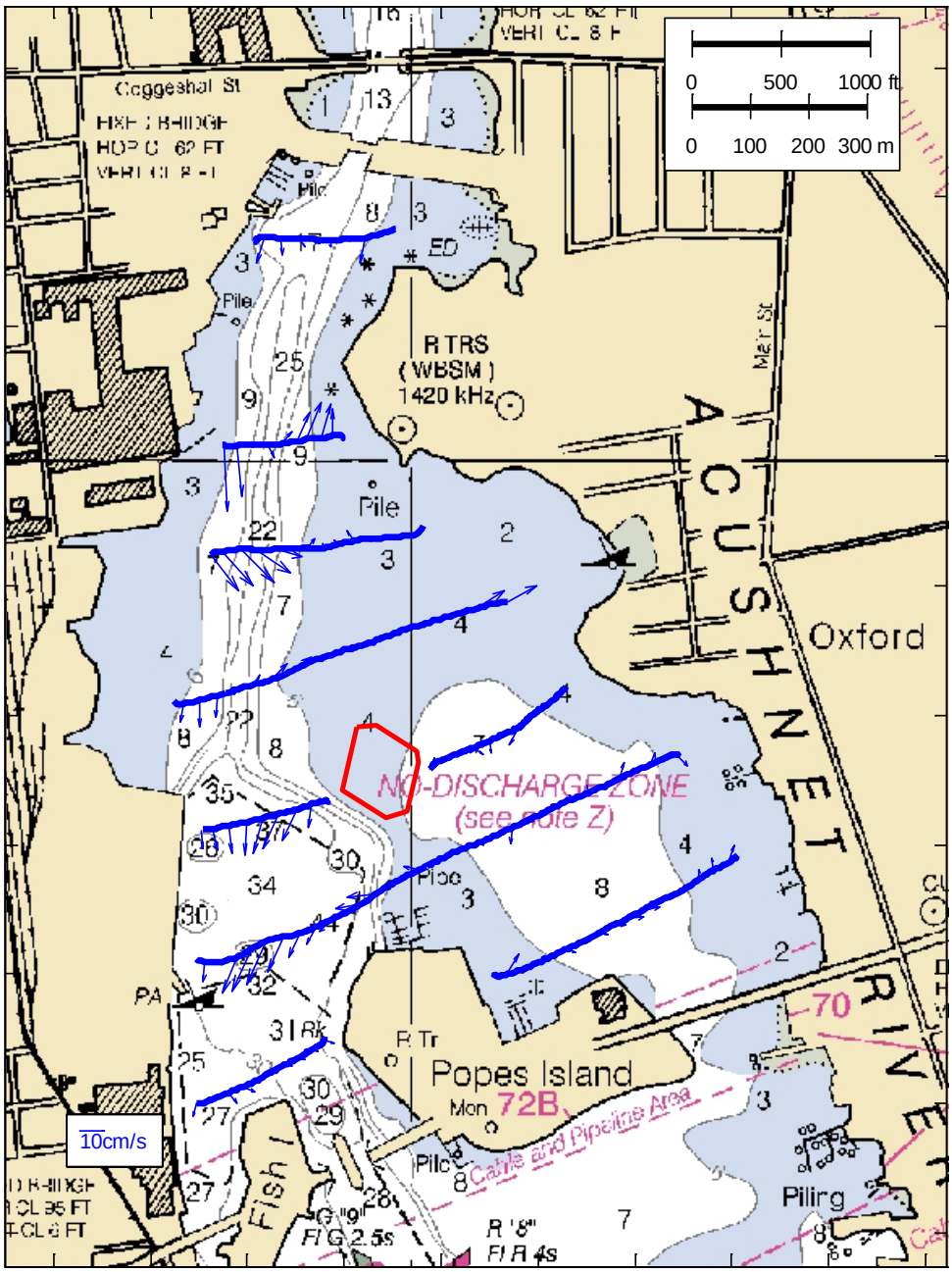

Figure E-17a Measured velocity vectors 1 hr after high water slack

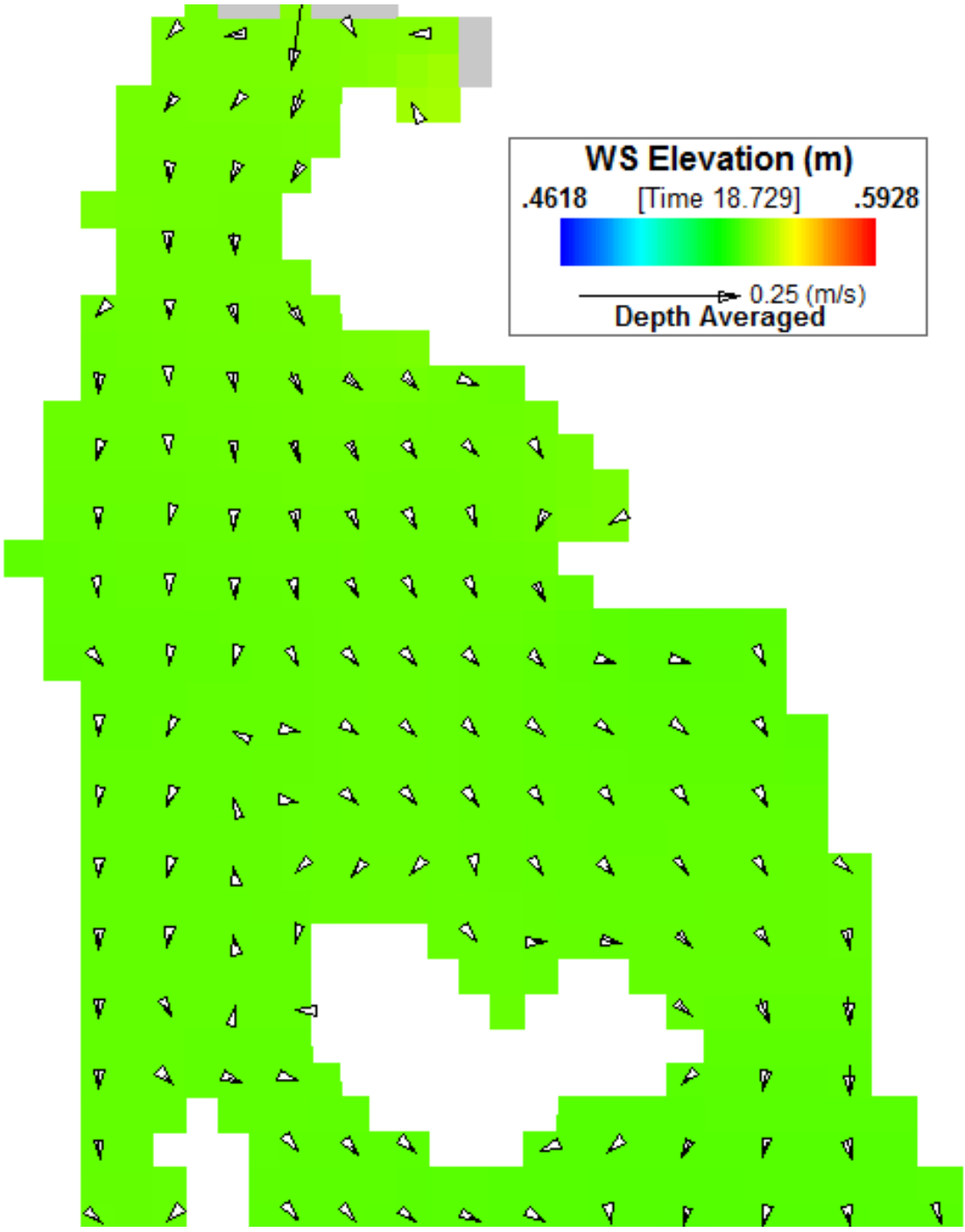

Figure E-17b Simulated velocity vectors 1 hr after high water slack

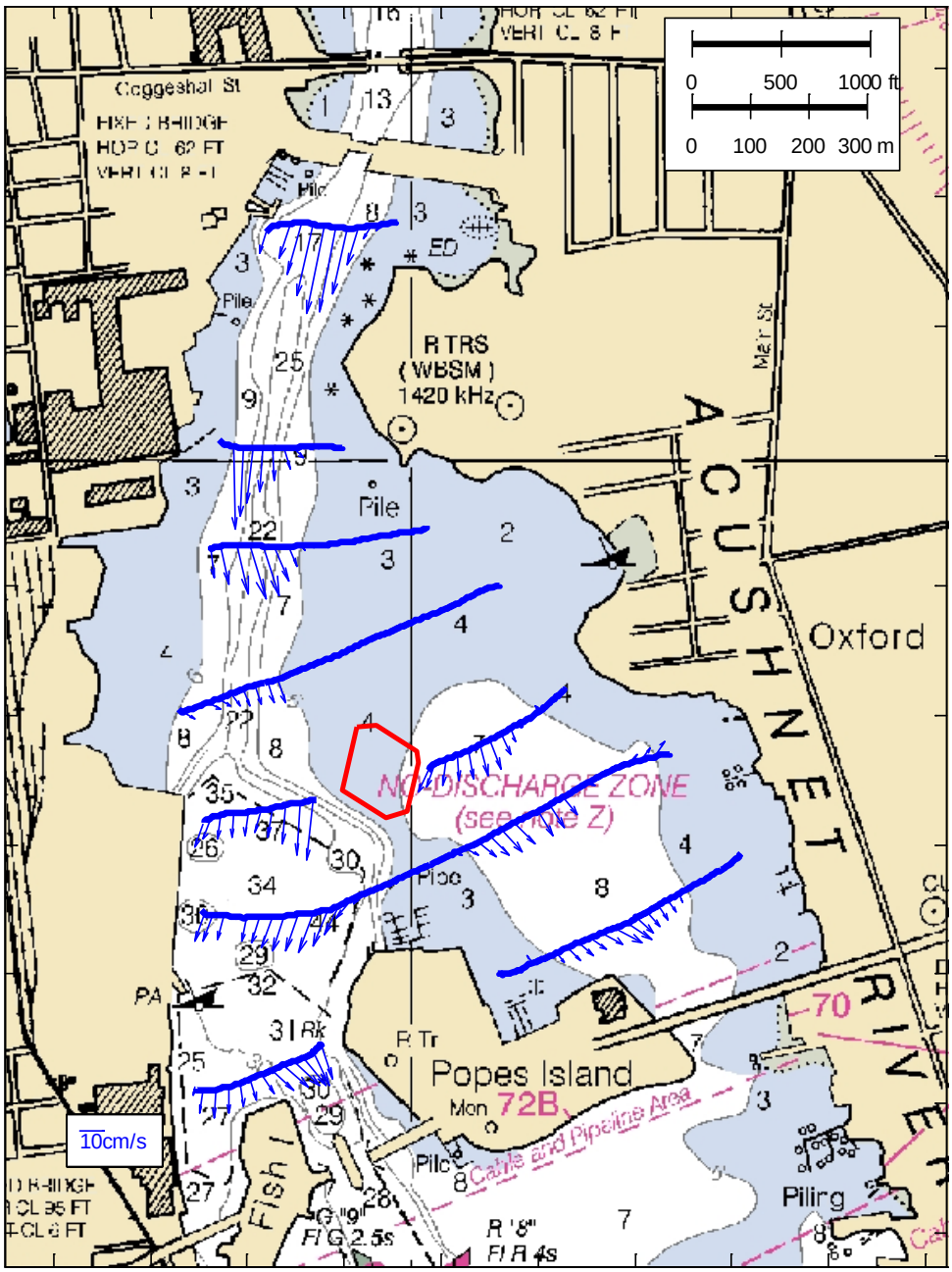

Figure E-18a Measured velocity vectors 2 hrs after high water slack

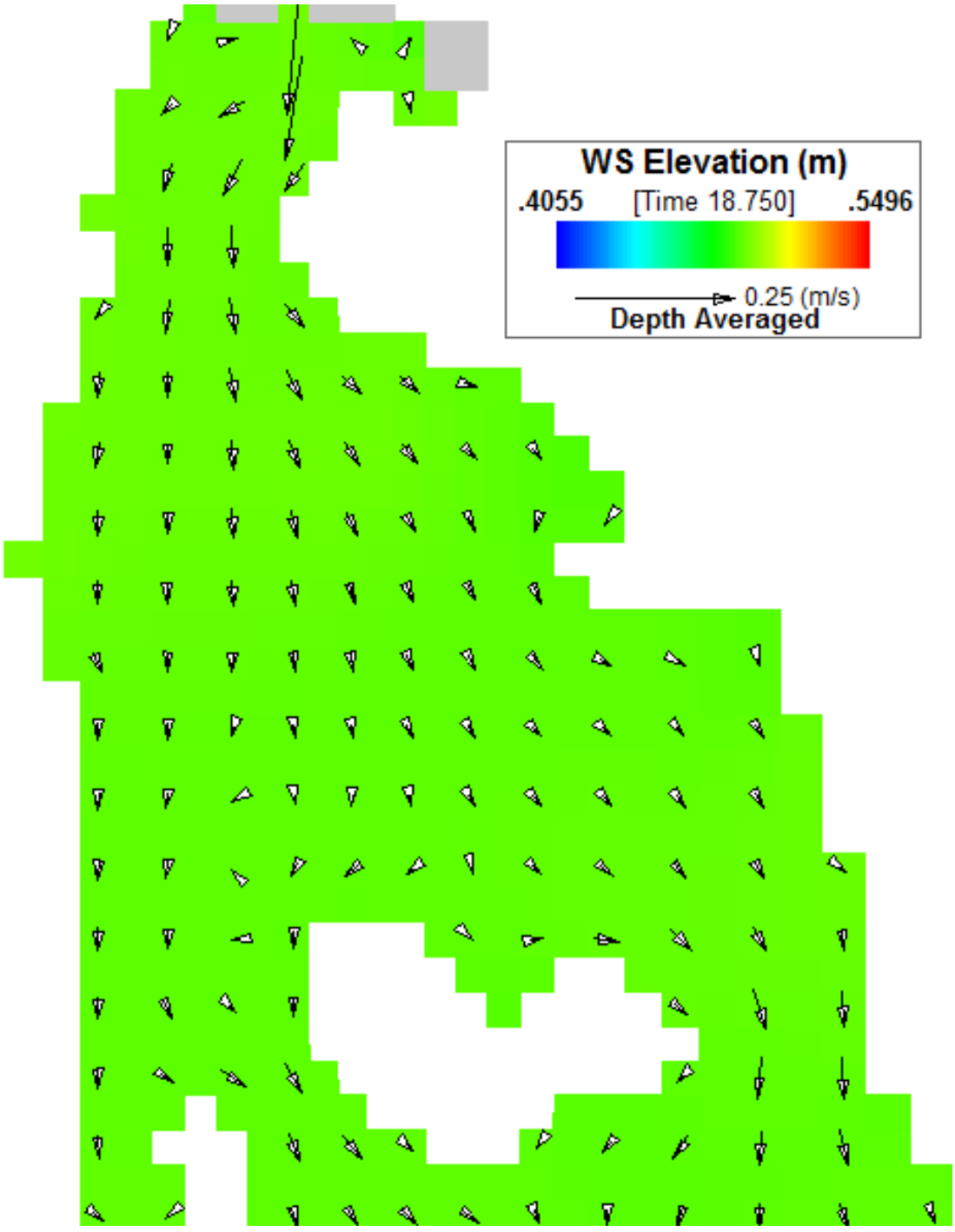

Figure E-18b Simulated velocity vectors 2 hrs after high water slack

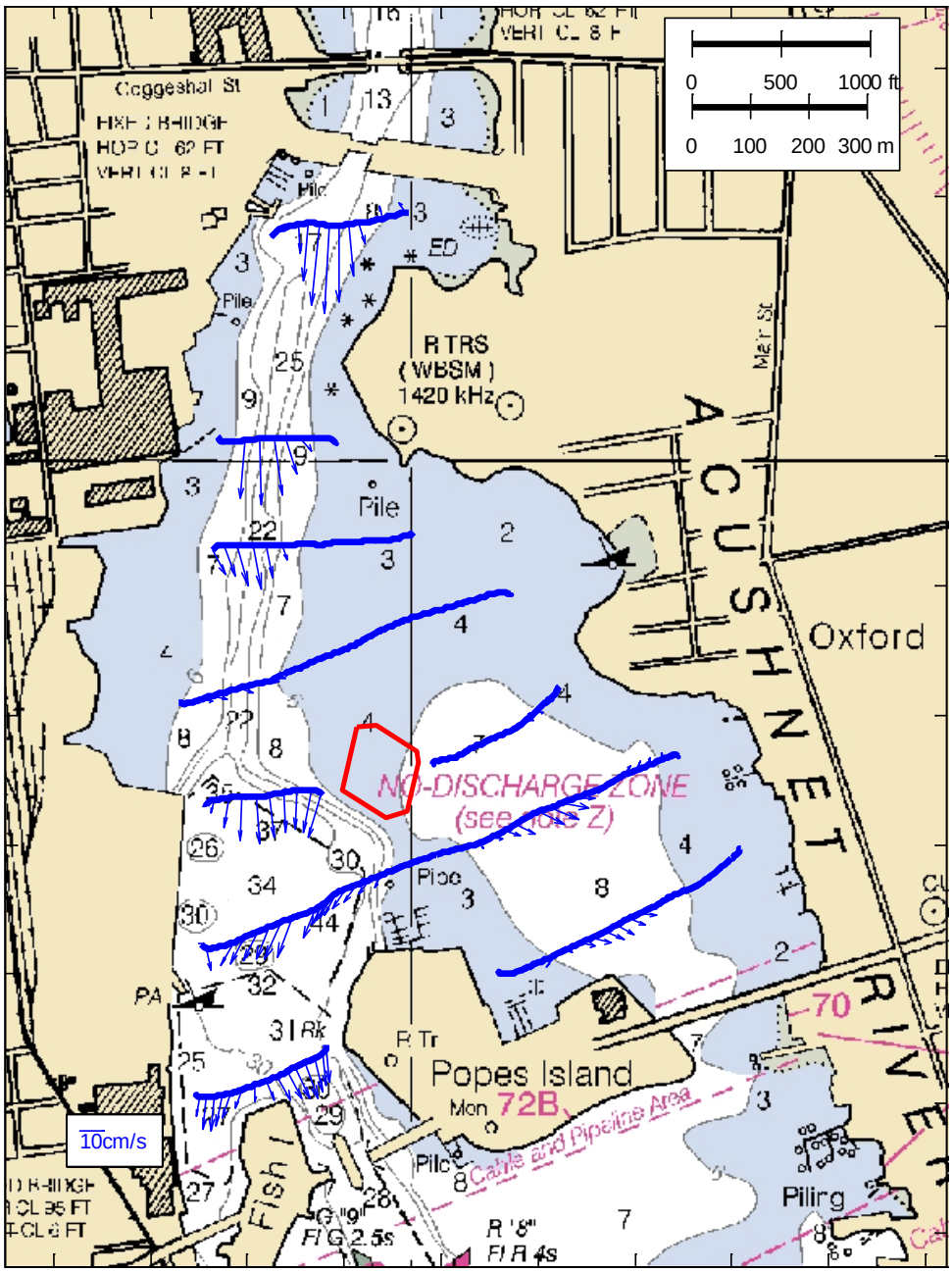

Figure E-19a Measured velocity vectors 3 hrs after high water slack

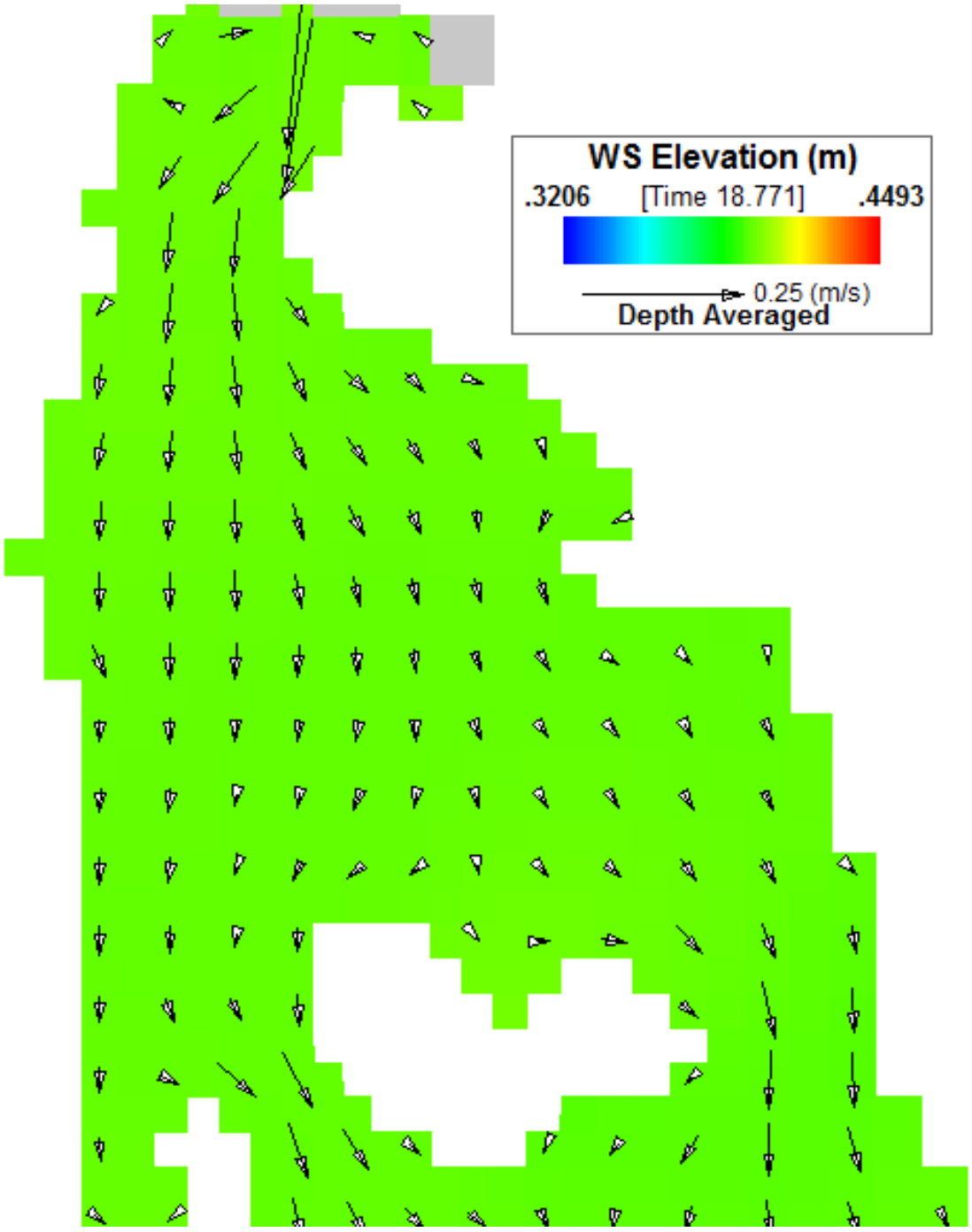

Figure E-19b Simulated velocity vectors 3 hrs after high water slack

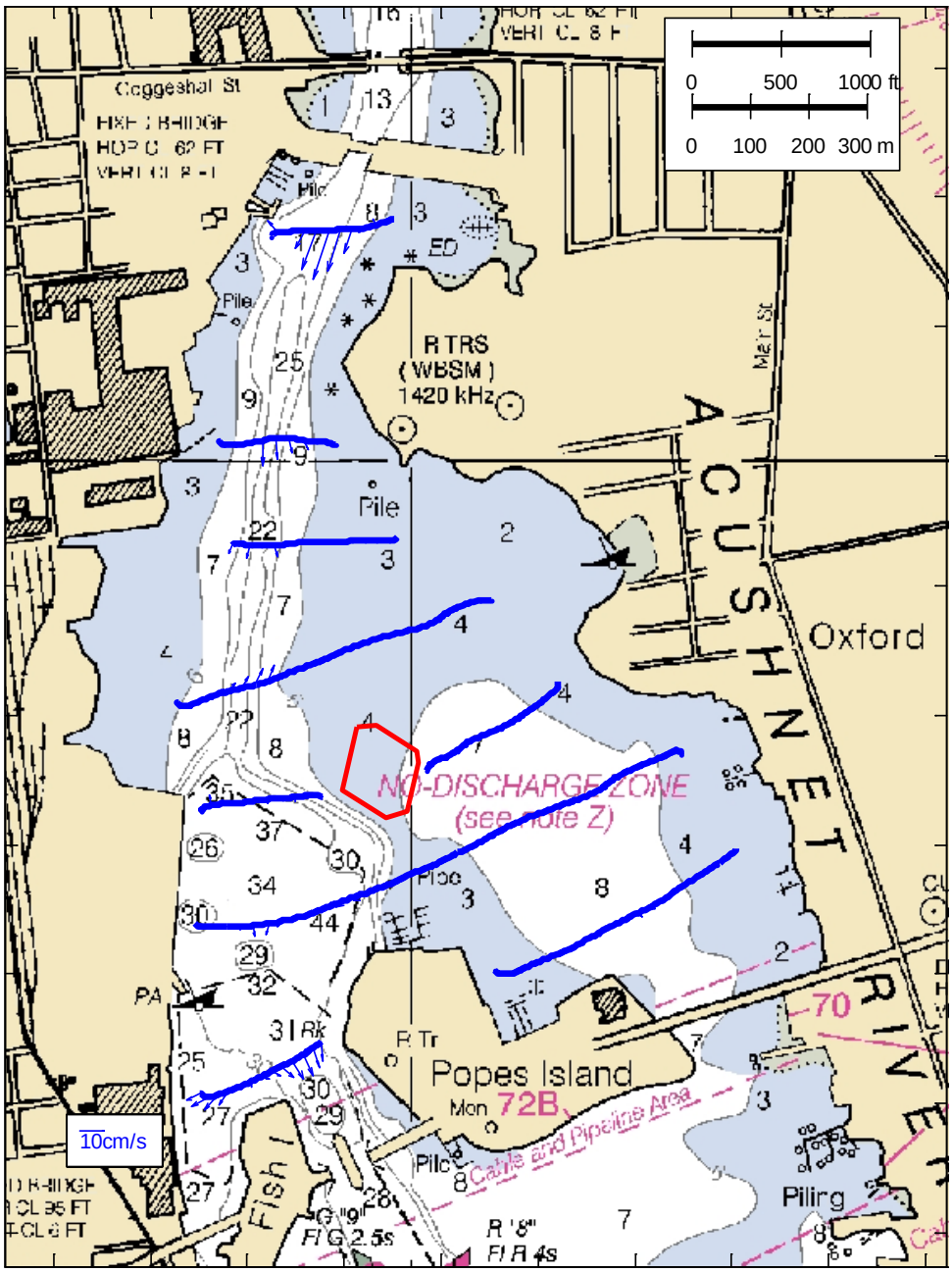

Figure E-20a Measured velocity vectors 4 hrs after high water slack

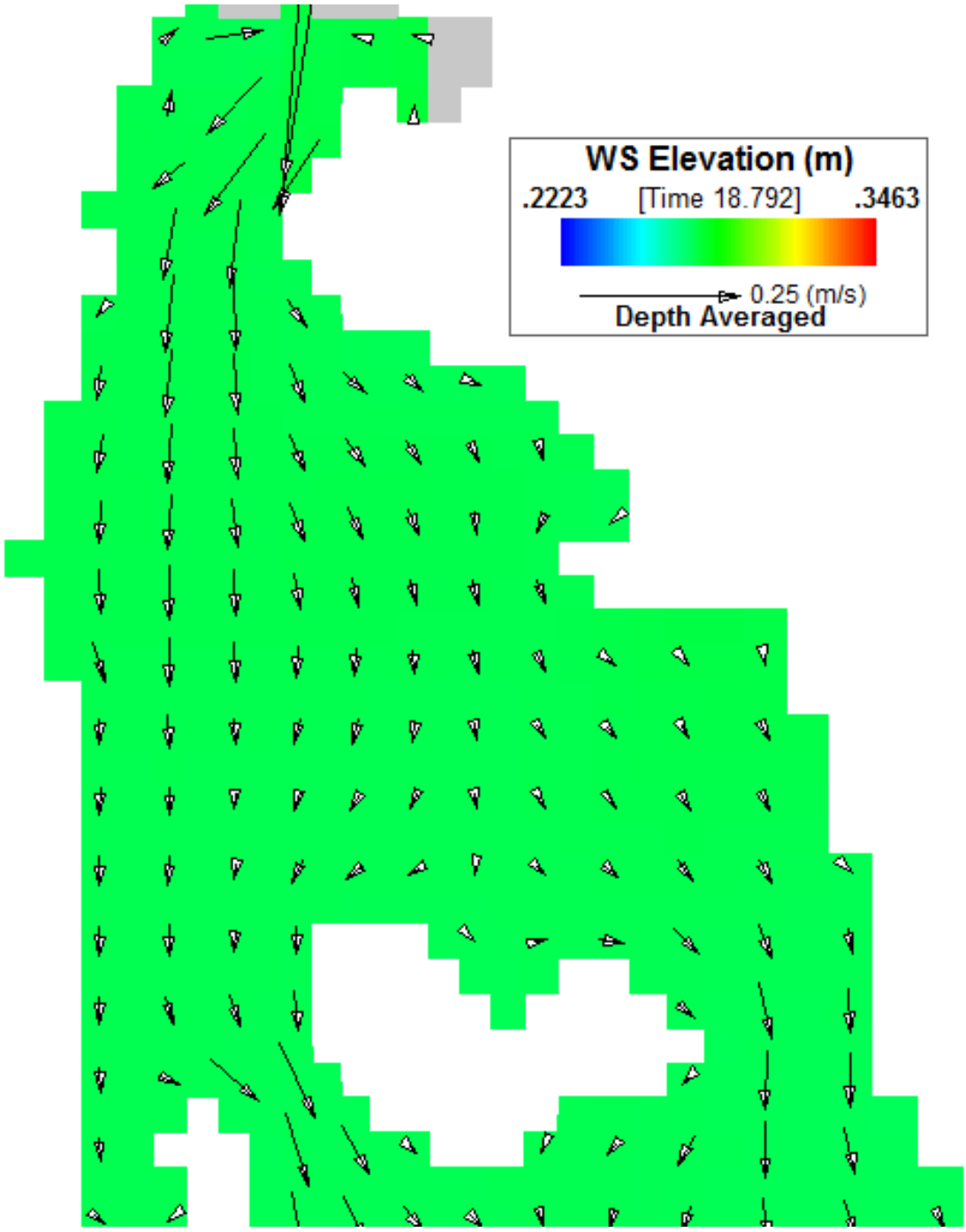

Figure E-20b Simulated velocity vectors 4 hrs after high water slack

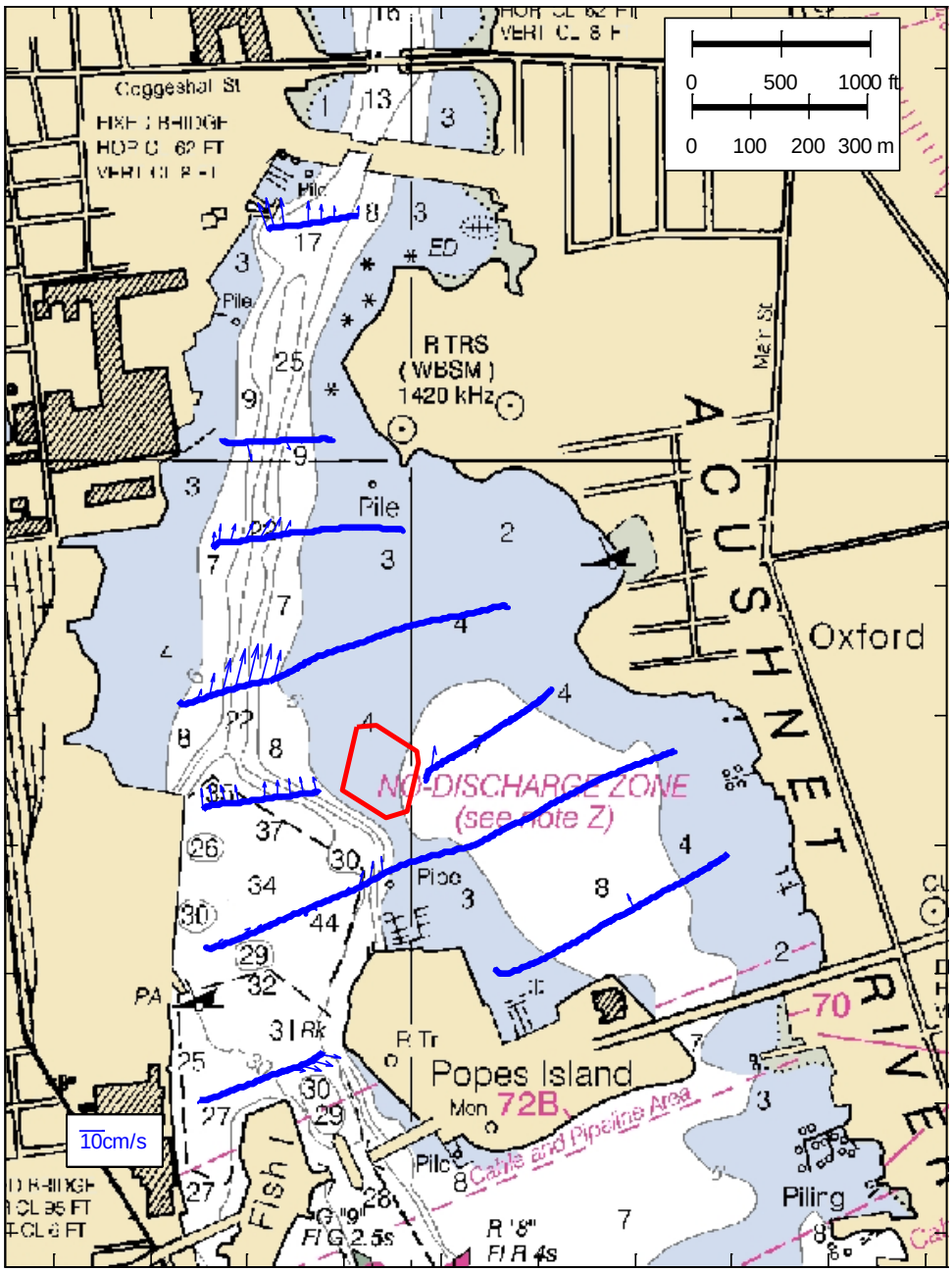

Figure E-21a Simulated velocity vectors 1 hr after low water slack

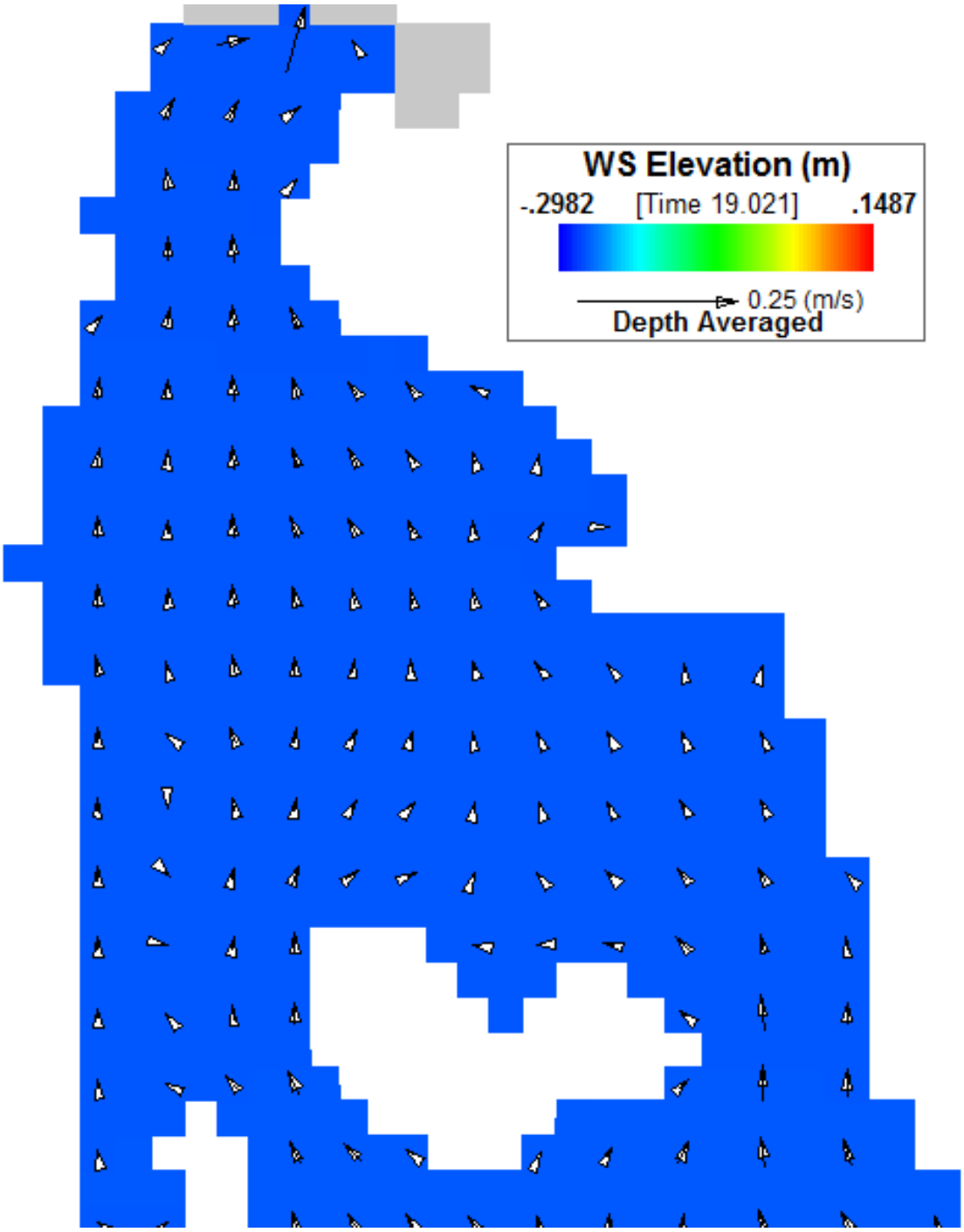

Figure E-21b Simulated velocity vectors 1 hr after low water slack